Chimeric antigen receptors cells targeting T cell malignancies

Candidate:

Hala Aldahshan

Supervisors:

Prof Waseem Qasim

Dr Christos Georgiadis

Dr Roland Preece

Great Ormond Street

Institute of Child health

University College London

A thesis submitted for the degree of Doctor of Philosophy

Declaration:

I, Hala Aldahshan, confirm that the content in this thesis is my own work. Where information has been drawn from other sources, I confirm that proper indication has been provided in this thesis.

Abstract

T cell leukaemias are characterised by the abnormal growth and dysfunction of T cells at various stages of development. Novel treatments for T cell malignancies, including adoptive cell transfer and chimeric antigen receptor (CAR) therapies, are being investigated. CAR-T cell therapy introduces a CAR transgene into T cells using viral or non-viral methods and redirects them against malignant cells. CAR-T cells have shown promise against B cell malignancies but face challenges in treating T cell malignancies due to fratricide during production and the risk of T cell aplasia post-administration. Genome editing allows for mitigating these challenges. Trials are underway testing base edited CAR7-T cells, targeting T cell receptor beta (β) chain (*TRBC)*, *CD7* and *CD52*, for elimination of graft-versus-host disease (GVHD), fratricide resistance and protection from serotherapy. This project investigated alternative base editor (BE) platforms incorporating rat or human cytidine deaminases that allow targeted C•G>T•A conversions in the genome independent of DNA breaks. These were tested for the multiplexed disruption of the *TCRαβ* and *CD7* loci in combination with lentiviral transduction strategies for expression of CAR7. All editors achieved on-target conversion with undetectable chromosomal translocations and no ectopic RNA aberrations. Optimal delivery timing for each BE mRNA was next investigated with respect to lentiviral CAR7 transduction to ensure orderly removal of shared antigens. Finally, site-specific 'knock-in' of a CAR transgene using clustered regularly interspaced short palindromic repeats (CRISPR)/CRISPR-associated protein 9 (Cas9) was investigated as it may favour more physiological levels of CAR expression and disruption of endogenous TCRαβ. A virus-free manufacturing timeline for anti-CD7 CAR-T cells was established using *Streptococcus pyogenes* (Sp) Cas9 ribonucleoproteins (RNPs) with single guide RNA (sgRNA) guides in combination with double-stranded (ds) DNA CAR templates flanked by regions of homology to T cell receptor alpha (α) chain *(TRAC)*, *CD3ζ or CD7*. Phenotypic profiling revealed CAR7+ expression and molecular analysis confirmed site-specific integration of CAR7 into *CD3ζ*, *CD7*, but not *TRAC.* CD3ζ-CAR7 effector cells exhibited potent cytotoxicity against CD7+ targets, comparable to lentivector expressed CAR7, warranting further investigation.

Impact statement

Immunotherapy has revolutionised the treatment of certain cancers that were previously untreatable. In the field of haematologic malignancies, anti CD19 chimeric antigen receptor (CAR) T cells have been successful, particularly in the treatment of B cell malignancies. These therapies have transitioned from being solely part of clinical trials to becoming licensed products. Immunotherapy options for T cell malignancies, however, have lagged as a result of key challenges in production due to the presence of shared antigens on both normal peripheral blood T cells and effector CAR T cells resulting in fratricide during manufacture. Additional complications faced in T cell targeting therapies and *in vivo* T cell aplasia, usually necessitating rescue by allogeneic hematopoietic stem cell transplantation (allo-SCT). It is crucial to note the pressing unmet clinical need for CAR targeting in T cell malignancies, especially among relapsed and refractory patients.

Genome editing has now made it possible to overcome key manufacturing hurdles enabling the targeted removal of surface antigens relevant to fratricide. Since the advent of clustered regularly interspaced palindromic repeats (CRISPR)/CRISPR-associated protein 9 (CRISPR/Cas9) which has democratised genome editing, technologies have rapidly evolved with innovative deaminase-based tools emerging, offering the capability to make precise edits in a seamless manner. Unlike traditional CRISPR/Cas9 methods that involve cutting the DNA strands, base editing techniques enable targeted changes at specific nucleotide positions without inducing double-strand DNA breaks. This advantage significantly reduces the risk of unintended mutations and simplifies the editing process, making base editing particularly attractive for applications requiring multiple simultaneous modifications with minimal off-target effects. As researchers refine base editors, they could revolutionise precision medicine, offering tailored genetic therapies for diverse disorders, advancing genomic medicine.

This work focused on the generation of T cell targeting CARs against T cell markers CD3 and CD7 for targeting T cell acute lymphoblastic leukaemia (T-ALL). However, it is important to note that CAR7 has broader potential applications beyond T-ALL. It can also be considered for diseases such as paediatric and adult acute myeloid

leukaemia (AML), given its ability to target CD7-expressing AML cells. Additionally, CAR7 provides a compelling alternative to traditional chemotherapy as a lymphodepletion strategy. Lymphodepletion involves reducing cells to create a more receptive environment for subsequent treatments, such as stem cell transplantation or CAR T cell therapy. The specificity of CAR7 in targeting CD7-positive cells reduces the risk of harming tissues, thus minimising treatment-related toxicity. The challenge of T cell aplasia following CAR7 treatment which can lead to protracted cytopenia is however a concern that would have to be addressed by the timely removal of the CARs. This precision, combined with the potential for combination therapies, positions CAR7 as an avenue for advancing the treatment of haematological malignancies while mitigating the negative effects of conventional therapies. Most CAR T cell products have relied on delivery of the CAR transgene by retroviral or lentiviral vectors. While highly efficient, viral vector manufacturing presents a significant bottleneck with high associated costs. Additionally, their use is not devoid of safety concerns related to potential immunogenicity and risk of insertional mutagenesis. This work has also explored the use of virus-free targeted delivery of CARs to precise gene loci in T cells. Avoiding the use of viral vectors will accelerate both research and clinical application.

Contribution to the publication:

R. Chiesa, C. Georgiadis, F. Syed, H. Zhan, A. Etuk, S. A. Gkazi, et al. Base-Edited CAR7 T Cells for Relapsed T-Cell Acute Lymphoblastic Leukemia. N Engl J Med 2023 Vol. 389 Issue 10 Pages 899-910

Publications arising from this work:

H. Aldahshan R. Preece H. Brezovjakova C. Georgiadis W. Qasim. Comparison of cytidine deaminase base editors for multiplexed editing of T cells. ESGCT 29th Annual Congress In collaboration with BSGCT Edinburgh, UK October 11–14, 2022 Abstracts.Volume:33 Issue 23-24: December 14, 2022.

O. Gough R. Preece H. Aldahshan C. Georgiadis W. Qasim. Virus-free production of CD20-targeted CAR-T cells via CRISPR-Cas9-mediated transgene insertion. ESGCT 29th Annual Congress In collaboration with BSGCT Edinburgh, UK October 11–14, 2022 Abstracts.Volume:33 Issue 23-24: December 14, 2022.

Acknowledgements

I would like to start these acknowledgements by expressing my gratitude to God, for blessing me with the strength and patience to reach this academic achievement.

I want to thank my supervisors, Professor Waseem Qasim, Dr Christos Georgiadis and Dr Roland Preece. Their unwavering guidance, support and invaluable insights throughout my research journey that have shaped my growth and professional development. I also extend my gratitude to the research team, whose expertise and guidance have been instrumental in shaping this body of work.

I am indebted to my family: my parents, Abdulrouf Aldahshan and Laila Alhamoudi, my brother Hamad, my sister Reema and my parents-in-law, Abdulmohsen Alghashiyan and Madawi Almugairen. Your unwavering belief in my abilities and your sacrifices to support my education have been crucial for my achievements. Your love and encouragement have carried me through challenging times.

I am truly grateful to my husband, Faisal Alghashiyan, and our precious children. Abdulmohsen, Nouf and Ahmad. They have willingly shared me with science while offering their support and understanding. Without their dedication it would have been impossible for me to come this far. Their patience, understanding and unending support have allowed me to balance project demands and family responsibilities. I could not have made it this far without their continued support and encouragement.

I want to express my gratitude to everyone who has been a part of this journey. This thesis reflects the combined effort and guidance of my loved ones and mentors. I will always be grateful for their presence in my life.

Table of Contents

List of Figures

List of Tables

Abbreviations

Adoptive cell therapies	ACT
Acute myeloid leukaemia	AML
Adeno-Associated Virus	AAV
Anaplastic large cell lymphoma	ALCL
Antigen binding regions	ABRs
Antigen presenting cell	APC
Alternative End Joining	Alt-EJ
Base editor	BE
Base excision repair	BER
B-cell acute lymphoblastic leukaemia	B-ALL
B-cell lymphoma	BCL
B cell non-Hodgkin lymphoma	B-NHL
Bispecific T cell engagers	BiTEs
Brentuximab vedotin	BV
Capsid	CA
Central polypurine tract	cPPT

Chemokine receptor 4	CCR4
Chimeric antigen receptor	CAR
Classical NHEJ	C-NHEJ
Class switch recombination	CSR
Cluster of differentiation	CD
Clustered-Regularly Interspaced Short Palindromic Repeats	CRISPR
CRISPR RNAs	crRNAs
Cytidine base editor	CBE
cyclic GMP-AMP synthase	cGAS
Cytomegalovirus	CMV
Deoxyribonucleic acid	DNA
Dimethyl sulfoxide	DMSO
DNA-dependent protein kinase	DNA-PKcs
DNA double-stranded break	DSB
Double stranded DNA	dsDNA
Dulbecco's Modified Eagle Medium	DMEM
Dulbecco's Phosphate-Buffered Saline	PBS

Escherichia coli	*E.coli*
Elongation factor 1 alpha	EF-1α
Foetal Calf Serum	FCS
Glyceraldehyde-3-phosphate dehydrogenase	GAPDH
Graft versus host disease	GVHD
Herpes simplex virus thymidine kinase	HSV-tk
Homology Directed Repair	HDR
Human immunodeficiency virus	HIV
Human leukocyte antigen	HLA
human phosphoglycerate kinase	hPGK
inducible caspase 9	iCasp9
Interleukins	IL
Immunoglobulin	Ig
Insertions and deletions	indels
Integrase	IN
Interferon-gamma	IFNγ
Ionic detergent compatibility reagent	IDCR

Jurkat, Clone E6-1	JE6.1
ligase IV	LigIV
Long terminal repeat	LTR
Lymphocyte-specific protein tyrosine kinase	LCK
Major histocompatibility complex	MHC
Matrix	MA
Meganucleases	MNs
Minimum Essential Medium	Opti-MEM
Minimal residual disease	MRD/
Microhomology-mediated end-joining	MMEJ
Multiplicity of infection	MOI
neoantigen-specific TCRs	neoTCRs
Natural killer	NK
Next generation sequencing	NGS
Non-Homologous End Joining	NHEJ
Nucleocapsid	NC
Nucleotide	nt

Overall survival	OS
Pattern recognition receptors	PRRs
Penicillin-Streptomycin	Pen-Strep
Peripheral blood mononuclear cells	PBMCs
Peripheral T cell lymphoma	PTCL
Peripheral T cell lymphoma not other specified	PTCL-NOS
piggyBac	PB
Polyethylenimine	PEI
Polymerase	Pol
Pre-integration complex	PIC
Replication-competent lentivirus	RCL
Programmed cell death protein 1	PD1
Protospacer Adjacent Motif	PAM
Recombinant TCR	rTCR
Reverse transcriptase	RT
Reverse transcription complex	RTC
Ribonucleic acid	RNA

Ribonucleoprotein	RNP
Self-inactivating	SIN
Single chain variable fragment	scFv
Single guide RNA	sgRNA
Single nucleotide polymorphism	SNP
Single stranded DNA	ssDNA
Single stranded RNA	ssRNA
Single-stranded synthetic oligodeoxynucleotide	ssODN
Somatic hypermutation	SHM
Stimulator of interferon genes	STING
Sleeping Beauty	SB
Streptococcus pyogenes Cas9	SpCas9
T cell acute lymphoblastic leukaemia	T-ALL
T cell receptor	TCR
T cell receptor alpha constant	TRAC
T cell receptor beta constant	TRBC
T cells redirected for universal cytokine-mediated killing	TRUCKs

Terminal deoxynucleotidyl transferase	TdT
Terminal inverted repeats	TIRs
Transactivating RNA	tracrRNA
Transcription-Activator-Like Effector Nucleases	TALENs
Transfer RNA	tRNA
Transducing units	TUs
Tris-acetate-EDTA	TAE
Tumour Necrosis Factor	TNF
Tyrosine-based activation motifs	ITAMs
Uracil DNA glycosylase	UDG
Uracil DNA glycosylase inhibitor	UGI
Universal CAR T cell	UCAR
Variable	V
Vesicular stomatitis virus glycoprotein	VSVG
Woodchuck hepatitis virus posttranscriptional regulatory element	WPRE
World Health Organization	WHO
X-ray cross complementing protein 4	XRCC4

XRCC4-like factor	XLF
Zinc Finger Nucleases	ZFNs
Zinc Finger Proteins	ZFPs

Chapter 1 Introduction

1.1 T lymphocytes

An effective immune response comprises a diverse array of cell types, with T lymphocytes (T cells), playing a pivotal role. T cells undergo a unique developmental journey, originating in the bone marrow and maturing in the thymus before being dispatched to the periphery (1). During T cell development, immature thymocytes proceed through many phases within the thymus, which is essential for proper immune system function and tolerance. As part of positive selection, thymic epithelial cells in the cortex introduce major histocompatibility complexes (MHCs) proteins to immature thymocytes. Thymocytes that successfully bind to MHC proteins continue maturation, while those that don't undergo apoptosis. This step ensures the development of T cells capable of recognising MHCs molecules (2). Transitioning to double-positive cells expressing CD4 and CD8 markers, thymocytes move to the cortex-medulla junction for negative selection. Here, self-antigens are presented, and thymocytes that bind to them are eliminated to prevent autoimmune responses. Exiting the thymus as single-positive T cells expressing either CD4 or CD8, mature T cells are equipped with diverse receptors. Shaped by both positive and negative selection, they effectively recognise foreign antigens while maintaining tolerance to self-antigens (2) (**Figure 1.1**). This journey gives rise to various T cell subsets, each with its distinct function. The T cell lineage encompasses naïve T cells, primed to respond to novel antigens, memory T cells, which confer long-term immunity following previous activations, and regulatory T cells, responsible for maintaining tolerance to self-antigens. Notably, memory and regulatory T cells can be broadly categorised into two main types: CD4+ helper T cells and CD8+ cytotoxic T cells (3). T cells recognise antigens through short peptide fragments presented by MHCs via their surface-expressed T cell receptor (TCR)-CD3 complex. Activation of T cells hinges upon the interaction between the TCR and its specific MHC-peptide complex, thereby initiating signalling cascades through the CD3ζ subunit. The recognition of antigens by T cells is highly specialised, with CD8+ cytotoxic T cells

targeting antigens presented by MHC class I complexes, while CD4+ helper T cells engage with antigens displayed by MHC class II complexes (3).

MHC class I molecules are universally present on all the nucleated cell surfaces. They play a crucial role in presenting intracellular pathogen-derived peptides, such as those from viruses or cancer cells to T cells. This pivotal interaction aids the immune system in identifying and subsequently eliminating infected or abnormal cells. In essence, MHC class I molecules serve as an immune alert system, allowing it to detect and target cells harbouring internal threats. In contrast, MHC class II molecules are predominantly found on specialised antigen-presenting cells. These molecules have the responsibility to present peptides to help T cells. This interaction serves as a regulatory checkpoint, controlling the immune response and modulating the activities of various immune cells. By presenting these extracellular pathogenic peptides, MHC class II molecules facilitate a coordinated and fine-tuned immune defence mechanism. The contrast between MHC class I and class II molecules play a critical role in recognising and responding to different pathogens, thereby improving the ability of the immune system. This division of work ensures that the immune response is both precise and adaptable, enabling the body to mount an effective defence against diverse threats while maintaining regulatory control over immune activities (4).

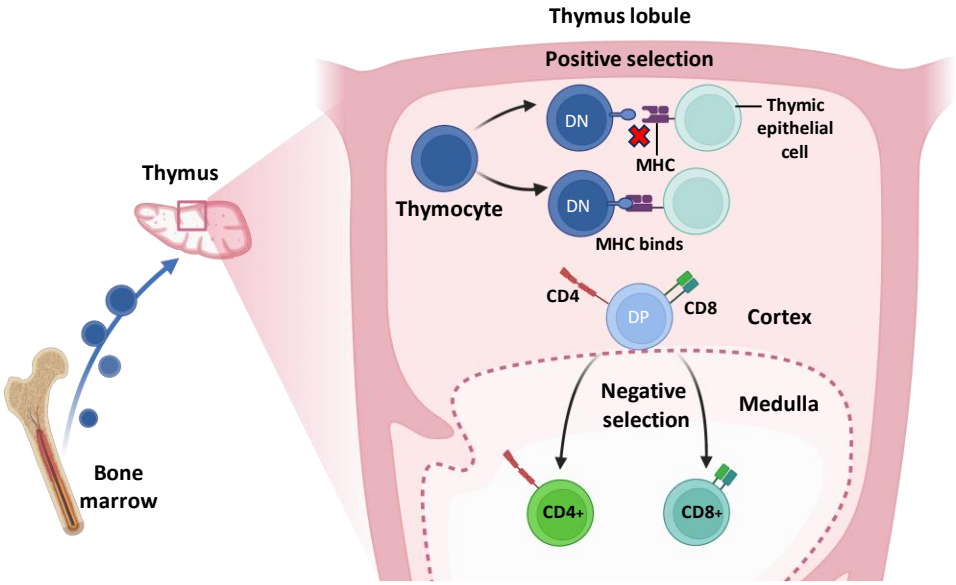

Figure 1-1 Overview of T cell development in the thymus

Immature thymocytes which are double negative (DN), (CD4-, CD8-) undergo a series of developmental stages within the thymus. In the cortex, thymic epithelial cells present major histocompatibility complex (MHC) proteins to immature thymocytes, a process known as positive selection. Thymocytes that successfully bind to MHC proteins progress in their maturation journey (black arrow), while those that fail to engage undergo apoptosis (red X). Transitioning to double-positive cells (DP) expressing both CD4 and CD8 receptors, thymocytes move to the cortex-medulla junction for negative selection. Self-antigens are presented, and thymocytes that bind to them are eliminated to prevent autoimmune responses. Finally, mature single-positive T cells expressing either CD4 or CD8 exit the thymus.

1.1.1 Structure of T cell receptor (TCR)

The T cell receptor (TCR) consists of two chains, alpha and beta or gamma and delta, linked by a disulfide bond. In human T cells, 95% of the TCR is made up of an alpha chain, a beta chain, and the CD3 complex. The remaining 5% consists of a gamma chain and a delta chain (3, 5). The variable (V) and constant (C) regions of the TCR alpha and beta chains include complementarity-determining domains (CDRs), which are required for antigen recognition. These CDRs, essential to binding antigens, undergo diversity generation through VDJ recombination. This process rearranges V, D, and J gene segments, leading to a distinct TCR sequence (5). When the TCR binds to MHC molecules, it transmits signals via CD3 family proteins such as CD3δ, CD3ε, CD3γ, and CD3ζ. TCR crystallisation studies have discovered immunoreceptor tyrosine-based activation motifs (ITAMs), a component of the CD3 complex. ITAMs trigger T lymphocytes internally and require the phosphorylation of two tyrosine residues upon the TCR's interaction with the MHC complex. This mechanism establishes sites for transduction molecules and initiates signalling pathways that lead to the activation of T lymphocytes (5, 6) **(Figure 1-2)**.

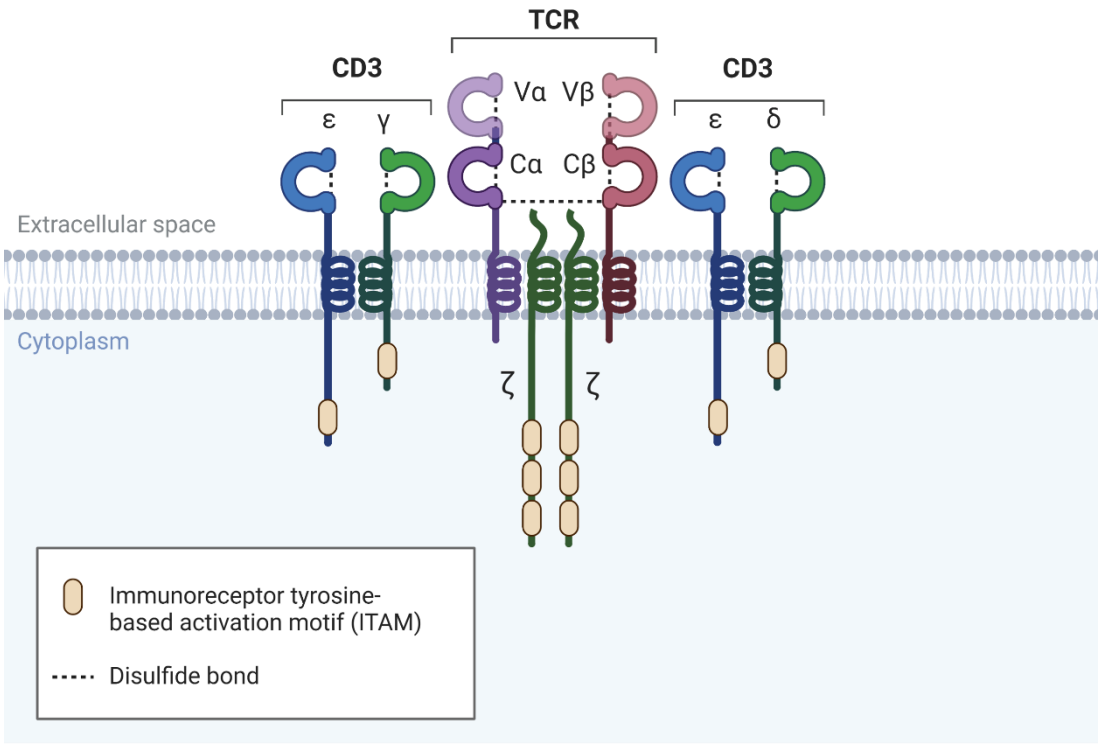

Figure 1-2 A diagram illustrating the TCR-CD3/ζ complex.

TCR comprises a disulphide-linked αβ heterodimer. The alpha(α) chain consists of a constant domain (dark purple) and a variable domain (light purple), while the beta (β) chain consists of a constant region (dark red) and a variable domain (light red). The αβ TCR is not covalently linked to CD3 proteins, which include CD3δ (green), CD3ε (blue), CD3γ (green), and the ζ chain (dark green). Phosphorylation of ITAM regions (yellow blocks) occurs at specific residues, creating a docking site for downstream effectors that induce T cell activation. ITAM: immunoreceptor tyrosine-based activation motifs.

1.2 T cell malignancies

T cell malignancies represent a group of aggressive cancers that specifically target the T cells of the immune system. These malignancies are further classified based on their clinical characteristics, genetic abnormalities, and the specific type of T cell they originate from. The most prevalent paediatric cancer is acute lymphoblastic leukaemia (ALL), a condition that can be broadly categorised into two primary subtypes: “B cell ALL (B-ALL) and T cell ALL (T-ALL)”. Additionally, there are other T cell malignancies such as peripheral T cell lymphoma (PTCL), which emerges from mature T cells and encompasses various subtypes like PTCL-not otherwise specified

(NOS), anaplastic large cell lymphoma (ALCL), and nodal PTCLs, each presenting distinct clinical and molecular features. These classifications play a crucial role in understanding and effectively managing the complexities of T cell malignancies (7, 8).

T-ALL is a highly aggressive malignant neoplasm originated in the bone marrow. It is estimated to affect around 10-15% of cases in paediatric and 25% cases in adult population, underscoring its significance in both age groups (9-11). T-ALL is characterised by high levels of white blood cells in the bloodstream, a condition called hyperleukocytosis, along with extramedullary involvement of lymph nodes and other organs. This may involve infiltration of the nervous system and the formation of a mediastinal mass originating from the thymus gland. According to the World Health Organization (WHO), T-ALL is identified as a precursor lymphoid neoplasm. It differs from adult T cell leukaemia/lymphoma, which is cancer affecting T cells caused by human T cell lymphotropic virus type 1 (12). The WHO classification of T-ALL involves assessing gene expression patterns and chromosomal abnormalities to categorise cases as high-risk or low-risk, guiding treatment decisions. T-ALL lymphoblasts are characterised by their positivity for terminal deoxynucleotidyl transferase (TdT) and variable expression of T cell markers such as CD1a, CD2, CD3, CD4, CD5, CD7, and CD8, indicative of different stages of T cell development. Additionally, despite surface expression variability, they often exhibit cytoplasmic positivity for CD7 and CD3. This immunophenotypic profile aids in distinguishing T-ALL from other acute lymphoblastic leukaemia and informs diagnostic and treatment approaches, reflecting the arrested maturation of malignant T cell precursors (13, 14).

The primary molecular drivers of T cell malignancies, notably T-ALL, encompass several key alterations. These include the constitutive activation of NOTCH1 signalling due to activating mutations in NOTCH1 and FBXW7 (15-17), inactivation of tumour suppressor genes like CDKN2A and other regulators such as RUNX1 and GATA3 (15), aberrant expression of transcription factor oncogenes resulting from chromosomal rearrangements such as TAL1, TAL2, LYL1, LMO1, LMO2, TLX1, TLX3, and HOXA (15, 16, 18), and dysregulation of cell signalling pathways involving genes like ABL1 and

PTEN (19, 20). Furthermore, epigenetic and chromatin remodelling alterations involving genes like KMT2C, SETD1B, ARID1A, ARID2, and CREBBP are also observed (14). Together, these molecular changes disrupt crucial pathways governing T cell development, proliferation, survival, and differentiation, contributing to the onset and progression of these aggressive haematological cancers.

The current standard of care for ALL treatment involves blocks of intensive chemotherapy based on a risk stratified approach followed by maintenance chemotherapy for 2-3 years. The risk stratification has evolved over the years and broadly includes disease type (B/T ALL), National Cancer Institute category, cytogenetics and disease response assessed by minimal residual disease (MRD) (21, 22). Over the years, there has been a substantial improvement in the 5-year overall survival (OS) rate, with recent studies reporting survival rates exceeding 90%, compared to 57% in the 1970s (21). This tremendous success in the outcome is the result of refinement of risk stratification and improvement in the supportive care.

Despite the improvement in the outcome of frontline T-ALL, 20-25% of children experience relapse. Unfortunately, standard therapies often fail to effectively treat relapsed cases, leading to poor survival rates (23, 24). Refractory T-ALL is another challenge, where the disease displays resistance to initial treatments, enhancing the difficulty of controlling and attaining successful results with a survival rate of only 19% (25). While nelarabine (26) and allogeneic stem cell transplantation (SCT) (27) are often used as salvage therapies, innovative treatments in T-ALL have not progressed as rapidly as in B-ALL. Addressing the challenges of relapsed and refractory (r/r) T-ALL necessitates a paramount focus on innovative therapeutic strategies, particularly the application of targeted therapies (28, 29). These novel approaches have the potential to improve the prognosis and overall quality of life for cancer patients. Additionally, chemotherapy has a growing recognition of the associated acute and long-term toxicities (30) and the corresponding impacts on mortality and health-related quality of life (HRQOL) (31-33).

In response to these challenges, the future of leukaemia treatment relies on innovative approaches, including novel therapeutic strategies, especially targeted novel immunotherapy.

1.3 Immunotherapy

Immune cells have the ability to recognise foreign and novel antigens and eliminate them via immune surveillance. This procedure is critical in protecting the host not only form infectious pathogens but also from cancer cells (34). Immunotherapy is a treatment approach that boosts the body's immune system to fight diseases, especially cancer. This approach has transformed the treatment of cancer in areas with previously unmet clinical needs. Most significantly, it has shown efficacy against a variety of haematological malignancies (35). As the field of immunology progresses, it led to the discovery of innovative therapies that use the immune cells and enhance their precision in targeting particular diseases through genetic modifications (10, 35, 36).

Immunotherapeutic strategies, redirecting the immune cells to effectively determine and eliminate tumour cells, have revolutionised the treatment of cancer to a great extent. One of the more promising avenues within this field is the utilisation of monoclonal antibodies (mAbs) to efficiently treat T-ALL. These specialised antibodies are developed to target particular proteins or antigens present on the surface of T-ALL cells, producing a significant anti-tumour effect (10). Monoclonal antibodies accomplish their anti-cancer goals with the help of different mechanisms. The key direct mechanism that results in apoptosis, or cell death, in cancer cells is the interference with the binding between growth factor receptors and their ligands. This disruption is primarily achieved by blocking the signalling pathways associated with these receptors. In addition, indirect mechanisms are also present relying on the engaging component of the host immune system. These mechanisms involve Complement-Dependent Cytotoxicity (CDC) and Antibody-Dependent Cellular Phagocytosis (ADCP). In CDC, the complement system is activated by antibodies to destroy tumour cells, while ADCP involves antibodies which facilitate the engulfment

and elimination of cancer cells with the help of phagocytic immune cells, such as macrophages. Additionally, another indirect mechanism is the antibody dependent cellular cytotoxicity (ADCC) where antibodies target immune cells, for instance natural killer cells, for targeting and eliminating cancerous cell effectively (37).

Numerous putative target antigens in T-ALL have been investigated, including , CD1a (38), CD38 (39), and CD5 (40). Notably, the FDA approved daratumumab, an anti-CD38 monoclonal antibody, as a stand-alone treatment for patients with relapsed/refractory multiple myeloma in 2015 and the European Medicines Agency approved it in 2016 (39). The persistent presence of CD38 on T-ALL and early T cell precursor ALL (ETP-ALL) cells at many illness stages, including diagnosis, chemotherapy, and relapse, has also made CD38 a prospective target for T-ALL treatment (41). This stability makes CD38 a strong option for the treatment of T-ALL. Current early-phase clinical trials are examining the use of anti-CD38 antibodies which induce an apoptosis effect on the cells, such as Isatuximab (NCT03860844) and Daratumumab (NCT03384654) for the treatment of T-ALL.

Antibody-drug conjugates (ADCs) represent another type of immunotherapy that combines the specificity of monoclonal antibodies with the potent cytotoxic properties of chemotherapeutic drugs (42). Researchers have also explored the use of monoclonal antibody immunotoxin therapy targeting CD7 as a potential treatment for T cell malignancies (43). Despite promising research, this approach was not ultimately developed into a commercial treatment option.

Genetically engineered adoptive cell therapies (ACT) that redirect T cells to target specific antigens while minimising side effects on healthy tissues have emerged as a promising area of immunotherapy research (44, 45). Currently, recombinant T cell receptors (rTCR) or chimeric antigen receptors (CARs) can be expressed to direct T cells towards a particular antigen (46). T cells have significantly changed cancer therapy and using them in adoptive T cell therapy has been proven to be highly effective for some cancer types. To be successful, adoptive T cell treatment must take into account a number of variables, including target antigen, immune evasion

strategies, and T cell subset selection (47). Nonetheless, the potential ability of T cells to identify and destroy cancerous cells has paved the way for multiple promising avenues in effective immunotherapy, raising hopes that more therapeutic options will be made available.

1.3.1 Recombinant TCR

The T cell receptor (TCR) is a complex assembly of multiple components, including two distinct chains, alpha (α) and beta (β), along with four additional membrane proteins: CD3γ (CD3 gamma), CD3δ (CD3 delta), CD3ε (CD3 epsilon), and an invariant CD3ζ (zeta). This intricate arrangement is essential for the TCR to function effectively in recognising and responding to antigens (48). This complex identifies enzymatically cleaved peptides displayed on the target cell surface via MHC. When TCRs bind to the matching MHC, it triggers the phosphorylation ITAMs within the intracellular CD3 subunits (49). Subsequently, this signalling cascade leads to T cell proliferation, cytokine release, and cytolysis through the secretion of granzyme and perforin (50). T cells are often genetically modified for the expression of the α- and β- chains of the TCR in the context of targeted TCR treatment, giving them the necessary specificity.

Although recombinant TCR (rTCR) T cells are limited to MHC recognition (**Figure 1-1 A**), they recognise extracellular and intracellular proteins. rTCR gene therapies have shown some encouraging outcomes across different cancer types, such as hepatocellular carcinoma (51), B-cell malignancies (52), sarcoma and melanoma (53). However, despite the promising effects of rTCR immunotherapy, there still remain several challenges. One of these challenges is the potential for off-target effects and receptor mispairing. Off-target recognition can lead to unintentional immune responses against healthy tissues, contributing to side effects and even patient fatalities in some cases (54, 55). Efforts have been made to establish predictive models for assessing the potential cross-reactivity of rTCRs before their clinical use. While these models provide significant insights into the risk of off-target effects, they are not yet perfect (56).

Another concern is receptor mispairing of rTCR, which involves improper association of the alpha (α) and beta (β) chains in T cell receptors. This can compromise antigen specificity and potentially result in unpredictable targeting. In some cases, this may lead to the development of rTCRs that target self-peptides, potentially causing autoimmunity or graft-versus-host disease (GVHD) (57, 58). To improve both safety and efficacy of TCR-based therapies and prevent mispairing of T cell receptors, researchers have employed genome editing techniques to eliminate both the endogenous TCR α and β genes (59). This approach was recently tested in a phase I clinical trial involving patients with refractory solid cancers. The goal was to replace their endogenous TCRs with neoantigen-specific TCRs (neoTCRs), providing an effective procedure for improving the precision of cancer immunotherapy as well as decreasing the likelihood of unintended immune responses towards healthy tissues (60).

1.3.2 Chimeric Antigen Receptors (CARs)

CAR-T cells, combine the antigen specificity of monoclonal antibodies with the cytotoxic potential of TCR signalling, allowing antigen recognition of cell surface protein in an MHC independent fashion (61, 62).

Chimeric antigen receptors are composed of an external target recognition domain, a transmembrane spacer domain, and an intracellular signal transduction domain. A single chain variable fragment (scFv) found in the extracellular domain functions to replicate the variable portions of heavy (vH) and light (vL) antibody chains, which are joined by a flexible linker (63) (**Figure 1-3 B**). A transmembrane spacer domain and a hinge region are located close to the scFv. These components are essential for keeping the CAR flexible, spaced out, and anchored to the cell membrane. Although it can also be generated from the CD8α chain, this spacer domain is often adopted from the constant IgG1 hinge-CH2-CH3 Fc domain (64). These components are linked to the intracellular signalling domain from the CD3ζ chain containing three immunoreceptor tyrosine-based activation motifs (ITAMs). This intracellular domain serves as the activation signalling hub (65). The modular design of CARs significantly

influences CAR-T cell signalling mechanisms, effector functions, and their potential efficacy and toxicity (66, 67). The downstream signalling cascades initiated by CAR-mediated antigen recognition primarily commence with the phosphorylation of the ITAMs situated within the intracellular domain of CD3ζ. This phosphorylation process is facilitated by the action of lymphocyte-specific protein tyrosine kinase (LCK), triggering signal 1 and activating the T cell. Co-stimulatory signals, generated by co-stimulatory molecules like CD28/B7, play a pivotal role in promoting the synthesis of IL-2, facilitating full T cell activation, and preventing apoptosis (signal 2). Consequently, CARs that only incorporate the CD3ζ sequence are unable to undergo full activation in the absence of a co-stimulatory signal. Following signal 2, cytokines like interferon-gamma (IFN-γ) and interleukins (IL) are released, augmenting immune responses and recruiting other immune cells (signal 3). The activated CAR-T cells subsequently eliminate target cells through cytotoxic mechanisms, including the secretion of cytotoxic granules containing granzyme and perforin and direct cell-cell interactions (68).

The CAR-T cells have evolved through different generations which are primarily differentiated through the presence of distinct endodomains **(Figure1-4**). In the first-generation CAR-T cells, a single intracellular signalling domain was present, the CD3ζ activation domain linked to an external scFv for T cell activation (63, 69). However, one of the drawbacks was that T cells engineered with these first-generation CARs did not facilitate IL-2 production, led to low persistence, and failed to generate potential anti-tumour effects *in vivo* (70). In the second-generation CAR-T cells, additional intracellular signalling domains were integrated, involving co-stimulatory domains such as CD28 or 4–1BB/CD137 (65), offering signal 2 to activate T cells. As a result, second generation CAR-T cells were significantly improved with better functionality, anti-tumour efficacy, and persistence, observed both in pre-clinical models (71, 72), as well as clinical trials (73-77). CAR molecules incorporating the CD28ζ signalling domain exhibit rapid expansion and increased effector T cell activity. However, their effects tend to be more transient than CARs based on 4-1BB signalling, which promotes sustained anti-tumour responses and prolonged T cell proliferation

(78, 79). Along with the frequently utilised co-stimulatory domains, alternative co-stimulatory domains have also been explored comprehensively. These alternatives mainly include the OX40 receptor (CD134), CD27, MYD88, CD40, the inducible T cell co-stimulator, and killer cell immunoglobin-like receptor 2DS2 (80). In third generation CARs, co-stimulatory signalling domains were combined, such as CD28 with 4-1BB, for improved CAR-T cell potency with better cytokine production, anti-tumour efficacy, and improved T cell proliferation (81). Even though third generation CARs have revealed promising outcomes in specific cancer types along with acceptable safety profiles (82, 83), the therapeutic benefits compared to second generation CAR-T cells is still not clear and requires further exploration.

Researchers have explored various cytokines to equip CAR-T cells with enhanced capabilities, leading to the development of what is referred to as T cells redirected for universal cytokine-mediated killing (TRUCKs). These engineered T cells are designed to produce and release specific cytokines, including interleukin-12 (IL-12), upon encountering their target cells, which are often cancer cells. This innovative approach aims to harness the power of cytokines, which are signalling proteins involved in immune responses, to bolster the CAR-T cell's therapeutic effects. When TRUCKs engage with their intended targets, they not only directly attack these cells but also release cytokines, which stimulate and recruit other immune cells to amplify the immune response against the malignancy (84). This dual mechanism, of both direct cytotoxicity and cytokine-mediated enhancement, represents a great potential in the evolution of CAR-T cell therapy, potentially offering improved effectiveness in treating a broader range of malignancies and providing a promising avenue for improving the treatment of a variety diseases. While TRUCKs show potential for broader applications compared to earlier CAR generations, encompassing viral infections, metabolic disorders, and heterogeneous tumour microenvironments, there are notable concerns. These concerns primarily revolve around the method of delivery and the risk of unintended off-target or off-tumour immune responses due to system leakage (65, 84, 85). These challenges must be carefully addressed to ensure the safety and precision of TRUCK-based therapies.

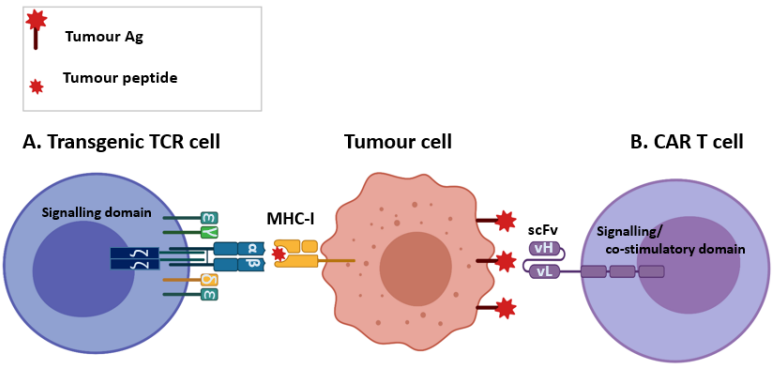

Figure 1-3 T cells genetically equipped with T cell receptors (TCRs) or chimeric antigen receptors (CARs) targeting a tumour cell

A. The transgenic TCR consists of an α and a β chain, which are linked with γ, δ and ε chains, and the signal-activating ζ chain, forming the CD3 complex. The TCR mediates recognition of antigenic peptides bound to MHC-I. Transgenic TCR engagement leads to its activation for the degranulation of the tumour cell. **B.** A second generation CAR includes the single-chain variable fragment (scFv) of a monoclonal antibody that binds to tumour antigens. This is fused to a transmembrane stalk, a 41BB or CD28 co-stimulatory domain, and a CD3ζ signalling domain. vH: variable heavy, vL: variable light.

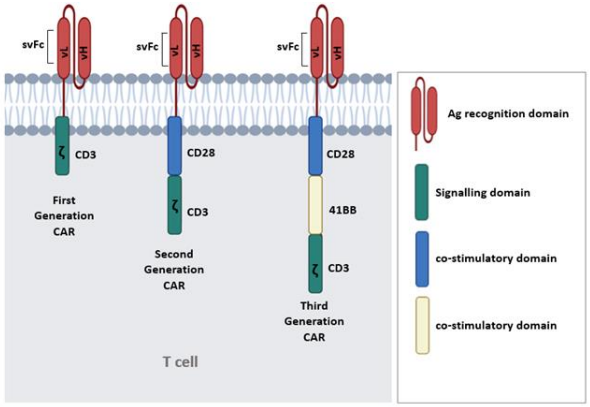

Figure 1-4 Structure of chimeric antigen receptor (CAR) and its design evolution.

The extracellular domain (scFv) is derived from the variable heavy (vH) and light (vL) antigen-binding domain of antibodies. A hinge links the scFv to the transmembrane and CD3ζ intracellular signalling domains in first-generation CARs. Second-generation CARs contain one co-stimulatory domain, such as CD28. Third-generation CARs contain at least two co-stimulatory domains, such as CD28 and 41BB.

1.4 Chimeric antigen receptors (CAR) for T cell malignancies

CAR-T cell therapy has demonstrated remarkable clinical efficacy in specific subsets of B cell leukaemia and lymphoma, with overall response rates up to 90% in some studies (86-91). The success of anti-CD19 CAR-T cell therapy against B cell malignancies led to its approval by the Food and Drug Administration (FDA) in 2017(92-94). The development of autologous anti-CD19 CAR-T cell therapy marked a significant advancement in treating relapsed or refractory B cell acute lymphoblastic leukaemia (R/R B-ALL), providing an additional therapeutic option. Currently, the two FDA-approved CD19-targeting CAR-T cell therapies for the treatment of R/R B-ALL are tisagenlecleucel (CTL019) based on the results of the ELIANA trial and brexucabtagene autoleucel (KTE-X19) based on the results of the ZUMA-3 trial. (93, 95). Although CAR-T cell therapy has shown effectiveness in treating B cell cancers, its use in treating T cell cancers faces challenges. One major obstacle is fratricide, a phenomenon where CAR-T cells mistakenly attack and destroy CAR-T cells. This unintended self-attack reduces the therapy's ability to eliminate T cells effectively. Overcoming fratricide is crucial for enhancing the efficacy of CAR-T cell therapy in treating T cell malignancies, necessitating innovative strategies to minimise off-target effects and optimise the specificity of CAR-T cell targeting. Additionally, CAR-T cell therapy can lead to T cell aplasia and immunodeficiency, which depletes healthy T cells and raises the risk of opportunistic infection (96). Therefore, the selection of a highly specific target for CAR-T cell therapy is fundamental to avoid T cell depletion. The ideal target should be predominantly expressed on tumour cells and minimally expressed on normal T cells, ensuring precise tumour identification by CAR-T cells. This choice plays a pivotal role in the therapy's success and safety.

Several strategies are being investigated to inhibit antigen-driven fratricide based on antigen and cell type. The first strategy has been to transduce CAR into alternative cell types. One potential cell type identified is natural killer (NK) cells, as these cells lack T cell antigens such as CD3 and CD5 (97, 98), and have demonstrated fast and pronounced cytotoxicity against tumour cells. The second strategy has been

identifying antigens on tumour T cells that are not highly expressed in normal and CAR-T cells. With this approach, fratricide can be limited to a subset of antigen-positive cells while promoting the expansion of the remaining cells with CAR-killing function (99). Antigens such as CD4, CD30, CD33, CD37, CD99, CD1a, CDR3, CCR7, CCR9 and TRBC1 or TRBC2 have limited expression in normal and CAR-T cells and are being investigated (99, 100). Integrating genome editing methods, for instance clustered regularly interspaced short palindromic repeats (CRISPR/Cas9) for eroding target antigen within the therapeutic cells, can lead to fratricide prevention in CAR-T cell treatments (71, 101). In addition to this, protein expression blockers (PEBLS) are considered a strategic tool for mitigating fratricide and facilitating the generation of CAR-T cells (102-104).

A recent study by Ye, Jia (105) showed that fratricide could be prevented in anti-CD7 CAR-T cells by blocking the CD7 antigen present on these cells with recombinant anti-CD7 blocking antibodies (105). Naturally occurring $CD7^-$ T cells have also been explored as means of avoiding cell fratricide. This led to the generation of $CD7^-$ CAR-T cells (NS7CAR), which showed potential anti-tumour effectiveness (106). One of the hurdles in the application of CAR-T cell therapy for T cell malignancies is the on-target, off-tumour effects that can lead to T cell aplasia. Unless followed by hematopoietic stem cell transplantation to restore the T cell compartment, this limits the effectiveness of CAR-T cell therapy (107). Targeting specific antigens on the surface of tumour cells that are not expressed or have limited expression on normal T cells would prevent T cell aplasia. Another strategy to mitigate this issue involves incorporating a "suicide" switch to ensure the controlled elimination of CAR-T cells post-treatment, which can be beneficial for haematopoietic stem cell transplantation (HSCT) or if unforeseen issues arise. This approach improves the safety profile of CAR-T cell therapy by providing a mechanism to manage and mitigate potential complications like aplasia (108). Various suicide switches, including Herpes simplex virus thymidine kinase (HSV-TK), inducible caspase 9 (iCasp9), and CD20, have been evaluated in clinical trials, although they do come with certain disadvantages, such

as premature eradication of the CAR-T cells limiting their effectiveness and on-target toxicity from the antibody (109).

Despite autologous CAR-T cell treatments that have shown encouraging results, obtaining material from paediatric and adult patients poses logistical difficulties due to batch variability and the need for specialised production equipment. These obstacles severely restrict the accessibility of CAR-T cell treatments. Another critical concern associated with infusing genetically engineered autologous cells is the potential incorporation of malignant blasts into the transduced T cell population, leading to treatment resistance (110). Genome editing techniques have eliminated alloreactive surface antigens, which has paved the way for developing "off-the-shelf" or "universal" CAR-T cells. These engineered cells can overcome HLA barriers, offering a solution to the limitations associated with personalised autologous therapies. A seminal study by Qasim *et al*. in 2017 demonstrated the clinical outcomes of universal CAR-T cell (UCART19) therapy, highlighting its potential in addressing this challenge (111). By implementing these strategies to reduce risks and continuously identifying novel antigens for targeting, CAR-T cell therapy holds great promise in the treatment of T cell malignancies.

1.4.1 Current investigations and ongoing clinical trials into CAR-T cell therapies against T cell malignancies

It is important to highlight that no CARs have been approved for T cell malignancies yet, and CAR technology for these cancers is still largely experimental compared to B cell malignancies. Presently, a wide range of CAR-T cells therapies for the management of T cell malignancies are under investigation. Important targets for T cell malignancies as well as ongoing clinical trials are presented in Table 1-1. Additionally, Table 2-2 presents the results from clinical trials and the treatment outcomes of CAR7-T therapy in the context of T cell haematological malignancies.

Table 1-1 Overview of different chimeric antigen receptors for targeting T cell malignancies under investigation

Target antigen	Therapy	Clinical trials	Autologous (Auto) and/or Allogeneic (Allo)
CD3	CAR-T cell (72, 101), CAR-NK (97)	-	
CD4	CAR-T (112, 113)	NCT03829540	Auto
		NCT04162340	Auto
		NCT04712864	Auto
CD5	CAR-T (98, 114-118), CAR-NK (119)	NCT03081910	Auto
		NCT04594135	Auto
		NCT05032599	Auto and Allo
		NCT05487495	Auto
		NCT05596266	Auto
CD7	CAR-T (71, 72, 102, 120-123), CAR-NK (124)	NCT03690011	Auto
		NCT04033302	Auto
		NCT04264078	Allo
		NCT04599556	Auto
		NCT04689659	Auto and Allo
		NCT04762485	Auto
		NCT04823091	Auto
		NCT04840875	Auto
		NCT04928105	Auto
		NCT04934774	Auto
		NCT04938115	Auto
		NCT04984356	Allo
		NCT05059912	Auto
		NCT05212584	Auto
		NCT05290155	Auto
		NCT05377827	Allo
		NCT05554575	Auto
		NCT05620680	Auto
		NCT04572308	Auto
		NCT04916860	Auto
		NCT04004637	Auto
		NCT05397184	Auto
		NCT05043571	Auto
		NCT05127135	Allo
		NCT04538599	Allo
		NCT04620655	Allo
		NCT04785833	Auto
		NCT04480788	Auto
CD30	CAR-T cell (125, 126)	NCT01192464	Auto
		NCT01316146	Auto
		NCT02259556	Auto
		NCT02663297	Auto
		NCT02690545	Auto
		NCT02917083	Auto
		NCT03383965	Auto
		NCT03602157	Auto

		NCT04083495 NCT04134325 NCT04268706 NCT04288726 NCT04526834 NCT04653649 NCT05208853 NCT05634785	Auto Auto Auto Allo Auto Auto Auto Auto
CD37	CAR-T cell (127)	NCT04136275	Auto
CD99	CAR-T cell (128)	-	
CD1a	CAR-T cell (129, 130)	NCT05679895	Auto
CDR3	CAR-T cell (131)	-	
CCR4	CAR-T cell (132)	NCT03602157	Auto
CCR9	CAR-T cell (133)	-	
TRBC1	CAR-T cell (134)	NCT03590574 NCT04828174	Auto Auto

Table 1-2 Representative clinical trials and outcomes of CAR7 for treating T cell hematologic malignancies

Study	Investigational product	Delivery vehicle	Modifications	Outcome	REF
Chongqing China	Healthy donor	Lentiviral vector	CRISPR/Cas9	4/5 remission	(76)
Beijing Boren Hospital, Beijing, China	Healthy donor or autologous	Lentiviral vector	PEBL anti-CD7	18/20 remission	(135, 136)
The First Affiliated Hospital, College of Medicine, Zhejiang University, China	Healthy donor	Lentiviral vector	CRISPR/Cas9	7/11 remission	(137)
Hebei Yanda Ludaopei Hospital, China	Healthy donor	N/A	CRISPR/Cas9	8/10 remission	(138)
Great Ormond Street Hospital for Children NHS Foundation Trust, London, UK	Healthy donor	Lentiviral vector	BE-CAR7	3/3 remission	(74)
ChiCTR1900025311	Healthy donor	Lentiviral vector	CRISPR/Cas9	11/12 remission	(75)

Multi-centre, clinical trial, China					
Hebei Yanda Ludaopei Hospital China	Autologous	Lentiviral vector	NS7CAR	19/20 remission	(139)
First Affiliated Hospital of Zhengzhou University China	Autologous	Lentiviral vector	PEBL anti-CD7	7/8 remission	(77)

1.4.2 CAR-T cells against different targets of T cell leukaemia

The CD3 complex is a hallmark of the T cell lineage and is commonly used as a T cell marker. In healthy cells, CD3 expression is confined to the hematopoietic system. It is typically associated with the TCR or the pre-TCR, found specifically on the surface of T cells and thymocytes. It is present at variable intensity levels on the cell surface of mature T cell lymphomas and mature T-ALLs (140, 141). TCR-associated CD3 molecules have been a prime target in therapeutic strategies for inducing tolerance in autoimmune diseases and preventing organ rejection. OKT3, a mouse anti-CD3ε monoclonal antibody (Muromonab), was the initial antibody used in humans to prevent the rejection of solid organ transplants, while anti-CD3 antibody therapy primarily aims to stimulate Treg cell production (142). Initially, CD3 was investigated as a therapeutic target in patients with T cell lymphoma through studies employing immunotoxin-loaded anti-CD3ε monoclonal antibodies (143). These antibodies resulted in partial remissions in certain patients, prompting the advancement of anti-CD3 CAR-engineered cells. Early endeavours in this area primarily focused on employing NK cells as the CAR-expressing cells, given their absence of surface CD3 (97) Moreover, our research team has effectively developed a CAR-T cell that targets the CD3 complex (anti-CD3ε CAR). This CAR3 construct is expressed using a third-generation self-inactivating (SIN) lentiviral vector, achieved through Transcription-Activator-Like Effector Nucleases (TALEN) mediated disruption of the TCRαβ-CD3 complex (101). These CAR3-T cells exhibited strong antileukemic effects in a human/murine chimeric model, suggesting that CAR3 cells could be used to achieve malignant T cell eradication (101). CAR3-T cells were also assessed against primary paediatric T-ALL samples from a tissue bank. Flow cytometry-based detection of

surface CD3 expression across six patients' T-ALL revealed heterogeneity in the levels of CD3 expression, which could lead to antigen escape. CD7 was instead found to be more homogenously expressed on T-ALL samples and was investigated further in this project.

CD7, a cell surface glycoprotein belonging to the immunoglobulin superfamily (144), is typically found on the surface of the majority of thymocytes, peripheral T cells, and NK cells (145, 146). It is highly expressed in lymphoblastic T cell leukaemia and lymphomas (>95%), as well as in a subset of PTCL (147-150) However, it is absent from at least a small portion of normal T cells (151) .Clinical evidence indicates that CD7 is consistently expressed at elevated levels on malignant T cells compared to healthy cells, suggesting its potential as a target for CAR-T cell therapy. Additionally, this expression remains stable across various disease stages, including newly diagnosed, relapsed, and minimal residual disease after chemotherapy (102). Previously, CD7 was assessed as a targeted protein for the immunotherapy given to patients who suffer from T cell cancer through the utilisation of an anti-CD7 monoclonal antibody, however, this possessed low cytotoxic response against tumours (43). The potency of anti-CD7 CAR-T cells in preclinical models of T cell cancer has previously been demonstrated (71, 102, 120). Expression of a CD7-specific CAR on T cells however results in fratricide during manufacture, preventing the expansion of *ex vivo* modified T cells. To enhance cell expansion, a commonly used approach involves genome editing techniques to disrupt the target (71, 72, 120). Additionally, alternative methods including restricting CD7 protein trafficking to the cell surface (102, 104), selecting T cells from naturally CD7-negative subtypes (106), or using anti-CD7 blocking antibodies (105), might also help reduce TvT fratricide.

The disruption of CD7 expression in these studies did not impact the proliferation or short-term effector function of T cells and maintained their effectiveness against tumours. CAR7-T cells exhibited *in vitro* and *in vivo* efficacy against primary CD7+ ALL and lymphoma. "Off-the-shelf" CD7-specific CAR-T cells were developed by deleting CD7 and TCR alpha chain (TRAC) and demonstrated efficient killing of human T-ALL cell lines and primary T-ALL cells *in vitro* and *in vivo* without inducing fratricide or

graft-versus-host disease (152). Our lab recently generated fratricide-resistant T cells via the orderly removal of shared antigens (CD7 and TCR/CD3) by a third generation human codon optimised cytidine deaminase (coBE3) prior to lentiviral-mediated expression of CARs specific for CD7 or CD3 (72). Several phase 1 clinical trials are ongoing to evaluate CD7-edited CAR-T cells (Table 1-1) or CD7-specific CAR-NK cells in patients with T cell malignancies.

CD5 is a pan-T cell marker that is also found on the surface of malignant T cells and expressed in approximately 80% of T-ALL and T cell lymphoma (115). CD5 is a negative regulator of TCR signalling and contributes to the survival of normal and malignant lymphocytes (153). Toxin-conjugated anti-CD5 antibodies have been shown to deplete malignant T cells in patients diagnosed with cutaneous T cell lymphoma and T-ALL with low toxicity and no irreversible off-target effects (40, 154). Based on these studies, second-generation T and NK cells expressing CD5-specific CARs with CD28, 4-1BB, or 2B4 intracellular signalling domains have been developed and demonstrated cytotoxicity against malignant T cell lines *in vitro* and control of disease progression in mouse models *in vivo* (98, 115, 155). Such cells are currently under investigation in patients with T-ALL and T cell lymphoma (NCT03081910) (Table 1-1). Recently CD5/CD7 bispecific CAR-T cells have been produced that are knocked for CD5 and CD7, thereby preventing fratricide. The authors reported that tandem CARs were observed to be more effective than dual CAR in preventing tumour escape in heterogeneous leukemic cells (117).

Several groups have developed CARs targeting antigens with restricted expression, such as CD30, TRBC1, CCR4, and CD1a, to limit fratricide to only a subset of antigen-positive T cells. CD30 is induced upon T cell activation and is present in T-ALL. Second-generation CD30-specific CAR-T cells exhibited cytotoxicity in preclinical and early phase clinical studies of relapsed/refractory Hodgkin lymphoma and anaplastic large cell lymphoma, even in patients who did not respond to the anti-CD30 monoclonal antibody, brentuximab (126, 156).

Although the TCR is a pan-T cell marker, T cells only express one of two genes encoding a TCR beta chain constant region, TRBC1 or TRBC2 (157, 158). Many lymphomas are TCR-positive, and about half express TRBC1. Therefore, Maciocia, Wawrzyniecka (134) developed TRBC1-specific CAR-T cells that specifically target TRBC1-positive normal and malignant T cells *in vitro* and *in vivo* while sparing normal T cells expressing TRBC2 (134). However, TRBC1-specific CAR-T cells may cross-link the TCR, decreasing the persistence of the CAR-T cells and limiting anti-tumour activity (99). A phase I/II study is ongoing to evaluate the use of TRBC1-specific CAR-T cells in patients with T cell lymphoma (NCT03590574) (Table 1-1).

CCR4 is a chemokine receptor that is expressed on regulatory T cells, Th2 cells, and Th17 cells of healthy individuals but also in malignant cells of patients with T cell leukaemia and lymphoma, and it can be an independent prognostic factor of poor survival (159). Mogamulizumab, an FDA-approved antibody that targets CCR4, has modest activity against adult T cell leukaemia/lymphoma and selectively depletes regulatory T cells, enhancing anti-tumour responses (160-162). Moreover, a strategy involving CCR4 CAR-T cells demonstrated robust cytotoxicity when targeted against patient-derived cell lines of T cell lymphoma. This suggests the potential feasibility of applying this approach to patients with T-ALL who express CCR4 (132).

CD1a is a cortical T cell surface antigen present in cortical T-ALL, a subgroup of T-ALL (163). Generation of second-generation CD1a-specific CAR-T cells exhibited robust cytotoxicity against cortical T-ALL cell lines and primary cells *in vitro* and *in vivo* (129). Importantly, as CD1a expression is transient and limited to developing thymus-restricted thymocytes, CD1a-specific CAR-T cells are unaffected by fratricidal effects (129).

The complementarity-determining region 3 (CDR3) on T cell receptors has recently been proposed as a good target for CAR-T therapies, offering greater precision and less off-tumour toxicity than current approaches (131).

The chemokine receptor, CCR9, can be found in more than 70 % of T-ALL cases and in greater than 85% of relapsed/refractory disease. In normal T cells, CCR9 is only present on less than 5% of cells making this receptor a suitable target for CAR-T therapy. Recent work by Maciocia, Wawrzyniecka (133) has demonstrated that anti-CCR9 CAR-T cells are resistant to fratricide and exhibit strong antileukemic activity (133).

This project utilised genome editing tools to produce fratricide resistance UCAR-T cells. These CAR-T cells are designed to target either the CD3 or CD7 T cell markers, enhancing their therapeutic potential.

1.5 CAR delivery

Over the past few decades, the delivery of CAR transgenes into T cells and other immune cells has been significantly optimised and refined. Various viral vector systems have been employed for transgene delivery, each with its unique advantages and challenges (164, 165). These delivery systems have played a crucial role in the development of CAR-T cell therapies, which have shown remarkable promise in treating various cancers.

Genetically engineered viral vectors, including lentiviral and retroviral vectors, stand out as the most commonly used vectors for generating CAR-T cells (165, 166). γ-retroviruses, for instance, exhibit high transduction efficiency but are limited to dividing cells and carry a risk of insertional mutagenesis (166, 167). In contrast, lentiviral vectors offer several advantages, such as the ability to transduce both dividing and non-dividing cells. They also have an improved safety profile due to semi-random integration, which favours gene bodies over promoter/enhancer elements, a preference of γ-retroviruses (165).

Non-viral DNA transposon systems have also been used as a more cost-effective approach to stably express CARs. DNA transposons are distinct DNA segments capable of repositioning themselves within the genome through a process known as

transposition, functioning like a 'cut and paste' mechanism (168). In their natural state, these elements consist of individual units containing the transposase gene, which is flanked by terminal inverted repeats (TIRs) housing transposase binding sites. DNA sequence of interest can be inserted between the transposon TIRs and mobilised by supplying transposase through an expression plasmid or *in vitro*-synthesised messenger RNA (mRNA) (169). During transposition, the transposase enzyme facilitates the removal of the element from its donor plasmid, followed by its reintegration into a specific chromosomal location (170). This unique characteristic makes transposons natural and manageable DNA carriers, serving as valuable tools in the field of gene therapy. A DNA transposons such as Sleeping Beauty (SB) (171) and *piggyBac* (PB) (172) have been used as genetic tools for cell and gene engineering. Transposons present advantages compared to retroviral delivery methods, as they eliminate the necessity for vector particle generation. This potential advantage could streamline and lower the cost of the gene delivery process. However, concerns about safety and long-term effects arose when two lymphoma cases were identified in a CAR-T cell trial that used *piggyBac* delivery (173, 174).

Alternatively, mRNA electroporation can transiently express CARs for a short duration, typically up to one week (175). This method helps circumvent potential on-target off-tumour effects resulting from target antigen expression by normal tissues. However, patients may require multiple infusions, as the transgene is rapidly lost. To address these drawbacks, ionizable mRNA-lipid nanoparticles have been designed for ex vivo CAR mRNA delivery to human T cells, showing substantially reduced cytotoxicity and potent cancer-killing activity (176).

Overall, the field of CAR-T cell therapy has witnessed significant advancements in the optimisation and safety of gene delivery systems over the years. Currently, retroviral vectors are considered the "gold standard" for delivering CAR transgenes into immune cells due to their efficiency and established safety profiles (164, 165, 177).

1.5.1 Lentiviral vectors

On the contrary to γ-retroviruses, which are unable to infect non-dividing cells, lentiviruses have a unique capability. They can enter into the genome and infect both dividing and non-dividing cells due to the presence of pre-integration complex, often called the virus's "shell". This complex makes the virus able to penetrate the intact nucleus membrane of the target cells, permitting it to efficiently deliver genetic material (178). It is crucial to understand that the genetically engineered versions of lentiviral vectors for gene therapy are found to be non-pathogenic and incapable of self-replication, ensuring their safety. These vectors have the ability to accommodate genetic material of up to 8.5 kilobases. Lentiviruses, derived from the human immunodeficiency virus (HIV-1), possess a provirus size of approximately 9 to 10 kilobases. Two linear, positive sense, single stranded RNA (+ssRNA) molecules are present in this provirus, encoding additional genes for regulatory and accessory proteins (179, 180).

Among these genes, *gag*, *pol*, and *env* are essential to all members of the *Retroviridae* family, including lentiviruses. The *gag* gene generates a polypeptide that is processed by the viral protease into three important structural proteins, involving capsid, nucleocapsid (NC), and matrix (MA) proteins. The *pol* gene, located downstream of *gag*, is expressed as a polypeptide processed by the viral protease during virus maturation into protease, integrase (IN), and reverse transcriptase (RT). The *env* gene encodes a polypeptide processed by cellular proteases into the surface (gp120) and transmembrane (gp41) subunits that assemble to form the Env protein of the surface of the mature virion. The Env glycoprotein is responsible for interacting with host cell receptors to facilitate viral-cell entry (181).

The lifecycle of wild-type HIV-1 begins with the attachment of the Env glycoprotein expressed on the surface of the virion to the receptor expressed on the surface of the host cell. As a result of this interaction, a transformational change occurs in the protein which results in the fusion of the viral envelope with the cell membrane and eventual release of the viral core into the cell (182). The cell is then infected by the

viral contents, forming the reverse transcription complex (RTC) which is responsible for synthesizing viral double stranded DNA from the single stranded RNA template. The transfer RNA (tRNA) binds to the primer binding site (PBS) at the 5'-end of the viral RNA genome to initiate reverse transcription. Double-stranded DNA is synthesised using one of the positive-single strands of RNA as a template and forms a pre-integration complex (PIC). The PIC is actively transported to the nuclear pore utilising ATP and then penetrates into the host genome with the help of viral integrase (IN) (183). The integrated viral DNA, also known as the proviral DNA, contains long-terminal repeats (LTRs) flanking the viral genome at the 5' and 3' ends. Each LTR contains three regions: 3' unique elements (U3), repeat elements (R), and 5' unique elements (U5), adjacent to cis-acting elements that produce the signals for genomic integration. The multi-step replication cycle results in a complete DNA copy of the viral DNA. The proviral DNA is then transcribed to form viral mRNA, which codes for viral proteins. The assembly of the viral proteins and viral RNA occurs at the plasma membrane to form viral particles, which are released from host cells by budding and subsequently mature into infectious particles (184).

To use lentiviruses as gene delivery vehicles, we can replace their genetic material with a transgene of interest. The necessary viral genes required for packaging and virion formation can then be supplied in *trans* on separate plasmids, meaning that the encoded transgene can be packaged into the viral vector without the need for the genes necessary for viral replication to be packaged alongside it. Further improvements to safety – such as the development of self-inactivating lentiviral systems and the removal of the dependence of viral packaging on the viral trans-activator gene *tat* – have led to the evolution several generations of lentiviral packaging systems (185) (**Figure 1-5**).

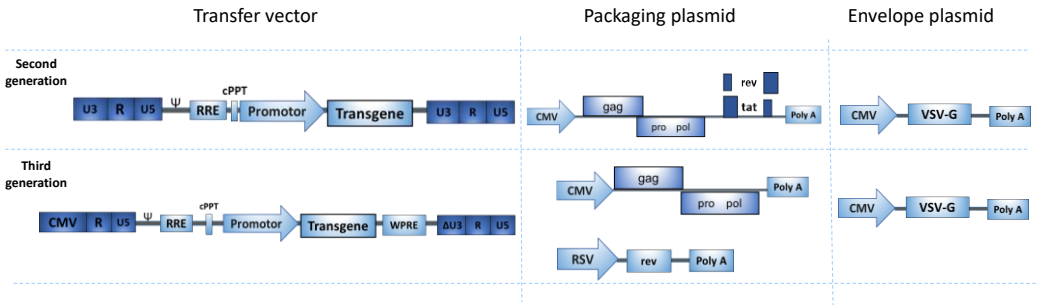

Figure 1-5 Evolution of lentiviral vectors

Second generation lentiviral vectors consist of three major components, involving the transfer plasmid containing the gene of interest flanked by long terminal repeats (LTRs), the packaging plasmids encoding gag, pol, rev, and Tat genes, and the envelope protein, particularly VSV-G or any other variant. On the contrary, third generation lentiviral protein possess additional features of safety. These vectors are divided into a two-plasmid system, with one containing packaging plasmids for gag and pol genes and a separate plasmid for the rev gene, reducing the risk of replication-competent lentiviruses (RCLs). Moreover, the third-generation system excludes the tat gene and swaps it with U3 region within the 5' LTR with Tat-independent CMV promoter, improving safety and control. CMV=cytomegalovirus, cPPT=central polypurine tract, LTR=long terminal repeat; RCLs=replication-competent lentiviruses; U3=3' unique element, RRE: rev responsive element, WPRE=Woodchuck hepatitis virus post transcriptional regulatory element.

To broaden the cellular tropism of lentiviral vectors, the envelope protein can be swapped with alternative versions from other viruses. This process is known as pseudotyping and can enhance the vectors' ability to target specific cell types or tissues (186). Most lentiviruses are pseudotyped with vesicular stomatitis virus G protein (VSV-G): a single-stranded, negative-sense RNA virus belonging to the *Rhabdoviridae* family. Due to its broad tropism, VSV-G pseudotyped viruses can transduce a wide range of cell types and maintain the stability of viral particles (187).

One of the crucial aspects of lentiviral vector development has been the elimination of the formation of replication competent lentiviruses (RCLs). This is usually accomplished through the separation of cis-regulatory elements required for packaging, reverse transcription, and integration from the sequences encoding the trans-acting viral proteins carrying out these processes. Third generation lentiviral

vectors are found to be safest due to the presence of three of the nine HIV-1 genes (*gag*, *pol*, and *rev*) as well as being divided into four separate plasmids, thereby decreasing the RCL formation risk. In these vectors, the *rev* gene is separated from the packaging plasmid and offered as a distinct plasmid construct (188). Moreover, the transfer plasmid is modified through deletion of the TATA box, SP1, and NF-KB transcription factor binding sites in the U3 region of the 3' LTR to produce self-inactivating (SIN) vectors: that is, vectors that have lost the ability to produce full-length vector RNA in transduced cells. During reverse transcription, the modified U3 region of 3' LTR is transferred to the U3 region of the 5' LTR in the proviral DNA, resulting in transcriptional inactivation (189). The removal of viral *tat* gene also occurs which is followed by replacing the native U3 promotor region with the active promotors, for instance the cytomegalovirus (CMV) promotor, excluding the requirement for a *tat*-dependent transcription mechanism (**Figure 1-5**) (190).

While these modifications improve vector safety, they can potentially decrease viral titres, leading to challenges for therapeutic purposes. To restore high-level transgene expression, post-transcriptional cis-regulatory elements such as woodchuck hepatitis virus (WPRE) have been integrated into the transfer vector (191). Furthermore, as the viral LTR is inactivated in SIN vectors, thus eliminating natural transcriptional activity, it is necessary to include an internal promoter that can drive transgene expression. Promoters that are commonly used in clinical trials and which have been approved originated from either viruses or humans. Examples include the Cytomegalovirus (CMV) and Spleen focus-forming virus (SFFV) of viral origin, as well as phosphoglycerate kinase (PGK) and EF1α from humans. These promoters enable stable transgene expression in both progenitor and differentiated cells. Notably, these promoters exhibit varying degrees of strength in transgene expression, with cellular human elongation factor 1 alpha (EF-1α) promotor driving the strongest transgene expression and CMV promotor from viruses showing the lowest. Interestingly, when evaluated in differentiated cell populations, the reverse trend was observed, suggesting that the choice of promoter can be optimised based on the specific target cell type (192). The PGK promoter, while not always the strongest for

transgene expression, is the most used due its long-term expression. Additionally, it has been documented to maintain its activity in a variety of cell types and lineages (193).

1.6 Genetic engineering tools

Genome editing tools present the opportunity to avoid fratricide through the removal of shared antigens. However, the use of genetic manipulation in therapeutic approaches requires highly efficient and accurate systems (194). There are nominally four types of genome-editing nuclease: programmable zinc finger nucleases (ZFNs) (195), meganucleases (MNs) (196), TALENs (197), and clustered regularly interspaced short palindromic repeats (CRISPR)/ CRISPR-associated (Cas) protein 9 (CRISPR/Cas9) (198, 199). These tools provide precise and efficient site-specific editing capabilities using nucleases that induce DNA double-stranded breaks (DSBs), which stimulates DNA repair mechanisms, including the non-homologous end joining (NHEJ) repair pathway or homology-directed repair (HDR).

Meganucleases are naturally occurring enzymes with high specificity due to their long recognition sequences, which are often not duplicated within the genome. However, their primary limitation is their restricted adaptability to novel target sequences (196). Customising Mns for specific gene editing tasks can be costly and time-consuming, making them less flexible than other methods. Zinc Finger Nucleases (ZFNs) represent an earlier generation of engineered nucleases. A ZFN is formed by combining a zinc finger domain with the commonly used FokI3 restriction endonuclease. Zinc finger domains have a unique ability to recognize three-base-pair sequences on DNA. By assembling a series of connected zinc finger domains, it becomes possible to identify longer DNA regions, achieving the desired precision in on-target specificity. The FokI endonuclease operates as a dimer, initiating double-strand DNA cleavage only at locations where two ZFNs attach to opposite DNA strands. This necessitates engineering two ZFNs to recognize closely adjacent nucleotide sequences within the target site, requiring their simultaneous recognition and binding for effective gene editing (200). Nevertheless, constructing ZFNs involves

protein engineering for each distinct target, which can be a costly and complex endeavour. TALENs, similar to ZFNs, can be customised for specific gene editing tasks. They offer an advantage in ease of design compared to ZFNs, which simplifies their application. In the context of TALENs, each individual TALE motif has the capability to recognise a single nucleotide, and by assembling an array of these TALEs, it becomes possible to associate with longer DNA sequences. Notably, the activity of each TALE domain is specific to one particular nucleotide and does not interfere with the binding specificity of adjacent TALEs. This unique feature simplifies the engineering process of TALENs in comparison to ZFNs. As ZFNs, TALE motifs are fused with the FokI endonuclease, necessitating dimerization for DNA cleavage. Consequently, for effective gene editing, it is essential that two distinct TALENs bind to opposite strands in close proximity to the target DNA (200).

Unlike ZFNs and TALENs which rely on protein-DNA interactions for site-specific binding, the CRISPR/Cas9 system operates via RNA guidance. Its ease of use, adaptability, and multiplex gene editing capabilities have propelled CRISPR/Cas9 to the forefront of genome editing (201-203), making it the genome editing tool of choice for this project. In addition, this delivery system requires only a single protein instead of two for both ZFNs and TALENs. The origin of CRISPR arrays was first observed in *Escherichia coli* (*E. coli*), characterised by five highly homologous repeated sequences of 29 nucleotides separated with 32 nucleotides (204). These repeat sequences are highly conserved within phylogenetic groups, suggesting a common ancestor and an important role for these sequences. Labelled CRISPR-associated genes (cas1 to cas4), were found adjacent to the CRISPR loci, suggesting a functional association (205). Comparative analysis of Cas protein functional domains revealed their DNA binding potential and possible roles in DNA metabolism, repair, or gene expression (205, 206).

The discovery that the spacer regions of CRISPRs were homologous to sequences of bacteriophages, plasmids, and viruses led to the hypothesis that CRISPR/Cas9 may function as a prokaryotic immune system (207-209). Interestingly, CRISPR/Cas resembled the adaptive immune system, as phage and plasmid infection did not

occur in strains containing homologous spacer sequences (208, 209). The role of CRISPR/Cas9 as a prokaryotic acquired immune system was confirmed experimentally by alternating the spacer sequences, which modified the phage-resistance phenotype of bacteria (210). Furthermore, viruses could evade a CRISPR-mediated response via extensive recombination of the viral genome, resulting in corresponding changes to the spacer sequences at CRISPR loci (211).

The CRISPR/Cas9 immune system operates in three phases, namely adaptation, expression, and interference. In the adaptation stage, new spacer sequences are acquired into the CRISPR locus by processing of foreign genetic material which has entered the cell. The new spacer is then integrated into the CRISPR locus (212). In the expression stage, the CRISPR locus is transcribed as a single long RNA (pre-crRNA), which is then processed into short guide CRISPR RNAs (crRNAs) of single repeat-spacer units by transactivating RNA (tracrRNA) and endogenous RNase III (213). These crRNAs interact with noncoding tracrRNA at a repeat region, enabling them to form ribonucleoprotein (RNP) complexes with Cas proteins. Finally, in the interference stage, the crRNA-Cas protein complexes direct nuclease activity towards the specific protospacer sequences on foreign DNA, resulting in cleavage of the target DNA (198, 214, 215). Cas proteins recognise short motifs adjacent to the precursor spacer, which are termed protospacer adjacent motifs (PAMs), on foreign DNA (216-218). Both the PAM and “seed” sequences, which are within the guide crRNA and complementary to the target sequence, are required for cleavage (219, 220). Importantly, PAM sequences are not present in the CRISPR loci, so self-cleavage will not occur.

CRISPR/Cas systems are classified as type I, type II, and type III, based on the encoded Cas proteins (221). The type II CRISPR system from *Streptococcus pyogenes*, which uses Cas9, was the first to be adapted as a gene editing tool in in human and mouse cells (199, 203), and remains the most widely used today. Although naturally occurring type II CRISPR is dependent on four components, namely mature crRNA, tracrRNA, RNase III and Cas9 endonuclease (222, 223), the gene editing system has been simplified by fusing the crRNA and tracrRNA into a single short guide RNA

(sgRNA) transcript, eliminating the necessity for RNase III and two separate RNA molecules (198).

1.6.1 DNA repair pathways post-*Streptococcus pyogenes Cas9* (SpCas9) genome editing

The CRISPR/Cas9 genome editing technique effectively employs the DSB repair pathways to introduce genetic variations into specific genomic locations. After the Cas9 enzyme makes a DSB, the DNA repair machinery is activated and recruited to promote end ligations through several damage repair pathways, such as NHEJ, microhomology-mediated end-joining (MMEJ), and HDR (194).

NHEJ, an error-prone repair mechanism, directly joins the broken DNA ends without requiring a template, leading to the insertion or deletion of small DNA segments (indels) at the repair site. These alterations can potentially disrupt genes, causing the introduction of premature stop codons or the knockout of protein expression (224, 225). When a DSB occurs, the Ku70-Ku80 complex (Ku) swiftly protects the ends, binding to them and activating the DNA-dependent protein kinase catalytic subunit (DNA-PKcs), which is crucial for NHEJ repair (226). Additionally, Ku helps recruit XLF-XRCC4, which, in turn, interacts with and stabilises DNA ligase IV (LigIV), an essential enzyme responsible for sealing the DSB (227).

MMEJ is a DNA repair mechanism that aligns broken DNA ends using short homologous sequences, or microhomologies, revealed by the end-resection machinery. Similar to NHEJ, MMEJ joins DNA ends devoid of an external template but needs initial short-distance end resection to uncover microhomologies for repair (228). The HDR pathway is an error-free DNA repair mechanism and is the preferred choice for targeted gene insertions and definite mutations. It depends on a homologous DNA sequence as a template for precise repair. If a homologous single- or double-stranded DNA template is introduced with the nuclease, HDR can insert the transgene and correct or replace genes (203, 225).

In mammalian cells, the primary DSB repair mechanism is the NHEJ pathway, which functions throughout the cell cycle without needing a homologous template (229-231). In contrast, homologous recombination (HR) typically operates during the S and G2 phases of the cell cycle (232, 233), when a homologous DNA template is available.

To enhance the efficiency of HDR, various approaches have been proposed, including inhibiting cell cycle progression and NHEJ DNA repair (231, 234), activating factors that promote HDR (235), suppressing or blocking key components of NHEJ DNA repair (236-238), and exploring modifications of the engineered nucleases (239, 240).

1.6.2 CRISPR delivery strategies

For the genome to be edited, the CRISPR/Cas9 components have to be delivered to the cells. This can be accomplished by the means of messenger RNA (mRNA) Cas9/sgRNA, Cas9 protein complexed with sgRNA (RNP), DNA plasmids encoding CRISPR sgRNA cassettes, or by transducing viral vectors expressing Cas9 and sgRNA (241). Selecting the delivery strategy for CRISPR/Cas9 is usually tailored to enhance the results of genome editing investigation, considering factors such as the specific cell type being targeted, the research objectives, and considerations regarding safety and precision. Delivering entire CRISPR/Cas9 cassettes via plasmids or lentiviral vectors is not suitable for clinical applications due to observed issues in initial experiments, including high T cell toxicity, off-target effects, and immunogenic responses. Therefore, the delivery has been adapted to introduce individual components of CRISPR/Cas9 by co-electroporation of sgRNA along with Cas9, which is provided as protein or mRNA (242-245).

Delivery of a DNA sequence also needs to be considered when using the HDR pathway. DNA sequences can be introduced using integration-deficient lenti- or adeno-associated viral vectors, which can deliver entire genes with efficiencies from 40% to 60%, and 10 kb in cargo delivery potential (246, 247). AAV- mediated donor template delivery has shown knock-in efficiencies of up to 85% in various primary

human cells. AAV Serotype 6 (AAV6) has exhibited the highest donor delivery efficiency across diverse cell types due to its high cell tropism (248, 249).

Non-viral templates come in various forms, each offering distinct advantages for achieving precise genetic modifications. Plasmids, both circular and linear, are versatile carriers capable of accommodating substantial genetic changes (250). Linear double-stranded DNA (dsDNA) fragments with homology arms offer efficient means for controlled genome modifications (247, 251), while long single-stranded DNA (ssDNA) templates enable intricate changes through annealing (252, 253). Single and double-stranded oligonucleotides (ODNs) provide rapid options for introducing single-point mutations or smaller alterations (251, 254). Emerging alternatives like minicircles and nanoplasmids are gaining prominence, indicating their viability as non-viral templates for HDR in the field of genome engineering (250, 255).

1.6.3 Off-target effects in CRISPR/Cas9 genome editing

The effectiveness of CRISPR/Cas9 genome editing depends on the selection of the sgRNA sequence, aiming to maximise on-target precision while minimising off-target effects. The CRISPR/Cas9 system uses a 100-nucleotide (nt) sgRNA, with the first 20nt complementary to the target DNA sequence, followed by the PAM (217). Depending on the location, a 1-2nt mismatch at the target sequence can inhibit Cas9 activity. However, cleavage activity has been reported with up to a 5nt mismatch, which could be detrimental to cell survival and potentially oncogenic (256). Although the CRISPR/Cas9 system has been vastly improved by using paired D10A nickase Cas9 (257), truncated protospacers (258), or high fidelity Cas9 variants (259, 260), off-target effects, large deletions and chromosomal alterations have still been reported (261-265).

The off-target effects in CRISPR/Cas9 genome editing occur when unintended cleavage happens at sites where the DNA sequences do not perfectly match the guide RNA. (266). Mitigating these off-target effects involves the development of techniques that enhance binding stability at the desired target sites while

concurrently destabilising the binding stability at off-target sites (267). The first method focuses on increasing on-target stability by using a Cas9 nickase mutant or pairs of sgRNA complexed with dimeric Cas9 proteins (268). This method is found to be effective as it increases the number of matched based pairs in the target site, potentially decreasing off-target frequencies. The second method is the inverse, where off-target effects are made more unstable without altering on-target binding. This can be achieved through methods like using truncated gRNA sequences (<20 bp) (258), generating unique Cas9 mutants such as high fidelity variants (259), or engineering Cas9 with improved specificity (269).

Identifying genome-wide CRISPR/Cas off-target sites is pivotal for assessing the precision and safety of genome editing. *In silico*, computational prediction tools like Cas-OFFinder, CRISPOR, and Benchling offer a convenient starting point for identifying potential off-target sites by analysing guide RNA sequences. These tools compare the guide RNA sequence to the target genome, allowing users to specify the number of allowed mismatches and their positions (270, 271). There are, however, limitations to this. *In silico* tools typically predict binding ability using simple sequence alignments and do not take into account how chromatin context may affect editing (272).

For more comprehensive assessments, cell-based assays such as Guide-seq and IDLV-CIRCLE-Seq, *in vitro* techniques such as Digenome-Seq, and targeted sequencing approaches like amplicon sequencing can be employed, which enable the detection of off-target mutations with high sensitivity. Biochemical methods using biotinylated guide RNAs and Guide-tag capture Cas9-bound DNA fragments for sequencing, can further enhance accuracy. These methods have been recently reviewed by Tao, Bauer and Chiarle (273).

The choice of genome-wide off-target prediction methods depends on the specific research goals and available resources. A combination of computational predictions and experimental validation methods offers a robust approach for identifying

genome-wide CRISPR/Cas off-target sites while ensuring the safety and precision of genome editing applications.

1.7 Site-directed CAR insertion

Genetic engineering approaches for the precise integration of therapeutic genes into specific genomic locations offer a promising solution to the challenges associated with random gene insertion caused by retroviral transduction. Achieving site-specific gene integration involves employing gene-editing tools such as CRISPR/Cas9, TALEN, and ZFN, which induce DSBs in the target DNA site and facilitate HDR using a donor DNA template (274) (Table 1-3). Directing expression creates safer therapeutic T cells as it reduces the likelihood of mutagenesis or TCR-induced alloreactivity, when compared to the CAR-T cells generated by viral transduction (275). This results in a safer and more efficient product with reduced chances of random DNA integration and TCR-induced alloreactivity. Ultimately, this allows the use of healthy allogeneic donors towards the development of universal CAR-T cells.

AAV's distinctive biological and biophysical characteristics, along with its tropism and capacity to transduce various cell types, position it as the preferred vector for numerous gene therapy applications (276). By combining targeted nucleases with AAV-mediated delivery of the HDR template, it becomes possible to insert a CAR transgene into a specific location within the T cell genome while disrupting endogenous TCR genes (248).

A study by Eyquem and colleagues, demonstrated this approach by electroporating Cas9 mRNA and delivering the HDR template via AAV, resulting in directed insertion of a CAR transgene into the coding region of the *TRAC* locus within T cells. This approach offered dual benefits: the targeted knock-in resulted in the disruption of the *TRAC* gene. Second, it allowed for the endogenous control of CAR expression from the *TRAC* locus. This approach has been reported to yield more consistent transgene expression in human T cells, enhancing their potency. It also prevents constant CAR signalling and re-expresses following exposure to antigens, thus reducing T cell

differentiation and exhaustion (275). Subsequently, AAV mediated delivery of the homology-directed repair template were adopted by other groups for site-specific insertion of CAR-T cells (Table 1-3). However, this approach is time-consuming, labour-intensive, and expensive, which requires cloning template DNA into the suitable vector and producing a high-titre viral supernatant before genome editing can commence.

Fully virus-free gene editing techniques using DNA templates for TCR or CAR knock-ins are rapidly emerging (Table 1-4). The majority of research groups have adopted electroporation as a method to introduce the CRISPR/Cas9 RNPs, along with the DNA HDR template, into the cell (277). Roth, Puig-Saus (278) characterised the use of virus-free knock-in to replace the endogenous TCR with an ectopic TCR targeting the NY-ESO-1 cancer antigen. They employed co-electroporation of Cas9 RNPs and a dsDNA HDR template with designed homology into the first exon of the *TRAC* locus. As a result, the TCR-engineered T cells exhibited precise recognition of NY-ESO-1 and effectively eliminated tumour cells expressing the antigen in both *in vitro* and *in vivo* settings (278).

To simultaneously overcome the drawbacks of viral vectors and random DNA integration, the development of non-viral, genome-specific targeted CAR-T cells through gene editing has become a key focus within the field (Table 1-4) (279, 280). The CRISPR/Cas9 gene-editing system mediates the insertion of the CAR at specific target regions of the genome with relative ease and few off-target edits. A long-linear non-viral double-stranded DNA (dsDNA) is used as an HDR template, yielding relatively high T cell viability and transgene insertion efficiencies. This approach combines the main advantages of non-viral manufacturing processes and precise genome editing: 1) easy manufacturing process; 2) reduced production costs; 3) reduced time to generate targeted gene modifications; and 4) increased safety and efficacy. Moreover, it generates CAR-T cells that recognise tumour antigens and mount an immune response, thus presenting great potential to generate universal allogeneic CAR-T cells. Such technology has shown safety and efficacy in several clinical trials (NCT04035434, NCT04244656, NCT04502446, NCT04438083,

NCT04637763, NCT05617755) and considerable potential to be translated from bench to bedside.

Table 1-3 Preclinical studies using AAV vectors and genome editing tools for knocking-in CAR into T cells

Condition	Transgene (CAR or TCR; target)	Target locus (Primary knock-in site)	Ref.
BCL	CD19 CAR	*TRAC*	(275)
Lymphoma	CD19 CAR	*TRAC*	(281)
B-cell malignancies	CD22 CAR	*TRAC*	(282)
B-cell malignancies	CD19 CAR	*TRAC*	(283)
B-cell malignancies	CD22 and CD19 CAR	*TRAC/ PDCD1*	(284)
B-ALL	CD19 CAR	*TRAC*	(285)
BCL & AML	CD19-, CD70- or BCMA-specific HLA-independent TCR(HIT) and CAR	*TRAC*	(286)
T-ALL	CD7CAR	*TRAC/CD7*	(121)

Table 1-4 Preclinical studies using non-viral CRISPR/Cas9-mediated genome editing for knocking-in CAR into T cell-based therapies

Condition	Transgene (CAR or TCR; target)	Target locus (Primary knock-in site)	Donor template format	Ref.
Solid tumours	NY-ESO-1 transgenic TCR	*TRAC*	Linear dsDNA	(278)
Haematological malignancies	CAR BiTE	*TRAC*	Linear dsDNA	(287)
Haematological malignancies	CD19 CAR	*TRAC*	Self-linearizing plasmid	(255)
Leukaemia	CD19 CAR	*TRAC*	Linear dsDNA	(288)
Solid tumours	NY-ESO-1 transgenic TCR CD19 CAR CMV TCR	*TRAC*	Nanoplasmid	(250)
Multiple myeloma	BCMA CAR	*TRAC*	Linear ssDNA	(253)
B-NHL	CD19 CAR	*PD1/PDCD1*	Linear dsDNA	(289)
Solid tumours	neoTCR	*TRAC*	Plasmid DNA	(290)
Haematological malignancies	CD19 CAR	*TRAC*	Linear dsDNA	(291)
Solid tumours	GD2 CAR	*TRAC*	Linear dsDNA	(292)
Adoptive T cell immunotherapy	Library of CMV-specific TCRs	*TRAC*	Linear dsDNA	(293)
Optimize HDR efficiency	NY-ESO-1 transgenic TCR	*TRAC*	Linear dsDNA	(294)

1.8 Base editing technology for seamless base conversion

Base editing is an advanced genome editing technique that enables precise alterations of individual DNA bases without causing direct DSBs in the genomic DNA. This process can be accomplished without using a DNA donor template or by relying on the cell's inherent homology directed repair mechanisms (**Figure 1-6 A&B**). DNA base editors (BEs) refer to a protein complex of a catalytically impaired Cas nuclease with a base modification enzyme. Initially, DNA base editors consisted of a catalytically-dead Cas9 (dCas9) nuclease linked to a deaminase enzyme. The dCas9 carries inactivating mutations in its two catalytic domains, which makes it unable to cleave the DNA. However, dCas9 still able to form a complex with the guide RNA (198), and find the target DNA locus of interest (known as the protospacer) using canonical base pairing between the guide RNA and the genomic DNA. This leads to binding of the base editor complex to the target sequence, displacing a small segment of single-stranded DNA (ssDNA) by the guide RNA. The deaminase enzyme then modifies the exposed ssDNA, resulting in a specific and targeted base conversion event, which can be used to generate stop codons or disrupt splice sites as needed (295, 296). In recent years, a number of DNA and RNA editors have been developed, greatly broadening the possibility of base conversion options to enable targeted transition and transversion mutations (296). There are two main classes of DNA base editors: cytosine base editors (CBEs), which convert cytosine to thymine (C>T), and adenine base editors (ABEs), which convert adenine to guanine. Combining CBEs and ABEs can mediate all transition mutations, without creating a DSB (297, 298).

1.8.1 Base editor variants

CBE incorporates a cytidine deaminase that acts on the exocyclic amine of the target cytosine and converts it to uracil. After binding the target locus, base pairing between the sgRNA and target DNA strands leads to the displacement of single-stranded DNA in an "R-loop", freeing it for modification by the deaminase. The first-generation CBE version (BE1) tethered the cytidine deaminase enzyme Apolipoprotein B mRNA editing enzyme catalytic subunit 1 (APOBEC1) to the dCas9 enzyme (297). Following

on from this, BE2 was improved by adding the bacteriophage PBS uracil glycosylase inhibitor (UGI), achieving three-fold higher efficiency of base editing when compared to BE1 (297). The third-generation base editor (BE3) combined a D10A mutant of the Cas9 nickase, rat (rAPOBEC1) cytidine deaminase, and a UGI. In the fusion BE3, the sgRNA specifies the activity, rAPOBEC1 induces C>T changes on the non-target strand, at position 4-8 bp distal to the PAM, while the nCas9 cleaves the target strand 3-4nt proximal to the PAM. The UGI prevents the endogenous uracil-N-glycosylase (UNG) from removing the U nucleotides from the genomic sequence. D10A Cas9-induced nicking of the unedited DNA strand prevents its use as a repair template for the complementary strand, increasing editing efficiency by two to six times compared to when dead Cas9 was used (297). Although conversion efficiency is high, there can be bystander conversions at other cytosines within the editing window, non-C>T changes, or insertions and deletions (indels), which are the result of the error-prone resolution of basic sites within the edited DNA strand formed by base excision repair (BER) (299). These can be resolved by the addition of a second UGI and extended linkers between APOBEC1 and D10A Cas9 as well as the D10 Cas9 and UGIs, increasing editing efficiency and forming the next (fourth) generation of base editors (BE4) (299).

In addition to the PAM and activity window restrictions, the deaminase enzyme used will also impose sequence context preferences that impact the efficiency of editing at a specific genomic site. For instance, rAPOBEC1 does not effectively edit cytidines within certain 5’-GC-3’ motifs. However, other cytidine deaminases such as activation-induced deaminase (AID) and cytidine deaminase 1 (CDA1), display different sequence context preferences and could be used where BE3 is not suitable (299). Additionally, DNA methylation reduces the editing efficiency of rAPOBEC1-mediated base editing at CpG nucleotides, which can be improved by utilising human APOBEC3A (hA3A) to edit cytidines found in CpG dinucleotides and in GC motifs more efficiently (300).

The ABE, replaces rAPOBEC1 with a modified *E. coli* TadA enzyme, allowing it to generate A to G modifications in DNA without the need for the UGI subunit (301).

Cytosine base editors (CBEs) and adenine base editors (ABEs) offer a high potential to correct pathogenic single nucleotide polymorphism (SNP) variants (296). However, as with all gene editing approaches, there are various limitations that have arisen over the last years. The ability to target a base editor to a particular locus and achieve a specific base editing outcome is dependent on the binding of the Cas9n portion of the editor to the target sequence. The sgRNA design must place the target base within the activity window of the base editor, which is normally restricted to bases 4-8 of the protospacer due to the strict architecture of the R-loop. Since most editors use the SpCas9n, they can only recognise NGG PAMs, which limits their applicability. Different approaches to circumvent this include substituting Cas9 that recognise other PAM motifs (302-305), replacing with other Cas9 proteins from other organisms (306), or modifying the activity window via circular permutation, which broadens the editing window of CBE by giving better access to the R-loop (307).

Recent research has demonstrated the feasibility of disabling gene function in primary human T cells using base editors. For instance, Webber, Lonetree (308) showed that it was possible to generate allogenic CAR-T cells by using a splice-site disruption to alter gene-processing at an RNA level. They successfully disrupted single (*TRAC*, *PDCD1*, *B2M*) and multiple gene targets with reductions in both RNA transcripts and protein. Moreover, prior work exhibited the successful disruption of *TRBC* and *CD7* by introducing stop codons (72).

1.8.2 Unwanted on-target effects of base editors

Unwanted on-target effects, which can be a concern in base editing, involve unintended modifications arising at the target sequence. This category of unintended effect includes what is referred to as "bystander editing," where changes beyond the desired edit can occur at the intended target site, potentially leading to undesired outcomes or genomic alterations. Bystander editing occurs when the base editor detects and alters extra cytosines or adenines inside the target window, depending on the sequence context (309). The most commonly used CBEs and ABEs have a five- and four-nucleotide editing window, respectively (309). The main cause of bystander

editing is due to multiple deamination incidents per Cas9 binding event (299). The main approach to reduce bystander editing is by introducing mutations that reduce the activity of APOBEC1 or its substrate binding, alter the conformation of bound DNA, or decrease substrate accessibility. This has been shown to narrow the activity window of BE3 (302, 310). The precision of CBE-mediated editing has been called into question by reports that cytosine editing does not always result in C>T conversions (296, 311-314). These editing errors occur in an unpredictable and locus-dependent manner resulting from the effect of UNG. Fourth- generation CBE (BE4), was designed with a more flexible linker and a second UGI domain, which in turn reduced editing errors by half (299).

CBEs can produce indels because deaminated bases can be eliminated through the BER pathway. Some proteins involved in the BER pathway have a lyase activity and can convert a basic site to ssDNA nicks. In the presence of those nicks, together with UGI and Cas9n, these could become DSBs following uracil DNA glycosylase (UDG) and apurinic/apyrimidinic (AP) lyase activity. Although the frequency of indels is significantly lower than that of base editing (297), it is still a potential issue that needs to be addressed. For this, the Gam protein from bacteriophage Mu can be bound to the DSBs to prevent additional processing from happening. Thus, fusing Gam to the amino termini of BE3 and BE4 reduces indel formation (299).

1.8.3 Off-target effects of base editors

The off-target effects of base editing encompass various unintended genomic alterations or modifications that can occur at sites other than the intended target locus during the base editing process. Off-target base editing events in genome and transcriptome editing can be categorised into three groups: gRNA-dependent off-targets, gRNA-independent DNA off-targets, and gRNA-independent RNA off-targets (315-320).

Off-target base editing resulting from gRNA-dependent events happens when Cas9 binds to a genomic site that shares some similarity with the target sequence, even if

there are mismatches between the guide RNA's protospacer and the corresponding genomic spacer. By engineering "high-fidelity" Cas variants in the form of nickase into the base editing system, these variants have reduced tolerance for mismatches, effectively reducing the occurrence of such off-target events (321-323).

gRNA-independent off-target editing arises when the deaminase enzyme gains entery to ssRNA (in both CBEs and ABEs) or ssDNA (only in CBEs) regions in the cell. These regions include mRNA molecules and areas associated with transcription or replication. In these regions, it can catalyse cytosine or adenine deamination events. Notably, several publications have detailed efforts to engineer the deaminase domain in both CBEs and ABEs to reduce or eliminate instances of off-target RNA editing (324-327). To reduce the occurrence of off-target DNA editing, scientists induced mutations into the rAPOBEC1 protein to restrict its catalytic activity. Additionally, naturally occurring APOBEC homologs with decreased gRNA-independent off-target editing activities have emerged (320, 328).

Both CBE and ABE are now established for single base conversions. Despite concerns regarding the system’s limitations and the potential for unwanted on-target effects and/or off-target editing, rapid technological improvements are continuously being implemented to increase safety, efficiency, and specificity.

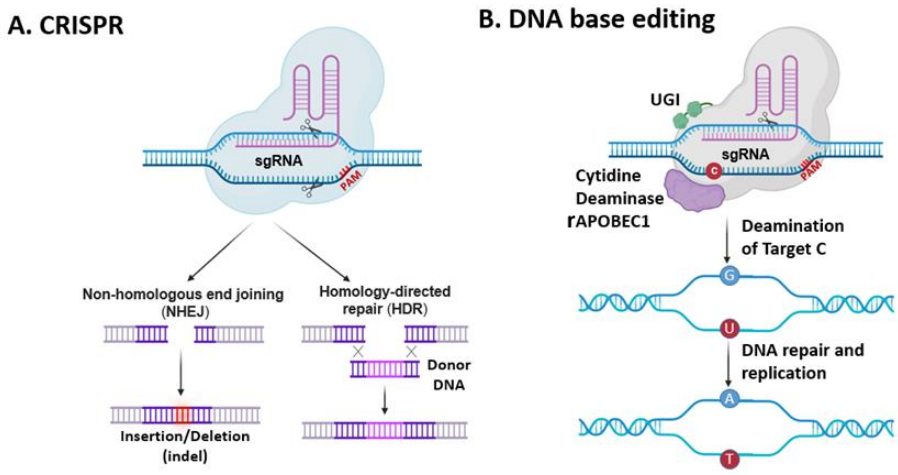

Figure 1-6 Comparison of the mechanism of action with CRISPR/Cas9 versus base editing

A. Schematic representation of CRISPR/Cas9 system in genome editing. The CRISPR/Cas9 systems enabled genomic alteration through the two main double-strand break (DSB) repair pathways, either through non-homologous end joining (NHEJ), which results in indel mutation and gene deletion, or by homology-directed repair (HDR), which results in gene insertion, correction, and replacement using a DNA donor template. **B.** Schematic representation of a third-generation cytidine deaminase base editor (BE3), comprising an N terminal rat APOBEC1 (rAPOBEC1, purple), D10A nickase SpCas9 (nCas9, grey), followed by an uracil glycosylases inhibitor (UGI, green). When nCas9 complexing with single guide RNA (sgRNA) and subsequent target site recognition occurs, the rAPOBEC1 deaminates cytidines (Cs) to uracils (Us) between protospacer positions 4-8 distal to the protospacer adjacent motif (PAM), on the single-stranded DNA (ssDNA). The UGI prevents the endogenous uracil DNA glycosylases (UDG) from recognising the U:G heteroduplexes, and removes these by base excision repair. Also, nCas9 cleaves the unedited sgRNA-bound DNA strand between positions 17 and 18 distal to the PAM, promoting correction from the uncut, edited strand. CBEs can be used to disrupt gene expression by removal of the start codon (silencing), mRNA splice donor site inference (retention of intronic sequence), mRNA splice acceptor inference (exon skipping), and introduction of a premature stop codon (truncated protein product). The advantage of base-editing is that it achieves precise, single base changes without a double-strand break (DSB).

1.9 Aims of current project

As described earlier, knowledge and expertise in CRISPR/Cas9 genome editing and T cell engineering for the advancement of immunotherapies have markedly expanded in the past decade. Broadly, this project aimed to enhance the accuracy, effectiveness, and safety of genome editing methods, with a specific focus on CRISPR/Cas9 technology. This effort was directed towards developing an innovative generation of CAR-T cell therapies that could be used universally, effectively overcoming the challenges associated with TvT fratricide. Moreover, a virus-free protocol for CAR-T cells was developed using SpCas9 ribonucleoproteins (RNPs) with an sgRNA and a dsDNA donor template encoding a self-cleaving CAR transgene cassette and homology arms that align with the intended target site.

The aims of this project were to:

1. Compare the efficiency and fidelity across human-derived cytidine base editor (CBE) versions and the original rat APOBEC1 iteration for multiplexed removal of CD7 and TCRαβ through transient delivery of guide RNA and CBE mRNA by electroporation of rat APOBEC1 (BE3), human activation-induced cytidine deaminase (hAID-BE3), and human APOBEC3A (hA3A-BE3).
2. Apply base editing strategies to terminal-CRISPR transduced T cells directed against CD3 or CD7 antigens to the CRISPR mediated disruption of TRBC, permitting CAR enrichment following TCRαβ depletion at the end of production.
3. Explore site specific integration into three distinct loci, *TRAC*, *CD3ζ*, and *CD7*, and assess the feasibility of non-viral generation of CAR7 and CAR3 products. This involved using SpCas9 ribonucleoproteins (RNPs) with an sgRNA guides, along with a double-stranded DNA homology flanked donor template.

Chapter 2 Materials and Methods

2.1 Materials

2.1.1 Reagents used for DNA processing

Table 2-1 List of the reagents used for DNA sample processing

Reagent	Manufacturer	Catalogue number
50X Tris-acetate-EDTA (TAE) buffer	ThermoFisher Scientific, Massachusetts, USA	B49
Nuclease-Free Water (not DEPC-Treated)	ThermoFisher Scientific, Massachusetts, USA	AM9939
1Kb plus DNA ladder	ThermoFisher Scientific, Massachusetts, USA	10787018
dNTP Set 100mM Solutions	ThermoFisher Scientific, Massachusetts, USA	R0181
Gel loading dye: Orange G 6X	ThermoFisher Scientific, Massachusetts, USA	R0631
UltraPure™ Agarose	ThermoFisher Scientific, Massachusetts, USA	16500500
SYBR™ Safe DNA Gel Stain	ThermoFisher Scientific, Massachusetts, USA	S33102
Branched Polyethylenimine (PEI)	Sigma-Aldrich, Dorset, UK	408727
T4 DNA ligase (5 U/µL)	ThermoFisher Scientific, Massachusetts, USA	EL0014
T4 Polynucleotide Kinase	NEW ENGLAND BioLabs, Massachusetts, USA	M0201S
FastAP Thermosensitive Alkaline	ThermoFisher Scientific,	EF0651

Phosphatase (1 U/µL)	Massachusetts, USA	
FastDigest BpiI (IIs class)	ThermoFisher Scientific, Massachusetts, USA	FD1014
FastDigest BamHI	ThermoFisher Scientific, Massachusetts, USA	FD0054
FastDigest MluI	ThermoFisher Scientific, Massachusetts, USA	FD0564

2.1.2 Reagents used for bacterial culture processing

Table 2-2 List of reagents used for bacterial culture processing

Reagent	Manufacturer	Catalogue number
Ampicillin Sodium salt	Sigma-Aldrich, Dorset, UK	A0166-25G
Kanamycin sulfate from Streptomyces kanamyceticus	Sigma-Aldrich, Dorset, UK	K1377-25G
LB broth	Sigma-Aldrich, Dorset, UK	L3022-250G
LB agar	Sigma-Aldrich, Dorset, UK	L3147-1KG
S.O.C. Medium	ThermoFisher Scientific, Massachusetts, USA	15544034
Stellar™ Competent Cells	Takara Bio Europe, Saint-Germain-en-Laye, France	636766

2.1.3 Reagents for cell culture processing

Table 2-3 List of reagents used during cell culture processing

Reagent	Manufacturer	Catalogue number
Dimethyl sulfoxide (DMSO)	Sigma-Aldrich, Dorset, UK	276855-100ML
Dulbeco's Modified Eagle Medium (DMEM), 500 mL	ThermoFisher Scientific, Massachusetts, USA	11960044
Foetal Calf Serum (FCS)	ThermoFisher Scientific, Massachusetts, USA	10-082-147
Trypsin-EDTA (0.25%)	ThermoFisher Scientific, Massachusetts, USA	25200056
Minimum Essential Medium (Opti-MEM™), Reduced Serum Medium, no phenol red, 500 mL	ThermoFisher Scientific, Massachusetts, USA	11058021
Penicillin-Streptomycin (Pen Strep), 10,000 U/mL, 100 mL	ThermoFisher Scientific, Massachusetts, USA	15140122
Dulbecco's Phosphate-Buffered Saline (DPBS),	ThermoFisher Scientific, Massachusetts, USA	14040117
TexMACS™ Medium	Miltenyi Biotech, Surrey, UK	130-097-196
Gemcell Human Serum Ab U.S. Origin	Seralabs, Brussels, Belgium	GEM-100-512-H
Human IL-2 IS, premium grade	Miltenyi Biotech, Surrey, UK	130-097-746
T Cell TransACT™, human	Miltenyi Biotech, Surrey, UK	130-111-160
OneComp eBeads™	ThermoFisher Scientific, Massachusetts, USA	01-1111-42
Anti-Biotin MicroBeads UltraPure	Miltenyi Biotech, Surrey, UK	130-105-637
LD Columns	Miltenyi Biotech, Surrey, UK	130-042-901

2.1.4 Flow cytometry antibodies

Table 2-4 List of primary and secondary antibodies used

Target	Fluorochrome	Manufacturer:	Catalogue number
CD3	VioBlue	Miltenyi Biotech, Surrey, UK	130-114-519
CD3	APC	Miltenyi Biotech, Surrey, UK	130-113-135
CD7	BV605	Biosciences, US	740392
CD7 Protein, Human, Recombinant (His Tag)	n/a	Sino Biological, UK	11028-H08H
Anti-6X His tag® antibody [AD1.1.10] (DyLight® 650)	APC	Abcam, UK	ab117504
CD45	VioGreen	Miltenyi Biotech, Surrey, UK	130-110-638
CD2	VioBlue	Miltenyi Biotech, Surrey, UK	170-078-000
CD7	PerCP/Cyanine 5.5	BioLegend, London, UK	343116
CD56	PE	Miltenyi Biotech, Surrey, UK	130-113-312
CD8	FITC	Miltenyi Biotech, Surrey, UK	130-122-718
CD4	VioBlue	Miltenyi Biotech, Surrey, UK	130-094-153
TCRαβ	APC	Miltenyi Biotech, Surrey, UK	130-091-237
TCRαβ	PerCP-vio700	Miltenyi Biotech, Surrey, UK	130-109-924
Biotin-SP (long spacer) AffiniPure F(ab') Fragment Goat Anti-Mouse IgG, F(ab') Fragment Specific antibody	n/a	Stratech Scientific Limited, Suffolk, UK	115-066-072-JIR
Streptavidin	APC	BioLegend, London, UK	405207
Streptavidin	PE	Miltenyi Biotech, Surrey, UK	130-106-789

CD247 (CD3 zeta)	PE	ThermoFisher Scientific, Massachusetts, USA	12-2479-82

2.1.5 Material Kits

Table 2-5 List of manufacture designed kits used

Reagent	Manufacturer	Catalogue number
Q5® High-Fidelity DNA Polymerase	NEW ENGLAND BioLabs, Massachusetts, USA	M0491L
Monarch® Plasmid Miniprep Kit	NEW ENGLAND BioLabs, Massachusetts, USA	T1010L
Plasmid Maxi Kit	QIAGEN, Hilden, Germany	12165
Monarch® PCR & DNA Cleanup Kit (5µg)	NEW ENGLAND BioLabs, Massachusetts, USA	T1030L
Monarch® DNA Gel Extraction Kit	NEW ENGLAND BioLabs, Massachusetts, USA	T1020L
DNeasy Blood & Tissue Kit (250)	QIAGEN, Hilden, Germany	69506
In-Fusion® HD Cloning Plus	Takara Bio Europe, Saint-Germain-en-Laye, France	638910
P3 Primary Cell 4D-Nucleofector™ X Kit L	Lonza, Basel, Switzerland	V4XP-3024
RNeasy® Plus Mini Kit	QIAGEN, Hilden, Germany	74134
QIAshredder	QIAGEN, Hilden, Germany	79656
High-Capacity cDNA Reverse Transcription Kit	ThermoFisher Scientific, Massachusetts, USA	4368813

Oligo(dT)$_{18}$ Primer	ThermoFisher Scientific, Massachusetts, USA	00480551
Pierce™ 660nm Protein Assay Reagent	ThermoFisher Scientific, Massachusetts, USA	22660
Ionic Detergent Compatibility Reagent	ThermoFisher Scientific, Massachusetts, USA	22663
BD Cytofix/Cytoperm™ Fixation/Permeabilization Kit	BD Bioscience, USA	554714

2.1.6 Buffers

Table 2-6 List of buffers

Buffer	Composition	Storage
dNTPs for PCR (10mM)	dNTPs from ThermoFisher Scientific come as 250 µL aliquots of dATP, dTTP, dGTP, and dCTP at 100mM. These were mixed to make up a 1 mL solution at 25 mM of each dNTP. Nuclease free water was used to dilute this to 10mM of each dNTP (total volume 2.5 mL).	-20˚C
Blocking solution	5% dried skimmed milk powder in 1X TBS-T wash buffer	4˚C
Western blot primary antibody	3% BSA in 1X TBS-T wash buffer	4˚C
Western blot secondary antibody	3% dried skimmed milk powder in 1X TBS-T wash buffer	4˚C
Lysis buffer	50 mM Tris/HCL (pH 8.0), (MW 121.4); 150 mM NaCl, (MW 58.44), 5 mM EDTA (Ethylenediaminetetraacetic acid, MW 380.2), 1:25 dilution of stock cocktail protease inhibitor (cOmplete cocktail tablets); 1 mM PMSF	
1X Laemmli buffer	94 mM Tris-HCl (pH 6.8), 2.25% SDS, 12.5% glycerol, 2.25% β-mercaptoethanol, 0.0075% bromophenol blue	N/A

10X running buffer	0.25 M Tris (MW 121.44 g/mol; 30.3 g), 1.92 M glycine (MW 75.07 g/mol; 144.0 g), 1% (w/v) SDS (10 g) Made up to 1 L with mqH_2O. Diluted with mqH_2O to 1X for use.	RT
10X TBS-T, pH 7.4-7.6	200 mM Tris (MW 121.44 g/mol; 24.2 g), 1.5 M NaCl (MW 58.44 g/mol; 87.7 g), 1% (v/v) Tween 20 (10 mL) Tris and NaCl dissolved in 800 mL mqH_2O, pH adjusted to 7.4-7.6 with HCl or NaOH, made up to 1 L with mqH_2O, and Tween 20 added. Diluted with mqH_2O to 1X for use.	RT
Flow cytometry washing buffer	2% FCS in PBS	4˚C
Column depletion MACS buffer	0.5% bovine serum albumin (BSA), 2mM EDTA, in PBS	4˚C
LB broth	20g LB broth powder per L of H_2O. Autoclaved at 121˚C for 15min. Once at room temperature, either Ampicillin (100 µg/mL) or Kanamycin (50 µg/mL) was added.	4˚C
LB agar	36g LB agar powder per L of H_2O. Autoclaved at 121˚C for 15min. Allow LB agar to cool to ~60˚C before adding either kanamycin (50 µg/mL) or ampicillin (100 µg/mL).	4˚C
Bacterial glycerol stock	100% glycerol was mixed in a 1:1 ratio with H_2O to make a 50% glycerol solution. This 50% glycerol solution was then mixed in a 1:1 ratio with overnight bacterial culture (500 µL: 500 µL) in a screw cap cryopreservation tube.	-80˚C
Primary T cell freezing mix	10% DMSO, 45% TexMACS, 45% human serum AB.	4˚C

2.1.7 Cell culture medium

Complete Dulbecco's Modified Eagle Medium (DMEM): DMEM with 10% FCS, and 1% Pen/Strep. Stored at 4˚C.

Complete Roswell Park Memorial Institute (RPMI): RPMI with 10% FCS, and 1% Pen/Strep. Stored at 4˚C.

T cell Medium: TexMACS with 3% human serum Ab, and 100 U/mL (20 ng/mL) IL-2. Stored at 4˚C.

2.1.8 Cell types

Table 2-7 List of cell types

Cell ID	Tissue type	Medium
HEK-293T (293T)	Human Embryonic Kidney Cell Line (Adherent)	Complete DMEM
Primary human T cells from healthy donors	Peripheral Blood, T lymphocyte (Suspension)	T cell medium
Jurkat, Clone E6-1 (JE6.1)	Peripheral Blood Cell Line, T Lymphoblast (Suspension)	Complete RPMI

2.1.9 Trilink biotechnologies (San Diego, USA) mRNA CleanCap® Cas9 mRNA (Cat. No. L-7606)

This off-the-shelf mRNA codes for the SpCas9 endonuclease (transcript length: 4521 bp). Trilink have incorporated two nuclear localisation signals, one at either terminus of the SpCas9 protein to increase trafficking to the nucleus. Also, co-transcriptional capping supported a naturally occurring Cap 1 structure which in conjunction with polyadenylation optimises mRNA expression and stability.

2.1.10 Custom made CleanCap® (coBE3, hAPOBEC3A, hAID) mRNA (Cat. No. L-7007)

These mRNA is a custom-made product from Trilink, encoding human codon optimised, third generation CBE (coBE3) (transcript length: 5664 bp), human APOBEC3A (hAPOBEC3A) (transcript length 5252 bp), human activation-induced cytidine deaminase (hAID) (transcript length 5249 bp). The plasmid DNA used for

mRNA synthesis containing the base editing sequence for (coBE3, hAPOBEC3A, or hAID) were sent to Trilink for mRNA production (180 µg). This involved template linearization by BtgZI restriction digest, and mRNA purification by silica membrane. Unlike the SpCas9 mRNA, the human base editors contain only a single nuclear localisation signal (NLS) at the C terminus. Trilink's CleanCap technology was used to add a co-transcriptional Cap 1 structure, and this mRNA was polyadenylated to increase expression and stability.

2.1.11 Synthego (California, USA) sgRNA

Synthetic sgRNA were manufactured by Synthego using automated solid-phase synthesis with 2'-Omethyl 3' phosphorothioate modifications in the 1st and last 3nt's. Single guide RNA containing a 20 nucleotide protospacer with an 80 nucleotide CRISPR scaffold were generated at either 1.5 nmol (~50 µg), or 3 nmol (~100 µg) production scale. These were eluted in nuclease-free Tris-EDTA buffer supplied by Synthego at 2 µg/µL.

2.1.12 sgRNA sequences

Table 2-8 Protospacer sequences

sgRNA name:	Target/ Exon	Sequence 5' – 3'	Nuclease	Benchling on-target (off-target) score
TRAC	Exon 1	TCTCTCAGCTGGTACACGGC	SpCas9	51.8 (85.6)
TRBC ex 1-2	Exon 1	CCCACCAGCTCAGCTCCACG	BE3	C1 0.8, C2 11.0, C3 5.7, C5 21.9, C6 21.4, (25.7)
CD7 (1)	Exon 2	CACCTGCCAGGCCATCACGG	BE3/SpCas9	0.8, 5.6, 9.3, 17.0, 8.7 (75.7)
CD7 SD (2)	Exon 1	GCTCTTACCTTGGGCAGCCA	BE3	0.5, 16.0, 21.9 (23.4)
CD7 SA (3)	Exon 3	CTGAGAAGGAAAAAAGA	BE3	21.7, 11.0, 4.1(27.2)
CD3ζ	Exon 2	CACCTTCACTCTCAGGAACA	SpCas9	62.7 (31.4)

Table 2-9 PCR Primers

All primers were ordered in the 5'-3' orientation provided by ThermoFisher Scientific, Massachusetts, USA. Primers were resuspended at 10µM.

Primer name:	Primer sequence 5' – 3'
hPGK FWD	TACCCTCGCAGACGGACAGC
WPRE REV	CCAGAGGTTGATTGTCGAGC
U6 FWD	GCGCTCTAGAGAGGGCCTATTTCCCATGA
U6 REV	GCGCACGCGTAAAAAAGCACCGACTCGGT
Vector FWD	AGCGGCCGCGACTG
Vector REV	TGGCCCAGGATTTTCCTCCAC
CAR3 infusion FWD	GAAAATCCTGGGCCAATGGAAACCGACACCCTGCT
CAR3 infusion REV	ACAGTCGCGGCCGCTTTATCTGGGGGGCAGGGCCT
CAR7 infusion FWD	GAAAATCCTGGGCCAATGGAAACCGATACACTGCTGC
CAR7 infusion REV	ACAGTCGCGGCCGCTTCATCTTGGAGGCAGGGCCTGCA
CD7 Exon2 FWD	ATCACCTGCTCCACCAGCGG
CD7 Exon2 REV	GTGTCCTCGCCAGCACACAC
TRBC FWD	ACACAGAGCCCCTACCAG
TRBC REV	GCTACCTGGATCTTTCCA
300 bp TRAC homology arm FWD	TCAGGTTTCCTTGAGTGGCA
300 bp TRAC homology arm REV	CATTCCTGAAGCAAGGAAACAG
300 bp CD7 homology arm FWD	GACTGATGGTGACAGCCCAG
300 bp CD7 homology arm REV	ATCCTTGGGACTGTTCCTCTG

300 bp CD3ζ homology arm FWD	GCCACATCTGCCGTTGGTGC
300 bp CD3ζ homology arm REV	ACCAGTAGCATCGCCTTCCC

2.1.13 Generated plasmids

pCCL-CAR7 and pCCL-CAR3: CAR7 was synthesised by codon optimisation (GeneArt) of variable heavy-chain and variable light-chain antigen binding elements of the anti-human CD7 murine hybridoma, 3A1e sequence. CAR3 was synthesized by codon optimization (GeneArt) of variable heavy-chain and variable light-chain antigen binding elements of the mouse anti-human CD3 monoclonal antibody, OKT3 sequence. The scFv was fused to a CD8 transmembrane domain and to activation domains derived from 41BB and CD3ζ. The resultant CAR7 construct or CAR3 was cloned into a lentiviral vector (pCCL) backbone under the control of a PGK promoter. The scFv was fused to a CD8 transmembrane domain as well as activation domains derived from 41BB and CD3ζ. The generated CAR7 construct was cloned into a lentiviral vector (pCCL) backbone under the control of a PGK promoter.

Terminal TRBC-CAR7 (TTRBC-CAR7) or Terminal TRBC-CAR3 (TTRBC-CAR3): third generation SIN terminal configurations placed transgene expression (CAR7 or CAR3) under the control of an RNA polymerase II (Pol II) human PGK promotor, and TRBC1/2 specific sgRNA under the control of an RNA polymerase III human U6 promoter within the ΔU3 region of the 3'LTR creating terminal TTRBC-CAR7 or TRBC-CAR3. Colonies were verified by Sanger sequencing using template forward and reverse primers.

TRAC HDR template: HDR template contains a CAR transgene (CAR20, CAR7, or CAR3) or GFP flanked by 300 bp TRAC homology arms. A P2A sequence has been placed at the 5' end of the CAR or GFP, additionally a bGH poly A signal has been added at the 3' end of the CAR sequence.

CD3ζ HDR template: HDR template contains a CAR transgene, without the CD3ζ element of CAR construct (CAR20, CAR7, or CAR3) or GFP flanked by 300 bp CD3ζ

homology arms. A P2A sequence has been placed at the 5' end of the ΔCAR or GFP, additionally a bGH poly A signal has been added at the 3' end of the GFP sequence only.

CD7 HDR template: HDR template contains a CAR transgene (CAR7) or GFP flanked by 300 bp CD7 homology arms. A P2A sequence has been placed at the 5' end of the CAR7 or GFP, additionally a bGH poly A signal has been added at the 3' end of the CAR sequence.

2.1.14 Software

FlowJo v10: used to import of FCS files used for all flow cytometry analysis shown in this report.

Graphpad Prism v8.0.0: used to arrange the data into appropriately formatted graphs.

SnapGene® v3.1.4: used in producing plasmid and gene maps, as well as restriction digest design. Also, this software was used to design sequencing primers for plasmid DNA and In-fusion cloning primers. Additionally, this software was used to align Sanger sequencing to a reference sequence.

All the illustrations were generated using the online tool BioRender, accessible at https://www.biorender.com/.

2.2 Methods

2.2.1 Transformation of chemically competent *E. coli*

All transformations were performed with 25 µL of Stellar chemically competent *E. coli* (636766, Takara Bio Europe, Saint-Germain-en-Laye, France). Competent cells were thawed for 10 minutes on ice before being mixed with T4 DNA ligation reaction (2 µL), or plasmids DNA (20-50ng). The mixture was allowed to rest on ice for 30 minutes, followed by a heat-shock step at 42°C for 45 seconds. Transformations were

rapidly cooled on ice for 2 minutes before the addition of 250 µL of S.O.C. medium (ThermoFisher Scientific), then moved to a 37°C shaking incubator at 250rpm, for 1 hour. Finally, 100 µL of the culture was plated out in LB agar supplemented with appropriate selection antibiotics: 50 µg/mL Ampicillin or Kanamycin, then incubated at 37°C overnight.

2.2.2 Plasmid DNA preparation

Individual colonies of *E. coli* containing plasmid DNA were picked and grown overnight at 37°C in 4 mL LB broth supplied with appropriate antibiotic. The plasmids were purified using an alkaline lysis method following manufacturer's guidelines (Qiagen Miniprep). Bacterial cultures were scaled up as needed by mixing them with fresh LB broth containing a selective antibiotic at a 1:1000 ratio (500 µL:500 mL), before incubating at 37°C and shaking at 250rpm overnight. Plasmid DNA was extracted from these large-scale bacterial cultures with the Plasmid Maxi Kit (QIAGEN).

2.2.3 Restriction endonuclease digest

In order to prepare the DNA for traditional cloning process, restriction enzymes were used to cut the DNA at a specific site. The DNA was digested with one or two restriction enzymes (<10% final volume), 0.1 mg/mL BSA, 1Xbuffer (supplied by manufacturer) to reach up a final reaction volume of 25 µL or 50 µL. The reaction was incubated at 37°C for 1 hour. DNA fragments generated by restriction enzymes, were identified by gel electrophoresis.

2.2.4 Dephosphorylation of 5' phosphate groups on vector

Before ligation and to avoid re-ligation of plasmid backbone (fragment of DNA that contains the Ampicillin or Kanamycin resistance gene) with compatible ends, 5' phosphate groups from DNA were released.

Plasmid backbone was dephosphorylated by adding 1 µL FastAP enzyme thermosensitive alkaline phosphatase (EF0651,ThermoFisher Scientific) to a final solution of 20 µL. The reaction was incubated for 30 minutes at 37°C and the enzyme was inactivated at 75° C for 10 minutes. This is done to release 5' and 3' phosphate groups from the DNA ends, therefore prevent re-annealing of the plasmid backbone during ligation reactions and reducing the presence of background colonies.

2.2.5 Protospacer cloning for sgRNA expression

Both terminal CAR7 plasmid DNA (1 µg) and terminal CAR3 plasmid DNA (1 µg) were digested with BpiI for 30 minutes at 37°C. The vector was dephosphorylated and purified as previously described. TRBC guide sequences were synthesized as two complementary single stranded DNA oligonucleotides. Following the protocol by Georgiadis, Preece (329), oligo annealing and phosphorylation by T4 Polynucleotide Kinase (M0201S, New England BioLabs) were completed. A ligation reaction (10 µL final volume) containing 50ng linear terminal Vector DNA, 1 µL (1:200 dilution) of annealed oligos and T4 DNA Ligase (EL0011, ThermoFisher Scientific) was incubated at 37°C for 10 minutes prior to bacterial transformation.

2.2.6 DNA Ligation reaction

For the ligation reaction, 1U of T4 DNA Ligase enzyme (EL0011, ThermoFisher) and 1X buffer was included at a 3:1 molar ratio (insert DNA: terminal-U6CRISPR SIN vector) to a final reaction volume of 20 µL for 10 minutes at room temperature. The ligation reaction was transformed into chemically competent *E. coli* bacteria.

2.2.7 Polymerase chain reaction

Polymerase chain reaction (PCR) was used to amplify specific DNA sequences for cloning new plasmids, assessing genome editing at the targeted locus, and producing a dsDNA template for HDR. All reactions were performed using Q5® High-Fidelity DNA Polymerase (New England BioLabs) according to the manufacturer's instructions. The dNTP were supplied from ThermoFisher Scientific and diluted to a concentration of

10 mM each. These reactions were carried out using a Mastercycler® nexus X2 thermocycler (Eppendorf, Hamburg, Germany). The optimal annealing temperature for new primer pairs was determined by performing gradient PCRs between 58 and 68˚C. The extension time was set to 30 seconds per kilobase (kb) for the first 5kb and 1 minute per kb afterwards. SnapGene® v3.1.4 was used to design primers for plasmid DNA amplification. To avoid background amplification while using genomic DNA as a template, primer pairs were designed using the NCBI Primer-Blast tool (https://www.ncbi.nlm.nih.gov/tools/primer-blast/).

2.2.8 In-Fusion HD cloning

The In-Fusion HD cloning process is a PCR based method for the seamless insertion of a desired sequence within the plasmid DNA with no restriction digest step. SnapGene® v3.1.4 software was used to design the primers to flank the insert with complementary overhangs to that of the backbone. Both plasmid backbone and insert were linearized by PCR using Q5® High-Fidelity DNA Polymerase (New England BioLabs) with approximately 1ng of template DNA. Once the reaction was completed, PCR products were resolved using gel electrophoresis to identify them, followed by a subsequent DNA extraction using Monarch® DNA Gel Extraction Kit (New England Biolabs). The eluted PCR products was then further purified using the Monarch® PCR & DNA Cleanup Kit (New England Biolabs). Purified PCR products were placed in an In-Fusion reaction comprising 2 µL In-Fusion enzyme mix (5X), 50ng of both backbone and insert DNA, and up to 10 µL ddH2O. As per manufacturer's instructions, the reactions were carried out in a thermocycler (Mastercycler® nexus X2) at 50˚C for 15 minutes before resting on ice for two minutes prior to transformation in the competent *E. coli*.

2.2.9 Agarose gel electrophoresis and DNA purification

Gel electrophoresis is a commonly used technique to separate DNA fragments by size for visualisation and purification. Vector and insert DNA were purified using agarose gel electrophoresis. Agarose was dissolved in 1xTAE buffer by heating, and SYBR Green was added to the final concentration of 1 µg/mL before it was allowed to

solidify. The agarose gel was cast in trays and allowed to set. DNA samples were loaded with the addition of a 10X loading dye, and a 1 kb Plus DNA ladder was run alongside as a size reference. Electrophoresis was carried out at 80 – 130 V, and gels were visualised under ultraviolet light using a UviDoc gel documentation system. Products from the gel were extracted using a gel extraction kit with further purification using a PCR purification kit (QIAquick gel extraction kit (28704) and QIAquick PCR purification kit, QIAGEN).

2.2.10 Third generation lentiviral vector production

Lentiviral vector stocks were produced by transient transfection of 293T cells with third generation packaging and transfer plasmids. All packaging plasmids were generated by the Trono laboratory and manufactured by PlasmidFactory (Bielefeld, Germany) at 1 µg/µL, in 0.1 x TE buffer (188).

Third generation lentiviruses require the transfection of four separate DNA plasmids; pMDLg/pRRE (Addgene #12251) containing the gag-pol proteins, pMDG2 (Addgene #12259) incorporating the vesicular stomatitis virus envelope, pRSV-Rev (Addgene #12253) the nuclear exporter rev signal, and a vector containing the transgene.

All third-generation transfer plasmids used in this project contained the HIV-1 central polypurine tract (cPPT) element, as well as a woodchuck post-transcriptional regulatory element (WPRE). In addition, internal RNA Pol II promoters were used for transgene expression. The U3 promoter has been replaced with a tat independent cytomegalovirus (CMV) promoter.

Viral stocks were produced by seeding twelve T-175 flasks with 293T cells at a density of 22-25x10^6 cell/ flask, a day before plasmid transfection. A transfection mixture was prepared including the relevant plasmids, and 1x10^{-7} mol/L PEI (Sigma-Aldrich), in reduced serum OPTI-MEM (ThermoFisher Scientific). Medium change was carried out using complete DMEM over both 4 hours and 24 hours post-transfection. Following transfection, media containing lentiviral particles was harvested at 48 and 72 hours

post transfection, and filtered through 0.45 µm filter (Merck Millipore,UK). The viral supernatant was concentrated by ultracentrifugation at 100,000x*g* for 2 hours, and resuspended in 100 µL OptiMEM (ThermoFisher Scientific). The virus was incubated on ice for one hour and moved for long term storage at -80˚C.

2.2.11 Virus titration

HEK-293T cells were initially plated at a density of $1x10^5$ cells per well in a 24-well plate and allowed to attach overnight. After 24 hours, concentrated viral stocks were serially diluted by a factor of 5 (10 µL, 2 µL, 0.4 µL, 0.08 µL, 0.016 µL, and 0.0032 µL) for transduction of 293T cells in DMEM/10% FCS. The cells were then incubated at 37˚C with 5% CO_2. On day 3 post-transduction, 1/10 of the HEK-293T cells from each well was harvested. These harvested cells were subsequently stained and analysed for vector expression by flow cytometry.

Flow cytometry analysis was performed using FlowJo software to calculate transducing units (TUs) per mL was performed as follows:

TUs/ per mL= [(% transgene positive – background) x 1000)] x (1000/ lentiviral vector volume)

Therefore, if the % transgene positive= 4 with 1% background at 0.016 µL of lentiviral vector:

TUs/ per mL = [(4-1) x 1000] x (1000/0.016)

TUs/ per mL = 3000 x 62500

TUs/ per mL = $1.8x10^8$

2.2.12 Optimisation steps for generating high-titre of lentiviral vector

The successful achievement of high-titre lentivirus (>10^8 TU/ml) is attributed to meticulous adherence to the laboratory protocol and specific optimization steps. Firstly, ensuring the health and viability of HEK293T cells a week prior to virus

production is crucial, involving careful microscopic examination, cell splitting, and regular media changes every two days. On the day before plasmid transfection, seeding twelve T-175 flasks with 293T cells at a density of 22-25x10^6 cells per flask is recommended, along with seeding additional flasks for potential use in virus titration or cell expansion. It is essential to ensure even cell distribution within flasks by levelling incubator racks to avoid uneven cell coverage, which could negatively impact virus production. During the infection stage, vertexing of virus and PEI mixtures before joining, followed by continuous agitation during incubation, enhances transfection efficiency. Rotating flasks during transfection aids in thorough coverage of cells by the transfection mixture, with an additional 180-degree rotation after half the incubation time to ensure comprehensive exposure of cells to the mixture. Early morning media change post-transfection is preferred, ideally within 16 hours, to optimize lentivirus production and minimize cellular stress. During the virus titration step, careful transduction of cells is crucial, involving the addition of virus without disturbing cells' bottom and pipetting virus in a circular motion to ensure uniform distribution to the majority of cells. Concentrating lentiviral vectors at a 350-fold increase during production offers several advantages. It enhances infectivity and transduction efficiency by increasing the density of viral particles per unit volume, leading to improved gene delivery into target cells and higher levels of gene expression. Additionally, concentrated vectors require smaller volumes for transduction experiments, simplifying storage and handling while reducing costs associated with media and reagents. These meticulous steps collectively contribute to the successful generation of high-titre lentivirus.

2.2.13 Isolation of peripheral blood mononuclear cells (PBMC) and T cell activation

Peripheral blood mononuclear cells (PBMC) were isolated from healthy adult donors following policies at the Institute of Child Health, UCL after gaining consent. Whole blood 50 mL were diluted 1:1 in phosphate buffer saline (PBS) (Invitrogen Life Technologies, UK). Up to 30 mL diluted blood was then divided into four 50 mL falcon tubes and carefully layered onto 15 mL Ficoll-Paque (GE Healthcare, UK), then

centrifuged at 1000x*g* for 25 minutes without a break on the centrifuge. The mononuclear cells were collected from the layer between plasma and Ficoll and washed with PBS three times. After the third wash, the harvested monocular cells were re-suspended in TexMACS medium (130-097-196, Miltenyi Biotech) supplemented with 3% AB human serum (GEM-100-512-HI, Seralabs, Brussels, Belgium) together with 100 international units per mL of human recombinant interleukin 2 (IL-2) (Miltenyi Biotech, Surrey, UK). Cells were counted and resuspended at $1x10^6$ PBMSs/mL, and activated with TransACT reagent (Miltenyi Biotech, Surrey, UK) for 48 hours.

2.2.14 Cell counting

A haemocytometer counting chamber (0.0025 mm^2, Marienfeld, Germany) was used to count the viable cells' density. Cells suspension of 10 µL was mixed with 90 µL Trypan blue dye (Sigma Life Sciences, USA) and loaded into the haemocytometer. Using direct-light microscopy, we can discriminate dead cells that ingest the trypan blue dye from the intact living cells. The total number of viable cells was counted in the four large squares within the counting chamber, and the resulting figures were input into the following equation:

Average of cell number in the four squares x 10 (dilution factor) $x10^4$= total number of cells/mL in the original suspension.

2.2.15 CRISPR single guide RNA design

Guide sequences compatible with wild-type SpCas9 targeting *CD7*, *TRBC*, *TRAC*, and *CD3ζ* were originally designed using Benchling (https://benchling.com).

Benchling provides a score to each prospective guide based on an *in-silico* estimate of on and off-target CRISPR cutting. The on-target score is based on the work of Doench and colleagues (2016), who offer a value ranging from 0 to 100 depending on the position of the predicted cut site within the translated gene sequence (330). The off-target score, on the other hand, is calculated using a method proposed by Hsu

and colleagues (2013), in which *in-silico* predicted off-target scores are subtracted from an initial score of 100. This means that guides with high off-target scores are preferable (223). Both systems then determine the least number of mismatches (MMs) required for these guides to bind to additional intronic and exonic genomic sites within the specified species. The minimum number of MMs required to target an exonic site was three.

Single guide RNA sequences compatible with BE3 targeting *TRBC 1/2*, *and CD7* loci were designed using a combination of tools. Guides predicted to introduce a pre-mature stop codon by utilising C>T conversion compatible with BE3 were designed using the iSTOP online tool (http://www.ciccialab-database.com/istop). Guides targeted disruption of splice acceptor sites, or splice donor sites were designed using spliceR (http://z.umn.edu/spliceR). This was used to locate and score the naturally occurring mRNA splice sites within the targeted gene. All guides that were compatible with BE3 were assigned an *in silico* predicted on- and off-target base editing score using Benchling, with the on-target score is based on *in vitro* analysis using a first generation base editor (299), whereas the off-target score is based on research conducted by Hsu and colleagues (2013) (223). Higher scoring guides were preferred in both cases.

2.2.16 Electroporation

Electroporation strategies were used for delivering mRNA and SpCas9 protein into the cells. All electroporation reactions were carried out with 4D-Nucleofector™ X Unit (Lonza) using the 100 µL cuvettes, at a cell concentration of $1X10^7$ cells/mL in buffer P3, using program EW138 for transfecting of mRNA or EH115 for HDR experiments. The application of this device has been indicated in the Results section.

Post-electroporation with mRNA cells was placed in a pre-warmed 24 well plate and incubated in a hypothermia condition (30˚C, 5% CO_2) overnight. The next day, cells were placed back into standard culture conditions (37˚C, 5% CO_2). Cells were kept under this culture condition until moved to G-rex the following day to expand the

cells for scaling-up purposes. However, cells electroporated with SpCas9 protein where directly placed into culture conditions (37˚C, 5% CO_2).

2.2.17 TCR depletion

In the final step of production, cells were collected from G-rex and pelleted by centrifugation at 400x*g* for 10 minutes. Cells pellets were then re-suspended in 98 µL MACS buffer and 2 µL of anti-TCRαβ biotin (130-113-537, Miltenyi Biotech) per $1x10^7$ cells, and this was incubated for 15 minutes in the fridge. Next, the cells were washed in 2-5 mL of MACS buffer and centrifuged at 400x*g* for 10 minutes. Cells pellets were re-suspended in in 80 µL MACS buffer and 20 µL anti-biotin ultra-pure beads per $1x10^7$ cells and incubated for 10 minutes at 4˚C. As previously explained, the cells were washed with MACS buffer and spun down at 400x*g* for 10 minutes. Then the cells were re-suspended in 500 MACS buffer and proceeded to depletion with LD column. During the last wash step, LD columns were inserted into a midi MACS separator, rinsed with 2 mL of MACS buffer and let run through columns. After passing the cells through the LD columns, the columns were washed twice with 1 mL of MACS buffer. Eventually, unlabelled cells which passed through the column were collected and labelled as depleted TCR negative fractions.

2.2.18 Cryopreservation and recovery of cells

All cells were suspended in T cell media, counted and collected by centrifugation. The cell pellets were resuspended in the appropriate volume of cold freezing media containing 10% Dimethyl Sulphoxide (DMSO4) + 45% TexMACS + 45% human serum AB to obtain a final concentration of $1x10^6$ cells/mL. A volume of 1 mL was transferred into individual cryovials. These cryovials were first placed into a Mr. Frosty™ freezing container (ThermoFisher Scientific) filled with 100% isopropanol and stored for 24 hrs at -80°C and then transferred to an LN_2 tank for long-term storage. Recovery of cells was performed by thawing the cryovials in a 37°C water bath for 1-2 minutes before transferring the 1 mL cell suspension to a 50 mL falcon tube containing pre-warmed T cell media. T cell suspension was centrifuged at 400x*g* for 5 minutes, and

the pellet was resuspended in 5 mL of T cell media. Cells were then counted and cultured accordingly.

2.2.19 RNA extraction

RNA was isolated from the cells following the RNeasy Plus Mini Kit (74134, QIAGEN). Cells pellet were lysed with 350 µL RLT Plus buffer, then moved to QIAshredder spin column. This biopolymer shredding system homogenizes cell lysate to reduce viscosity. This was spun for 2 minutes at 8000x*g*. The homogenized lysate was transferred to the gDNA Eliminator spin column and then centrifuged for 1 minute at 8000x*g*. Afterwards, 350 µL ethanol was added to the cells, and 800 µL of that was transferred into the RNeasy spin column. This was centrifuged for 1 minute at 8000x*g*. Then 700 µL Buffer RW1 was added to the RNeasy Mini spin column and centrifuged for 1 minute at 8000x*g*. Following, 500 µL Buffer RPE was added twice to the RNeasy spin column and then centrifuged for 2 minutes at 8000x*g*. Finally, cells were eluted in 50 µL dH2O.

2.2.20 Genomic DNA extraction

After re-suspending the cell pellet in 200 µL of PBS, genomic DNA was isolated from the cells following the DNeasy Blood and tissue kit (69504, QIAGEN). The resuspended samples were mixed with 20 µL proteinase kinase and 200 µL lysis buffer. Afterwards, 200 µL of ethanol was added to the cells then transferred into a binding column. This was centrifuged at 8000x*g* for one minute. The column was washed twice with 500 washing solution. Finally, the DNA was eluted in 100 µL of dH2O and stored at -20˚C.

2.2.21 Whole cell lysate extraction

To extract whole cell lysate (WCL), cells were washed twice with DPBS and pelleted by centrifugation at 350x*g* for 5 minutes. The supernatant was fully removed, and the protein was frozen at -80˚C for later extraction. The cells were then resuspended in 5

pellet volumes of 1X Laemmli buffer, vortexed, lysed through mechanical shearing by passing through a syringe, and boiled at 95°C for 5 minutes.

2.2.22 Protein quantification

The total protein concentration in the whole cell extract was calculated using the Pierce™ 660nm Protein Assay (sensitivity range 50-2000 µg/mL; 22660, ThermoFisher). All measurements were performed in duplicates. The assay was carried out in a 96-well format with 10 µL of sample or standard/reaction and 200 µL of assay reagent (with Ionic Detergent Compatibility Reagent; 22663, ThermoFisher).

2.2.23 660nm Protein Assay

Before conducting the assay, one pack of Ionic Detergent Compatibility Reagent (IDCR) was added to 20 mL of the Pierce 660nm Protein Assay Reagent. In a 96-well flat-bottom plate, 10 µL of each standard and diluted sample were loaded, then 150 µL of the Assay Reagent containing IDCR was added. The well's contents were mixed through pipetting the fluids up and down avoiding generating bubbles.

A standard curve was constructed by plotting the average blank-660nm measurement for each BSA standard versus its concentration in µg/mL. Using the standard curve, the protein concentration of each sample was determined.

Prior to loading, cytoplasmic extracted samples were normalised, diluted in Laemmli buffer to a final sample volume of 20 µL using a 12-well and boiled for 5 minutes at 95°C to denature the protein.

2.2.24 SDS-PAGE and protein transfer

The samples were subjected to electrophoresis at 100 V in 1X running buffer after being loaded on SDS-PAGE gel. Following electrophoresis, protein was transferred to a 0.2 µm polyvinylidene fluoride (PVDF) membrane (part of the Trans-Blot Turbo Mini 0.2 µm PVDF Transfer Pack) using the Bio Rad Trans-Blot Turbo Transfer System. The

electrophoretic transfer programme used was the Bio-Rad preprogramed protocol 'Mixed MW (Turbo)' (1.3 A; 25 V; 7 minutes).

2.2.25 Immunoblotting and protein detection

The membrane was blocked in 5% milk for 1 hour at room temperature on shaker. The membrane was washed once in 1X TBS-T and incubated with the primary antibody solutions which were prepared in PBS containing 3% BSA (10 mL anti-CRISPR/Cas9 antibody abcam 1:1000, and 10 mL anti-β-Actin 1:200). Then, the membrane was washed 3 to 5 times for 10 minutes at room temperature in 1X TBS-T and incubated with HRP-conjugated secondary antibody (5 mL/ membrane, 1:5000 Amersham ECL HRP-linked whole Ab, in secondary stain buffer). The membrane was then washed 3 to 5 times for 10 minutes at room temperature in 1X TBS-T and the signal was detected by applying the Clarity Western ECL Substrate on the Bio-Rad ChemiDoc MP. For re-probing, the membrane was stripped using the Restore™ Western Blot Stripping Buffer. First, the membrane was washed once for 5 minutes in TBS-T to remove the chemiluminescent substrate, followed by 6 minutes incubation in Restore™ Western Blot Stripping Buffer at room temperature with gentle shaking. The stripped membrane was then washed twice for 5 minutes in PBS and blocked ahead of continuing with the second immunoprobing.

2.2.26 Next Generation Sequencing

Total RNA was extracted from primary T cells edited with SpCas9, coBE3, AID, and hA3A at 48 hours and 7 days post transduction. cDNA of CAR scFv was synthesised using High-Capacity cDNA Reverse Transcription Kit (4368813, ThermoFisher).

Library prep was carried out using scFv primers with Eurofins Illumina adapter sequences added. Illumina adapter sequence that has been added on the 5'- end of the forward primer: 5'- ACACTCTTTCCCTACACGACGCTCTTCCGATCT -forward primer target sequence-3' Illumina adapter sequence that has to be added on the 5'- end of the reverse primer: 5'- GACTGGAGTTCAGACGTGTGCTCTTCCGATCT -reverse primer target sequence-3'. Amplified products were detected by running on gel and provide

Eurofins with 50 µL 2 ng/ µL. The library preparation step was carried out by Eurofins the generated FastQ files were uploaded to Galaxy platform for comprehensive quality assurance and subsequent analysis (331) The data preprocessing involved adapter trimming with Trim Galore and Trimmomatic. Alignment was performed using Bowtie2 with a custom reference sequence containing the expected CAR7 scFv cDNA. Variant calling was done using Naïve variant caller followed by variant annotator.

2.2.27 Sanger sequencing analysis of non-homologous end joining, and targeted Cytidine deamination events

Genomic DNA extraction was performed using DNeasy Blood and Tissue Kit (69504, QIAGEN) and a PCR reaction designed in order to amplify 400-800 bp over the protospacer binding site. PCR products were detected by running the sample on 1% agarose gel electrophoresis, before purification by Monarch® DNA Gel extraction Kit (New England Biolabs), followed by Monarch® PCR & DNA Cleanup Kit (New England Biolabs). DNA samples were sent to Eurofins Genomics for Sanger sequencing with the appropriate forward and reverse primers. The Sanger sequencing results were further analysed by Synthego ICE online tool (ice.synthego.com), to determine the frequency of indels, at the predicted SpCas9 cleavage site. When analysing C>T conversion rates generated by cytidine deaminase base editing technologies, EDITR software was used (moriaritylab.shinyapps.io).

2.2.28 Production of double stranded DNA template for homology directed repair (HDR)

PCR was used to amplify specific sequences of dsDNA template with 300 bp homology arms to the DNA break site. Q5® High-Fidelity DNA Polymerase (New England Biolabs) was used for all reactions and set up in accordance with manufacturer's instructions.

In order to achieve sufficient concentration of PCR products, PCR purified products were concentrated by an isopropanol precipitation method. Briefly, a 1/10 of the volume 3M sodium acetate was added to the purified DNA. Then two volumes of cold

isopropanol were added, with the contents being vortexed at full speed for 5 seconds. The tube was then incubated at -80˚C for 45 minutes and centrifuged at 16000xg for 10 minutes at 4°C. The supernatant was removed, and the tubes were washed with 200 µL of ice-cold 80% ethanol. The centrifugation step was repeated, and the ethanol removed, with the pellet allowed to air-dry. After the pellet was dried, 3 µg/µL of Tris-EDTA (TE) buffer was added to each pellet. For quantification on the Nanodrop spectrophotometer, 0.5 µL solution was diluted with 4.5 µL of TE and the size of the product was confirmed on an agarose gel.

2.2.29 SpCas9-RNP complexes

SpCas9 protein (Alt-R® S.p. Cas9 Nuclease V3, ThermoFisher Scientific, Massachusetts, USA), was incubated at room temperature with the sgRNA (synthetic sgRNA were manufactured by Synthego) at a 1:1.2 molar ratio for 10 minutes, prior to electroporation. Where more than one locus was targeted RNP complexes were incubated separately before being mixed together. When performing HDR experiments RNP complexes were incubated for 8 minutes before the addition of dsDNA template and then incubated for a further 2 minutes.

2.2.30 ^{51}Chromium release assay

Cytotoxic activity of CD3ζ-CAR7 was assessed by ^{51}Cr release assay. Wild-type Jurkat cells (target cells) were harvested and re-suspended in RPMI media at 11x10^6 cells per mL. Target cells were labelled with 100 µCi of ^{51}Chromium and incubated at 37˚C using 5% CO_2 for one hour. During the incubation period, effector T cells (CD3ζ-CAR7, pCCL-CAR7, UTD cells, RNP cells, and GFP cells) were counted and resuspended at a concentration of 1x10^6 /mL of culture medium RPMI in a 96-well and a U bottom plate was loaded in triplicate so that the highest concentration contained 1x10^5 cells and two-fold dilutions were performed thereafter. Twelve well-replicates were plated with RPMI alone to measure spontaneous release and twelve with 10% triton to measure the maximal ^{51}Cr release assay. ^{51}Cr-labeled targeted cells, 5x10^4 cells/mL, (5x10^3 target cells / well) were co-cultured with either CD3ζ-CAR7, pCCL-CAR7 as a positive control, or un-transduced cells, RNP cells, GFP cells as a negative

control for 4 hours 37˚C with 5% CO_2. Then the 50 µL supernatant was removed and added to 150 µL scintillation fluid in 96-well isoplates and incubated at room temperature overnight. The next day ^{51}Cr release effect was measured by beta-counter. The specific killing activity of the cells was calculated using the formula:

[(experimental release - spontaneous release)/ (maximum release - spontaneous release) x 100].

2.2.31 Flow cytometry

For flow cytometry analysis, cells were harvested and pelleted by centrifugation at 300x*g* for 5 minutes. For CAR staining, CAR19, CAR20 and CAR3 were stained with Fab Fragment Goat Anti-Mouse IgG fragment-specific antibody (Stratech Scientific Limited) followed by Streptavidin-APC (BioLegend) or Streptavidin-PE (Miltenyi Biotech). CAR7 was stained with recombinant CD7 (His-Tag) (Sino Biological), followed by anti-His-APC (Abcam). Cells were then stained with the appropriate monoclonal antibody diluted in FACS buffer (PBS with 2% FCS) then incubated for 30 minutes at 4˚C in the dark.

A fixation/permeabilization kit (BD Bioscience) was used to fix and permeabilize cells before staining intracellular cytokines with fluorochrome-conjugated anti-cytokine antibodies.

Compensation between fluorochromes was carried out by using OneComp eBeads™ (ThermoFisher Scientific). Half of these beads are conjugated to anti-lambda/Kappa chain antibodies, allowing them to recognise hamster, mouse, and rat antibodies and functioning as ideal single colour control.

At the end of the staining cells were washed with PBS before resuspending for flow analysis. The cell pellet was then resuspended in about 300 µL of FACS buffer and analysed using the LSRII cytometer (BD Biosciences) and all data were analysed using FlowJo software version 10.

Chapter 3 Comparison of cytidine deaminase base editors for multiplexed editing of T cells

3.1 Introduction

Genome-editing has been effectively applied to modify T cell receptors, HLA and other molecules required for generation of 'universal' CAR-T cells. These modifications have also been utilised to make CAR-T cells fratricide resistant when targeting shared T lineage antigens (332).

Base editing, an alternative approach to traditional gene disruption, offers site-specific base conversion without the need for DSBs or dependence on cellular HDR (297). Furthermore, base editors can induce targeted mutations in dividing and non-dividing cells, as they depend on excision repair or mismatch repair processes, which, contrary to HDR, occur in nearly every cell cycle phase (296).

Cytidine deaminase base-editors (CBE) cause conversion of C•G>T•A nucleotides and have been used for gene knockout though the introduction of premature stop codons or disruption of splice sites (295, 308, 333). First generation CBEs contained a rat Apolipoprotein B mRNA editing enzyme catalytic subunit 1 (rAPOBEC1), fused to the N-terminus of dCas9, and with an optimal linker length of 16 nt. While successful as a proof of concept, editing efficiencies in human cell lines were only 0.8-7.7% within a five nucleotides editing window (297).

In the pursuit of improvement, a second-generation base editor (BE2), with uracil DNA glycosylase inhibitor (UGI) fused to the C-terminus of the dCas9 was developed, achieving threefold efficiency with indel formation remaining lower than 0.1% (297). This was followed by BE3 (APOBEC–XTEN–nCas9(D10A)–UGI) which raised the efficiency up to 37%, with indel frequency averaging at 1.1%, operating in an activity window 5 nt wide, at positions 4-8 distal to the PAM (297). To further enhance efficiency and generate CBEs with different editing windows/ sequence preferences, BE3 variants were generated that replaced the rAPOBEC1 deaminase with other

cytidine deaminases, including: human activation-induced cytidine deaminase (hAID) (300, 327) and human APOBEC3A (hA3A) (300, 310, 325). These enzymes are ssDNA specific cytidine deaminases each with distinct sequence preferences.

AID and APOBEC3 are both enzymes that belong to the AID/APOBEC family of proteins. While they share some similarities, they have distinct functions and origins. AID is primarily involved in the immune response, specifically in the processes of somatic hypermutation (SHM), class switch recombination (CSR), and gene conversion. These processes, together with gene conversion are essential to produce functional T and B cells lymphocytes (334). On the other hand, APOBEC3 forms part of the innate antiretroviral immune activity against retroviruses, by inducing mutations within the viral genome. This activity leads to hypermutation and degradation of viral genetic material, with these genes displaying a lot of diversity to provide a broad spectrum of antiviral defence mechanisms (335). Each fused deaminase in base editors exhibits distinct sequence preferences: hAID preferentially deaminates cytosine in WRC (W=A/T, R=A/G) motifs, (336), while APOBEC3A showed preferential deamination of cytidines in a TCR motif (R = A/G) (337, 338).

Recently studies have used base editors, to manipulate human primary T cells (72, 308). Notably, compared to SpCas9 editing, base editing showed a lower frequency of translocation events in primary T cells edited at three loci (*TRAC*, *B2M*, and *PDCD1*) (308). Moreover base editors have also shown potential in a pre-clinical study where a BE3 was employed to remove shared CD3 and CD7 antigens on primary T cells ahead of anti-CD3 and anti-CD7 CAR-T cell production and subsequent combinational effects against primary T-ALL cell targets and *in vivo* models of T-ALL (72). This has subsequently resulted in the world first therapeutic application of base-edited CAR-T cells designed for children with T-ALL. BE-CAR7 were engineered to delete three genes encoding *CD52* and *CD7* receptors, as well as TCRαβ, strategically designed to evade complications associated with lymphodepleting serotherapy, fratricide, and GVHD. The preliminary results of this clinical trial involved three patients. The first patient, a 13-year-old girl with relapsed T-ALL following HSCT, achieved molecular remission just 28 days after BE-CAR7 infusion. This enabled her to undergo a

nonmyeloablative HSCT, with sustained remission in the bone marrow still evident 9 months post-HSCT. BE-CAR7 also exhibited anti-leukemic activity in the other two patients, enabling one to undergo HSCT successfully, while the third patient experienced a fatal fungal complication (74).

The objective of this chapter is to investigate base editors incorporating rAPOBEC1 (BE3), hAID (AID-BE3), or hA3A (A3A-BE3), for the development of 'universal' fratricide-resistant CAR-T cell therapies targeting the CD7 antigen. All editors were tested with the BE3 architecture with the cytidine deaminase fused to the N-terminus of a nickase SpCas9 (D10A), and a singular UGI fused at the C-terminus (**Figure 3-1 A**).

3.2 Optimisation of genome base editing effects in primary T cells to remove TCR and shared antigens (CD7, CD3)

Single guide RNA compatible with coBE3 targeting both the *CD7* and *TRBC1/2* loci had previously been designed and validated. The CD7 sgRNA mediates a C>T nucleotide conversion at protospacer position C8, leading to a premature STOP codon in exon 2 (Gln115*) (72). Similarly, the TRBC1/2-specific sgRNA mediated C>T conversions at positions C5 and/or C6 leading to the generation of a premature STOP codon in exon 1 (Trp44*), to allow downstream generation of $CD7^-/TCR^-$ cells (72).

An alternative method of achieving genomic disruption involves the targeting of splice-sites which by promoting exon skipping or intronic sequence retention, both of which have shown high levels of efficiency for other gene targets (308, 333). Therefore, two additional CD7 guides were designed alongside CD7 sgRNA (1), to disrupt either the exon 1 splice donor (SD) site (CD7 sgRNA (2)) or the exon 3 splice acceptor (SA) site (CD7 sgRNA (3)) (**Figure 3-1 B**). Comparative testing was performed using the three different sgRNA to determine which sgRNA sequence offered optimal disruption of CD7.

Healthy donor PBMCs (n=3) were isolated and activated for 48 hours using TransACT reagent. Activated T cells were electroporated with 50 µg/mL of either SpCas9 or

coBE3 mRNA and 10 μg/mL of both CD7 and TRBC1/2 sgRNA. Knockout was assessed at seven days post electroporation by flow cytometry, T cells were stained with CD2 antibody to identify T cell populations (**Figure 3-1 C**). Although, all CD7 guides presented with high knockout when used with SpCas9, only CD7 sgRNA 1 showed high levels of knockout ranging from 66%-79% when used in conjunction with coBE3. I therefore opted to use this guide in all subsequent experiments (**Figure 3-1 D**). High knockout of TCRαβ was achieved with both SpCas9 (96%-99%) and coBE3 (91%-97%) across all conditions (**Figure 3-1 D**).

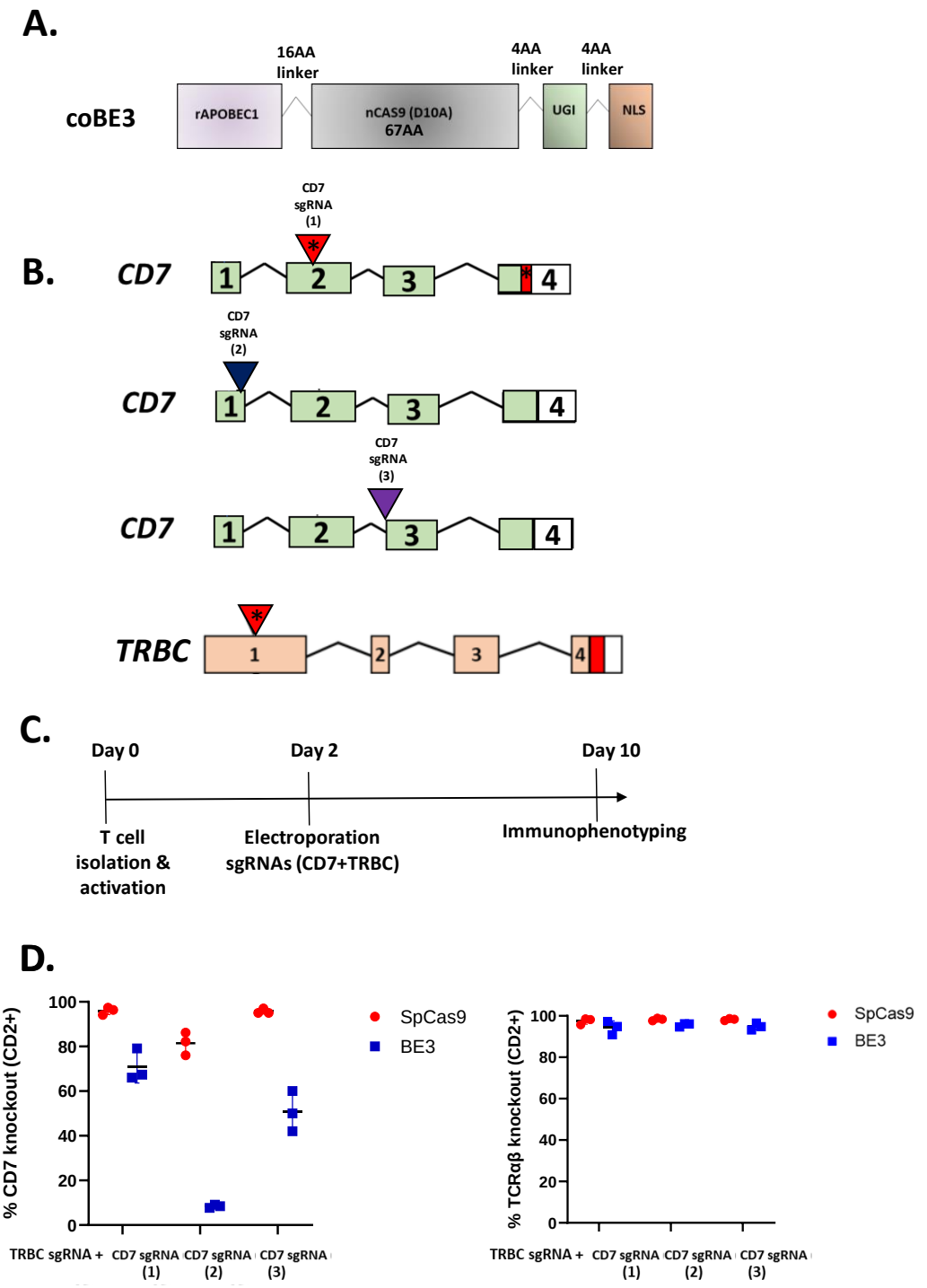

Figure 3-1 Comparison of CD7 targeting sgRNAs when multiplexed with TCRαβ knockout

A. A third-generation cytidine deaminase base editor (BE3) architecture of rat APOBEC1 (rAPOBEC1), cas9 nickase (nCas9) D10A, uracil glycosylase inhibitor (UGI) and nuclear localisation signal (NLS) elements. **B.** Schematic representations of the exonic regions within the *CD7* and *TRBC* genes, the red marking denoting the genomic translation stop sites in exon 2 of CD7, followed by their respective 5'

untranslated regions (white boxes). The blue triangle indicates the splice donor (SD) site, and the purple triangle indicates the splice acceptor (SA) site. The red triangle with asterisks indicates the positions of base conversions that resulted in the formation of premature stop codons in exon 1 of TRBC **C.** Timeline of the experiments, transient delivery of sgRNA and CBE mRNA by electroporation (EP) in primary donor T cells was compared (n=3) for rat APOBEC1 (BE3) **D.** Phenotyping of CD7 and TCRαβ knockout results across n=3 donors, CD7 sgRNA (1) showed the highest knockout with both SpCas9 and coBE3, while CD7 sgRNA (2) showed high knockout with SpCas9 only, with low knockout with coBE3. The CD7sgRNA (3) showed moderate knockout with coBE3 and high knockout with SpCas9. The error bars represent the standard deviation (SD). TCRαβ showed high levels of disruption when co-electroporated with each CD7 gRNA with both SpCas9 and coBE3. The error bars represent the standard deviation (SD).

3.3 Assessment of the effectiveness of genome editing by cytidine deaminases

To assess third generation CBEs incorporating either rAPOBEC1 (BE3), hAID (hAID-BE3), or hA3A (hA3A-BE3), primary T cells were electroporated with CD7 and TRBC targeting sgRNAs detailed above. Genome editing efficiencies, molecular signatures, and fidelity were compared.

To this end human codon optimised mRNA encoding BE3, hAID-BE3, or hA3A-BE3 was produced and delivered to primary T cells at 50 µg/mL alongside CD7 and TRBC sgRNAs at 10 µg/mL. SpCas9 mRNA was used in parallel as an endonuclease-type control of CD7 and TCRαβ disruption.

As seen in the previous section, flow cytometry revealed high knockout of CD7 when using SpCas9 (n=4, 83%-95%), while BE3 ranged between 43%-78%. Although, hAID was able to achieve CD7 knockout, more variability across the donors was observed (17%-62%). However, hA3A achieve CD7 knockout comparable to SpCas9 (79%-94%) (**Figure 3-2 A&B**). All editors demonstrated a comparable level of TCRαβ knockout with SpCas9 and hA3A being the highest (91.5%-98% and 91.7%-97% respectively), closely followed by coBE3 and hAID (84%-94% and 82%-94% respectively, **Figure 3-2 A&B**).

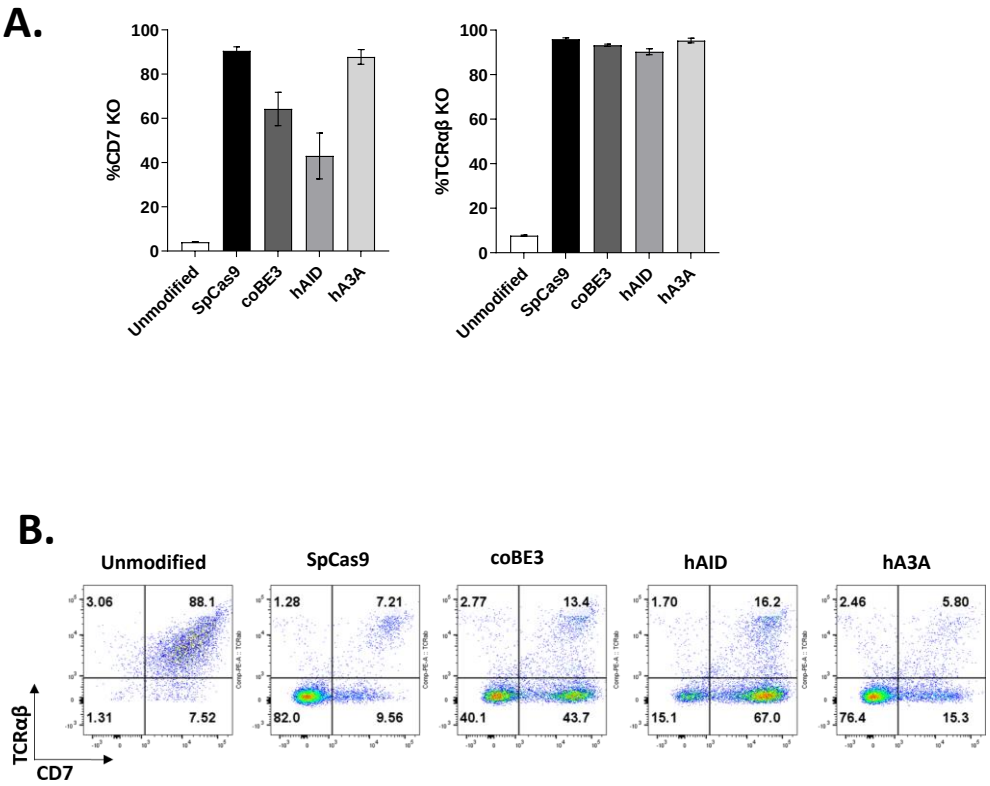

Figure 3-2 Comparison of different BE mRNA for editing efficiency

A. Summary of phenotypic analysis (n=4) of Spcas9, coBE3, hAID, and hA3A edited cells gated on CD2+ cells, expression reduction of CD7 and TCRαβ surface antigens following targeted disruption. The error bars represent the standard error of the mean (SEM). **B.** Representative flow plot for CD7 and TCRαβ disruption with each base editor; mRNA SpCas9 were used as a positive knockout control.

To verify the disruptive effects of base editing at the genomic level, specific primer pairs were designed to amplify the across the genomic regions surrounding the protospacer sequences. The amplified PCR products from edited and unedited cells were sequenced by Sanger sequencing and analysed using the EditR online tool (http://baseeditr.com/).

Consistent with the flow cytometry analysis hA3A-BE3 displayed the highest C>T conversion at the target nucleotide within the *CD7* locus (C8, 88%-98%). However, hA3A-BE3 also resulted in C>T conversion outside the predicted editing window (between nucleotides 4-8 distal to the PAM sequence) at positions C1, C3, and C16 (**Figure 3-3 Ai&ii**). Similarly, BE3 showed C>T nucleotide conversion at protospacer

position C8 ranging from 61%-81%, additional editing also observed at C4 and C7, as well as outside the optimal editing window at position C3 (**Figure 3-3 Bi&ii**).

In contrast, T cells electroporated with hAID-BE3 demonstrated a relatively low level of C>T nucleotide conversion at protospacer position C8, ranging from only 2% to 3%. However, high C>T conversion was observed at other C positions within the hAID editing window (C1, C3, C4, and C7), indicating high levels of activity at other specific positions close to the target sequence (**Figure 3-3 Ci&ii**).

Similar to the *CD7* loci, hA3A-BE3 resulted in relatively high G>A (antisense) conversion rates throughout the TRBC-targeting protospacer. At the target nucleotides (G5 and G6) hA3A resulted in high G>A conversion (G5 44%-83% and G6 35%-81%) consistent with observations made by flow cytometry. However, high range of non-target editing was again observed with this base editor outside the 4 bp-8 bp PAM distal editing window at (G1, G2, G3, G9, G11, G16, and G17) (**Figure 3-4 Ai&ii**).

T cells edited with coBE3 showed G>A conversion at position G5 and G6 of 32%-92% and 21%-66% respectively, with minimal editing observed outside the PAM distal 4 bp-8 bp editing window at only G11, where G>A conversion ranged from 1%-18%.

Unlike at the *CD7* loci hAID showed high G>A conversion at both target nucleotides (G5 41%-72% and G6 28%-68%). In addition, moderate level of editing was also observed within the 1 bp-8 bp PAM distal editing window at G1, G2 and G3. Outside the editing window, low levels of editing were observed at G9, G11, G16 and G17 (**Figure 3-4 Ci&ii**).

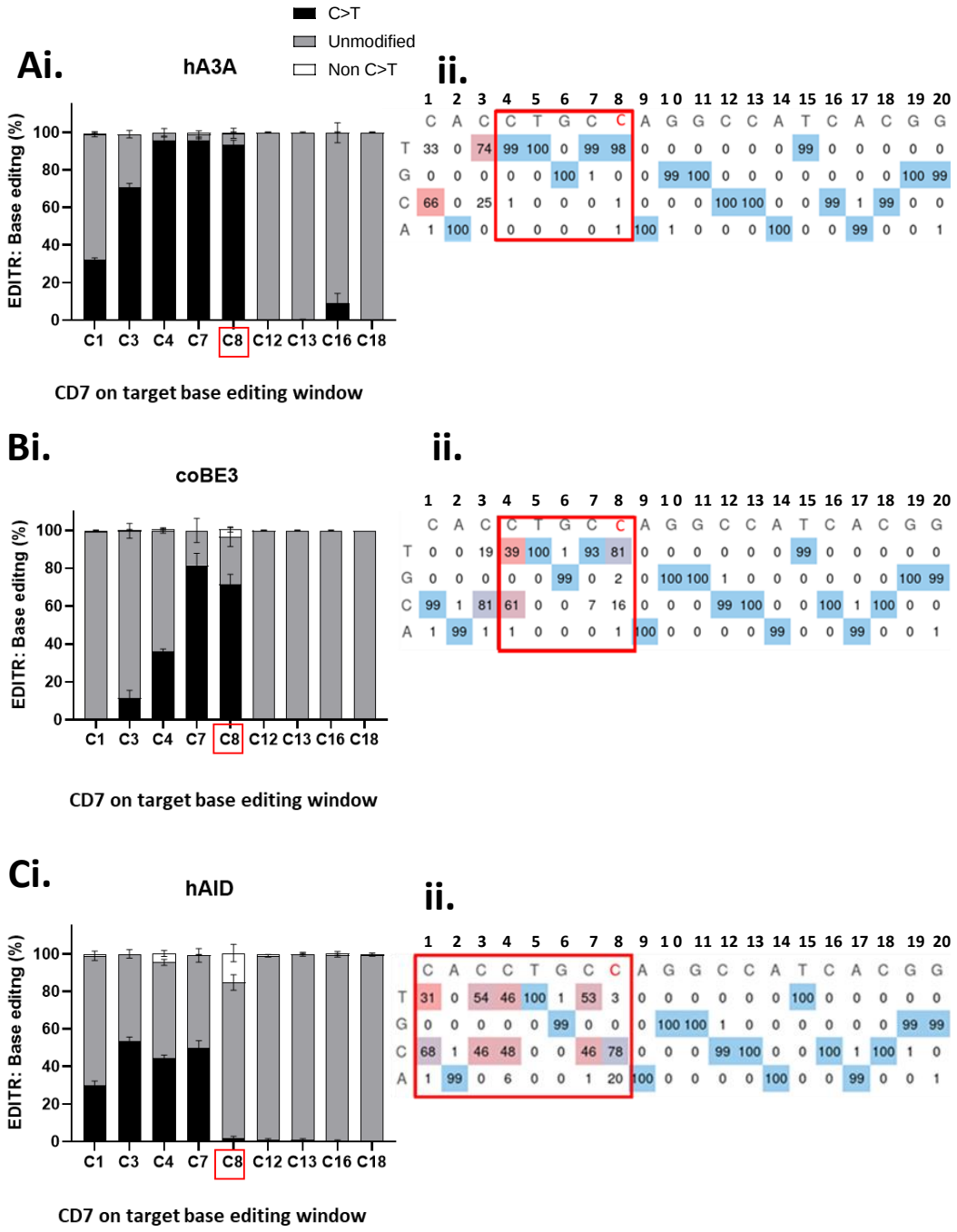

Figure 3-3 Sanger sequencing of *CD7* locus confirms C>T conversions at 'on-target' sites for all editors

A (i). Summary of EDITR output of Sanger sequencing results of *CD7* genome editing (n=4). A window of deaminase activity was anticipated at cytidine (C) positions (red box) within an editor-specific window for hA3A: 4-8 bp, distal to the target PAM sequence. High percentage of C>T conversion throughout CD7-targeting protospacer, on target C8, C7, and C4. Out of the optimal window editing showing at C1, C3 and C16 **A (ii).** Representative EDITR output of Sanger sequencing results of *CD7* genome editing showing C>T conversion measured at position C8 of the

target window, as well as indicating the occurrence of C>T changes outside the optimal window. **B (i).** Summary of EDITR output of Sanger sequencing results of *CD7* genome editing (n=4). A window of deaminase activity was anticipated at cytidine (C) positions (red box) within an editor-specific window for coBE3: 4-8 bp, distal to the target PAM sequence. High percentage of C>T conversion throughout CD7-targeting protospacer, on target C8, C7, and C4. Editing out of the optimal editing window only on C3 with low percentage. **B (ii).** Representative EDITR output of Sanger sequencing results of *CD7* genome editing showing C>T conversion measured at position C8 of the target window. **C (i).** Summary of EDITR output of Sanger sequencing results of *CD7* genome editing (n=4). A window of deaminase activity was anticipated at cytidine (C) positions (red box) within an editor-specific window for hAID: 1-8 bp, distal to the target PAM sequence. Moderate percentage of C>T conversion throughout CD7-targeting protospacer**.** Low editing percentage on target C8, and higher editing was observed on C7 and C4.**C (ii).** Representative EDITR output of Sanger sequencing results of *CD7* genome editing showing C>T conversion measured at position C8 of the target window. The error bars represent the standard error of the mean (SEM).

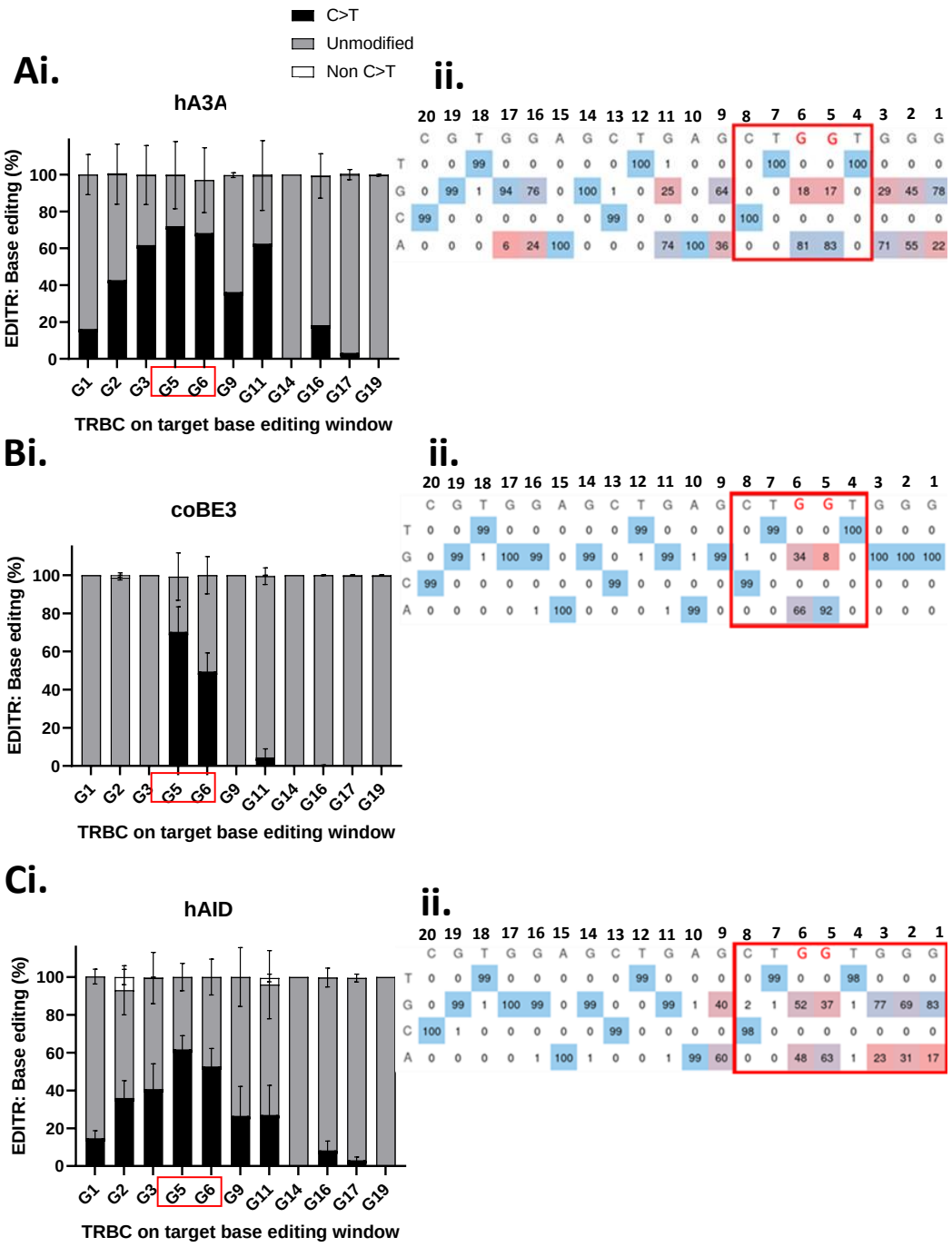

Figure 3-4 Sanger sequencing of *TRBC* locus confirms G>A conversions at 'on-target' sites for all editors

A (i). Summary of EDITR output from Sanger sequencing results of *TRBC* genome editing (n=4). A window of deaminase activity was anticipated at cytidine (C) positions (red box) within an editor-specific window for hA3A: 4-8 bp, distal to the target PAM sequence. The percentage of G>A (antisense) conversion throughout TRBC-targeting protospacer at target position G5 and G6. Editing of G nucleotides was observed outside the editing window **A (ii)**. Representative EDITR output from Sanger sequencing results of *TRBC* genome editing showing G>A conversion at

position G5 and G6, as well as indicating the occurrence of high-level G>A changes outside the optimal window, occurring on G1, G2, G3, G9, G11, G16, and G17. **B (i)**. Summary of EDITR output from Sanger sequencing results of *TRBC* genome editing (n=4). A window of deaminase activity was anticipated at cytidine (C) positions (red box) within an editor-specific window for coBE3: 4-8 bp, distal to the target PAM sequence. The percentage of G>A (antisense) conversion throughout TRBC-targeting protospacer at target position G5 and G6. Editing outside the editing window was observed at G11 only. **B (ii)**. Representative EDITR output of Sanger sequencing results of *TRBC* genome editing showing G>A conversion at position G5 and G6. **C (i)**. Summary of EDITR output from Sanger sequencing results of *TRBC* genome editing (n=4). A window of deaminase activity was anticipated at cytidine (C) positions (red box) within an editor-specific window for hAID: 1-8 bp, distal to the target PAM sequence. The percentage of G>A (antisense) conversion throughout TRBC-targeting protospacer at target position G5 and G6, also on G1, G2, G3. Editing outside the editing window was observed in different Gs, including G9, G11, G16 and G17. **C (ii)**. Representative EDITR output of Sanger sequencing results of *TRBC* genome editing showing G>A conversion at position G5 and G6. The error bars represent the standard error of the mean (SEM).

The SpCas9 control was assessed by tracking of indels by Sanger sequencing across the protospacer sequence, followed by ICE analysis. Across the four primary T cell donors SpCas9 induced between 71%-80% and 67%-85% at the *CD7* and *TRBC* loci respectively (**Figure 3-5 A&B**). Notably, ICE analysis of all base editors (coBE3, hA3A, AID) confirmed seamless editing with no indels detected. This underlines the precision and accuracy of the base editing techniques used, further supporting their efficiency as genome editing tools, with BE3 offering a balance of efficient editing within a defined window of activity. One explanation of these findings could relate to how protein expression was after electroporation of the relevant mRNA. To investigate, serial protein expression assessments were undertaken next.

A.

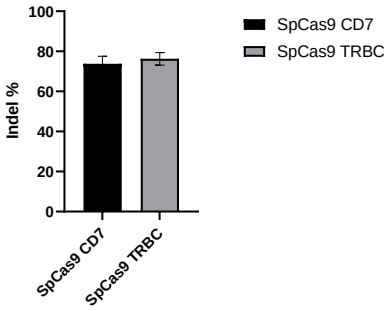

B.

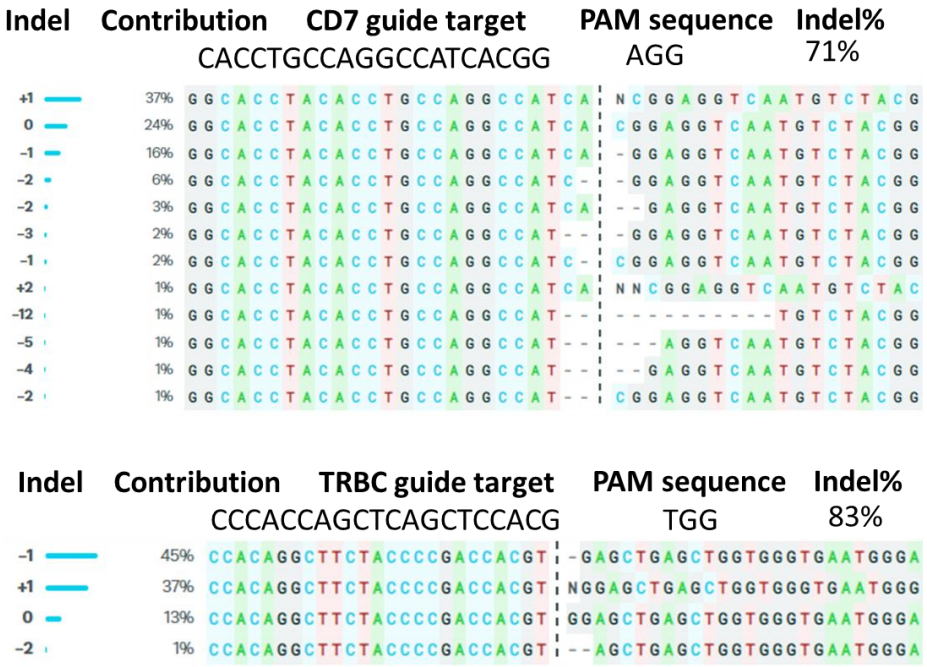

Figure 3-5 Detection of insertions/deletions (indels), induced by SpCas9 in primary T cells

A. Summary of indel% (n=4) SpCas9-CD7 indels. On-target editing effects of DNA extracted from primary T cells treated with SpCas9 + sgRNA for CD7 and TRBC were measured by direct sequencing and bioinformatic analysis using Tracking of Indels by Inference of CRISPR Edits (ICE) software for signatures of non-homologous end joining (NHEJ) demonstrating efficient disruption at both target sites. The error bars represent the standard error of the mean (SEM). **B.** Quantification of on-target editing was accomplished using direct sequencing, and bioinformatic analysis of indels following NHEJ repair confirmed multiplexed knockout. PAM, protospacer adjacent motif.

3.3.1 Serial detection of SpCas9, BE3, hA3A and hAID protein expression after mRNA delivery

To explore the potential impact of protein expression and stability on the variations observed in editing efficiency between SpCas9 and CBEs (coBE3, hA3A, and hAID), serial Western blot analysis was performed to measure how transient these editors are over time.

To track editor protein expression over time, T cell pellets from one of the donors mentioned in section 3.3 were collected at different time points following electroporation with the different CBE (coBE3, hA3A and hAID) mRNA and sgRNAs against CD7 and TRBC. The on-target editing frequency was measured at day 7 post electroporation by flow cytometry (SpCas9 = 91.5%, coBE3 = 83.8%, hAID=82.1%, hA3A 91.7%, TCRαβ knockout gated on CD2+) confirming activity of each editor (**Figure 3-2**). Molecular corroboration was provided by Sanger sequencing analysis of the *TRBC* and *CD7* loci using the Synthego ICE tool for samples treated with SpCas9 (**Figure 3-5**), and the EDITR for samples treated with coBE3, hA3A and hAID (**Figure 3-3 & Figure 3-4**).

Total protein was extracted from the cell pellets and equal amounts of protein, as measured by a Bicinchoninic acid (BCA) assay, were loaded into an SDS-PAGE gel. Subsequently, the membranes were stained for the presence of Cas9 protein, which is present in all the CBE configurations for SpCas9, coBE3, hA3A, hAID edited cell lysates. Recombinant SpCas9 protein was used as a positive control for the anti-Cas9 antibody, protein from unmodified cells were used as negative controls, and displayed no anti-Cas9 staining (**Figure 3-6 A**).

Cells treated with SpCas9 mRNA showed detectable levels of SpCas9 protein 7 days post electroporation (**Figure 3-6 B**). However, BE3 and hAID proteins were considerably more transient, displaying a peak at 16 hours, after which BE3 protein was undetectable, while low levels of hAID expression could still be seen at 48 hours (**Figure 3-6 C&D**). Unlike coBE3 and hAID, expression of hA3A seemed to peak at 16

hours and persisted, for up to 72 hours post-electroporation (**Figure 3-6 E**). It is conceivable that longer persistence of hA3A was related to its higher levels of activity, both in and outside its anticipated window of activity.

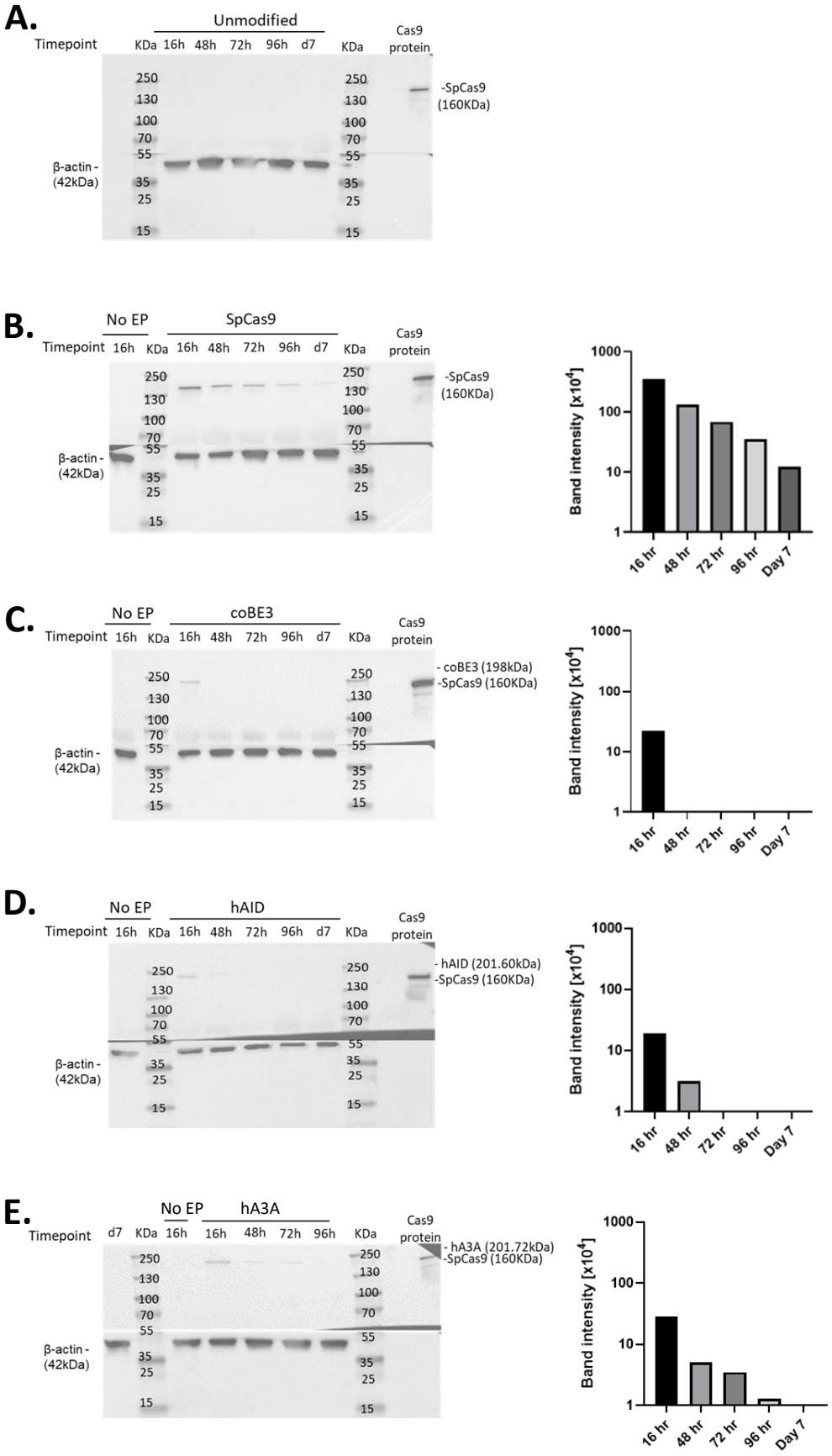
A.
Unmodified
Timepoint
KDa 16h 48h 72h 96h d7 KDa
Cas9 protein
250
130
100
70
55
35
25
15
β-actin - (42kDa)
-SpCas9 (160KDa)
B.
No EP
SpCas9
Timepoint 16h KDa 16h 48h 72h 96h d7 KDa
Cas9 protein
β-actin - (42kDa)
-SpCas9 (160KDa)
Band intensity [x10⁴]
1000
100
10
1
16 hr
48 hr
72 hr
96 hr
Day 7
C.
No EP
coBE3
Timepoint 16h KDa 16h 48h 72h 96h d7 KDa
Cas9 protein
β-actin - (42kDa)
- coBE3 (198kDa)
-SpCas9 (160KDa)
Band intensity [x10⁴]
1000
100
10
1
16 hr
48 hr
72 hr
96 hr
Day 7
D.
No EP
hAID
Timepoint 16h KDa 16h 48h 72h 96h d7 KDa
Cas9 protein
β-actin - (42kDa)
- hAID (201.60kDa)
-SpCas9 (160KDa)
Band intensity [x10⁴]
1000
100
10
1
16 hr
48 hr
72 hr
96 hr
Day 7
E.
No EP
hA3A
Timepoint d7 KDa 16h 16h 48h 72h 96h KDa
Cas9 protein
β-actin - (42kDa)
- hA3A (201.72kDa)
-SpCas9 (160KDa)
Band intensity [x10⁴]
1000
100
10
1
16 hr
48 hr
72 hr
96 hr
Day 7

Figure 3-6 Temporal (16 - 72 hours) analysis of editor expression using serial Western blot

A. Western blot from non-edited cells (n=1) were used as negative controls. Purified SpCas9 protein (15.6 ng), was used as a positive control. β-actin staining was used as a loading control. **B.** Serial sampling of cells electroporated with SpCas9 mRNA post electroporation (n=1). Highest intensity of SpCas9 staining visible at 16 hours and had mostly dissipated by day 7. **C.** Serial sampling of cells electroporated with coBE3 mRNA (n=1). BE3 protein appeared highly expressed at 16 hours, but had mostly dissipated by 16 hours post electroporation. **D**. Serial sampling of cells electroporated with hAID mRNA (n=1). hAID protein appeared highly expressed at 16 hours, slightly detected by 48 hours but starting dissipating by 72 hours post-electroporation. **E.** Serial sampling of cells electroporated with hA3A mRNA (n=1). Loading positions have been adjusted, day 7 sample was plotted first before the no EP sample. hA3A protein appeared highly expressed at 16 hours, with gradual loss over subsequent measurements. Band intensity was calculated for each protein band expressed on Western blot using Image Lab software.

3.3.2 Screening for predictable major translocation events

One of the key advantages of using base editors lies in their reduced potential for causing genomic aberrations, particularly when targeting two or more genomic loci simultaneously. Previous studies have linked translocation events to gene editing tools like, TALENS, and CRISPR/Cas9 because of their reliance on dsDNA break formation (111, 262, 308, 339). Data screening for signatures of NHEJ were reassuring in that BE activity was not associated with dsDNA break and repair by Cas9 nuclease effects. For further reassurance, potential translocation events between two previously edited genomic loci, *CD7* and *TRBC* were identified using targeted PCRs. Genomic DNA from three primary T cell donors previously shown to have high levels of editing at TRBC ex1-2 and CD7 ex2 with each editor **(Figure 3-2, 3-3 and 3-4)** were analysed for the presence of translocations using primers designed to amplify chromosomal fusions between the *TRBC* locus on the q-arm of chromosome 7 and the *CD7* locus on the q-arm of chromosome 17 (**Figure 3-7**).

Gel electrophoresis of PCR products from genomic DNA extractions showed the presence of all predicted translocation events in control SpCas9-treated samples (n=3), while as expected, none were detected in unmodified control samples (**Figure**

3-8 A). Sanger sequencing of DNA from the bands seen in SpCas9 treated samples confirmed positive alignment across all three donors with the predicted chromosomal fusions. Importantly, DNA bands corresponding to the four chromosomal fusions were absent across all cells edited with coBE3, hAID and hA3A suggesting no translocations were occurring (**Figure 3-8 A&B**). Where bands were detected, subsequent Sanger sequencing analysis was performed to confirm that these bands were non-specific and not indicative of chromosomal translocations.

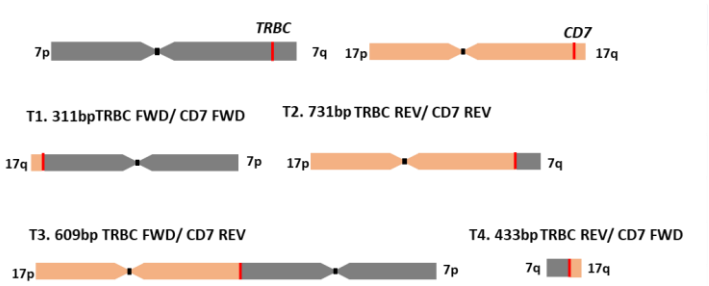

Figure 3-7 Molecular analysis corroborates the absence of chromosomal translocations in base-edited cells compared to conventional Cas9-treated cells

The four translocations that are predicted to occur upon simultaneous cleavage between *TRBC* and *CD7* loci (T1-T4). Schema of chromosomes *TRBC* (grey) and CD7 (orange), with a red line indicating the approximate location of TRBC ex1-2 and CD7 ex2 protospacer binding. FWD: forward primer, REV: reverse primer.

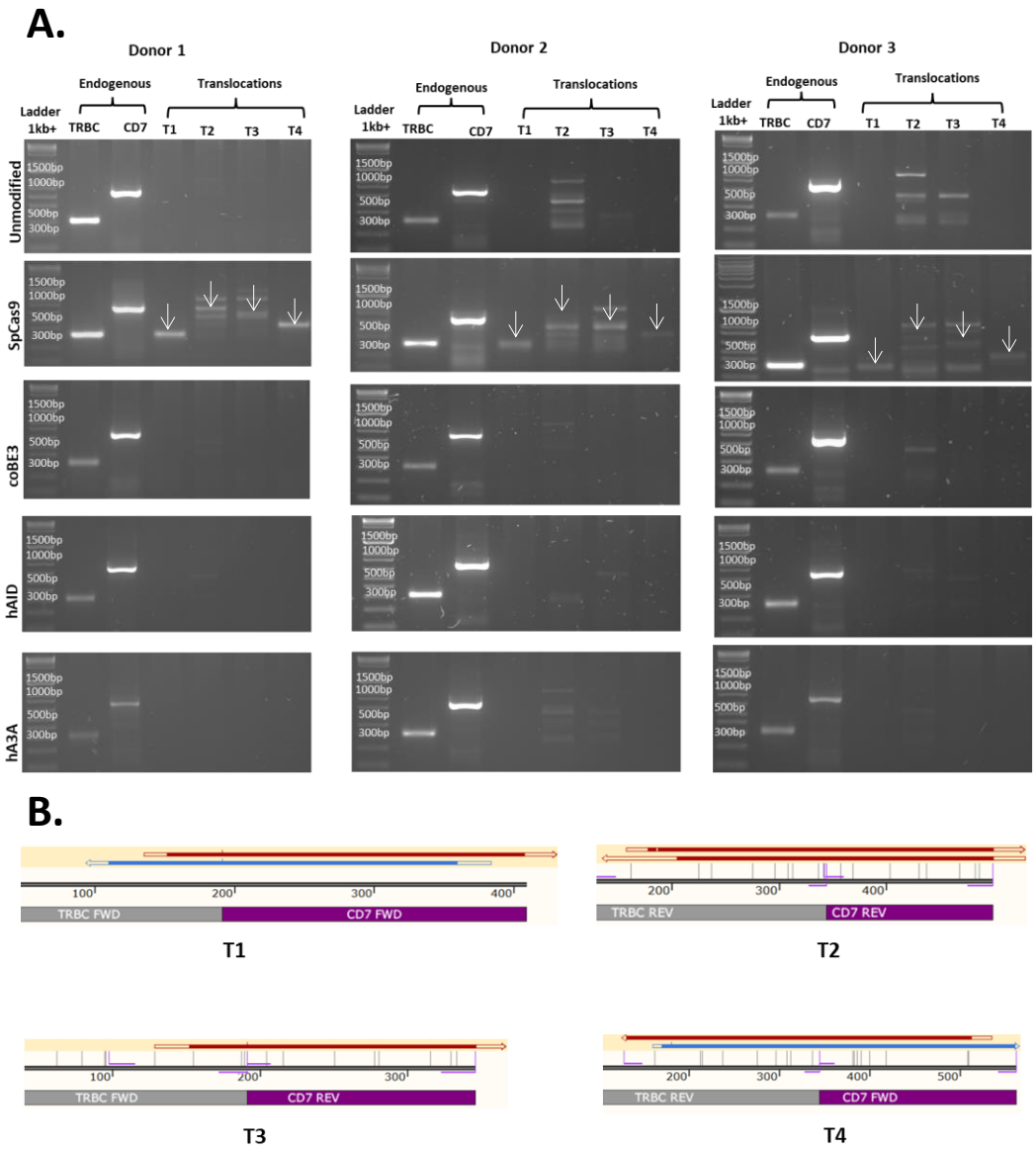

Figure 3-8 Comparison of reduction in large translocation events with CBEs (BE3, hAID, and hA3A) versus SpCas9 editing in primary human T cells

A. Gel electrophoresis of DNA products (n=3) from either unmodified or edited with SpCas9 or CBEs (coBE3, hAID and hA3A) mRNA following PCR amplification with TRBC Fwd – CD7 Fwd, TRBC Rev – CD7 Fwd, TRBC Rev – CD7 Rev and TRBC Fwd – CD7 Rev combinations of primers. PCR amplification from n=3 donors of the *TRBC* and *CD7* loci spanning the protospacer binding site, as well as the four predicted translocation events (T1-T4), T1=311 bp, T2=731 bp, T3=609 bp, T4=433 bp. Positive bands seen in SpCas9 treated samples (T1-T4) point to the predicted translocation events. Bands seen in unmodified samples are non-specific and confirmed by sequencing. **B.** Snapgene maps of the four predicted translocation events (T1-T4), showing alignment of Sanger sequence traces from positive translocation bands from SpCas9 edited cells.

3.4 Comparative analysis of deamination efficiency using pCCL-CAR7

Lentiviral vector stocks for pCCL-CAR7 were produced as previously described through transient transfection of HEK293T cells (Chapter 2, Section 2.2.10) (**Figure 3.9 A**). The virus particles were collected at two time points and concentrated using ultracentrifugation. The viral titre was determined by transducing HEK293T cells with serial dilutions of the virus stock, and flow cytometry analysis assessed the expression of the CAR transgene. High titre lentiviral vector was produced for pCCL-CAR7 of $1.2x10^8$ transducing units per mL (TU/mL).

Primary T cells were electroporated with a mixture of CD7 and TRBC sgRNAs at 10 µg/mL and 50 µg/mL mRNA of each of the editors. SpCas9 mRNA was used alongside as a positive control of CD7 disruption. T cells were then transduced with pCCL-CAR7 at MOI 5 24 hours post-electroporation and cell pellets collected at 48hr, 96hr, and 7 days post mRNA delivery.

Phenotypic analysis of transduced cells at day 4 showed similar CAR7 transduction efficiency across all samples ranging between 60% to 77%. Notably, high knockout of CD7 was seen with SpCas9, hA3A and coBE3 (69%, 68%, 62%, respectively, gated off CD2+), followed by hAID with 40% CD7 knockout. With all editors, a remarkable level of TCRαβ disruption, ranging from 87% to 98%, was consistently achieved (**Figure 3-9 B&C**).

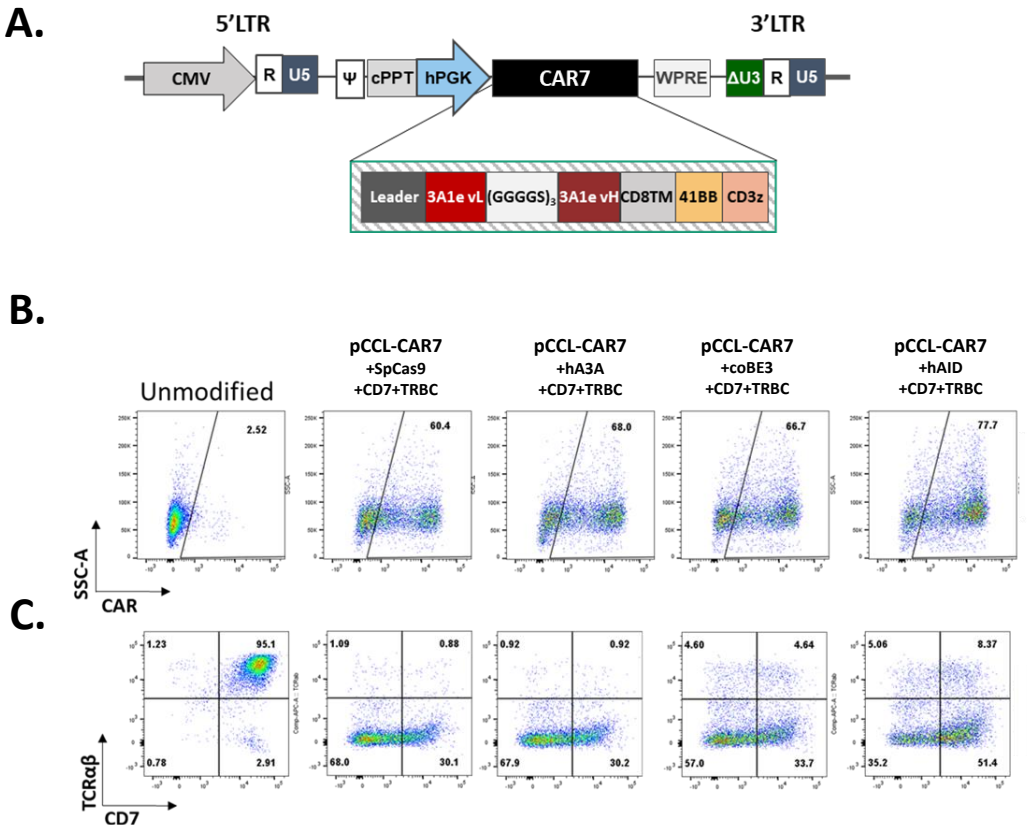

Figure 3-9 Comparing editing efficacy of *CD7* locus and *TRBC* locus with pCCL-CAR7 vector, using different base editor iterations

A. Schematic representation of pCCL-CAR7 plasmid configuration expressing CAR7 with 41BB/CD3ζ activation domains **B**. Flow cytometry analysis of CAR7 expression (n=1) at MOI5, gated-off CD2+ cells. **C.** CD7 and TCRαβ knockout at day four post electroporation (n=1) indicating high double negative population with SpCas9, hA3A, and coBE3, with moderate double negative with hAID.

Molecular investigation of the *CD7* locus of base edited CAR7 cells 7 days post-electroporation revealed high levels of on-target C8 C>T conversion. Among the editors, hA3A achieved an efficiency of 100%. Editing using coBE3 and hAID, while not as efficient, was still moderately high at 78% with both editors (**Figure 3-10 A&B**). As seen above hA3A showed high editing at the *TRBC* locus with G>A conversion reaching 100% at both G5 and G6. Although as described previously hA3A induced substantial G>A conversions outside the editing window (G1 (27%), G2 (54%), G3 (78%), G11 (79%)). Outside-of-window editing was not observed when using BE3 while retaining highly efficient editing within the window (99% at G5 and 55% at G6).

Efficacy was slightly reduced when using hAID (60% G>A conversion at G5 and 44% at G6), with no editing detected outside the editing window (**Figure 3-10 C&D**).

Analysis of SpCas9 control group showed indel frequencies of around 94% at both the *CD7* and *TRBC* loci (**Figure 3-11**), while importantly the molecular profile for all base editors (coBE3, hA3A, and AID) was verified to be indel-free.

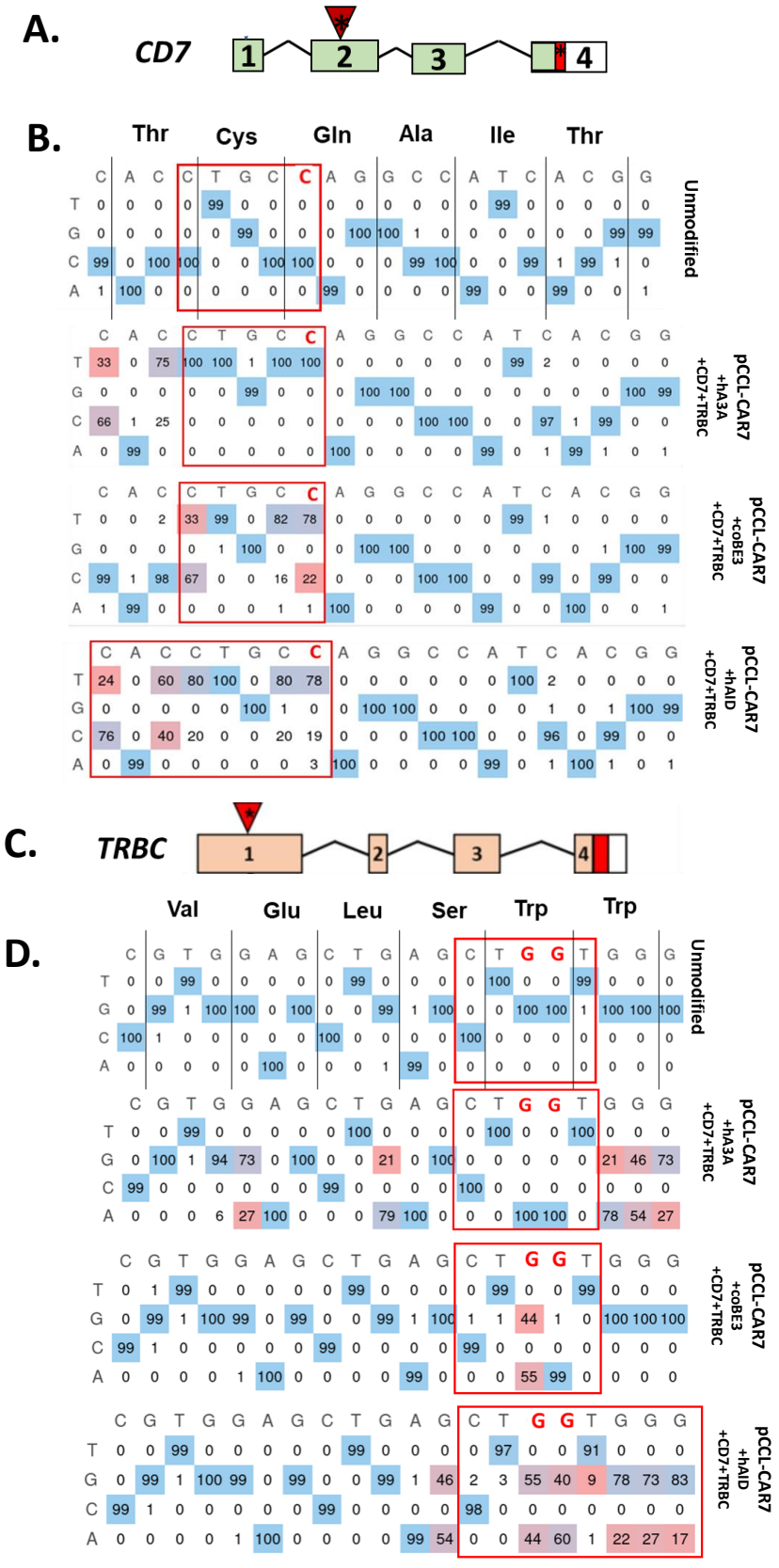

Figure 3-10 Molecular verification of CD7 and TCRαβ disruption in pCCL-CAR7 edited cells

A. Schematic of exonic regions within *CD7* gene. The red marking in exon 2 of *CD7* represents the genomic translation stop site, followed by 5' untranslated regions (white box). The red triangle with asterisk indicates the position of the base conversion that led to premature stop codon formation. **B.** EDITR output of Sanger sequencing results of *CD7* genome editing (n=1). The anticipated base conversion sites are shown in red boxes. The unmodified negative control showing no editing. The percentage of C>T conversion throughout CD7-targeting protospacer and on target C8 leading to a premature STOP codon in exon 2 (Gln115*), using hA3A, coBE3, and hAID. **C.** Schematic of exonic regions within *TRBC* gene. The red marking in exon 1 of *TRBC* represents the genomic translation stop site followed by 5' untranslated regions (white box). The red triangle with an asterisk indicates the position of the base conversion that led to premature stop codon formation. **D.** EDITR output of Sanger sequencing results of TRBC genome editing (n=1). The unmodified negative control showing no editing. The anticipated base conversion sites are shown in red boxes. The percentage of G>A (antisense) conversion throughout TRBC-targeting protospacer conversion at position G5 and/or G6 leading to the generation of a premature STOP codon in exon 1 (Trp44*), using hA3A, coBE3, and hAID.

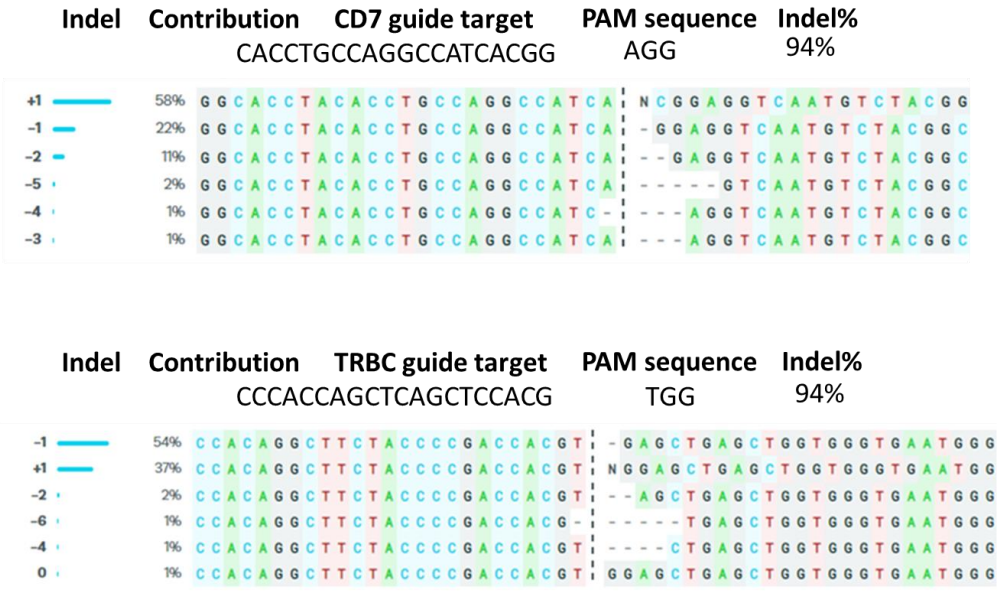

Figure 3-11 Detection of insertions/deletions (indels) created by SpCAS9 in pCCL-CAR7 transduced cells

The on-target editing effects of DNA extracted from primary T cells treated with SpCas9 + sgRNA for CD7 and TRBC (n=1) were measured by direct sequencing and bioinformatic analysis using Tracking of Indels by Inference of CRISPR Edits (ICE) software for signatures of non-homologous end joining (NHEJ) demonstrating efficient disruption at both target sites. Quantification of on-target editing was accomplished

using direct sequencing, and bioinformatic analysis of indels following NHEJ repair confirmed multiplexed knockout. PAM, protospacer adjacent motif.

3.4.1 Screening for ectopic cytosine deamination effects

Current CRISPR/Cas9 base editors employing rAPOBEC1, including coBE3, have induced off-target DNA and RNA edits through deamination across the entire transcriptome, affecting both protein-coding and non-coding regions (319, 320, 325, 327, 340).

One particular concern revolves around the possibility of deamination-mediated editing of the scFv antigen recognition elements. The process of somatic hypermutation in antibody variable regions of B cells, mediated by human cytidine deaminase, is known to enhance receptor diversity (341). However, if such deamination events occur at either the DNA or RNA level within the CAR scFv sequence region, then target recognition could be deviated.

To address these concerns, I investigated the potential for promiscuous deamination effects on scFv antigen recognition elements that confer CAR antigen specificity. Total RNA was extracted from SpCas9 and CBE mRNA modified T cells at 48 hours and day 7 post-electroporation. cDNA of CAR scFv were generated using universal primers flanking the CAR sequences as described in Section 2.2.26 and the PCR products were verified by gel electrophoresis. Amplification of Glyceraldehyde-3-phosphate dehydrogenase (GAPDH) across exons 2 and 3 was used as a control for RNA extraction and cDNA production (**Figure 3-12**).

Samples were prepared and analysed by next generation sequencing (NGS) for cytidine-specific base conversion. NGS analysis performed by Dr Gough, with a focus on the heavy and light antigen binding regions (ABRs). The quantification of cytidine transitions and transversions suggested that C>N transitions were uncommon, occurring across SpCas9 and CBEs edited samples, and generally ranged from 0% to 1% in the ABRs (**Figure 3.13 A**). Notably, there was minimal C>T conversion across the entire CAR transgene in either spCas9 or CBEs edited cells and the frequency of

events detected 48hrs after mRNA delivery was comparable to that observed after the end of production on day 7 **(Figure 3.13 B**). These findings indicate that there were no signs of sustained mutational corruption of antigen specificity in CAR-T cells resulting from base editing from any of the editors tested.

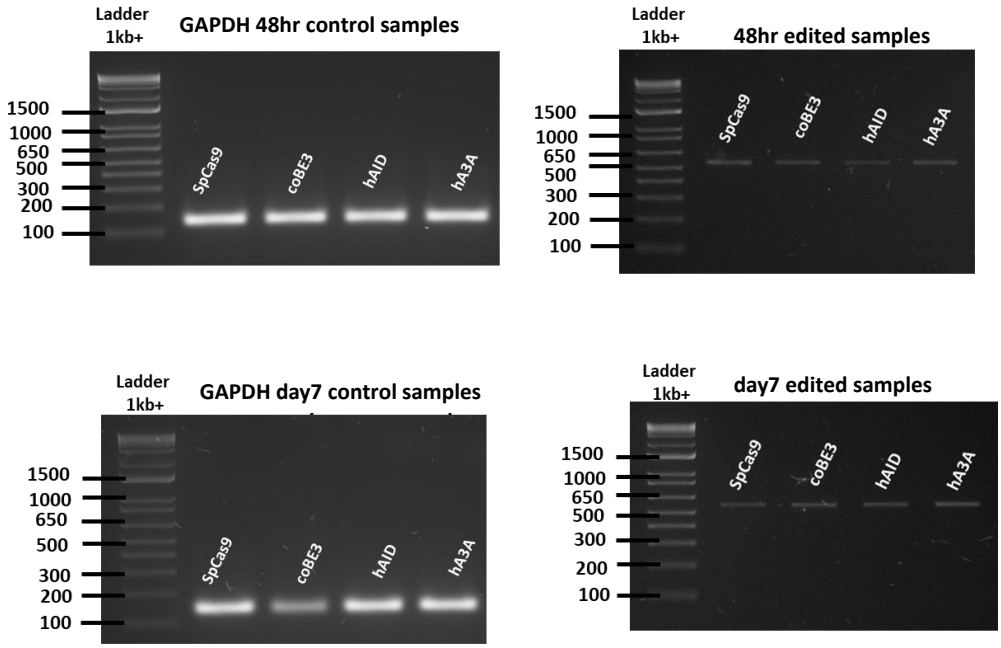

Figure 3-12 Amplification of CAR scFv from edited cells with SpCas9, coBE3, hAID or hA3A, at 48hr and 7days

Successful amplification of CAR scFv cDNA from primary T cell samples treated with different editors SpCas9, coBE3, hAID, and hA3A. Gel image showing predicted band size with the adaptor 552 bp at 48hr and 7days. GAPDH was used alongside as a positive control with band size of 143 bp.

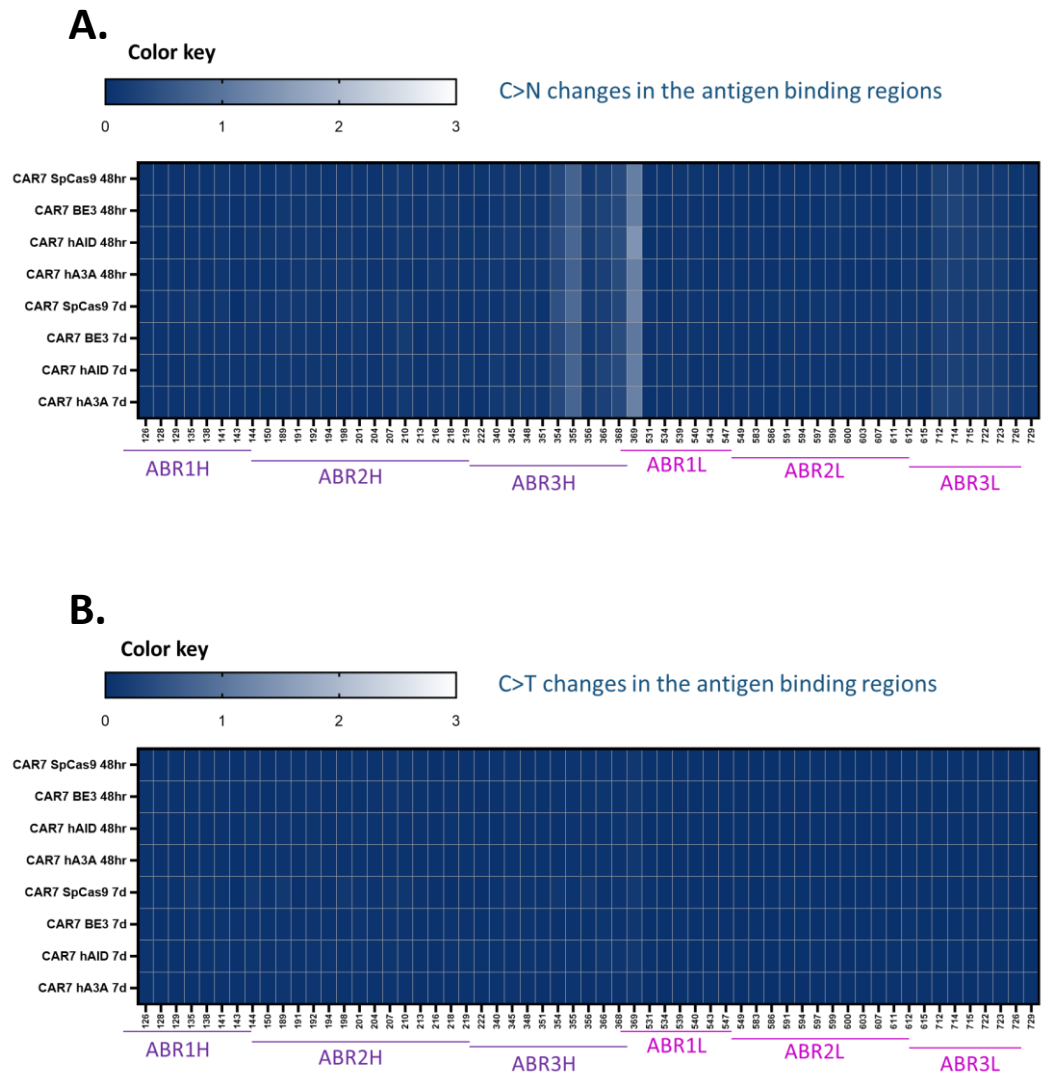

Figure 3-13 Cytidine deamination displays lack of promiscuous editing of CAR sequences

Serial examination of CAR7 scFv RNA sequences (n=1) 48 hrs and 7days after electroporation with SpCas9, coBE3, hAID, or hA3A mRNA. **A.** Amplicons of CAR7 vH and vL sequences including ABR presented mapped as heatmap using the *gplots* library for C>N conversion rates at the marked location. **B.** CAR7 scFv ABR presented mapped as a heatmap for C>T conversion rates. ABR: antigen binding regions. vH: variable heavy, vL: variable light. The colour key denotes the editing percentage, ranging from 0% represented by dark blue to the maximum of 3% indicated by white. As the editing percentage increases, the dark blue shade gradually lightens until it reaches white at 3%.

3.5 Chapter summary

This chapter explores the application of cytidine base editing technology towards multiplexed gene knockout, with the ultimate goal of creating 'universal' CAR-T cells capable of circumventing fratricide effects. The initial experiments were conducted on primary T cells to assess the genome-editing efficacy of several base editors, including coBE3, hA3A, and hAID.

Remarkably, efficient multiplexed indel-free disruptions of both *TRBC* and *CD7* loci in primary T cells was achieved using human-derived CBE versions or ratAPOBEC1 control. The high editing percentage of C observed within the optimal editing window leading to conversion of all C>T, is not a concern for several reasons. Firstly, it's important to note that editing within this window is expected, as it falls under the influence of the base editor deaminase enzyme's optimal activity window. This means that the enzyme is most effective at inducing edits within this specific genomic region, leading to a higher frequency of editing events observed therein. Since our primary objective is gene knockout rather than introducing specific amino acid substitutions, the occurrence of these C>T alterations is in line with our ultimate goal and does not deviate from our intended outcome.

hA3A-BE editor demonstrated particularly high levels of wider C>T conversion outside the predicted editing window, highlighting both efficiency and fidelity of editing as crucial factors for downstream applications.

In terms of transient protein expression, all editors had transient expression except for SpCas9, where Cas9 protein was detected up to 7 days post-electroporation. This transient effect may reduce the likelihood of off-target editing. The expression of coBE3 and hAID had dissipated after 16 hours, while hA3A persisted for 72 hours.

This chapter further shows that CBE allows multiplex knockout without the chromosomal aberrations seen in SpCas9-treated samples. Interestingly, the study did not find detrimental changes in the antigen-binding regions of the scFv for CAR7,

suggesting that the tested CBEs did not affect antigen-binding specificity when delivered transiently as mRNA. The next chapter aims to explore the generation of CAR7 or CAR3 cells using base editing variants by the terminal lentiviral vector platform.

Chapter 4 Base editing with lentiviral vectors incorporating 3' sgRNA expression cassettes

4.1 Introduction

Our group previously reported the generation of anti-CD3 and anti-CD7 CAR-T cells, by removal of shared antigen expression (CD3 or CD7) prior to CAR expression to limit fratricide during manufacture (72, 101). Similarly, to overcome fratricide effects, CRISPR/Cas9 genome editing has been used to knock out CD7 expression in CAR-T cells, allowing CAR-T cells to expand without impairing their antitumour effect (71).

In this chapter, I investigate coupled cytidine deamination using BE3 of shared TCRαβ antigen to CAR expression using the terminal CRISPR/CAR platform. The lentiviral plasmid configuration described places a second-generation CAR transgene under the control of an internal human phosphoglycerate kinase (hPGK) promoter, whereas CRISPR sgRNA expression is driven off a human U6 promoter (**Figure 4-1 A**). This lentiviral vector configuration is referred to as "terminal-CRISPR" because the sgRNA expression cassette is integrated within the ΔU3 region, of the 3' LTR (329). The incorporation of the sgRNA expression cassette into the 3' LTR exploits the lentiviral lifecycle, in which this region is duplicated to the 5' LTR by reverse transcription of the ssRNA viral genome, thereby increasing transcription levels while minimising interference with transgene expression (**Figure 4-1 B**). The results from Chapter 3 demonstrated that high knockout efficiency similar to SpCas9 can be achieved at both *TRBC* and *CD7* loci when using CBEs. Achieving comparable efficiencies from a vector expressed TRBC sgRNA from a 'terminal' vector remains a possibility. These configurations allow coupling of knockout and CAR expression and have been used in trials with highly homogenous CAR19+TCR- T cell products (73).

Therefore, the aim of this chapter is to evaluate the adaptability of the terminal CRISPR lentiviral vector, which couples a cytidine deaminase-specific sgRNA targeting TRBC1/2, for the generation of "universal" fratricide-resistant CAR3 and CAR7-T cells. Additionally, I seek to investigate whether the timing of knockout would be influenced by using the terminal configuration with the coupled TRBC sgRNA, as

compared to using the pCCL lentiviral vector with free sgRNA. Furthermore, the chapter aims to explore the generation of CAR7 or CAR3 cells using alternative base editing variants (AID-BE3 and APOBEC3-BE3) by the terminal lentiviral vector platform.

4.2 Generation of lentiviral plasmids with 3' sgRNA expression cassettes

Initial work involved the transfer of human codon-optimized CAR3 and CAR7 transgenes from a 3rd generation pCCL lentiviral backbone into a 3rd generation SIN terminal-CRISPR lentiviral vector configuration under the transcriptional control of a human PGK RNA polymerase II (Pol II) promoter (Section 2.2.2). Restriction digestion was used to cut out the CAR7 and CAR3 sequences with BpiI restriction enzyme, resulting in predicted product sizes of 1465 bp and 1482 bp, respectively (**Figure 4-1 C**). Each of these sequences was next ligated into a linearised 'terminal' lentiviral backbone, and Sanger sequencing confirmed successful insertion.

The TRBC1/2-specific sgRNA used in the previous chapter was subsequently cloned into the ΔU3 region of the 3'LTR under the control of an RNA polymerase III human U6 promoter. These constructs are hereon referred to as Terminal TRBC-CAR3 (TTRBC-CAR3) and Terminal TRBC-CAR7 (TTRBC-CAR7).

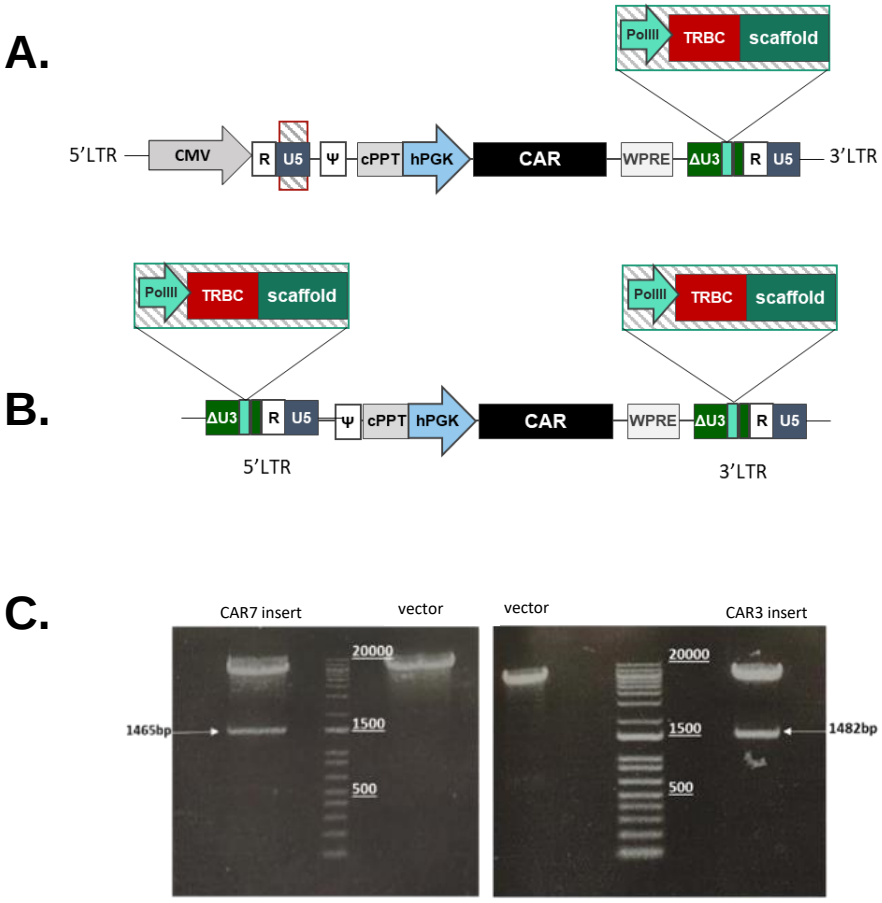

Figure 4-1 Terminal-CRISPR configuration coupling lentiviral sgRNA and CAR expression

A. Third-generation self-inactivating (SIN) lentiviral plasmid DNA configuration, coupling CAR transgene expression from an internal RNA Pol II promoter, and T cell receptor beta constant (TRBC) specific single guide RNA (sgRNA) from an RNA Pol III promoter (U6), inserted in the deleted unique 3' (ΔU3) region of the 3' long terminal repeat (LTR). This plasmid configuration is referred to as terminal-TRBC-CAR. **B.** Following reverse transcription and integration of the single-stranded RNA (ssRNA) lentiviral genome, the proviral DNA of the TTRBC-CAR vector exhibits duplication of the 3' ΔU3 region, copying the sgRNA expression machinery into the proviral 5'LTR. **C.** Restriction digestion and agarose gel electrophoresis of expected CAR7 (1465 bp) and CAR3 (1482 bp) DNA bands before ligation into lentiviral 'terminal' plasmid. hPGK: human phosphoglycerate kinase promoter, cPPT: central polypurine tract, WPRE: woodchuck post-transcriptional regulatory element. Ψ: Psi, R: repeat R region, CMV: Cytomegalovirus.

4.2.1 'terminal-CRISPR' lentiviral vector stock production

In order to generate the lentiviral vector stocks, the transient transfection of HEK293T cells was carried out using a transfer plasmid, and third-generation lentiviral packaging plasmids. The viral particles were collected from the culture media at 48 and 72 hours post transfection and concentrated using an ultra-centrifuge.

To determine the lentiviral titre, HEK293T cells were transduced with serially diluted viral stock. The CAR transgene expression was checked using flow cytometry. The viral titre was calculated based on the percentage of transduced cells at a specific viral vector dilution (Section 2.2.10).

Lentiviral vectors with high titre were produced for TTRBC-CAR3 and TTRBC-CAR7 of $5.6x10^8$ transducing units per mL (TU/mL) and $1.5x10^8$ TU/mL respectively (**Figure 4-2 A&B**). Additionally, a TTRBC-CAR19 was used as a process control, achieving the titre of $6x10^8$ TU/mL (**Figure 4-2 C**).

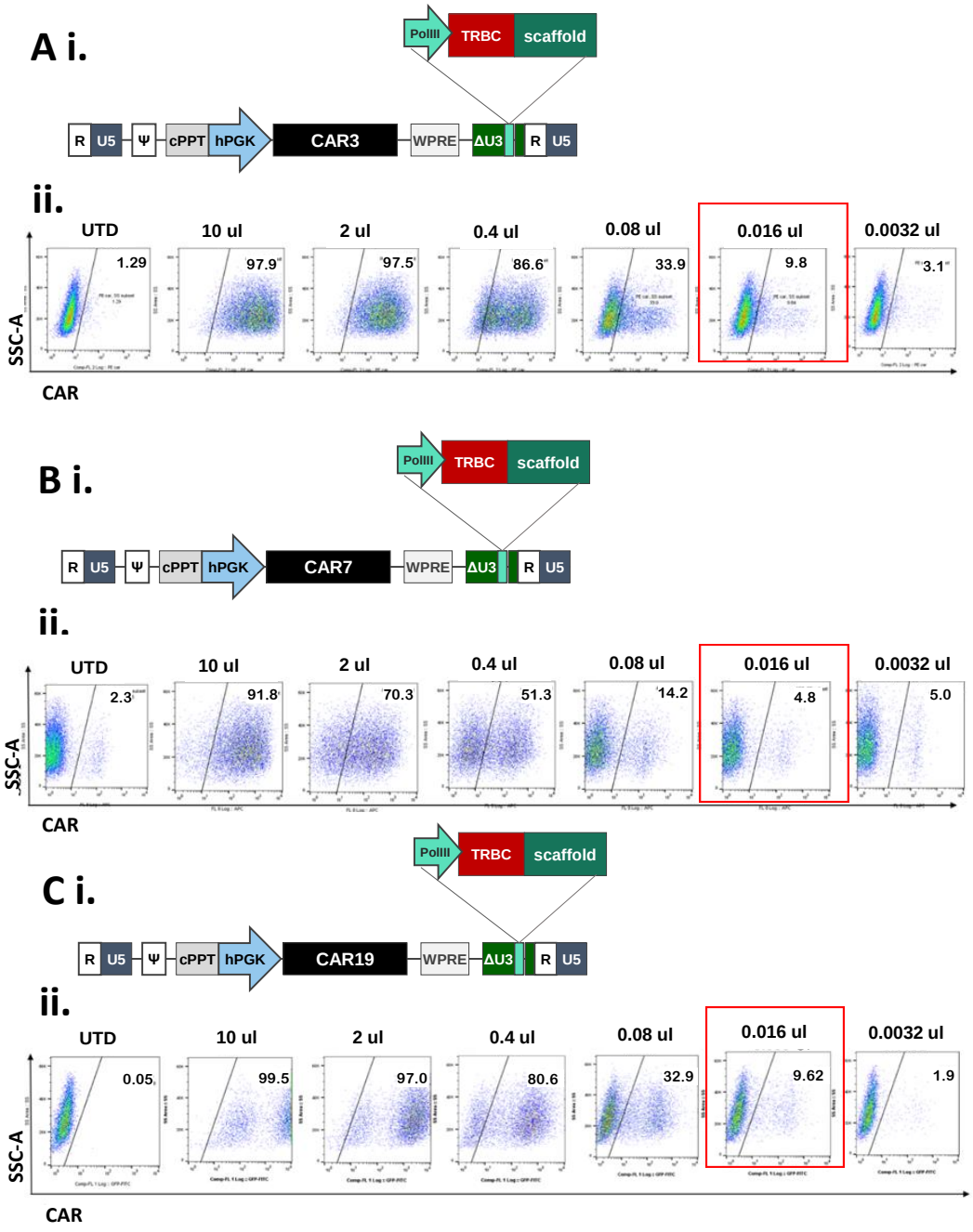

Figure 4-2 Titration of CAR vector stocks

A (i). Schematic representation of terminal TRBC-CAR3 plasmid configuration. **A (ii).** Flow cytometry analysis demonstrating TTRBC-CAR3 transduction efficiency using serial dilution of concentrated virus supernatant titre of $5.6x10^8$ TU/mL was achieved. The dilution of 0.016 µL was chosen to calculate the titre. **B (i).** Schematic representation of terminal TRBC-CAR7 plasmid configuration. **B (ii).** Flow cytometry plot data demonstrated virus (TTRBC-CAR7) transduction efficiency using serial dilution of concentrated virus supernatant titre of $1.5x10^8$ TU/mL was achieved. The dilution of 0.016 µL was chosen to calculate the titre. **C (i)**. Schematic representation of TTRBC-CAR19 plasmid configuration. **C**

(ii). Flow cytometry titration plot of TTRBC-CAR19 titre of $6x10^8$ TU/mL was achieved. The dilution of 0.016 µL was chosen to calculate the titre. UTD: un-transduced, cPPT: central polypurine tract, hPGK: human phosphoglycerate kinase promoter.

4.3 Terminal TRBC-CAR7 and terminal TRBC-CAR3 transduction of primary T cells

During the pilot investigation to access the vectors' ability to support CAR expression, TTRBC-CAR7 and TTRBC-CAR3 lentiviral vectors were used to transduce primary human T cells. However, in this initial experiment, genome editing was not used to remove shared antigens.

This experiment involved isolating PBMCs from consented healthy blood donors (n=3) and activating them for 24 hours using TransACT reagent Subsequently, lentiviral vector transduction was carried out in activated T cells at a multiplicity of infection (MOI) of 2.5, 5, or 10 to compare transgene expression efficiency (**Figure 4-3 A**). Similar lentiviral configuration expressing CD19 targeting CAR (TTRBC-CAR19) was used as a positive control of transduction in activated T cells.

Flow cytometry analysis was carried out at 72 hours post-transduction, with resulting CAR19 expression ranging from 63% to 76.6% at an MOI of 5 (**Figure 4-3 B&C**). CAR7 expression could be detected in T cells transduced with TTRBC-CAR7 vector, ranging from 60% to 88% at MOI 5 (**Figure 4-3 B**). In contrast, no CAR3 expression was detected by flow cytometry above background at any of the tested MOIs (**Figure 4-3 B&C**).

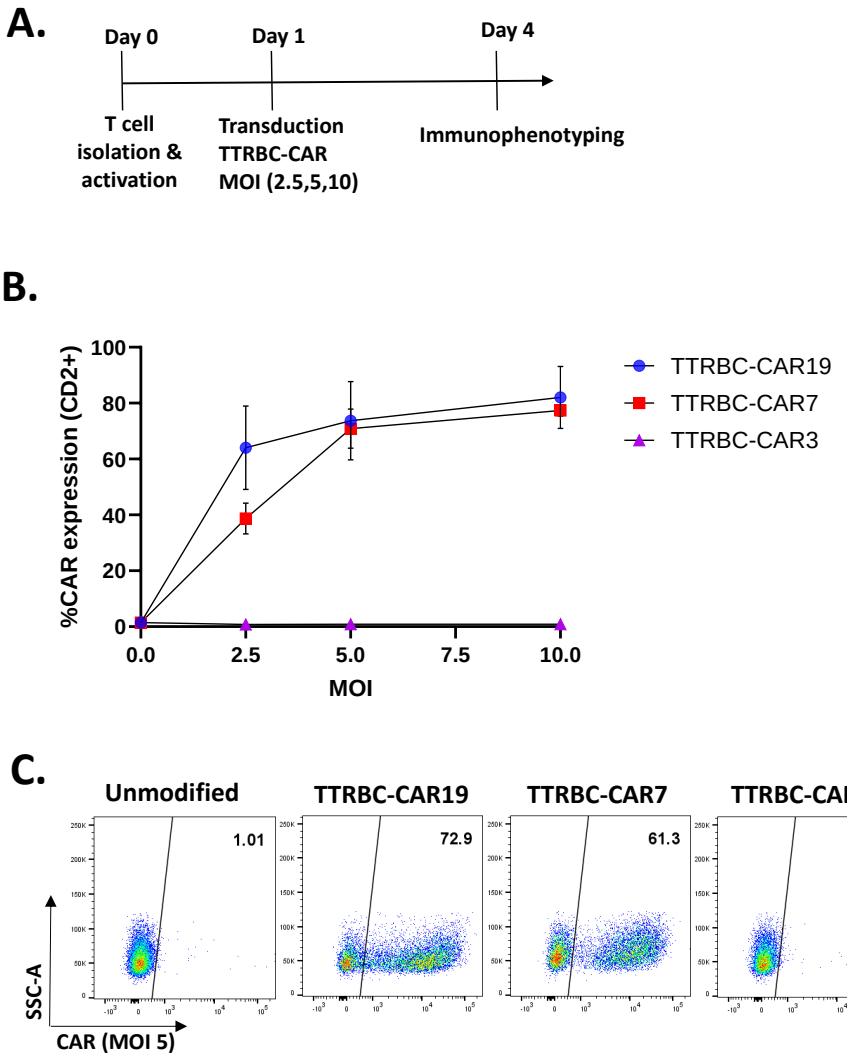

Figure 4-3 Transduction of primary human T cells with TTRBC-CAR vector

A. Experimental timeline: 24 hours following T cell isolation and activation, cells were transduced with TTRBC-CAR vectors at MOI 2.5, 5, and 10. Cells were analysed using flow cytometry at day 4. **B.** Summary of flow cytometry analysis of CAR expression at different multiplicities of infection (MOI). Gated-off CD2+ cells in n=3 donors. Error bars represent the standard deviation (SD). **C.** Representative flow plots of CAR expression at MOI 5.

4.4 Testing TCRαβ knockout coupled to CAR transduction (strategy A)

In order to test the terminal vector configurations in combination with gene knockout T cells were transduced with terminal TRBC-CAR vector expressing the TRBC sgRNA, followed by electroporation with coBE3 and CD7 sgRNA. This workflow is hereon referred to as 'Strategy A'.

Primary T cells were isolated using a Ficoll density gradient, activated with TransACT reagent before being transduced at MOI 5 with TTRBC-CAR7 or TTRBC-CAR3 vectors. Both of these terminal vector configurations incorporated a minimal U6 promoter for TRBC sgRNA expression, rather than the wild-type promoter as used above. Both wild-type and minimal U6 variants have previously demonstrated similar genome editing efficiencies incorporated into a lentiviral vector (342). Next, cells underwent electroporation with 50 µg/mL coBE3 mRNA and 10 µg/mL CD7 specific sgRNA followed by a hypothermic overnight culture at 30°C (**Figure 4-4 A**). As before, the TTRBC-CAR19 vector was used as a positive control, with unmodified cells used as a negative control. Un-transduced cells electroporated with TRBC and CD7 sgRNAs were maintained in parallel as a positive control for surface protein disruption.

The expression of CAR19 and CAR7 following transduction was similar in all three donors (70% to 85% and 74% to 80% respectively, **Figure 4-4 B**). Flow cytometry analysis 7 days post-electroporation showed between 30.2%-60% double $TRBC^{-}CD7^{-}$ knockout in un-transduced cells electroporated with coBE3 mRNA and CD7, TRBC guides, while the level of disruption in cells transduced with TTRBC-CAR19 or TTRBC-CAR7 was markedly lower due to the reduced TRBC editing, accounting for 11.5%-22.6% and 11.9%-40% $TRBC^{-}CD7^{-}$ of $CD2^{+}$ cells, respectively (**Figure 4-4 C**).

Interestingly, the CD8:CD4 ratio in T cells transduced with TTRBC-CAR7 was skewed towards CD4+ cells (CD8:CD4 ratio 1:12.4), which was not observed in the genome edited un-transduced cells or TTRBC-CAR19 transduced controls (with ratios of 1:1.2 and 1:2.2, respectively) (**Figure 4-4 D**). Similar results were observed across replicate experiment from separate T cell donors (n=3) (**Figure 4-4 E**).

Employing this strategy, a successful CAR3 product could not be generated. This can be attributed to the lack of protective TCRαβ disruption, with only a 6.3% TCRαβ knockout achieved, causing fratricide-mediated elimination of the cells (**Figure 4-4 F**).

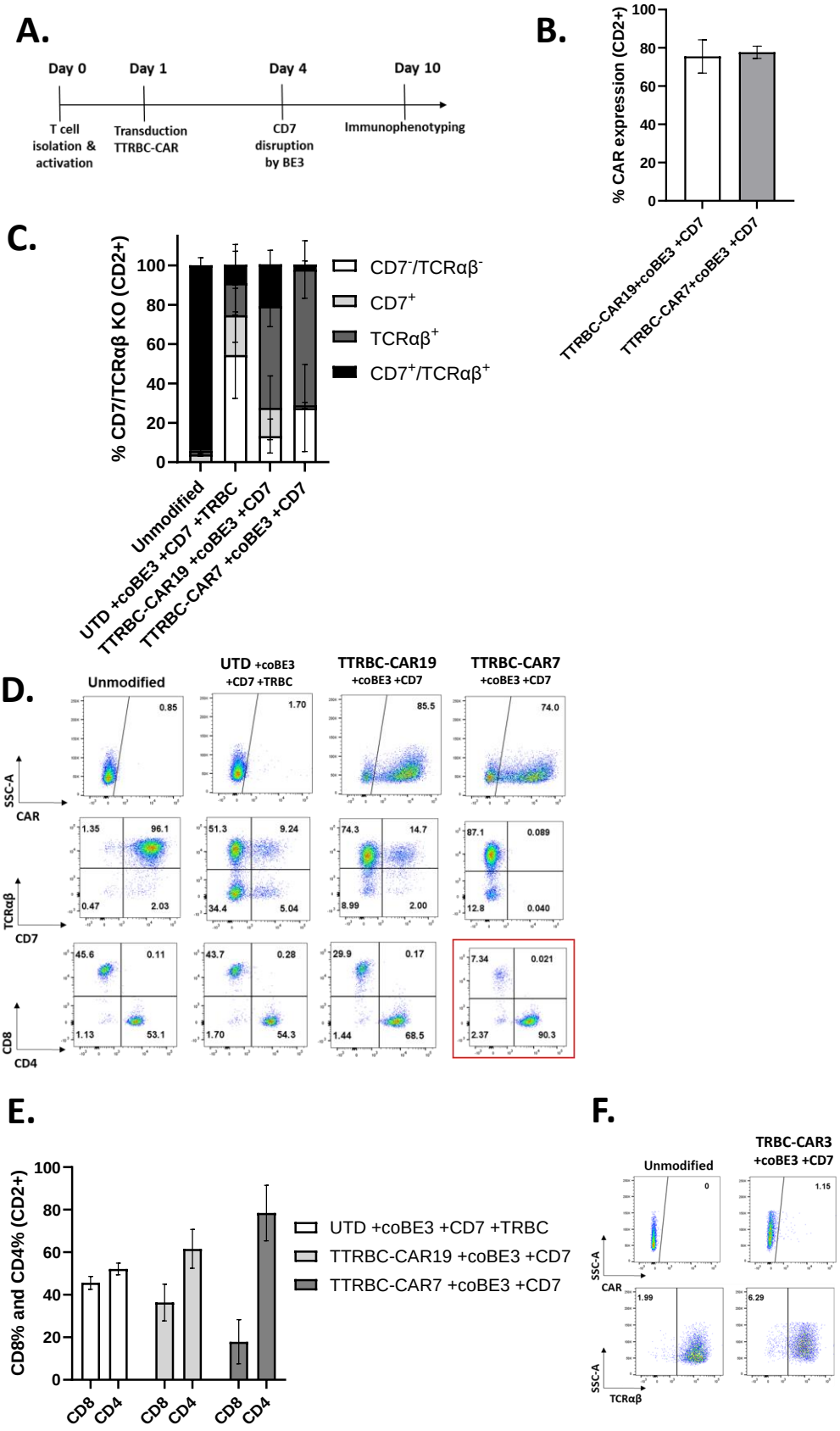
A.
Day 0
Day 1
Day 4
Day 10
T cell isolation & activation
Transduction TTRBC-CAR
CD7 disruption by BE3
Immunophenotyping
B.
% CAR expression (CD2+)
TTRBC-CAR19+coBE3 +CD7
TTRBC-CAR7+coBE3 +CD7
C.
% CD7/TCRαβ KO (CD2+)
CD7-/TCRαβ-
CD7+
TCRαβ+
CD7+/TCRαβ+
Unmodified
UTD +coBE3 +CD7 +TRBC
TTRBC-CAR19 +coBE3 +CD7
TTRBC-CAR7 +coBE3 +CD7
D.
Unmodified
UTD +coBE3 +CD7 +TRBC
TTRBC-CAR19 +coBE3 +CD7
TTRBC-CAR7 +coBE3 +CD7
SSC-A
CAR
TCRαβ
CD7
CD8
CD4
E.
CD8% and CD4% (CD2+)
UTD +coBE3 +CD7 +TRBC
TTRBC-CAR19 +coBE3 +CD7
TTRBC-CAR7 +coBE3 +CD7
CD8
CD4
F.
Unmodified
TRBC-CAR3 +coBE3 +CD7
SSC-A
CAR
TCRαβ

Figure 4-4 Base-editing-mediated chemical deamination results in CD7 disruption in primary human T cells

A. Schematic of electroporation and transduction timings; editing following CAR transduction. **B.** Summary of phenotypic analysis of CAR expression across n=3 donors gated-off CD2+ cells. The error bars represent the standard deviation (SD). **C.** Histogram representing the CD7 and TCRαβ knockout results across n=3 donors. The error bars represent the standard deviation (SD). **D.** Representative flow plots of CAR expression, CD7 and TCRαβ knockout, and CD8:CD4 ratio, the red box highlighted the skewed T cell population. **E.** Histogram showing the skew of the T cell population towards CD4 across three donors (n=3). The error bars represent the standard deviation (SD). **F.** CAR3 failed to be expressed on the surface of the T cells, and limited knockout of TCRαβ could be detected in edited cells.

Genome editing was qualified at the genomic level by PCR amplification and Sanger sequencing across the protospacer sequence, and analysed using the EditR online tool (http://baseeditr.com/). Our observations revealed high levels of editing in TTRBC-CAR7 cells electroporated with coBE3 mRNA and CD7 sgRNA, with 85% C>T conversion measured at position C8 of the target window for *CD7* (**Figure 4-5 A&B**), whereas no editing was seen in non-edited control cells. Similar levels of C>T conversion were observed at position C7 (86%). Consistent with my previous results C>T conversion was also detected outside the 4 bp-8 bp coBE3 window at position C3 (17%). Editing of C>T at position C8 in UTD cells and in TTRBC-CAR19 cells was 71% and 70%, respectively (**Figure 4-5 B**). However, while TCRαβ editing showed a 32% and 21% G>A conversion at positions G5 and G6 in UTD cells electroporated with uncoupled TRBC sgRNA, only limited conversion was detected in coBE3 mRNA electroporated TRBC-CAR19 and TRBC-CAR7 transduced cells (19% and 4%, 16% and 2% G>A at positions G5 and G6, respectively) (**Figure 4-5 C&D**).

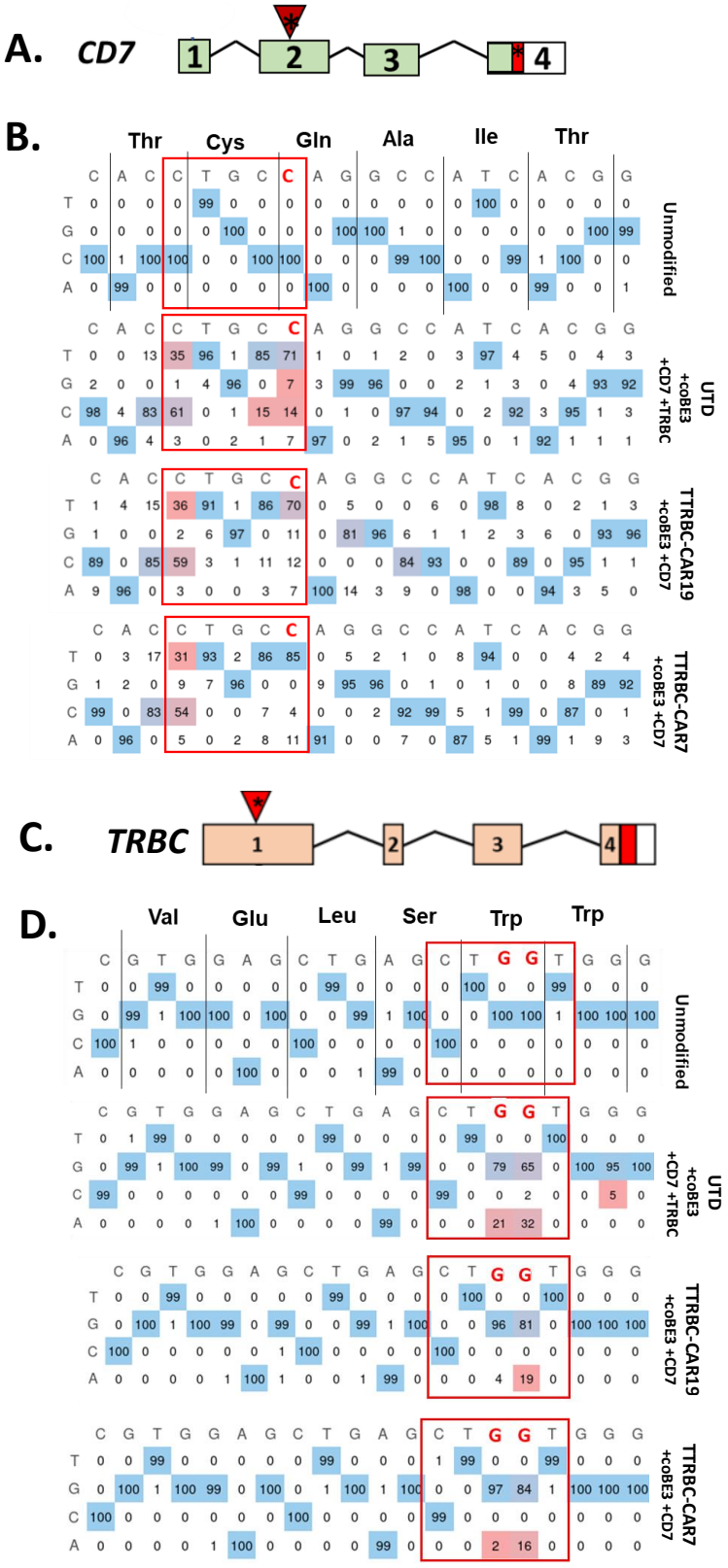

Figure 4-5 Molecular verification of CD7 and TCRαβ disruption (Strategy A)

A. Schematic of exonic regions within the *CD7* gene. The red marking in exon 2 of CD7 represents the genomic translation stop site, followed by

5’ untranslated regions (white box). The red triangle with an asterisk indicates the position of base conversion that results in a premature stop codon formation. **B.** EDITR output of Sanger sequencing results of *CD7* genome editing. The anticipated base conversion sites are shown in red boxes. The percentage of C>T conversion throughout CD7-targeting protospacer. **C.** Schematic of exonic regions within the *TRBC* gene. The red marking in exon 1 of TRBC represents the genomic translation stop site, followed by 5’ untranslated regions (white box). The red triangle with an asterisk indicates the position of base conversion that led to premature stop codon formation. **D.** EDITR output of Sanger sequencing results of *TRBC* genome editing. The anticipated base conversion sites are shown in red boxes. The percentage of G>A (antisense) conversion throughout TRBC-targeting protospacer.

4.5 Alternative order: BE3 mRNA delivery before TTRBC-CAR (Strategy B)

Due to concerns regarding fratricide, genome editing efficiency, and skewed CD4:CD8 ratios, I investigated an alternative experimental timeline. I hypothesised that perhaps coBE3 mRNA and CD7 sgRNA delivery ahead of transduction with TTRBC-CAR could be advantageous in generating a CAR+, TCRαβ-, CD7- cell population. This is hereon referred to as ‘Strategy B’.

Activated primary T cells (n=3) were first electroporated with 50 µg/mL coBE3 mRNA and 10 µg/mL CD7 sgRNA 24 hours prior to transduction (**Figure 4-6 A**). T cells were then transduced at MOI 5 with either TTRBC-CAR7, TTRBC-CAR3, or TTRBC-CAR19 coupling TRBC sgRNA and CAR transgene expression. The experimental controls included CD7-edited TTRBC-CAR19 transduced cells and un-transduced cells electroporated with uncoupled sgRNA (CD7 and TRBC).

Flow cytometry analysis at day 10 showed successful transduction, with between 43.4% - 69.5% of the cells positive for CAR7 and 54.5% - 64.2% positive for CAR19. However, it was not possible to generate CAR3 product, due to insufficient TCRαβ disruption (double knockout population 11% to 15%) ahead of CAR expression, resulting in fratricide (**Figure 4-6 B&C**).

Although high levels of surface antigen knockout were seen in un-transduced cells electroporated with coBE3 mRNA and sgRNA targeting both CD7 and TRBC (60.9% to

73.7% double knockout), little TCRαβ knockout was observed when using the terminal vector. Transduction with TTRBC-CAR19 and TTRBC-CAR7 exhibited considerably lower double knockout (11% to 23.7% and 10% to 26.9%, respectively) as a result of the lower TRBC editing (**Figure 4-6 C&D**).

The ratio of CD4:CD8 expression in n=3 T cell donors transduced with the TTRBC-CAR7 (1:1.6) still appeared mildly skewed but was more comparable to unmodified and CAR19 controls (with ratios of 1:1 and 1:1.1, respectively) (**Figure 4-6 D**).

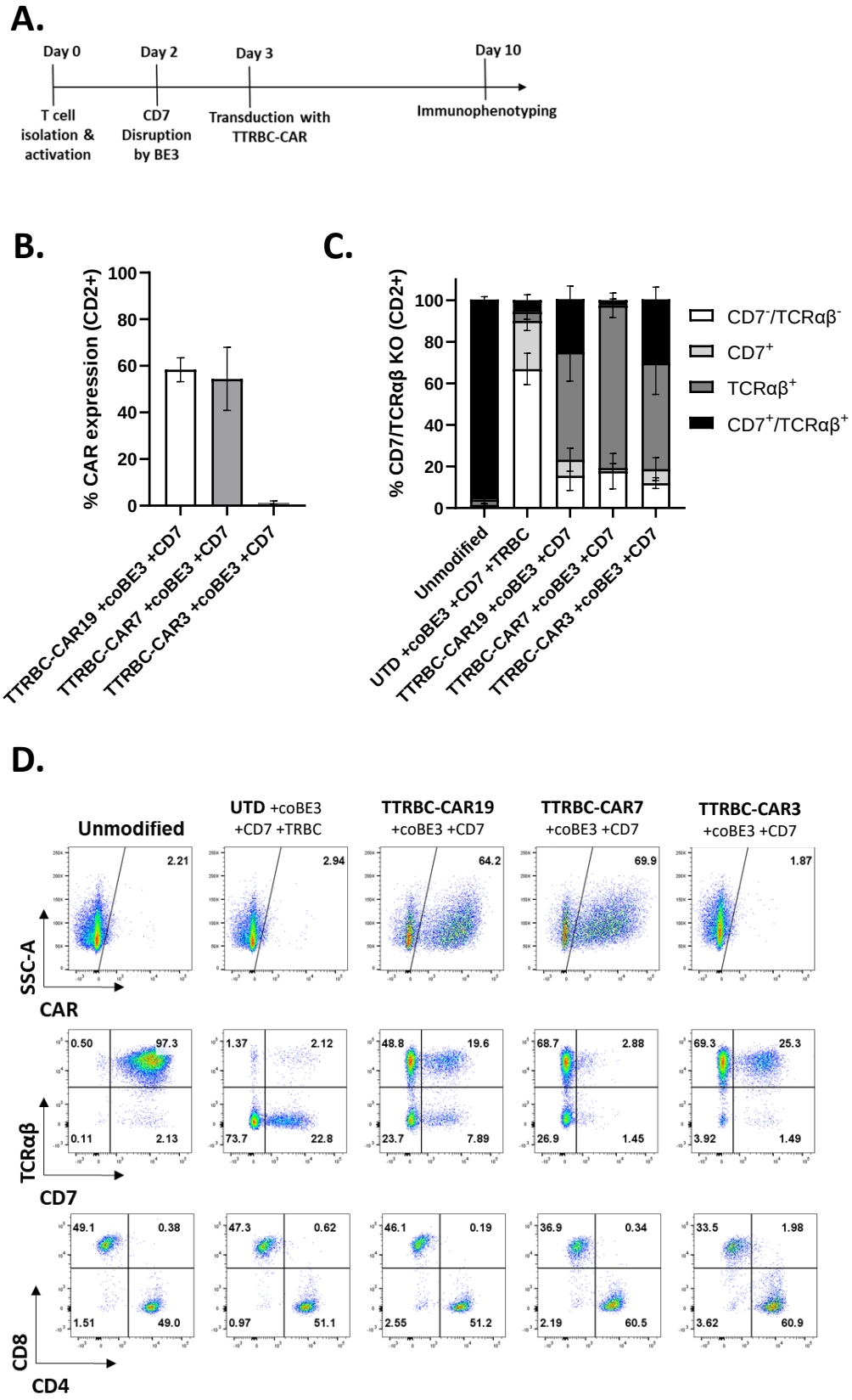
A.
Day 0
Day 2
Day 3
Day 10
T cell isolation & activation
CD7 Disruption by BE3
Transduction with TTRBC-CAR
Immunophenotyping
B.
% CAR expression (CD2+)
TTRBC-CAR19 +coBE3 +CD7
TTRBC-CAR7 +coBE3 +CD7
TTRBC-CAR3 +coBE3 +CD7
C.
% CD7/TCRαβ KO (CD2+)
CD7-/TCRαβ-
CD7+
TCRαβ+
CD7+/TCRαβ+
Unmodified
UTD +coBE3 +CD7 +TRBC
TTRBC-CAR19 +coBE3 +CD7
TTRBC-CAR7 +coBE3 +CD7
TTRBC-CAR3 +coBE3 +CD7
D.
Unmodified
UTD +coBE3 +CD7 +TRBC
TTRBC-CAR19 +coBE3 +CD7
TTRBC-CAR7 +coBE3 +CD7
TTRBC-CAR3 +coBE3 +CD7
SSC-A
CAR
TCRαβ
CD7
CD8
CD4

Figure 4-6 Strategy B - coBE3 mRNA with CD7 sgRNA delivery ahead of transduction with TTRBC-CAR

A. Timeline of experimental Strategy B: BE3 mRNA delivery and endogenous CD7 knockout occurs prior to transduction. **B.** Summary of phenotypic analysis of CAR expression (n=3) in T cell donors gated-off CD2+ cells. The error bars represent the standard deviation (SD). **C.** Histogram representing the CD7 and TCRαβ knockout results in n=3 donors. The error bars represent the standard deviation (SD). **D.** Representative flow plots of CAR expression, CD7 and TCRαβ knockout, CD8:CD4 ratio.

Sanger sequencing traces of on-target amplified genomic DNA showed high levels of editing in TTRBC-CAR7 cells electroporated with coBE3 mRNA and CD7 sgRNA, with 99% C>T conversion measured at position C8 of the target window for CD7 (**Figure 4-7 A&B**), whereas no editing was seen in unmodified control cells. Similar levels of C>T conversion were observed at position C7 (96%). Additionally, a modest C>T conversion was also detected outside the 4 bp-8 bp coBE3 window at position C3 (69%).

Similar levels of editing were also observed in genome edited un-traduced T cells (C8: C>T 70%) and in TTRBC-CAR19 cells (C8: C>T 92%), following editing with sgRNA and coBE3 mRNA (**Figure 4-7 B**). At the *TRBC* locus, 100% and 73% G>A conversion rates were seen at positions G5 and G6, respectively, in UTD cells electroporated with sgRNA TRBC, whereas no editing was seen in non-electroporated control cells. However, where TRBC sgRNA was expressed from the terminal vector no G>A conversion was detected in electroporated TRBC-CAR19 and TRBC-CAR7 (**Figure 4-7 C&D**).

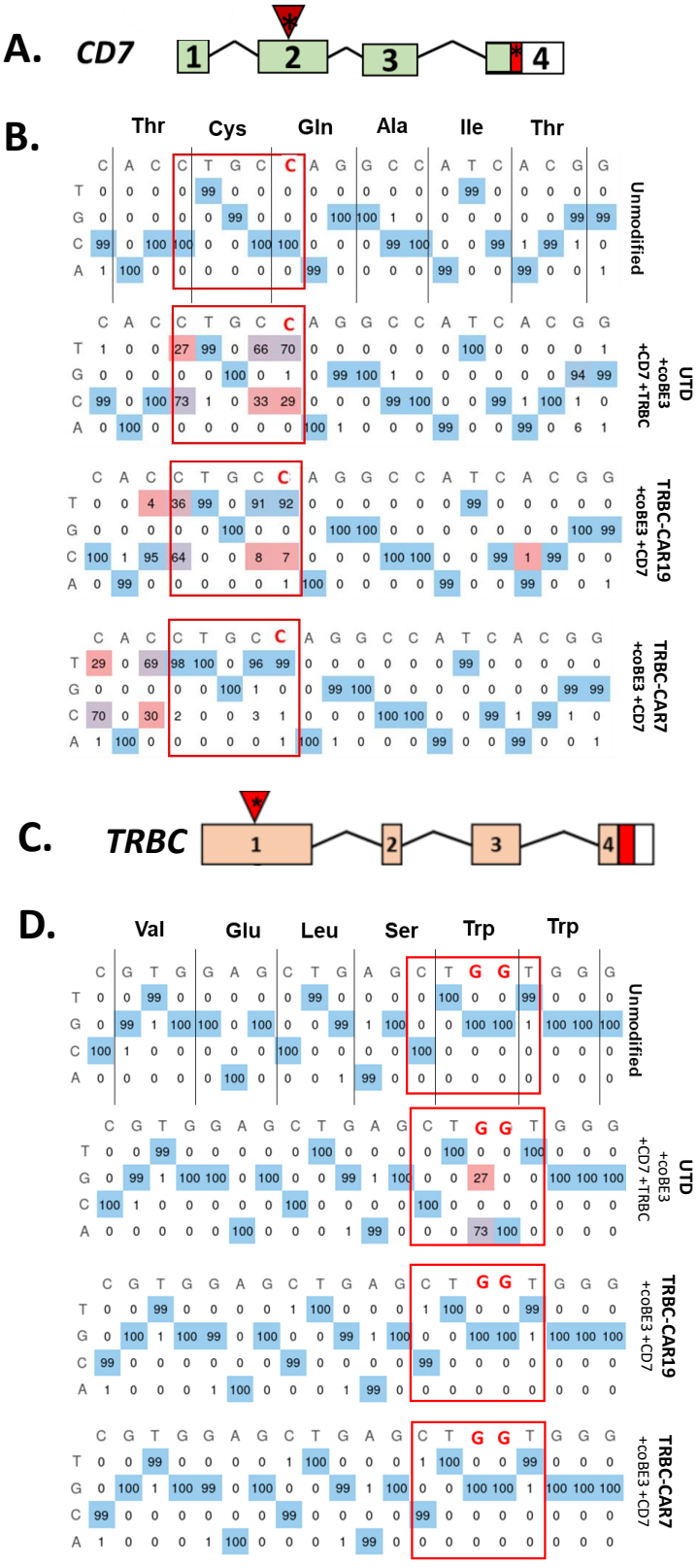

Figure 4-7 Verification of CD7 and TCRαβ disruption at the molecular level (Strategy B)

A. Schematic of exonic regions within *CD7* gene. The red marking in exon 2 of CD7 represents the genomic translation stop site, followed by 5' untranslated regions (white box). The red triangle with asterisk indicates the position of the base conversion that led to premature stop codon formation. **B.** EDITR output of Sanger sequencing results of *CD7* genome editing (n=1). The anticipated base conversion sites are shown in red boxes. The percentage of C>T conversion throughout CD7-targeting protospacer. **C.** Schematic of exonic regions within *TRBC* gene. The red marking in exon 1 of *TRBC* represents the genomic translation stop site followed by 5' untranslated regions (white box). The red triangle with an asterisk indicates the position of the base conversion that led to premature stop codon formation. **D.** EDITR output of Sanger sequencing results of *TRBC* genome editing (n=1). The anticipated base conversion sites are shown in red boxes. The percentage of G>A (antisense) conversion throughout TRBC-targeting protospacer.

4.6 TTRBC-CAR vector transduction time course

Although achieving successful TRBC knock out was not as successful as knocking out CD7 in either of the tested strategies, I reasoned that it might be possible to improve the results by determining an optimal time point for the transduction of CAR following delivery of the base editor and the CD7 sgRNA. Based on the above results, it was hypothesised that the coBE3 may have been saturated by uncoupled sgRNA or degraded before the vector contained TRBC sgRNA was expressed in the cells. This observation was based on the data from previous chapter that showed that coBE3 protein was not detectable by Western blotting 48 hours post-electroporation. To mitigate the potential fratricide effects observed when expressing the CAR7 transgene, the TTRBC-CAR19 construct was employed in the transduction time course experiment. By using TTRBC-CAR19, the risk of fratricide among the experimental CAR-T cells is minimised, allowing for a more accurate evaluation of their behaviour over the course of the transduction experiment. This approach helps to ensure that any observed effects are primarily attributed to the experimental CAR -T cells' response to the editing and transduction time rather than interference from fratricidal interactions.

To test this hypothesis, as previously described, primary T cells were electroporated 48 hours post-activation with 50 µg/mL coBE3 mRNA and 10 µg/mL CD7 sgRNA. Next,

cells were transduced at MOI 5 with TTRBC-CAR19, either immediately (0 hours) following electroporation or at 4, 8, 12 or 24 hours (**Figure 4-8 A**). Little variation was seen in transduction efficiency across the time course with the highest efficiency seen when transduction occurred immediately (0 hours) following electroporation (61%) (**Figure 4-8 A&B**). Flow cytometry analysis at the end of the experiment showed no discernible change in TCRαβ expression across the time course (**Figure 4-8 C&D**), which was confirmed at the molecular level (**Figure 4-9 A&B**). This highlights the requirement for further refinement of the selected genome editing strategy, which will be explored in the next experiments.

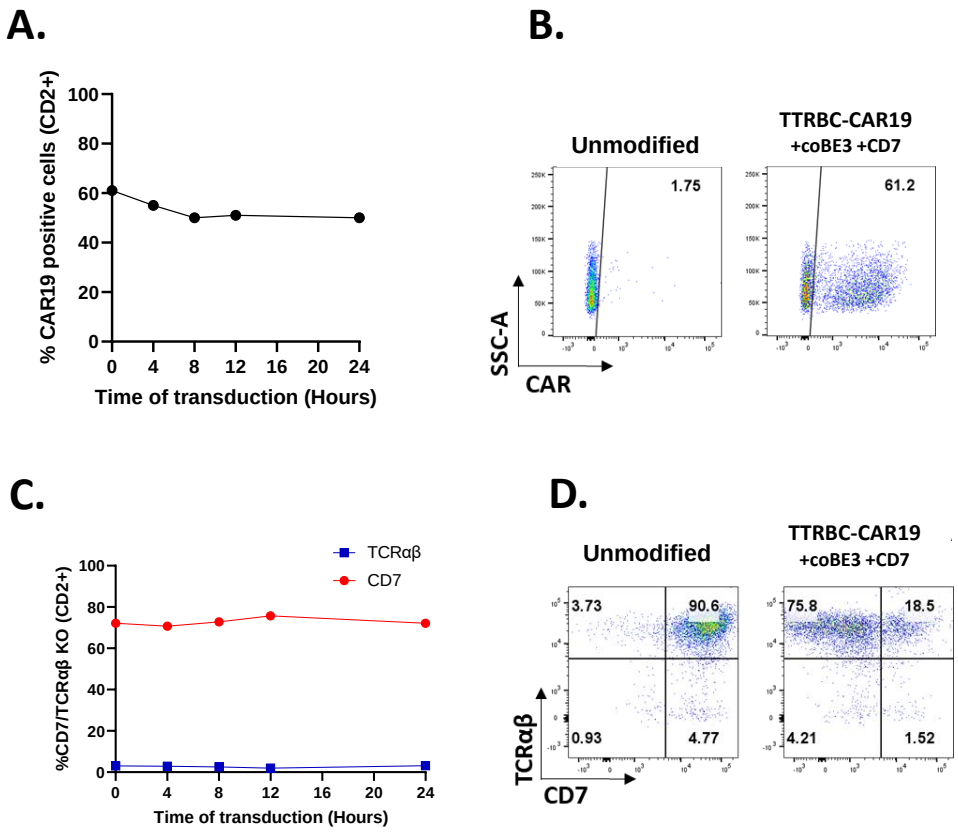

Figure 4-8 Transduction time course

A. Phenotypic analysis at day 10 of CAR19 expression following transduction at serial timepoints (n=1). **B.** Representative flow plot of CAR19 expression in transducing cells 0 hours post electroporation. **C.** Phenotypic analysis of CD7 and TCRαβ protein knockout at serial timepoints showing robust CD7 disruption but negligible knockout of TCRαβ. **D.** Representative flow plot of CD7 and TCRαβ knockout in transduced cells 0 hours post electroporation.

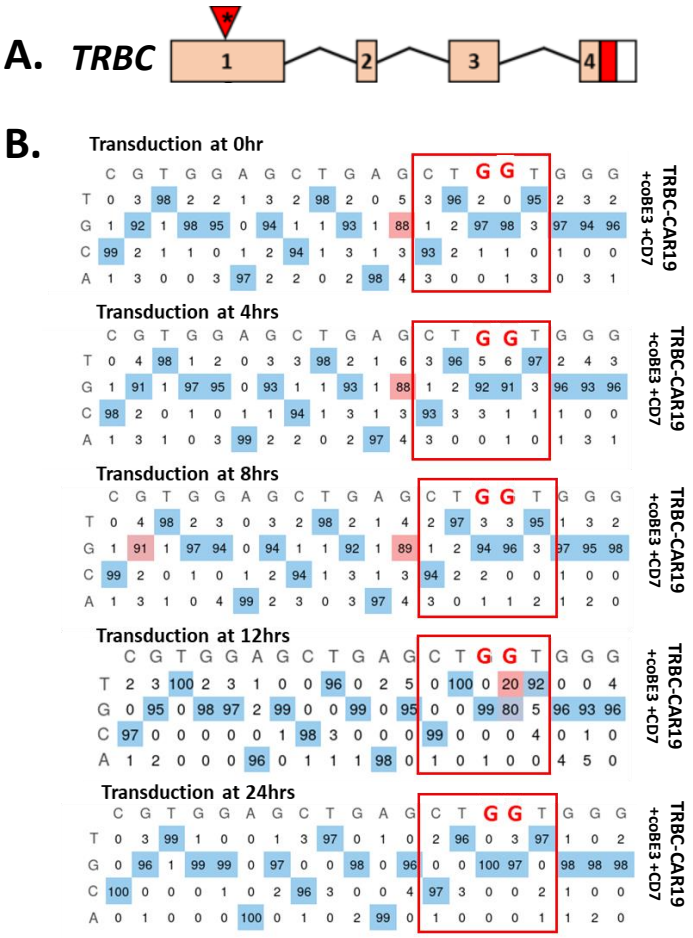

Figure 4-9 Molecular verification of TRBC disruption across transduction time course

A. Schematic of exonic regions within *TRBC* gene. The red marking in exon 1 of TRBC represents the genomic translation stop site followed by 5' untranslated regions (white box). The red triangle with an asterisk indicates the position of the base conversion that led to premature stop codon formation. **B.** EDITR output of Sanger sequencing results of *TRBC* genome editing (n=1). The anticipated base conversion sites are shown in red boxes. The percentage of G>A (antisense) conversion throughout TRBC-targeting protospacer.

4.7 Selection of base editors for the terminal platform (TTRBC-CAR)

Next, alternative deaminases hAID-BE3 and hAPOBEC3-BE3 were explored to improve knockout for sgRNAs embedded within the terminal vector configuration.

To compare the multiplexed genome editing efficiency from vector-coupled and uncoupled sgRNAs using each base editor (coBE3, hA3A and hAID), and assess

whether this approach could lead to successful generation of TCRαβ^{-}CD7^{-} CAR7-T cells, primary T cells (n=3) were electroporated with a combination of CD7 sgRNA 10 µg/mL and each of the editors 50 µg/mL delivered as mRNA. SpCas9 mRNA 50 µg/mL was used alongside as a positive control of CD7 disruption. T cells were then transduced 24 hours post electroporation at MOI 5 with either TTRBC-CAR7, TTRBC-CAR3, or TTRBC-CAR19 control coupling TRBC sgRNA and CAR transgene expression (**Figure 4-10 A**). Un-transduced cells electroporated with uncoupled sgRNAs (CD7 and TRBC) served as positive controls for gene disruption.

Flow cytometry analysis 8 days post electroporation showed similar TTRBC-CAR19 and TTRBC-CAR7 transduction efficiency across all base editors ranging from 45.6% to 62.9% in primary T cell donors (n=3) (**Figure 4-10 B**).

Both CD7 and TCRαβ knockout 8 days post electroporation in UTD cells showed similar editing efficiencies to those observed in Section 3.3. Furthermore, phenotypic analysis demonstrated that T cells treated with SpCas9 ahead of TTRBC-CAR19 had high disruptions in CD7 (93%-97%) and TCRαβ (70%-90%) expression, as expected. This level of CD7/TCRαβ disruption was closely followed by hA3A where the disruption of CD7 ranged from 88%-96%, and TCRαβ from 45%-70%. In the case of coBE3, the level of TCRαβ disruption mediated by the coupled guide in the TTRBC-CAR19 vector appeared lower at 15%-31%, while CD7 disruption from the uncoupled sgRNA was still able to achieve relatively high efficiency (55%-78%). Similar results were observed in cells treated with hAID where CD7 disruption was between 47.5%-57% and TCRαβ disruption ranging from 14% to 40% (**Figure 4-10 C&D**). Phenotypic analysis of cells transduced with TTRBC-CAR7 showed increased CD7 loss across all editors SpCas9 (95%-99%), hA3A (86%-99%), coBE3 (81%-99%), or hAID (88%-97%), suggesting a level of enrichment CD7^{-} cells due to fratricide. However, TCRαβ disruption was high with both SpCas9 and hA3A, achieving (60%-86% and 60%-81%, respectively), lower disruption was detected with coBE3 and hAID (10%-35% and 9%-34%, respectively) (**Figure 4-10 C&D**).

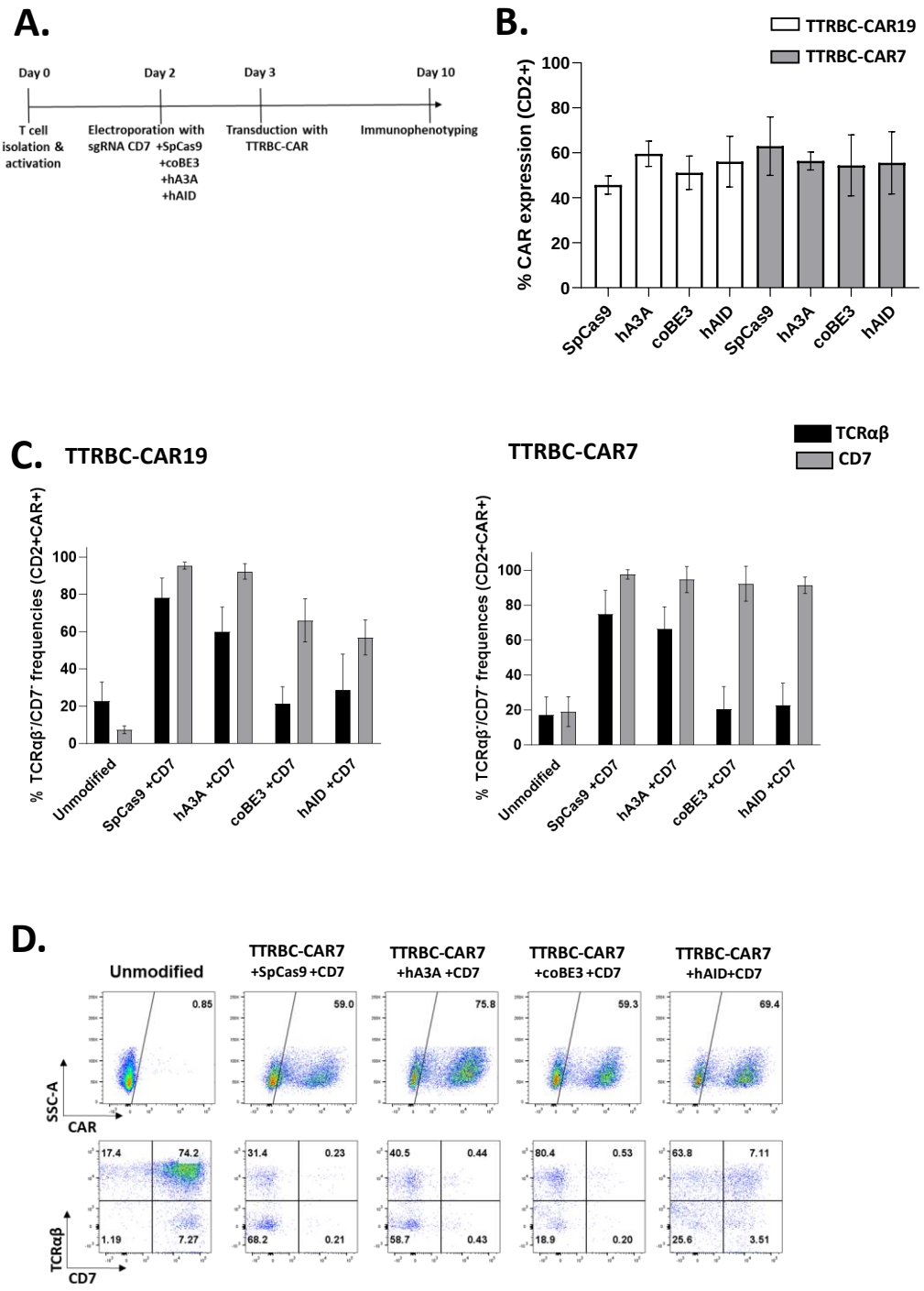

Figure 4-10 Comparing editing efficacy of *CD7* locus and *TRBC* locus with TTRBC-CAR vector, using different base editor iterations

A. Schematic timeline for the experiment, mRNA delivery and endogenous CD7 knockout occurs prior to TTRBC-CAR transduction. **B.** Summary of phenotypic analysis of CAR expression in primary T cell donors n=3 gated-off CD2+ cells. The error bars represent the standard deviation (SD). **C.** Histogram representing the CD7 and TCRαβ knockout results (n=3) in TTRBC-CAR19 and TTRBC-CAR7 transduced cells. The error

bars represent the standard deviation (SD). **D.** Representative flow plots of CAR7 expression, knockout of CD7 and TCRαβ in TTRBC-CAR7 transduced cells.

Molecular investigation of the base edited TTRBC-CAR7 transduced cells at the *CD7* locus confirmed the intended STOP inducing C>T nucleotide conversion at protospacer position C8 across all samples. Efficiency was highest when hA3A and coBE3 were used, with a conversion rate of 99%. However, editing with hAID as previously observed produces relatively low editing of the target cytidine (C8, 18% C>T) with the majority of editing seen at C 1, 3, 4, and 7 ranging from 38-64% (**Figure 4-11 A&B**).

In cells edited with hA3A, substantial editing was observed outside the 4 bp-8 bp PAM distal editing window with C>T conversions detected at positions C1 and C3. On the other hand, coBE3 showed out-of-window editing was only observed at C3. Investigation of the *TRBC* locus showed editing was observed only when treated with hA3A resulting in a conversion frequency of 80% G>A at G5 and 36% at G6. Substantial editing was detected outside the 4 bp-8 bp PAM distal editing window with G>A conversions detected at positions G1 (15%), G2 (52%), G3 (22%), G11 (24%) (**Figure 4-11 C&D**).

In contrast, when SpCas9 was used ahead of TTRBC-CAR7, indels in CD7 were as high as 95% while only at around 35% in TRBC (**Figure 4-12**). Notably, no indels were detected at either genomic locus in Sanger sequence traces, regardless of base editor used.

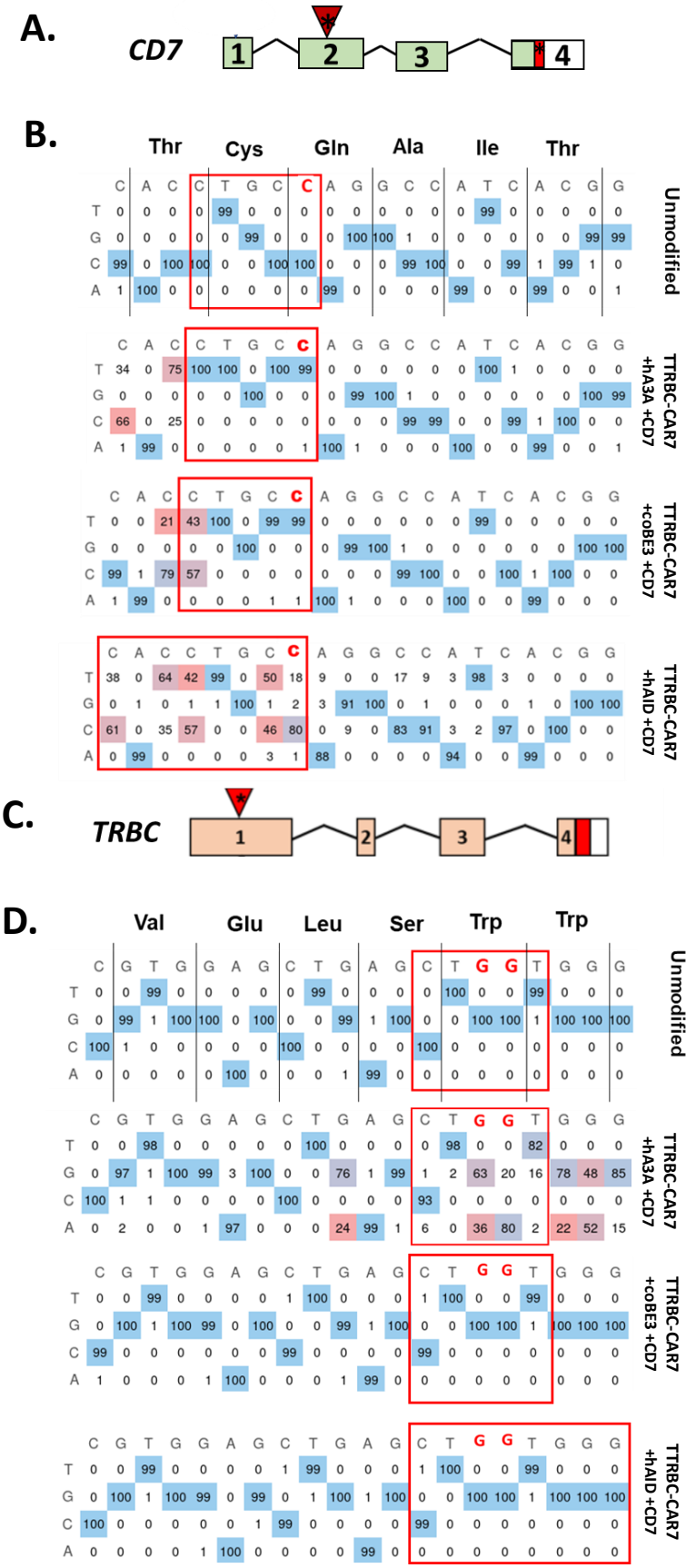
A.
CD7
1
2
3
4
B.
Thr
Cys
Gln
Ala
Ile
Thr
Unmodified
TTRBC-CAR7 +hA3A +CD7
TTRBC-CAR7 +coBE3 +CD7
TTRBC-CAR7 +hAID +CD7
C.
TRBC
1
2
3
4
D.
Val
Glu
Leu
Ser
Trp
Trp
Unmodified
TTRBC-CAR7 +hA3A +CD7
TTRBC-CAR7 +coBE3 +CD7
TTRBC-CAR7 +hAID +CD7

Figure 4-11 Molecular verification of CD7 and TRBC disruption at the molecular level in TTRBC-CAR7 edited cells

A. Schematic of exonic regions within CD7 gene. The red marking in exon 2 of CD7 represents the genomic translation stop site, followed by 5' untranslated regions (white box). The red triangle with asterisk indicates the position of the base conversion that leads to premature stop codon formation. **B.** EDITR output of Sanger sequencing results of *CD7* genome editing (n=1). The anticipated base conversion sites are shown in red boxes. The percentage of C>T conversion throughout CD7-targeting protospacer. **C.** Schematic of exonic regions within *TRBC* gene. The red marking in exon 1 of *TRBC* represents the genomic translation stop site followed by 5' untranslated regions (white box). The red triangle with an asterisk indicates the position of the base conversion that leads to premature stop codon formation. **D.** EDITR output of Sanger sequencing results of TRBC genome editing (n=1). The anticipated base conversion sites are shown in red boxes. The percentage of G>A (antisense) conversion throughout TRBC-targeting protospacer.

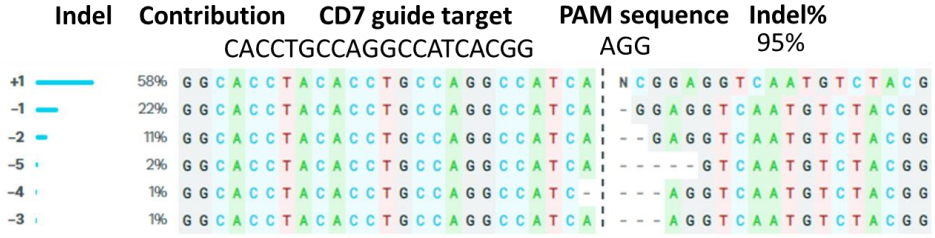

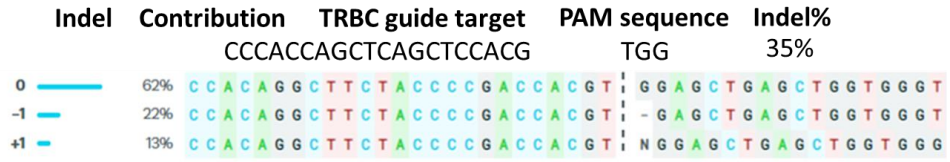

Figure 4-12 Identification of insertions/deletions (indels) created by SpCas9 in TTRBC-CAR7 transduced cells

On-target editing effects in DNA extracted from primary T cells treated with SpCas9 and sgRNAs against CD7 and TRBC (n=1) were measured by direct sequencing and bioinformatic analysis using Tracking of Indels by Inference of CRISPR Edits (ICE) software for signatures of non-homologous end joining (NHEJ) demonstrating efficient disruption at both target sites. PAM, protospacer adjacent motif.

In TTRBC-CAR3 transduced cells, limited CAR3 cells could be detected, and only when SpCas9 and hA3A were used (18%, 12%, respectively, gated on $CD2^+$). The level of

TCRαβ knock out achieved in these cells was 67% and 43%, respectively (**Figure 4-13**). Notably, CAR3 was not detected when the cells were treated with either coBE3 or hAID base editors while also 95% of cells remained positive for TCRαβ when edited with coBE3 or hAID.

However, at the CD7 locus, 93% of knockout was achieved using both SpCas9 and hA3A with slightly lower yet comparable levels (87%) achieved with coBE3. hAID displayed the lowest levels of editing of 26%. Interestingly, editing the cells with uncoupled sgRNAs (CD7 and TRBC) and SpCas9 ahead of pCCL-CAR3 transduction resulted in 59% CAR3 expression, with 85% CD7/TCRαβ double knockout efficiency (**Figure 4-13**).

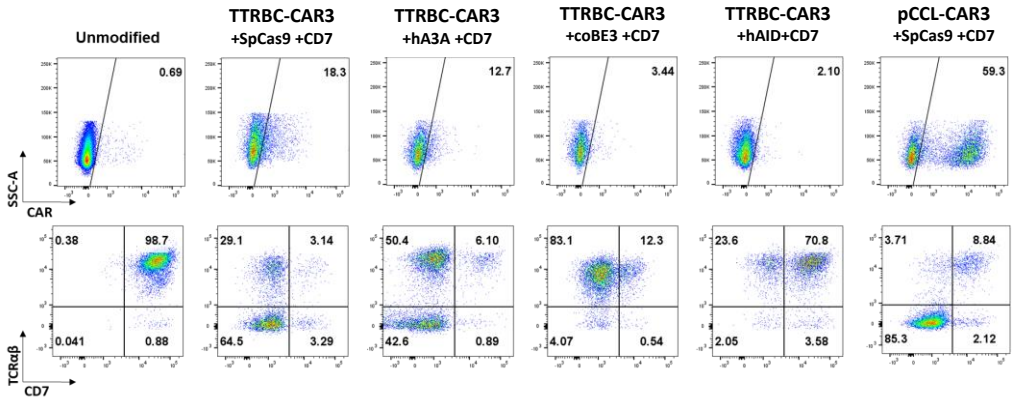

Figure 4-13 Expression of CAR3 in TTRBC-CAR3 transduced cells edited with SpCas9, or CBEs (coBE3, hA3A and hAID)

Successful CAR3 generation was achieved using the pCCL-CAR3 vector. In the context of TTRBC-CAR3, CAR3 expression was limited when SpCas9 and hA3A were employed, while coBE3 or hAID did not yield detectable CAR3 expression. TCRαβ knockout was efficient with SpCas9 and hA3A, but the use of coBE3 or hAID resulted in a lower efficiency of TCRαβ knockout. CD7 disruption was accomplished using SpCas9 and hA3A, followed by coBE3, with moderate CD7 knockout observed using hAID.

4.8 Chapter summary

In this chapter, the terminal-CRISPR platform was adapted for use against T cell malignancies by coupling CD3 or CD7 targeting CAR sequences to the CRISPR mediated disruption of TRBC. However, in order to overcome the additional hurdle of TvT fratricide, a CD7 targeting sgRNA was delivered alongside.

Two different strategies were tested. In Strategy A, the cells were initially transduced with TTRBC-CAR7 or TTRBC-CAR3 vectors before electroporation with coBE3 and a CD7 specific sgRNA to knock out TCRαβ and CD7. This strategy successfully generated CAR7-T cells with high knockout of CD7. However, limited TCRαβ knockout was observed.

Interestingly, when the base editor and CD7 sgRNA were delivered after TTRBC-CAR7 transduction, it was observed that the population of CD8+ cells was noticeably reduced, an observation that was not evident in the CAR19 control group. Use of this strategy did not allow successful generation of CAR3-T cells due to the lack of protective TCRαβ/CD3 disruption leading to cell fratricide.

An alternative workflow, termed Strategy B, activated primary T cells were first electroporated with coBE3 mRNA and CD7 sgRNA 24 hours prior to transduction. This led to successful production of CAR7-T cells with high levels of CD7 disruption, but limited disruption of TCRαβ. As a result, CAR3-T cells could not be manufactured successfully using this approach.

One key hurdle that was faced when using the TTRBC-CAR vector was the reduced TRBC knockout, which was the case whether the BE3 base editor mRNA was delivered before or after TTRBC-CAR transduction. This was particularly problematic when coBE3 mRNA preceded TTRBC-CAR7 transduction, where the majority of cells remained positive for TCRαβ. However, as this was the preferred timing strategy for CAR7 production and additionally did not result in a CD4:CD8 ratio imbalance, further steps were considered to optimise the precise timing for the delivery of TTRBC-CAR

in relation to coBE3 mRNA and CD7 sgRNA delivery. In order to identify whether expression of the CAR or knockout of TRBC occurred first in the TTRBC-CAR coupled vector, cells were transduced with TTRBC-CAR19 either immediately or over a course of time points up until 24 hours following electroporation with coBE3 mRNA and CD7 sgRNA. However, there did not appear to be any discernible difference in TCRαβ knockout across the time course. Moreover, the absence of TCRαβ knockout might be attributed to the potential degradation of coBE3 mRNA before the expression of the vector contained TRBC sgRNA occurs.

The outcomes of transient protein expression presented in Chapter 3 indicated that the coBE3 and hAID expressions diminished after 16 hours, while hA3A persisted for 72 hours. The prolonged presence of the hA3A editor could have contributed to successful editing when using the TTRBC-CAR7 configuration, but with some C>T conversions outside the expected editing window. However, attempts to generate TTRBC-CAR3 cells were unsuccessful due to fratricide-mediated elimination caused by the lack of protective TCRαβ disruption.

Chapter 5 Investigation of CRISPR/Cas9 mediated site-specific CAR insertion by homology directed insertion

5.1 Introduction

The previous chapters explored the use of lentiviral vectors for delivery of CAR transgenes to T cells, a technique widely employed in the field of CAR-T cell engineering. These vectors are preferred due to their high transduction efficiency, stable integration into the host genome, broad cell tropism, and ability to accommodate larger genetic payloads (approximately 9 Kb) (46, 343). However, it is important to note that lentiviral vector integration is semi-random, which may disrupt endogenous gene regulation and lead to potential risks such as oncogenic transformation and clonal expansion (344, 345). Insufficient access to these therapies results from high costs and supply chain limitations tied to manufacturing GMP grade vectors. Furthermore, early-stage trial innovation is restricted by extended lead times and costly viral vector production (346, 347). Non-viral methods, such as transposon systems (348) and mRNA transduction (349), aim to produce CAR-T cells without viral vectors. However, challenges arise from reduced uniformity due to random integration and short-lived CAR expression. Safety concerns also arise from observed insertional mutagenesis and T cell-lymphoma cases in patients treated with CD19CAR-T cells using potent *piggyBac* transposon systems (173).

Recently, alternative strategies, employing genome editing technologies, have been demonstrated enabling site-directed insertion of a CAR transgene into a targeted locus. CRISPR/Cas9 in conjunction with adeno-associated virus (AAV) enables precise genome modifications via HDR, potentially decreasing the risk of insertional mutagenesis when compared to random insertions introduced by retroviruses, while simultaneously allowing for the knockout of a target gene of interest (121, 275, 284, 285, 350). Eyquem *et al*. (2017) reported a successful CD19-CAR knock-in to the coding region of the *TRAC* locus of T cells through electroporation of Cas9 mRNA and AAV mediated delivery of the homology-directed repair (HDR) template. This led to enhanced and consistent CAR expression in T cells, reduced baseline (tonic)

signalling, and increased potency both *in vitro* and *in vivo* compared to CAR-T cells produced through viral transduction (275).

AAV production, however, is complex, expensive, and requires the removal of impurities to meet clinical standards (351), making it a costly option for CAR integration. Alternative options have included non-viral donor templates for site-specific CAR integration, which can be synthesised using either single-stranded DNA (ssDNA) or double-stranded DNA (dsDNA). Roth *et al*. (2018) introduced the virus-free knock-in approach to replace the native TCR. They used non-viral dsDNA as an HDR template, which was generated via conventional PCR amplification (278). This innovative technique overcomes challenges linked to viral vectors. Although, delivery of dsDNA templates has been associated with innate immune responses leading to toxicity, they are commonly used in favour of their affordability, rapid manufacture, and commercial availability. Furthermore, dsDNA templates can be delivered in multiple formats including linearized plasmid DNA, self-cleaving circular plasmid DNA, or as a PCR product (352-354). ssDNA is less toxic, but these are currently more challenging and costly to produce (355).

This chapter will explore the non-viral site-specific integration of a transgene using a dsDNA HDR template in combination with SpCas9 RNP complexes. Templates encoding eGFP and CAR20 will be used as a control alongside templates encoding a CAR (CAR7, or CAR3). GFP is a well-established positive control with known expression and fluorescence characteristics, aiding in the procedure's overall validation. It allows for non-invasive, longitudinal expression tracking, valuable for dynamic studies, and can serve as a normalisation control to eliminate insertion process-related variations. CAR20 targeting CD20 is a positive control demonstrating the capacity to express effectively while simultaneously mitigating the fratricide effect observed with CARs designed to target T-ALL.

Multiple loci were assessed in this project for targeted insertions, with initial work focusing on insertion into the *TRAC* locus. This choice was based by earlier research that had already validated successful insertions into the *TRAC* locus, as reported by

others (287, 288, 356, 357). The *CD247* locus, encoding CD3ζ was also tested, as this could allow the use of an endogenous sequence within the CAR construct, potentially taking advantage of the natural regulatory elements and cellular machinery associated with CD3ζ for controlling CAR expression. Additionally, this chapter investigated the possibility of site-specific insertion of CAR7 into the *CD7* locus to determine whether the transcriptional control of the CAR7 from this site could mitigate fratricide.

5.2 Multiplexed knockout of *TRAC* and *CD7* loci by SpCas9 RNP complexes

In previous studies, highly efficient and rapid editing approaches were demonstrated using modified CRISPR/Cas9 systems (287, 288, 356, 357). By co-electroporating T cells with CRISPR/Cas9 RNP and a long dsDNA without viral vector, others have achieved direct insertion of dsDNA sequences larger than 1 kb into the first exon of the *TRAC* locus. This approach allowed them to replace the endogenous T cell receptor locus with a new TCR that redirected T cells to the NY-ESO-1 cancer antigen (278). To replicate the study conducted by Roth, Puig-Saus (278), RNP complex titration was first optimised for efficient simultaneous disruption of *CD7* and *TRAC* loci, with the aim of further testing site-directed insertions into the *TRAC* loci. The CD7 sgRNA, which had been used in the prior chapters and which induced a double strand break in exon 2 when complexed with an SpCas9 nuclease, was combined with the TRAC guide, which targets exon 1 (**Figure 5-1 A**). By targeting the *TRAC* locus, it is anticipated that fratricide can be avoided through the disruption of TCRαβ before CAR3 integration, and similarly, the knockout of CD7 is expected to help minimise fratricide upon CAR7 expression. A range of sgRNA concentrations were titrated for both CD7 ex2 and TRAC ex1 sgRNAs ranging from 10 to 35 µg/mL, pre-complexed with SpCas9 protein and electroporated into primary T cells.

Complexes for TRAC and CD7 guide RNA were incubated separately to avoid competition between the sgRNAs while complexing. T cells not exposed to electroporation, or those electroporated with either TRAC or CD7 RNP complexes alone were used as experimental controls. Using flow cytometry 4 days post-

electroporation, the optimal sgRNA concentration, measured by surface removal of TCRαβ and CD7 proteins, was 20 µg/mL (89.3% $CD7^-/TCR\alpha\beta^-$), In contrast, the range of double knockout achieved with other concentrations varied between 25.4% and 85.5% (**Figure 5-1 B&C**).

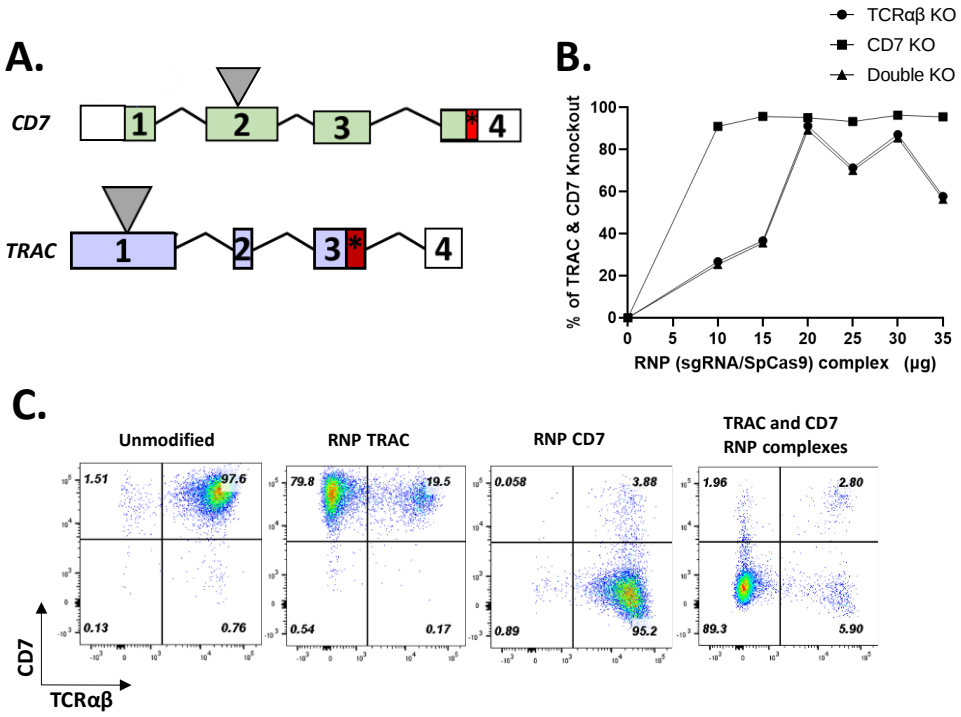

Figure 5-1 Optimisation of simultaneous distribution of *CD7* and *TRAC* loci by spCas9 RNPs

A. Schematic of exonic regions within the *CD7* gene and *TRAC* genes. 5' and 3' untranslated regions (white box), black lines represent the intronic sequence. The grey triangle indicates the position where at the sgRNA break site. **B.** Titration of RNP (sgRNA/SpCas9) complex at 10-35 µg/mL in primary T cells (n=1). Flow cytometry displays efficient knockout of CD7 and TCRαβ at 20 µg/mL. **C.** Flow plots of efficient disruption of CD7 and TCRαβ at 20 µg/mL.

5.3 Design of templates for non-viral mediated delivery of transgene to the *TRAC* locus

Once the optimal concentration of RNP complexes required for simultaneous disruption of both *TRAC* and *CD7* loci was established, targeted knock-in efficiency of

a transgene of interest at the *TRAC* locus was assessed. First, templates were designed as follows:

Each template encoded a transgene (GFP, CAR3 or CAR7 or CAR20) upstream of a P2A self-cleaving peptide and followed by a stop codon and bGH polyA sequence which were flanked at 5' and 3' ends by 300 bp sequences of TRAC homology. The P2A sequence incorporated between TRAC and GFP/CAR genes within a single mRNA transcript, acts as a "self-cleaving" peptide. During translation, the ribosome encounters the P2A sequence and undergoes a "ribosome skipping" event. This results in the release of the nascent polypeptide chain upstream of the P2A sequence from the ribosome, while the ribosome continues translation of the downstream polypeptide chain. GFP's lack of transmembrane regions contributes to its cytoplasmic localisation, as it lacks the structural elements necessary for membrane integration or transport across organelle membranes. Therefore, GFP primarily resides in the cytoplasm, where it can display its fluorescent properties without being directed to specific organelles (**Figure 5-2 A**).

To produce the dsDNA TRAC donor template, PCR was used to amplify each sequence from template encoding transfer plasmids followed by an isopropanol precipitation step as explained in Section 2.2.27. Template production was confirmed by agarose gel electrophoresis post purification and concentration (**Figure 5-2 B**).

These dsDNA templates (20 µg) were delivered to healthy donor T cells through electroporation along with separately complexed RNP:sgRNA against *TRAC* and *CD7*. The RNP complexes were formed at a 1:1.2 (SpCas9: sgRNA protein) molar ratio and incubated for 10 minutes at room temperature. Following this, dsDNA templates were introduced at the end of the incubation and before electroporation (**Figure 5-3 A&B**). These were tested for CRISPR/Cas9 mediated cleavage of the *TRAC* locus and subsequent repair by homologous directed repair (**Figure 5-3 C**).

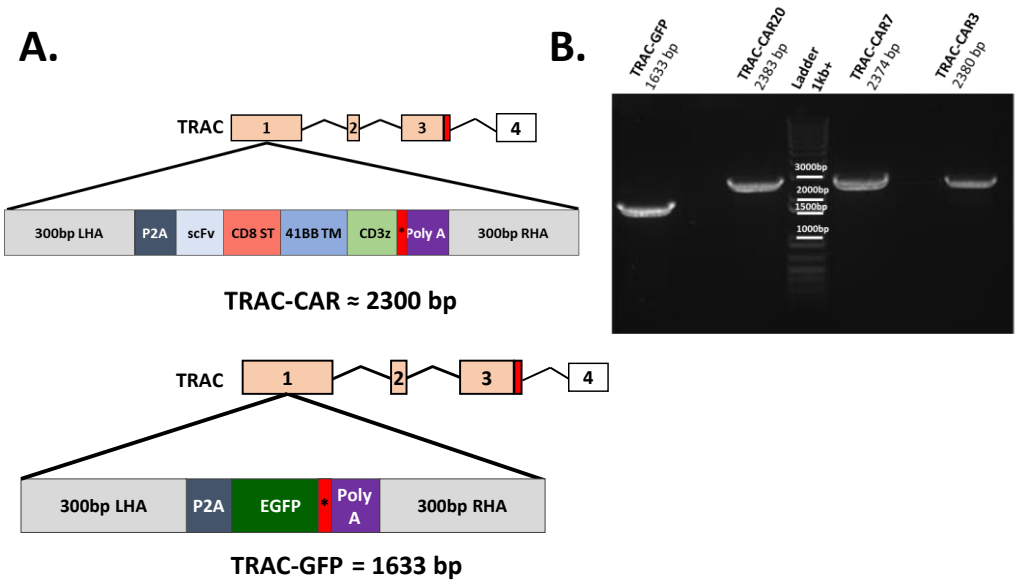

Figure 5-2 dsDNA TRAC donor template design

A. Iterations of transgene encoding dsDNA templates with 5' and 3' homology regions to endogenous TRAC. TRAC-CAR construct incorporating synthetic CD3ζ domain, or TRAC-GFP construct flanked by upstream P2A and downstream STOP codon and bGH polyA sequence. 5' and 3' 300 bp TRAC homology arm sequence included. **B.** Amplification of synthetic templates flanked by 300 bp TRAC homology arms. DNA was gel extracted, concentrated and purified for downstream complexing with RNP and electroporation into T cells. TRAC: T Cell Receptor Alpha Constant, GFP: green fluorescence protein. LHA: left homology arm, RHA: right homology arm.

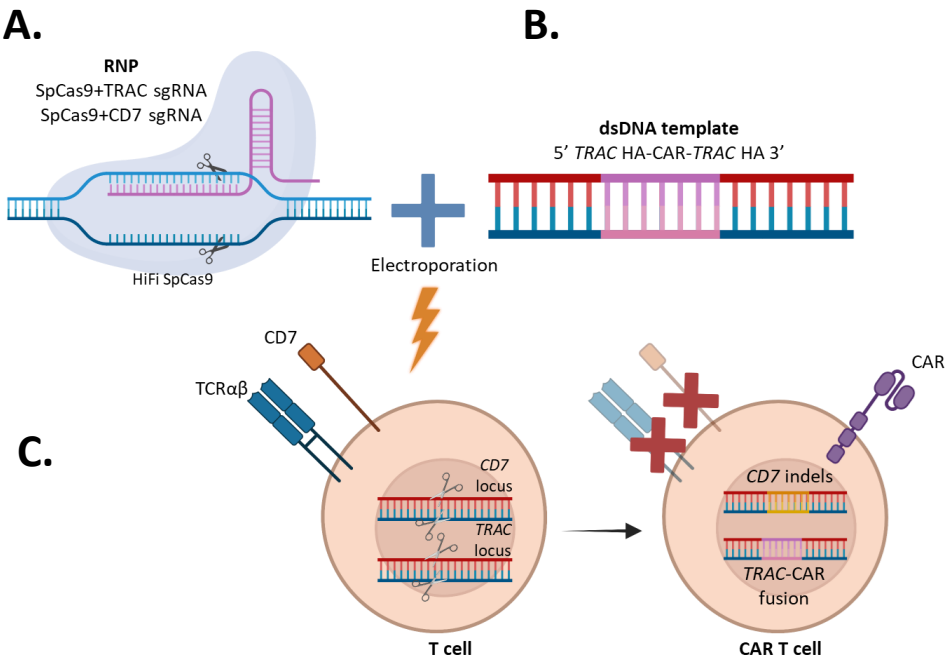

Figure 5-3 CRISPR-mediated integration of CAR template into *TRAC* locus

A. Ribonucleoprotein (RNP) complex of *Streptococcus pyogenes* Cas9 (SpCas9) protein with sgRNA targeting *TRAC* and *CD7*, sgRNA is combined with dsDNA template encoding transgene sequence flanked by 300 bp homology regions (HR) of the *TRAC* gene. **B.** RNP and dsDNA template are electroporated into healthy donor T cells leading to CRISPR/Cas9 mediated cleavage of *TRAC* and repair by homologous directed repair (HDR). Disruption of TRAC leads to removal of surface TCRαβ. **C.** Expression of CAR sequence integrated within *TRAC* locus. Disruption of TCRαβ and CD7. TRAC: T cell receptor alpha constant.

PBMCs from three healthy donors were isolated and activated with TransAct for 48 hours prior to electroporation with a combination of sgRNA TRAC and CD7 RNP complexes at a 1:1.2 (SpCas9: sgRNA protein) molar ratio and dsDNA templates coding CAR3 or CAR7 homology flanked transgenes. Previously validated eGFP and CAR20 dsDNA templates were run in parallel as controls alongside cells electroporated with RNP alone. High titre pCCL-CAR7 ($1.2x10^8$ TU/mL) lentiviral vector was used at MOI of 5 as a vector delivered control of CAR (**Figure 5-4 A**).

Flow cytometry analysis performed at 4 days post-electroporation on a sample size of three revealed a high disruption of TCRαβ and CD7 expression across all experimental conditions. The percentage of T cells lacking both CD7 and TCRαβ

expression ($CD7^-/TCR\alpha\beta^-$) in the population electroporated with RNPs exclusively (SpCas9-TRAC sgRNA and SpCas9-CD7 sgRNA) ranged from 78.8% to 85.4%. Inclusion of dsDNA GFP in the electroporation, resulted in a double knockout population ranging from 74% to 94.1%, which was overall comparable to T cells electroporated with dsDNA CAR20 template (76.2% to 82.3%), dsDNA CAR3 (88% to 95.7%) or dsDNA CAR7 (69.0% to 92.8%). Edited cells transduced with control pCCL-CAR7 vector displayed a double knockout population ranging from 76% to 85% (**Figure 5-4 B&D**).

Interestingly, eGFP and CAR20 dsDNA template delivery resulted in modest levels of HDR-mediated transgene expression of 10%-21.6% and 9.4-17.5%, respectively (**Figure 5-4 C&D**). However, no detectable expression of CAR3 was observed above background with limited CAR7 expression (1.6% to 3.5%), as opposed to lentiviral vector control transduced cells where 40%-51.7% expressed CAR7-T cells (**Figure 5-4 C&D**).

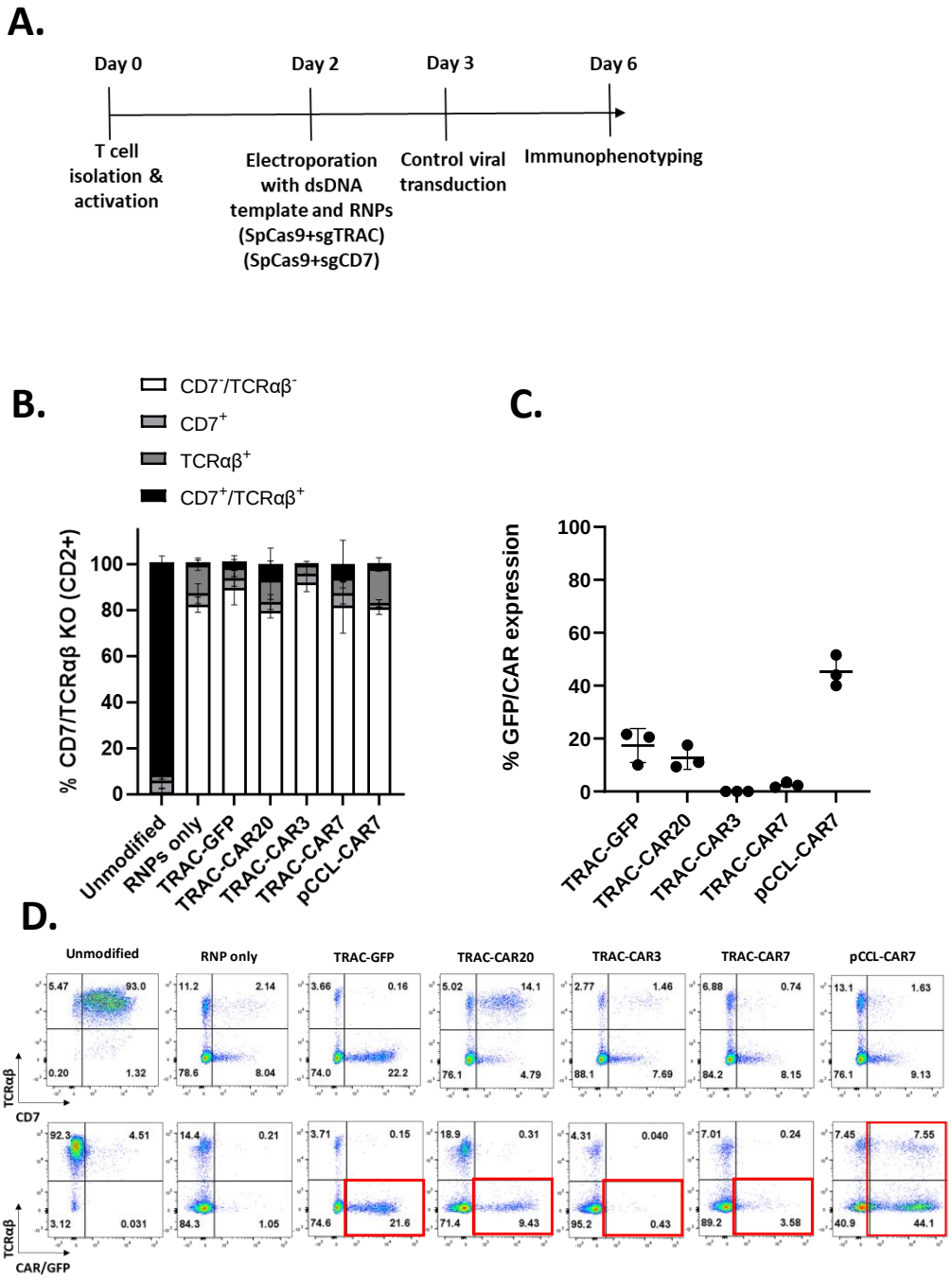

Figure 5-4 CRISPR-mediated transgene knock-in to *TRAC* locus

A. Experimental timeline: primary PBMCs (n=3) were isolated and T cells activated with anti-CD3/CD28 for 48hrs. T cells were next electroporated with an RNP complex of SpCas9-TRAC and SpCa9-CD7 targeting sgRNA and combined with respective dsDNA CAR encoding template. pCCL-CAR7 encoding lentiviral vector used as positive CAR control in T cells electroporated with SpCas9 RNP-TRAC sgRNA and SpCas9 RNP-CD7 sgRNA **B.** Flow analysis of TCRαβ and CD7 disruption showed successful double knockout population across all conditions. The error bars represent the standard deviation (SD). **C.** Flow analysis of GFP/CAR

expression in cells from three donors' on day 6. The error bars represent the standard deviation (SD). **D.** Representative flow plots showing successful double knockout of TCRαβ and CD7 across all conditions with the expression of CAR20 and GFP, no expression of CAR3 and limited expression of CAR7, their expression is highlighted with red boxes. Successful CAR7 expression from pCCL-CAR7 transduced cells. TRAC: T cell receptor alpha constant, GFP: green fluorescence protein.

5.3.1 Time course of cell surface antigen expression and GFP template incorporation

Insight into the optimal timing for surface expression mitigation, which may explain the absence of CAR7 and CAR3 integration into the *TRAC* locus, was sought through a time-course experiment using a control dsDNA GFP template. To achieve this objective, a control dsDNA GFP template was directed to the *TRAC* locus following SpCas9 delivery.

Further investigations were needed to determine the chronological sequence and underlying mechanisms of these events. Therefore, PBMCs were isolated from a healthy donor, activated with TransAct prior to electroporation with GFP template in combination with TRAC/CD7 RNP complexes (**Figure 5-5 A**). Cells were harvested at 24 hours and 48 hours following electroporation and immunophenotyped by flow cytometry. GFP expression was readily detectable at 24 hours post-electroporation (26.4%) which slightly increased to 29.8% at 48 hours (**Figure 5-5 B**). However, the mean fluorescence intensity (MFI) of CD7 and TCRαβ had not fully decreased by 24 hours post-electroporation, confirming residual surface expression which continued to drop by 48 hours (**Figure 5-5 C**).

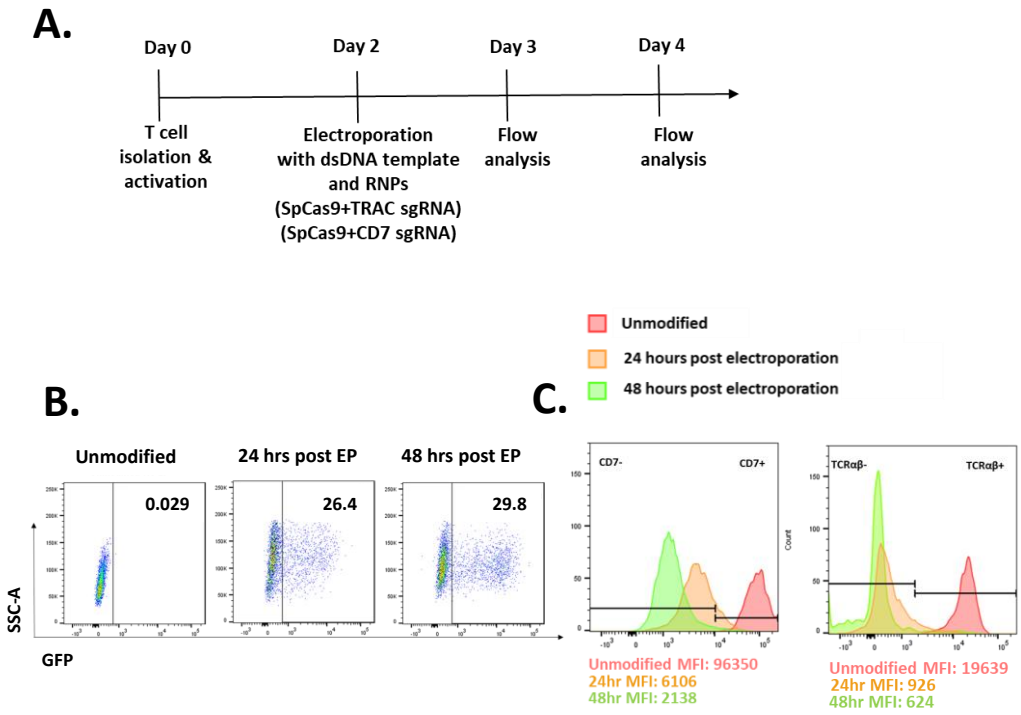

Figure 5-5 Insertion of GFP template in *TRAC* locus

A. Experimental timeline: Primary PBMCs were isolated and T cells activated with anti-CD3/CD28 for 48hrs. T cells (n=1) were next electroporated with an RNP complex of SpCas9-TRAC and SpCa9-CD7 targeting sgRNA and combined with dsDNA GFP encoding template. **B.** Flow analysis of GFP expression after electroporation gated on $CD2^{+}$ showing GFP expression percentage at 24h hrs and 48 hrs. **C.** Histogram showing the CD7 (left) and TCRαβ (right) MFI at 24 or 48 hours post-electroporation. EP: electroporation, TRAC: T cell receptor alpha constant, GFP: green fluorescent protein, MFI: mean fluorescence intensity.

5.3.2 Orderly base edited disruption of TCRαβ and CD7 prior to nuclease mediated insertion of dsDNA template (CAR7/CAR3)

The data suggested that the low CAR3 and CAR7 yields may have been a result of fratricide against residual T cell CD3/CD7 antigen as delivery of control CAR20 and GFP template controls resulted in greater knock-in and transgene expression. To test this hypothesis an experiment was conducted where TCRαβ/CD3 and CD7 expression were disrupted using an additional multiplexed base editing step prior to transgene template integration delivery by SpCas9 at the *TRAC* locus. To achieve this T cells

were electroporated with sgRNAs targeting both *TRBC1/2* and *CD7* loci and coBE3 mRNA 48 hours post activation (**Figure 5-6 A**). By targeting *TRBC1/2,* it ensured TCRαβ expression was disrupted, but the *TRAC* gene, and therefore Cas9 mediated integration site, would remain unaffected. Additionally, using coBE3 for the disruption ensured no DSBs were present which could interfere with template integration and increase the likelihood of translocation events. Two days following disruption of *TRBC1/2* and *CD7* the cells were subjected to a second round of electroporation with TRAC targeting sgRNA, in combination with CAR3 or CAR7 dsDNA template and SpCas9 protein. For this step the electroporation conditions were as previously described in Section 5.3.1 using RNPs (SpCas9+TRAC sgRNA) at 1:1.2 molar ratio. GFP and CAR20 templates were used alongside as positive controls and a separate pCCL-CAR3 lentiviral vector was used as a positive control of CAR expression. Six days post-electroporation cells were analysed by flow cytometry and compared against GFP and CAR20 dsDNA template controls which showed around 5.3% and 9% template integration, respectively (**Figure 5-6 B**). Similarly, CAR7 integration resulted in expression of 8.9%. Interestingly, CAR7 template integration resulted in enrichment of the CD7 negative fraction from 64.5% to 93.6%. However, in the case of CAR3 less than 2% template expression was still observed (**Figure 5-6 B**).

For genomic confirmation of transgene insertion, DNA was extracted from the cells and amplified using primers designed to bind upstream of the TRAC homology arm sequence (reverse primer) and within the template (forward primer). The expected band sizes for GFP and CAR20 were detected using both one-step and two-step editing strategies (**Figure 5-6 C**), however CAR7 could only be detected with the two-step editing approach (**Figure 5-6 D**). Gel extraction of positive bands and Sanger sequencing of these corroborated the template insertion.

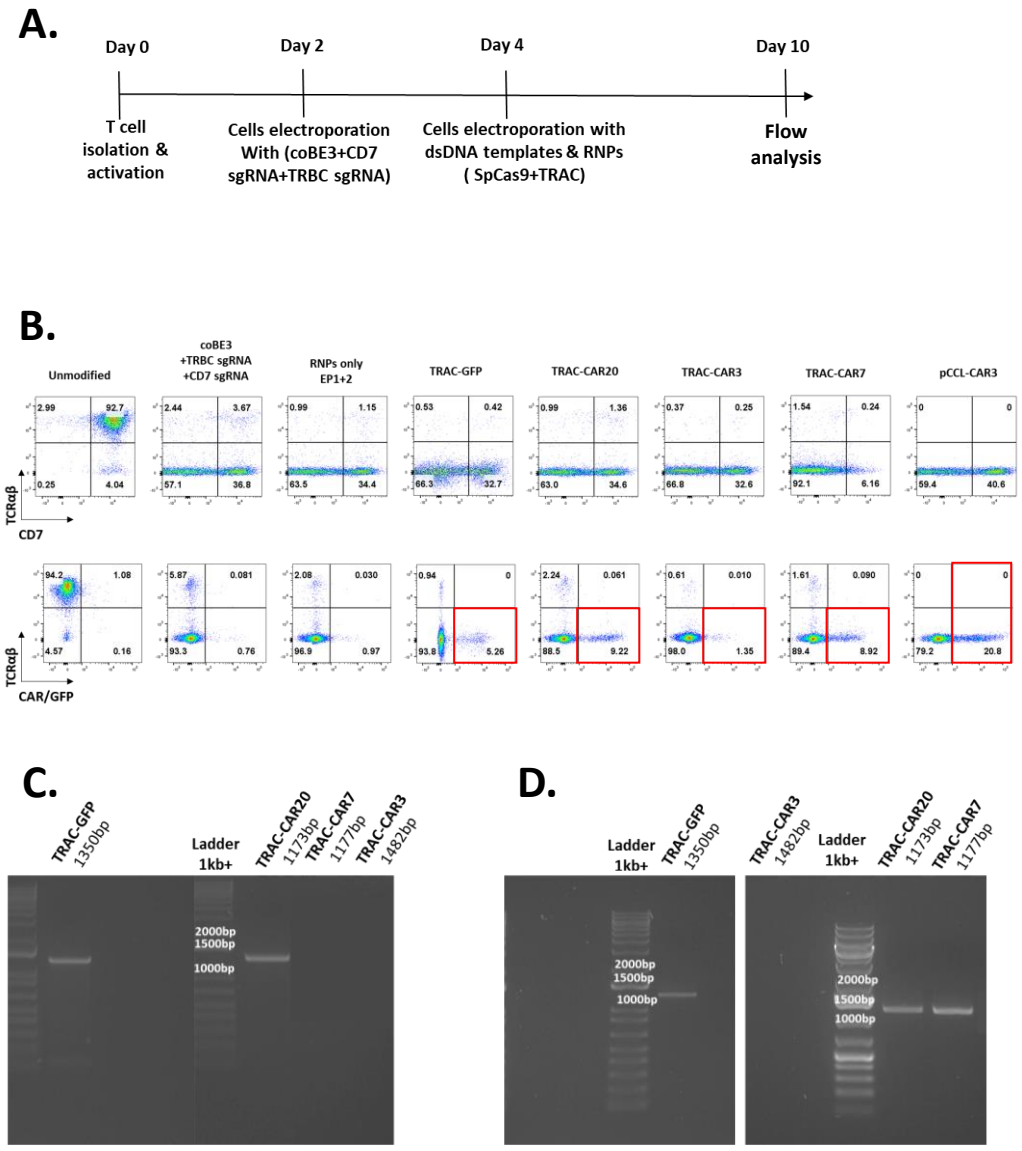

Figure 5-6 Two-step TCRαβ removal enables expression of CAR7 dsDNA template

A. Experimental timeline: primary PBMCs were isolated and T cells activated with anti-CD3/CD28 for 48hrs. T cells (n=1) were next electroporated with sgRNAs targeting both *TRBC1/2* and *CD7* loci and coBE3 mRNA, second cell electroporation at day 4 with TRAC targeting sgRNA, CAR3 or CAR7 dsDNA template and SpCas9 protein. **B.** Flow analysis at day 10 showing successful expression of CAR7 template, similar to the control template CAR20 and GFP. **C.** Gel picture showing the expected band size of CAR20 and GFP insert using the single step editing strategy. **D.** Gel picture showing the expected band sizes of CAR20, GFP and CAR7 when applying the two-step electroporation strategy, with no detection of CAR3. TRAC: T cell receptor alpha constant, GFP: green fluorescence protein. The red boxes highlighting the percentage of transgene expression.

5.4 Investigation of an alternative CAR integration site: endogenous *CD3ζ* locus

The possibility of inserting CAR transgenes using CRISPR/Cas9-mediated knock-in approach to insert either CAR3 or CAR7 transgenes into the *CD3ζ* locus was studied, for its potential in knocking-out CD3ζ, which consequently results in the removal of the TCR (similar to TRAC knockout). By inserting the CAR transgenes into the endogenous *CD3ζ* locus, the existing CD3ζ transcriptional machinery might be relevant for the control of CAR expression. The endogenous *CD3ζ* locus contains the regulatory sequences and transcription factors that control the expression of CD3ζ chains, which are integral components of the T cell receptor complex. By placing the CAR transgenes within this locus, the existing transcriptional machinery that governs CD3ζ expression can also impact the expression of the CAR. This can lead to more consistent and appropriate levels of CAR expression, as they are guided by the same regulatory elements as CD3ζ. This approach has the advantage of delivering a modestly reduced-sized template, preservation of both CD3ζ isoforms and ensures compatibility with T cell signalling. Integrating the CAR transgenes into the *CD3ζ* locus results in a relatively smaller genetic modification compared to inserting them into other genomic locations. This can have practical benefits such as improved efficiency of the genetic modification process and potentially reduced cellular stress caused by large genetic alterations. Two alternatively spliced transcript variants encoding distinct isoforms of *CD3ζ* (CD247-201 and CD247-202) have been identified that play distinct roles in T cell signalling. Integrating the CAR transgenes into this locus can ensure that the expression of these isoforms is preserved.

T cell activation and signalling pathways are intricately linked to the CD3ζ molecules. By integrating the CAR transgenes into the same genomic region, the signalling pathways that are initiated upon CAR engagement and can therefore be integrated with the natural T cell signalling pathways more seamlessly. This can enhance the overall functionality and responsiveness of the CAR-modified T cells.

The exploration of alternative integration sites is important for optimising CAR design and function, considering different transcriptional machinery and potential expression variations that may impact CAR-T cell behaviour and prevent fratricide.

An innovative sgRNA design, which specifically targeted the region between the transmembrane domain (typically what incorporates within a CAR configuration) and the intracellular domain of CD3ζ was designed and tested demonstrating high knockout efficiency.

A CD3ζ homology template, as opposed to the TRAC template, was designed without the CD3ζ element of the CAR construct. This reduced the CAR7 size from 2374 bp to 1785 bp. The truncated ΔCAR7 template incorporated a P2A linked scFv to CD8α stalk/transmembrane and 4-1BB regions in frame with the endogenous CD3ζ sequence. In this configuration the internal stop codon and bGH polyA sequence were excluded and endogenous elements from the -C terminus of CD3ζ employed The P2A sequence, located between the CD3ζ and GFP or CAR genes in a single mRNA transcript, acts as a "self-cleaving" peptide during translation. This causes a "ribosome skipping" event, where the ribosome releases the nascent polypeptide chain upstream of the P2A sequence while continuing translation downstream. Since GFP lacks transmembrane regions, it mainly stays in the cytoplasm, displaying its fluorescent properties without being targeted to specific organelles (**Figure 5-7 A**). Similar to TRAC template production, CD3ζ templates were produced with 300 bp of homology regions of endogenous CD3ζ sequence (**Figure 5-7 B**).

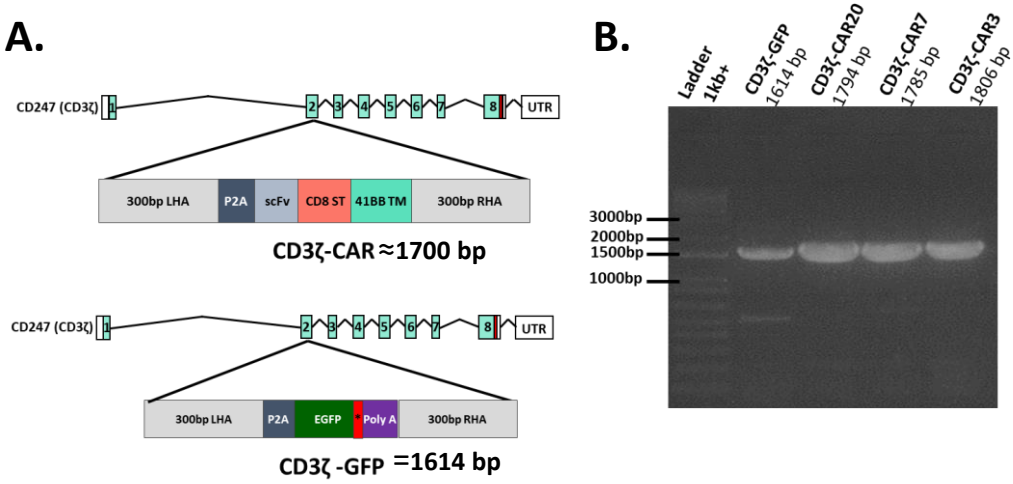

Figure 5-7 dsDNA CD3ζ-CAR donor template design

A. Iterations of transgenes encoding dsDNA templates with 5' and 3' homology regions to endogenous CD3ζ. CD3ζ-CAR construct preceded by P2A and incorporates scFv, CD8α stalk/transmembrane, and 4-1BB regions flanked by CD3ζ homology arms. EGFP coding templates preceded by P2A and incorporating downstream STOP codon and bGH polyA sequence flanked by CD3ζ homology arms. **B.** Amplification of synthetic templates flanked by 300 bp CD3ζ homology arms. DNA was gel extracted, concentrated and purified for downstream complexing with RNP and electroporation into T cells. GFP: green fluorescence protein, LHA: left homology arm, RHA: right homology arm.

5.4.1 Targeted insertion of GFP into the endogenous *CD3ζ* locus

To determine the impact of simultaneous *CD3ζ* and *CD7* knockout on the efficiency of CRISPR-mediated transgene knock-in to the *CD3ζ* locus a GFP control dsDNA template was designed.

PBMCs from healthy donors were isolated and activated for 48 hours prior to electroporation with dsDNA templates encoding eGFP either with RNP CD3ζ alone or with a combination of RNP CD3ζ and CD7 RNP complexes at a molar ratio of 1:1.2 (sgRNA: SpCas9 protein).

Flow analysis at day 4 post-electroporation showed high levels of TCRαβ and CD7 disruption and up to 90.7% double knockout ($TCR\alpha\beta^-/CD7^-$) when RNP CD3ζ and CD7 RNP complexes were combined. GFP expression was comparable in cells electroporated with RNP CD3ζ alone (23.5%) or in combination with CD7 RNP (24.5%)

(**Figure 5-8**) indicating that simultaneous disruption at two loci does not interfere with the desired knock-in event.

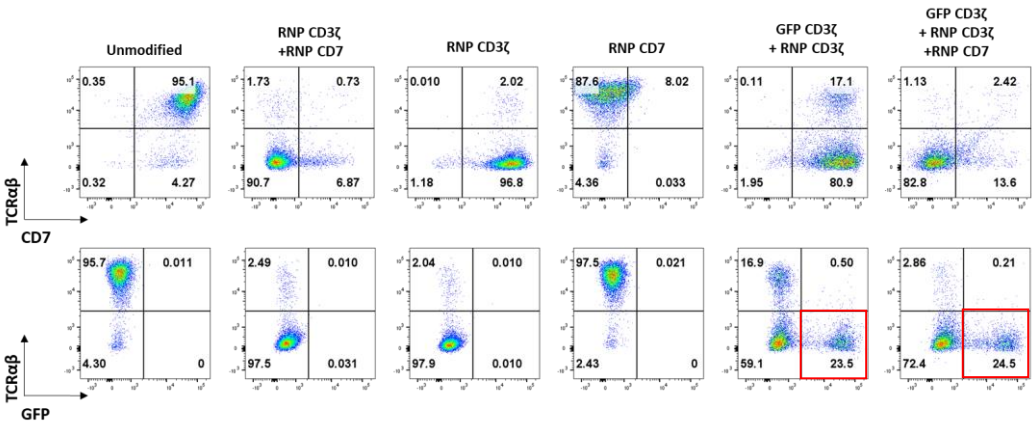

Figure 5-8 CRISPR-mediated GFP knock-in to *CD3ζ* locus

Primary PBMCs were isolated and T cells activated with anti-CD3/CD28 for 48hrs. T cells (n=1) were next electroporated with either RNP CD3ζ only or with RNP CD3ζ and RNP CD7 complexes and combined with dsDNA of GFP encoding template. Flow analysis at day 4 post-electroporation showed successful insertion of GFP following electroporation of single RNP CD3ζ or dual RNP CD3ζ/CD7 complex. The red boxes highlighted the percentage of GFP expression.

5.4.2 Insertion of CAR7/CAR3 into endogenous *CD3ζ* locus

To test the insertion of CAR7 and CAR3 into *CD3ζ* locus, PBMCs from healthy donors were isolated and activated with TransAct for 48 hours prior to electroporation with a 1:1.2 (sgRNA: SpCas9 protein) molar ratio of CD3ζ and CD7 RNP complexes and 20 µg of dsDNA templates expressing either CAR7 or CAR3 (**Figure 5-9 A**). As controls, previously validated eGFP and CAR20 dsDNA templates were run in parallel with electroporated RNP-only cells. Lentiviral vectors for pCCL-CAR7 and pCCL-CAR3 served as positive controls of CAR expression and were used to transduce cells 24 hours after electroporation resulting in 17.3% CAR7 and 31.3% CAR3 expression (**Figure 5-9 B&C**).

Four days post-electroporation, the phenotypic analysis revealed a high percentage of double knockout in T cells (TCRαβ$^-$/CD7$^-$) across all experimental conditions. T cells electroporated with RNP complexes but no template displayed a double knockout

percentage of 95.7%, whereas there was a slight drop when CAR20 or GFP templates were co-delivered, measured at 61.2% and 79.4%. Targeted knock-in for each dsDNA donor template was 14.7% for CAR20 and 9% for GFP. Interestingly, although the CAR3 T cells demonstrated a high double knockout percentage of 96.6%, flow cytometry analysis only detected 2.2% expression of CAR3. Conversely, the CAR7-T cells also displayed a double knockout percentage of 90.6% but had a successful insertion rate of 17.1%, comparable to the expression rate achieved by the pCCL-CAR7 vector in this experiment (**Figure 5-9 B&C**).

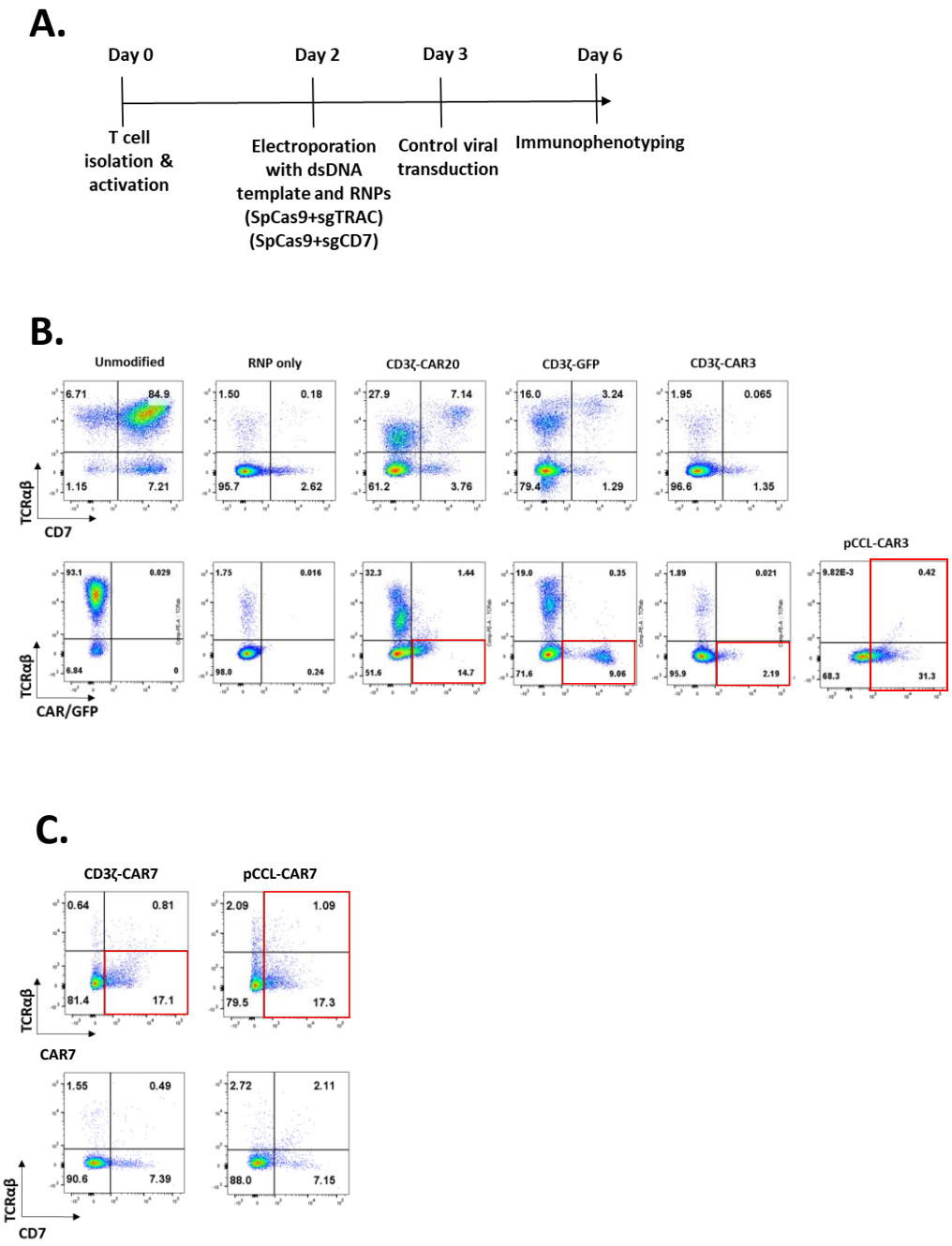

Figure 5-9 CRISPR-mediated transgene knock-in to *CD3ζ* locus

A. Primary PBMCs were isolated and T cells activated with anti-CD3/CD28 for 48hrs. T cells were next electroporated with an RNP complex of SpCas9 and CD3ζ-CD7 targeting sgRNA and combined with respective dsDNA CAR of GFP encoding template. pCCL-CAR7 and pCCL-CAR3 encoding lentiviral vectors used as positive CAR control in T cells electroporated with SpCas9 RNP-CD3ζ and SpCas9 RNP-CD7 sgRNA. **B.** Flow analysis at day 4 post- electroporation showed high double knockout percentage of TCRαβ^{-}/CD7^{-} with successful insertion of CAR20 and GFP. Unsuccessful insertion of CAR3 into CD3ζ, while control pCCL-

CAR3 vector showed successful CAR3 expression. **C.** Flow analysis on day 4 post-electroporation of CAR7 showed high double knockout percentage of TCRαβ$^-$/CD7$^-$, and successful CAR7 insertion with expression level similar to pCCL-CAR7 vector in this experiment. The red boxes highlighting the percentage of transgene expression.

This strategy was repeated in multiple donors (n=4) testing the insertion of dsDNA of CAR7 alongside with GFP, and cell viability was initially assessed to exclude any potential toxicity associated with dsDNA template. Four days after electroporation, both conditions exhibited high levels of viability of 82.3% to 96.0% electroporated with the GFP dsDNA template and 72.8% to 94.4% with the CAR7 dsDNA template (**Figure 5-10 A**). Following expansion in G-Rex flasks, flow analysis was performed on day 13 to assess the TCRαβ/CD7 disruption. The analysis revealed a high proportion of double knockout (TCRαβ$^-$/CD7$^-$) in CD3ζ-GFP cells and CD3ζ-CAR7 cells, with percentages ranging from 78.8% to 98.9% and 91.2% to 97.9%, respectively (gated on CD2+) (**Figure 5-10 B**). Successful template knock-in of CD3ζ-GFP and CD3ζ-CAR7 constructs was also confirmed across all four donors an average insertion rate of 43.1% ± 4.3% SEM for CD3ζ-GFP and 26.1% ± 3.0% SEM for CD3ζ-CAR7. These results demonstrated more efficient and consistent incorporation of the CD3ζ-GFP and CD3ζ-CAR7 constructs in four donor samples (**Figure 5-10 C**). Two of the four donors underwent further enrichment using magnetic bead depletion of residual TCRαβ-positive cells, yielding a >99% TCRαβ- population expressing either GFP or CAR7 (**Figure 5-10 D**). In the initial examination of T cell flow staining, conducted four days post-electroporation, some residual CD7 was still detected on the cell surface. However, as the cells continued to be cultured in G-Rex and were re-evaluated on day 13, an evident in-culture CAR7-mediated enrichment was observed (**Figure 5-10 D**). This suggests a dynamic process of CD7 reduction and CAR7 enhancement during the culture period.

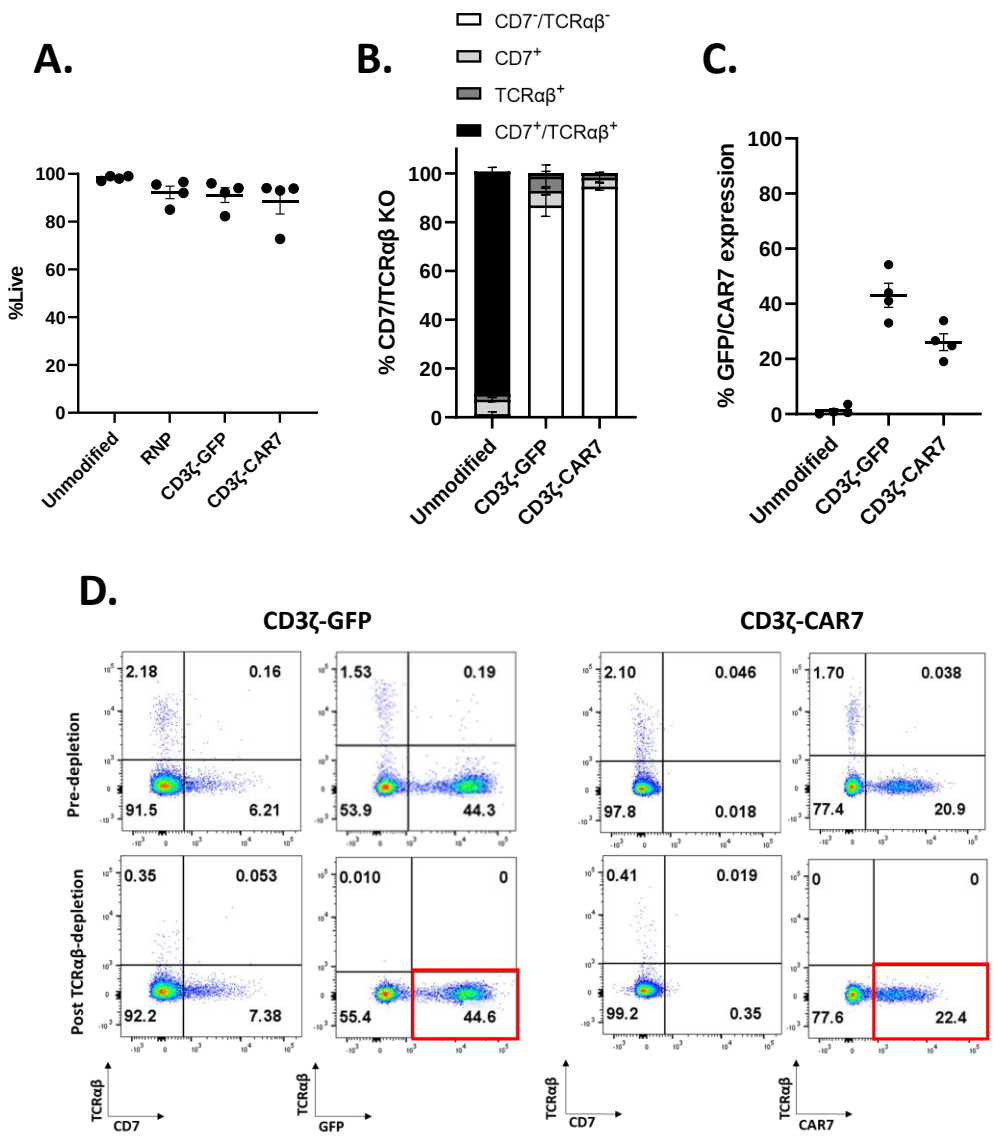

Figure 5-10 Targeted template knock-in into *CD3ζ* locus in multiple primary donors

A. Cell viability detection at day four post dsDNA GFP or CAR7 template insertion. **B.** Histogram representing the CD7 and TCRαβ knockout results across n=4 donors. Error bars represent the standard error of the mean (SEM). **C.** Expression of CAR7 at end of culture (pre-TCRαβ depletion) following electroporation with SpCas9-CD3ζ + SpCas9-CD7 RNPs combined with respective CAR7 encoding or GFP encoding dsDNA templates. Histograms depict mean of expression levels measured by flow cytometry in four donors. Each point represents an individual donor. **D.** Flow analysis of cells on days 13 (pre-TCRαβ) or 14 (post-TCRαβ)

depletion showing surface TCRαβ/CD7 and GFP or CAR7 expression levels. Red boxes showing the expression level of GFP and CD3ζ-CAR7 post-TCRαβ deletion.

For genomic verification of transgene insertion into *CD3ζ*, DNA was extracted and PCR amplified using primers designed to bind endogenous CD3ζ sequence upstream of the CD3ζ homology arm (forward primer) and within the template sequence (reverse primer). Gel electrophoresis of the amplicon confirmed the presence of the full-length template (1452 bp) for CAR7, and further Sanger sequencing of the gel extracted amplicon confirmed the template sequence and corresponding junctions with the endogenous *CD3ζ* locus (**Figure 5-11 A&B**).

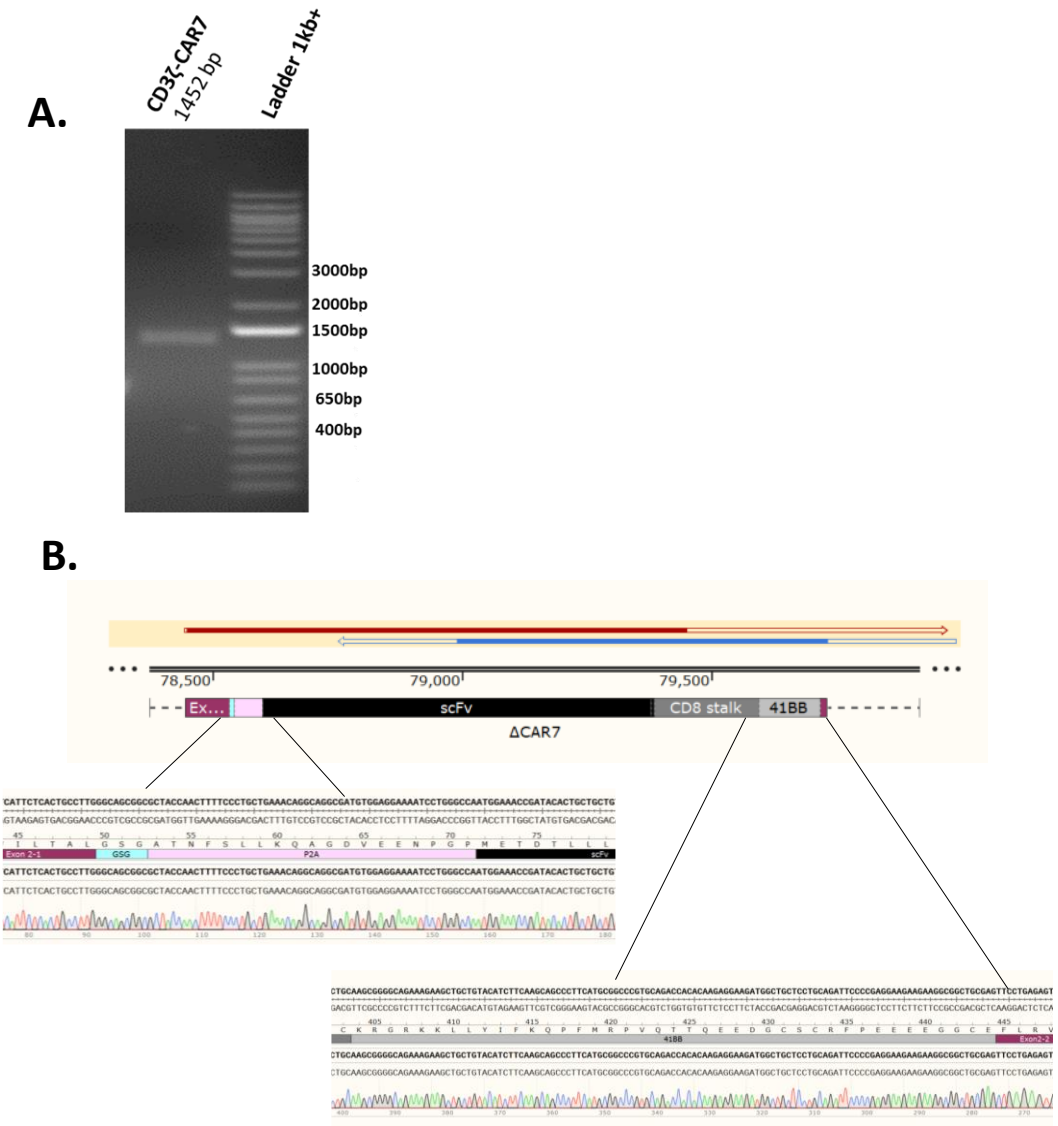

Figure 5-11 Confirmation of CAR7 insertion into *CD3ζ* locus

A. PCR amplification of ΔCAR7 inserted into *CD3ζ* loci indicates successful in frame integration, gel picture showing the expected band size of 1452 bp. This band was gel extracted and PCR purified before sending for Sanger sequencing **B.** The Sanger sequencing of ΔCAR7 in to the *CD3ζ* loci showing successful in frame integration. The left black dashed line represents Intron 1, followed by Exon 2, where the ΔCAR7 insertion took place, then the black dashed line of Intron 2. The blue arrow represents sequence alignment from the forward primer, and the red arrow represents the reverse primer's sequence alignment. Representative zoomed-in chromatogram trace figure demonstrates in frame integration of CD3ζ-CAR7 expression.

5.4.3 Transcript detection of CD3ζ -CAR7 expression

The objective of this investigation was to evaluate the splicing patterns of the CD3ζ transcript downstream of the CAR7 insertion and whether this would induce alternative splicing events, crucial in understanding the potential implications for the overall functionality of CAR-T cell therapies.

RNA was extracted from the cells and cDNA was synthesised. GAPDH was used as a control of RNA extraction and cDNA production. Following PCR amplification, the expected band size of CD3ζ-CAR7 was detected by gel electrophoresis and confirmed by Sanger sequencing, with two different CD3ζ isoforms detection (CD247-201 and CD247-202) (**Figure 5-12**).

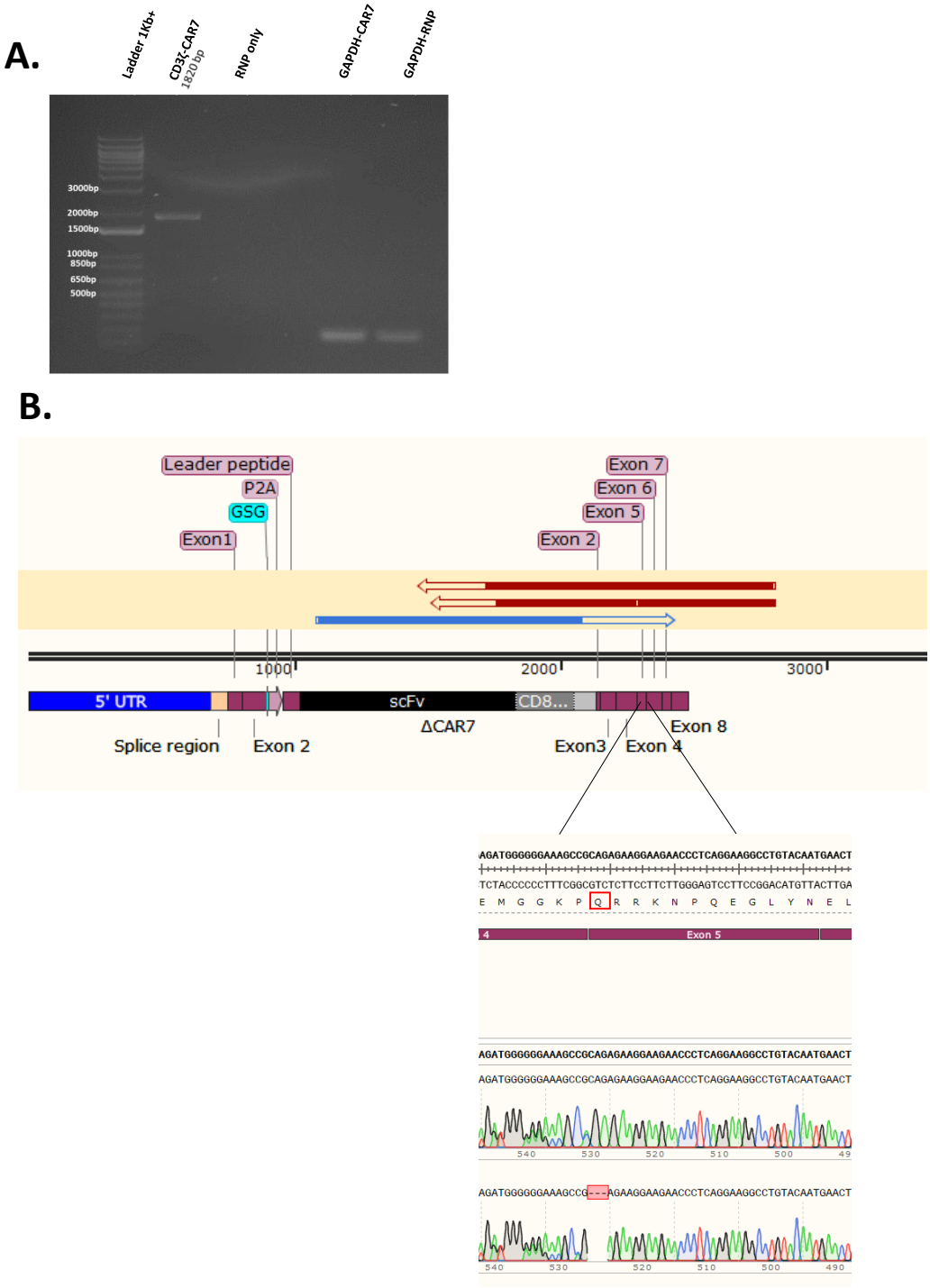

Figure 5-12 Successful production of cDNA for CD3ζ-CAR7

A. PCR amplification of cDNA for CD3ζ-CAR7 amplifying the insert of the CAR7 into the *CD3ζ* locus showed the expected band size of 1820 bp, RNP alone without a template as negative control. GAPDH amplification across exons 2 and 3 control for successful RNA extraction and cDNA production. **B**. Sanger sequencing of the cDNA verifies in frame insertion of the ΔCAR7, as indicated by SnapGene alignment. The red arrow represents sequence alignment from the forward primer, and the blue arrow

represents the reverse primer's sequence alignment. Representative zoomed-in chromatogram trace figure demonstrates in frame integration with two distinct CD3ζ isoforms identification.

5.4.4 Intracellular staining for CD3ζ cytoplasmic tail

To further assess whether the insertion of CAR7 was in frame with *CD3ζ* locus and correctly spliced downstream of the CAR insertion site, intracellular staining targeting the cytoplasmic tail of CD3ζ was performed. T cells from Section 5.4.2 were used to detect CD3ζ cytoplasmic protein. Intracellular staining of CD3ζ was conducted following cell fixation and permeabilization. Four days post-electroporation flow analysis of the control unmodified cells showed 91% expressed CD3ζ cytoplasmic tail. RNP electroporated cells where CD3ζ had been knocked out no longer stained positive for CD3ζ. pCCL-CAR7 transduced cells were 43.5% double positive for intracellular vector-derived CD3ζ and surface CAR expression, while CD3ζ-CAR7 knock-in cells showed matched expression of endogenous CD3ζ expression and CAR7 (20.8%) verifying correct insertion of CAR7 in frame with the endogenous CD3ζ chain (**Figure 5-13**).

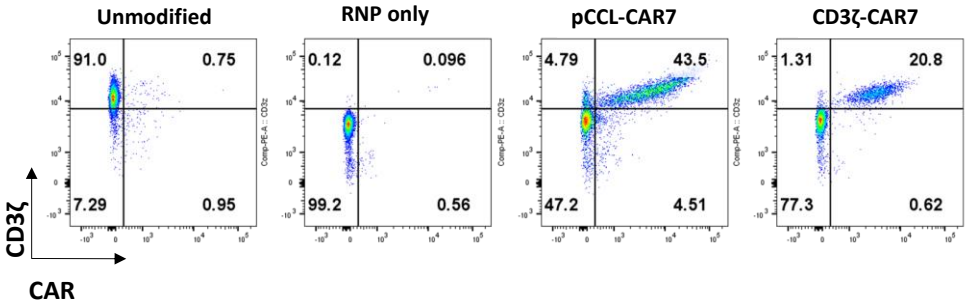

Figure 5-13 Successful expression of intracellular CD3ζ cytoplasmic tail in CAR7+ cells

Expression of intracellular CD3ζ cytoplasmic tail in CD3ζ-CAR7 knock-in cells. Knock-in of CAR7 devoid of CD3ζ in frame with endogenous CD3ζ site was detected by intracellular staining for CD3ζ. Control pCCL-CAR7 lentiviral vector transduced cells included CD3ζ within the CAR construct.

5.4.5 Chromium release assay of *in vitro* cytotoxicity

In order to assay whether expressing CAR7 from a CD3ζ-CAR7 knock-in template impacted the cytolytic potential of the T cells, a ^{51}Cr release assay was performed, comparing killing efficiency of CD7+ target cells to conventional lentiviral pCCL-CAR7 expressing T cell effectors. T cells expressing CD3ζ-GFP or un-transduced, unedited (UTD) T cells were included as negative controls of killing. CD3ζ-CAR7 effectors exhibited high levels of cytotoxic activity against Jurkat cells across a wide range of effector:target (E:T) ratios compared to unmodified controls. In this experiment vector expressing CAR7 control cells unexpectedly did not result in a positive signal (**Figure 5-14 A**). Effector batches generated from an alternative donor were tested where CD3ζ-CAR7 effectors were normalised for CAR expression to pCCL-CAR7 effectors as the expression of CAR7 varied between the two (CD3ζ-CAR7: 22%; pCCL-CAR7: 44%). The normalisation process involved adding a greater number of CAR7 T cells to achieve a comparable CAR count between both groups (**Figure 5-10 D**). Target lysis on this occasion was comparable between CD3ζ-CAR7 and pCCL-CAR7 effectors achieving high level (>35%) of targeted killing even at reduced E:T ratios of 0.63-2.5:1 compared to CD3ζ-GFP or unmodified T cell controls (**Figure 5-14 B**).

A.

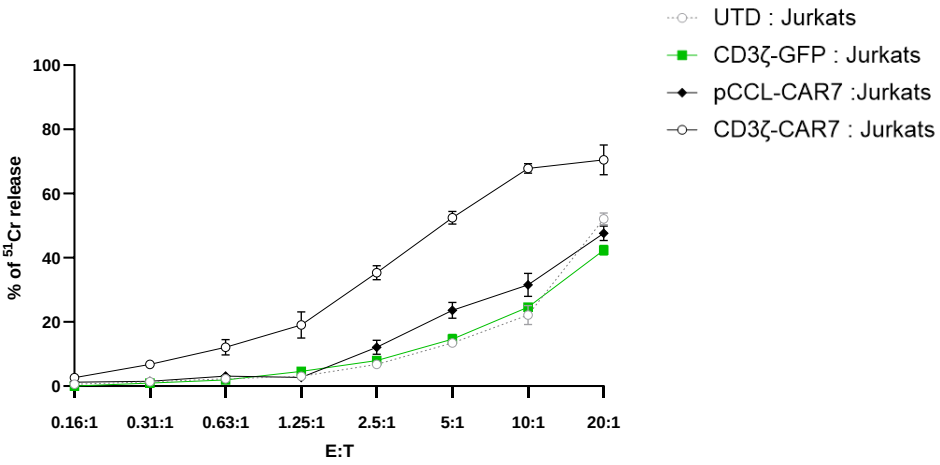

B.

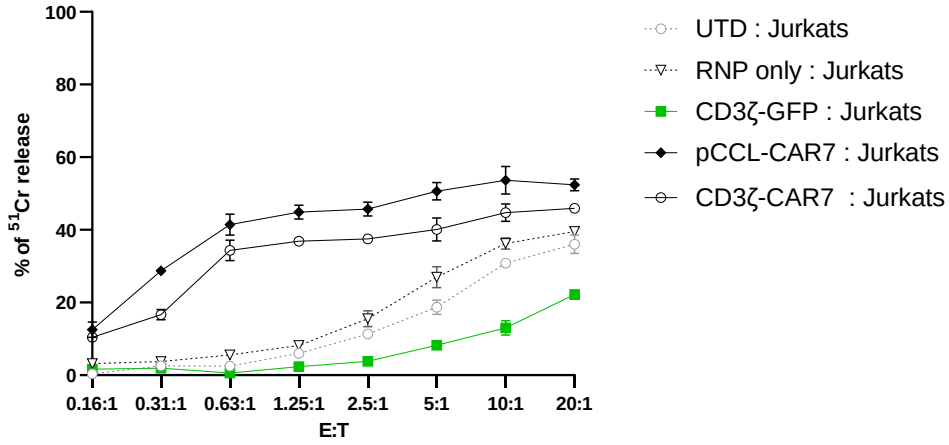

Figure 5-14 CD3ζ-CAR7 T cells exhibit comparable target cell lysis to vector expressed CAR7

A. First donor 4hr *in vitro* cytotoxicity of TCRαβ depleted CD3ζ-CAR7 effectors against ^{51}Cr loaded Jurkat cells across a range of Effector:Target (E:T) ratios. pCCL-CAR7 lentiviral vector transduced and TCRαβ knockout effectors acted as positive controls and CD3ζ-GFP expressing T cells or un-transduced unedited (UTD) T cells acted as negative controls. **B.** Second donor 4hr *in vitro* cytotoxicity of TCRαβ depleted CD3ζ-CAR7 effectors against ^{51}Cr loaded Jurkat cells across a range of Effector:Target (E:T) ratios. pCCL-CAR7 lentiviral vector transduced and TCRαβ knockout effectors acted as positive controls and CD3ζ-GFP expressing T cells or untransduced unedited (UTD) T cells, and RNP only acted as negative controls. Error bars represent the standard deviation (SD) of three technical replicates.

5.5 Non-viral insertion of transgene within the *CD7* locus

An alternative site that was considered for the insertion of CAR7 was the *CD7* locus, as it offers the advantage of disruption CD7 expression and thereby tackles the effects of fratricide.

Similar to previous experiments, dsDNA CAR7 templates were designed but with 5' and 3' homology arms to the *CD7* locus. The CD7-CAR7 construct was flanked by an upstream P2A self-cleaving peptide and downstream stop codon and bGH polyA sequence with symmetrical 300 bp of endogenous CD7 homology sequence at 5' and 3' ends The P2A sequence, located between the CD7 and GFP/CAR genes in a single mRNA transcript, acts as a "self-cleaving" peptide. During translation, the ribosome encounters the P2A sequence, causing a "ribosome skipping" event. This releases the nascent polypeptide chain upstream of the P2A sequence (CD7) while allowing continued translation of the downstream polypeptide chain (CAR). Due to its lack of transmembrane regions, GFP primarily resides in the cytoplasm, which displays its fluorescent properties without specific organelle targeting. (**Figure 5-15 A**). The chimeric sequence was manufactured by GeneArt and purified dsDNA template was amplified by PCR and concentrated by isopropanol precipitation. Templates for CD7-CAR7 and control CD7-GFP were confirmed for size by agarose gel electrophoresis (**Figure 5-15 B**).

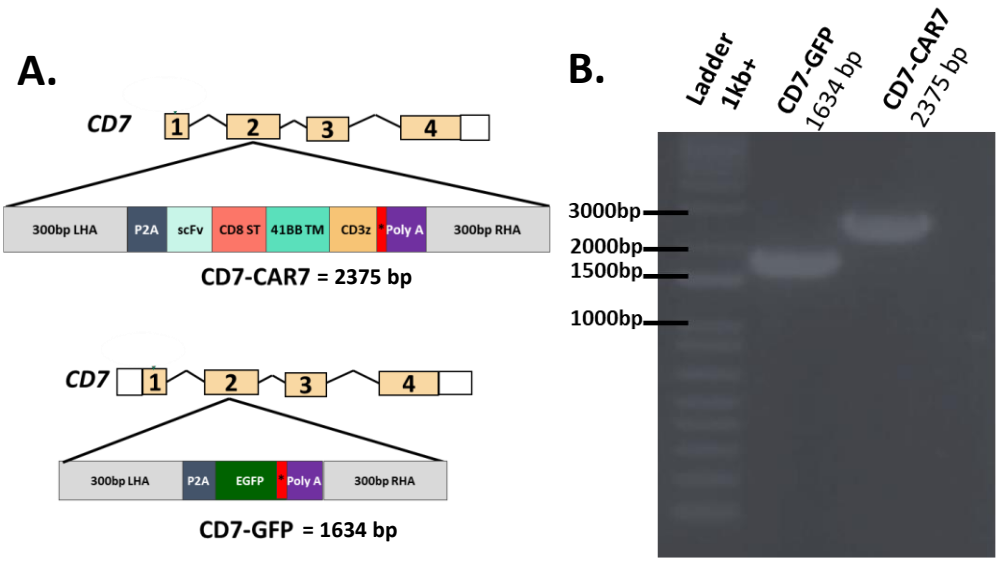

Figure 5-15 dsDNA CD7-CAR7 donor template design for knock-in into *CD7*

A. Iterations of transgenes encoding dsDNA templates with 5' and 3' homology regions to *CD7* locus. CD7-CAR7 construct incorporating synthetic CD3ζ domain, or CD7-GFP construct flanked by upstream P2A and downstream STOP codon and bGH polyA sequence. 5' and 3' 300 bp CD7 homology arm sequence incorporated. **B.** Amplification of synthetic templates flanked by 300 bp CD7 homology arms. DNA was gel extracted, concentrated and purified for downstream complexing with RNP and electroporation into T cells. GFP: green fluorescence protein. LHA: left homology arm, RHA: right homology arm.

To test the insertion of GFP and CAR7 into *CD7* locus, PBMCs from healthy donors (n=4) were isolated and activated with TransAct for 48 hours prior to electroporation with a combination of CD7 and TRAC RNP complexes at a 1:1.2 (SpCas9:sgRNA) molar ratio and 20 µg of dsDNA templates expressing GFP or CAR7. Electroporated cells with RNP alone (SpCas9-TRAC and SpCas9-CD7) were run in parallel as negative control and pCCL-CAR7 lentiviral transduction 24 hours post- electroporation was used as a positive control of CAR expression (**Figure 5-16 A**). Four days after electroporation, both conditions revealed high levels of cell viability, with 75% to 97.6% viability in CD7-GFP dsDNA template and 68% to 96.3% viability in CD7-CAR7 dsDNA (**Figure 5-16 B**). Flow analysis revealed a high proportion of double knockout ($TCR\alpha\beta^-/CD7^-$) in CD7-GFP cells and CD7-CAR7 cells, with percentages ranging from 77.6% to 90% and 67.5%% to 85.6%, respectively (gated on CD2+) (**Figure 5-16 C&D**).

All four donors had successful template knock-in of the CD7-GFP and CD7-CAR7 constructs, with an average insertion rate of 18.7% ± 3.5% SEM for CD7-GFP and 16% ± 3.5% SEM for CD7-CAR7 (**Figure 5-16 E&F**).

For genomic confirmation of transgene insertion into CD7, DNA was extracted from the cells and PCR amplified using primers designed to bind upstream of the CD7 homology arm sequence (forward primer) and within the template sequence (reverse primer). Gel electrophoresis of the amplicon confirmed the expected size for CAR7. Subsequent gel extraction and Sanger sequencing of positive band further corroborated the successful insertion (**Figure 5-17 A&B**).

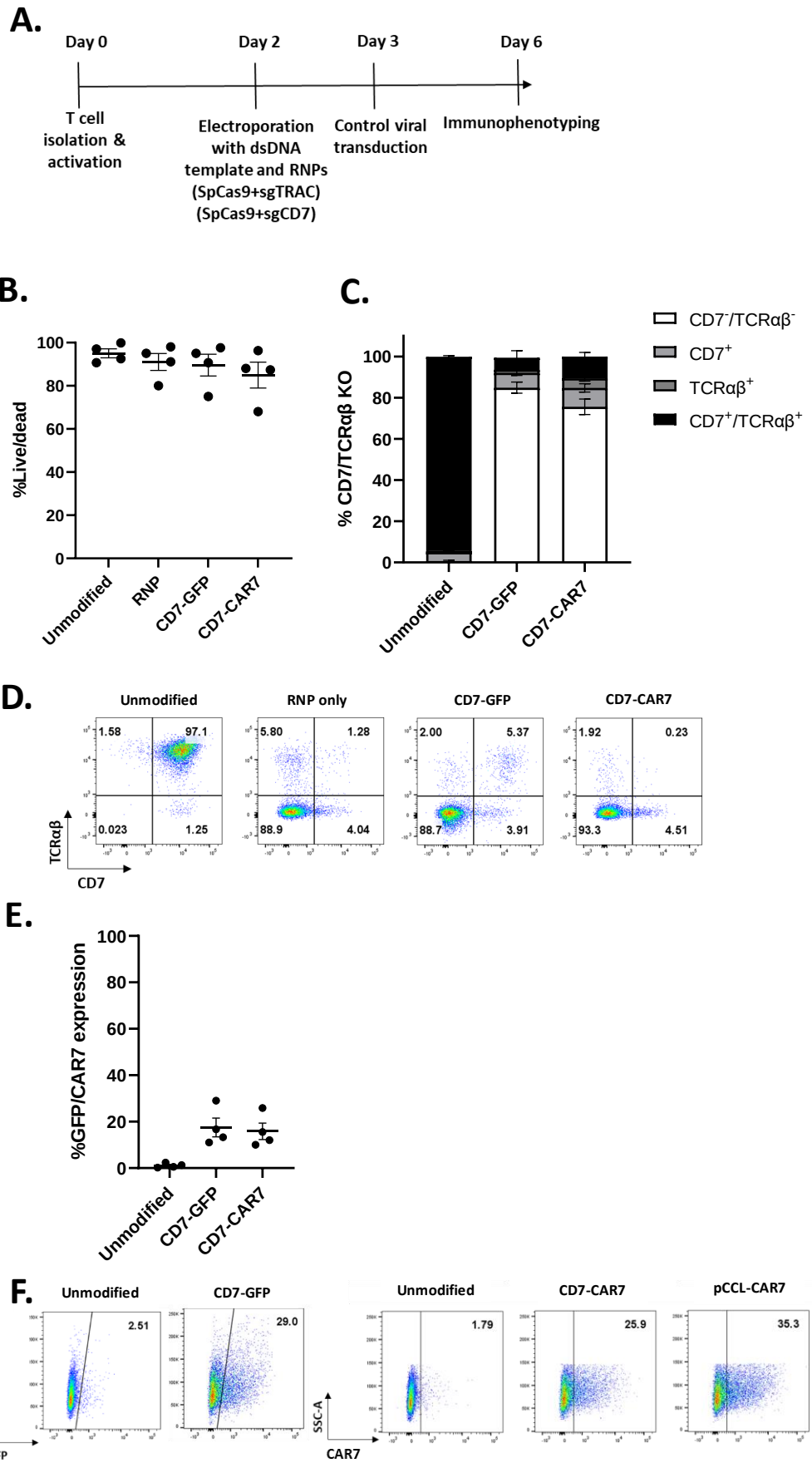
A.
Day 0
Day 2
Day 3
Day 6
T cell isolation & activation
Electroporation with dsDNA template and RNPs (SpCas9+sgTRAC) (SpCas9+sgCD7)
Control viral transduction
Immunophenotyping
B.
%Live/dead
Unmodified
RNP
CD7-GFP
CD7-CAR7
C.
% CD7/TCRαβ KO
CD7-/TCRαβ-
CD7+
TCRαβ+
CD7+/TCRαβ+
D.
Unmodified
RNP only
CD7-GFP
CD7-CAR7
TCRαβ
CD7
1.58
97.1
0.023
1.25
5.80
1.28
88.9
4.04
2.00
5.37
88.7
3.91
1.92
0.23
93.3
4.51
E.
%GFP/CAR7 expression
F.
Unmodified
CD7-GFP
2.51
29.0
SSC-A
GFP
Unmodified
CD7-CAR7
pCCL-CAR7
1.79
25.9
35.3
SSC-A
CAR7

Figure 5-16 CAR7 expression following integration into *CD7* locus in multiple primary donors

A. Primary PBMCs were isolated and T cells activated with anti-CD3/CD28 for 48hrs. T cells were next electroporated with an RNP complex of SpCas9-TRAC and SpCas-CD7 targeting sgRNA and combined with respective dsDNA CAR encoding template. pCCL-CAR7 encoding lentiviral vector used as positive CAR control in T cells electroporated with SpCas9 RNP-TRAC and SpCas9 RNP-CD7 sgRNA. **B.** Cell viability at day four post dsDNA GFP or CAR7 template delivery. **C.** Histogram representing the CD7 and TCRαβ knockout results across n=4 donors. The error bars represent the standard error of the mean (SEM). **E.** Expression of CAR7 at day four following electroporation with SpCas9-TRAC + SpCas9-CD7 RNPs combined with respective CAR7 encoding or GFP encoding dsDNA templates. Histograms depict mean of expression levels measured by flow cytometry across four donors. Each point represents an individual donor. **D.** Representative FACS plot showing the successful double knock out of TCRαβ/CD7 cell population in RNP only, CD7-GFP, and CD7-CAR7. **F.** Representative FACS plot at day four post-electroporation showing expression of CD7-GFP and CD7-CAR7. Successful CAR7 expression by pCCL-CAR7 vector.

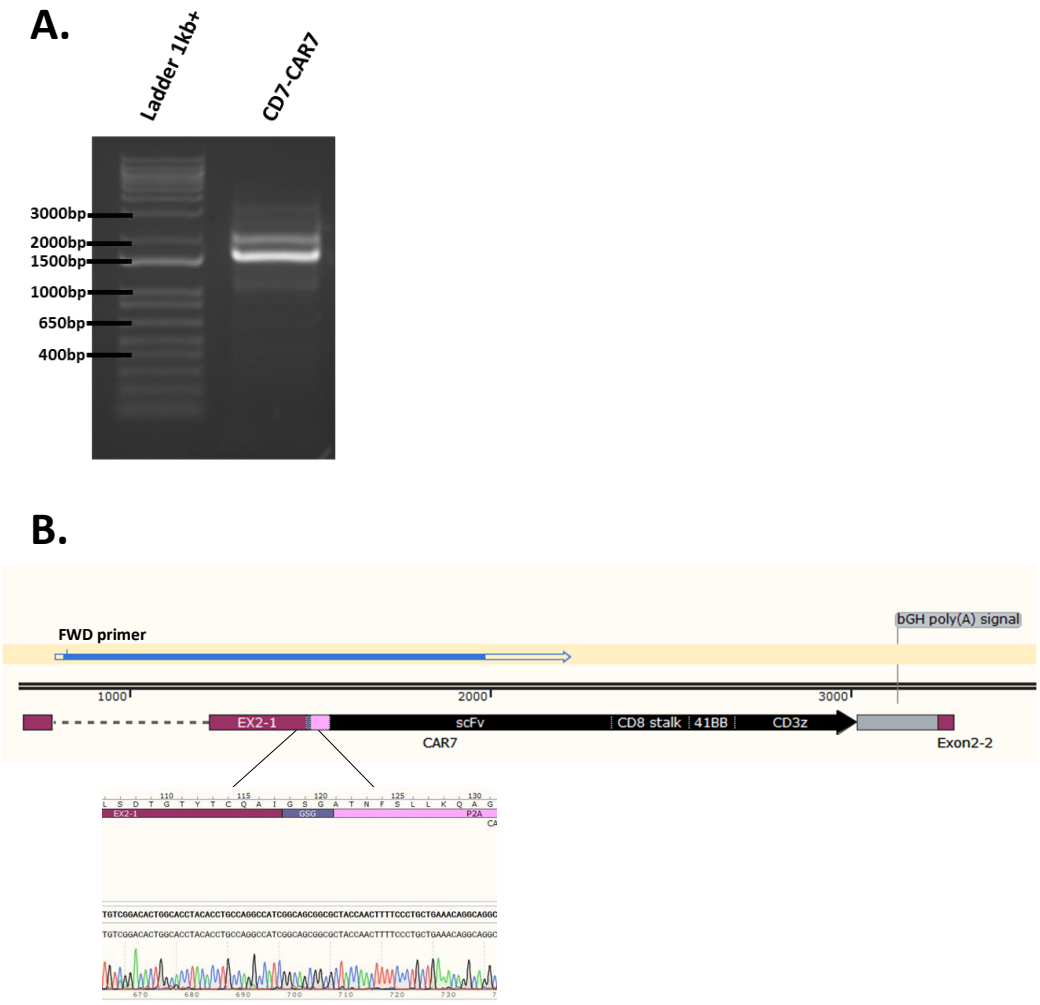

Figure 5-17 Confirmation of CAR7 insertion into *CD7* locus

A. PCR amplification of CAR7 into *CD7* loci indicate successful insertion, gel picture showing the expected band size of 1550 bp. **B.** Confirmation of CAR7 template in frame insertion into *CD7* loci by Sanger sequencing, and alignment to SnapGene map. The blue arrow represents sequence alignment from the forward primer. Representative zoomed-in chromatogram trace figure demonstrates in frame integration.

5.6 Chapter summary

In summary, this chapter investigated a virus-free strategy for the expression of a CAR transgene, thereby minimising production costs, manufacturing bottlenecks and improving the safety profile. This was investigated by using SpCas9 ribonucleoproteins (RNPs) with an sgRNA targeting the desired insertion site and a

dsDNA donor template encoding a self-cleaving CAR transgene cassette and homology arms of three distinct loci, *TRAC*, *CD3ζ*, and *CD7*.

The initial aim was to determine whether a CAR7 or CAR3 encoding dsDNA templates could be targeted to the *TRAC* locus using CRISPR-mediated transgene knock-in. The knock-in of a CAR transgene into the *TRAC* locus through CRISPR/Cas9 has been shown to enable more physiological levels of CAR expression while disrupting endogenous TCRαβ expression. Transcriptional activity mediated by the endogenous TRAC promoter machinery has been suggested to enhance CAR-T cell function.

Multiple attempts at inserting the dsDNA template into the *TRAC* locus were unsuccessful when CAR3 or CAR7 templates were used, contrary to when CAR20 or GFP templates were delivered. This could have been due to timing and residual fratricide effects, if TCRαβ and CD7 expression take longer to be lost from the cell surface than HDR-mediated CAR template insertion and expression. It was therefore necessary to complete a time-course experiment using a control dsDNA GFP template directed to the *TRAC* locus following SpCas9 delivery to determine at which point surface expression is abrogated. Using a dsDNA GFP template, it appeared that transgene expression could be robustly detected by 24 hours and peaked at 48 hours, highlighting that transgene expression occurs within the first 24 hours post-electroporation.

However, when evaluating protein knockout through CRISPR-mediated targeting of the *TRAC* and *CD7* genes to introduce a GFP dsDNA template, it was noted that TCRαβ expression had diminished within 24 hours. In contrast, CD7 expression remained detectable, suggesting the timing prior to CAR7 expression would need to be extended. Once the extended timing for surface CD7 expression to be cleared was taken into account, a proof-of-concept experiment was designed to prove the hypothesis. By disrupting alternative sites within *CD7* and *TRBC* using cytidine base editing 48 hours ahead of CRISPR RNP with dsDNA template insertion, successful, yet modest expression of CAR7 could be seen.

An alternative strategy investigated the CRISPR-mediated knock-in of CAR3 and CAR7 transgenes into the *CD3ζ* locus. Unfortunately, the approach was not successful in generating CAR3 cells. However, across multiple donors, the insertion of CAR7 into the *CD3ζ* locus was effectively achieved, as confirmed at the genomic level. The CD3ζ-CAR7 T cells that were generated were expanded and tested for their *in vitro* cytotoxicity. It was found that CD3ζ-CAR7 T cells exhibited potent killing capabilities, which were comparable to those of T cells expressing the CAR7 vector. The efficient insertion of CAR7 into the *CD3ζ* locus ensured that it was in frame with *CD3ζ*, allowing for strong expression of the CAR from endogenous CD3ζ machinery. This was validated through the production of cDNA and the expression of the intracellular CD3ζ cytoplasmic tail.

In an attempt to overcome TvT fratricidal effects during non-viral CAR7 production, the *CD7* locus was selected as a potential integration site. The results were promising, with successful CAR7 expression achieved across multiple donors. This finding opens possibilities for using the *CD7* locus as an effective site for CAR7 integration, potentially minimising any negative effects associated with fratricide.

Chapter 6 Discussion

This project's overarching objective was to optimise CRISPR/Cas9-based genome editing technology for the engineering of universal CAR-T cell therapeutics that can overcome TvT fratricide. Particular focus has been given to comparing different CBEs incorporating human cytidine deaminases (either hAID or hA3A), alongside the rat APOBEC1 used in BE3 for their ability to disrupt *TRBC* and *CD7* gene expression. Additionally, investigation involved coupling cytidine deamination of the *TRBC* loci to CAR expression via the terminal CRISPR-CAR platform. Furthermore, virus-free CAR-T cells were generated by using long dsDNA as a template for HDR when combined with RNP complexes.

One of the key challenges in developing CAR T-based techniques for treating T cell malignancies stems from the fact that both CAR and tumour cells of the T-lineage express shared target antigens (358). Innovative strategies such as protein expression blockers (102, 135) or genome editing (71, 72, 101, 120), seem essential for disruption of the target antigen in T cells prior to CAR expression to prevent self-antigen-driven fratricide. Other strategies aimed at mitigating fratricide in engineered T cells involve epitope masking, a technique that decreases the intensity of fratricidal interactions by reducing the accessibility of antigen molecules on the cell surface. This is particularly evident in T cells that have been genetically modified to express CD38-specific chimeric receptors, as demonstrated by Gao, Tong *et al*. (2019) (103). Similarly, in the context of CAR7 epitope masking, innovative approaches include using a recombinant anti-CD7 antibody to specifically block the CD7 antigen on the T cell surface (105).

In the pursuit of evading T cell fratricide, alternative effector cell sources have been explored leading to the emergence of CAR-NK cells. As NK cells do not express the TCR/CD3 complex, they are able to express an anti-CD3 CAR without the risk of fratricide. Preclinical studies have explored CAR-modified NK cells for treating T cell malignancies. Notably, three CAR-NK cell therapies directed at CD3 (97), CD5 (155), and CD7 (124) have been developed for T cell malignancies, demonstrating

substantial anti-tumour cytotoxicity against T cell lymphomas and T-ALL both *in vitro* and *in vivo*, employing engineered CAR-NK-92 cells (359). CAR-NK cell therapy holds promise in the treatment of malignant tumours due to its potential to circumvent GVHD concerns (360). However, CAR-NK cells exhibit limitations, including their challenging scalability due to difficulties in obtaining and transducing sufficient NK cells (359), a shorter lifespan compared to T cells (360), susceptibility to NK cell-mediated killing, particularly for NK-92 cells (361), and the need for vigilant monitoring in clinical applications due to their potential for malignant expansion stemming from their origin in a lymphoma patient (362).

Moreover, in an effort to counter fratricide within CD7-CAR T cells, researchers turned to naturally occurring $CD7^-$ T cells as a solution, resulting in the generation of $CD7^-$CAR-T cells by two-step magnetic bead separation, which exhibited promising antitumor efficacy (106). The first human phase 1 clinical trial with naturally selected CD7 CAR-T cell therapy, involving 20 patients with relapsed/refractory T cell malignancies, demonstrated promising results. The outcomes were highly encouraging, with most patients achieving complete remission (139). This work has highlighted that using naturally selected CAR-T cells avoids the need for extra genomic modifications, making the procedure simpler and potentially lowering the risk of unintended side effects. However, a challenge lies in the limited numbers or low frequency of naturally occurring $CD7^-$ T cells, which could hinder practical application. Therefore, alternative strategies involving genomic modifications can provide a greater degree of control over the cell population, enabling optimisation of their characteristics and potential for enhanced therapeutic outcomes.

This project explored the possibility of mitigating TvT fratricide effects through genomic disruption using SpCas9 or base-editing technologies for the orderly removal of shared TCR/CD3 and CD7 from T cells prior to CAR expression.

6.1 Cytidine deaminase base editors for multiplexed editing of T cells

Genome editing technologies, such as TALENs and CRISPR/Cas9, depend on targeted DNA cleavage and repair through NHEJ, and while they offer a high level of editing, they also induce DSB formation which can result in translocations, large deletions, and upregulation of p53 tumour suppressor protein (265, 339, 363, 364). Translocation events commonly arise due to on-target cleavage followed by recombination with a homologous genomic region. They can also result from concurrent cleavage at both on-target and off-target sequences, or as a result of multiple on-target cleavage events in cases of multiplexed editing (365). Instances of chromosomal translocations have been sporadically documented in preclinical studies involving human T cells that have been engineered using genome-editing techniques such as TALENs or CRISPR/Cas9 (60, 308, 366).

Previous work indicates that TALEN-mediated genome editing in T cells may result in chromosomal alterations, including karyotypic abnormalities. These karyotypic aberrations were seen in around 5% of TALEN-edited CAR19-T cells with breaks at both the *TRAC* and *CD52* loci (111), highlighting the potential influence of this genome editing technique on cellular genomic stability. In a Phase 1 clinical trial with six paediatric patients with relapsed/refractory CD19-positive B-ALL, CRISPR/Cas9 engineered universal CAR19-T cells were employed with similar edits in the *TRAC* and *CD52* loci. The study also detected translocations between *TRAC* and *CD52* through ddPCR, occurring at a frequency of up to 1% (73).

A recent comprehensive study revealed that chromosome loss is a universal consequence of site-specific Cas9 genome editing (265). Stadtmauer *et al*. (2020) showed that triple knockout using CRISPR/Cas9 to delete *TRAC*, *TRBC*, and *PDCD1* has the potential to cause frequent chromosomal alterations (60). Translocations, chromothripsis events, and other unintended editing outcomes have been documented as outcomes of CRISPR/Cas editing in human cells (367). Emerging base editing technologies rely on targeted base conversion instead, without requiring a dsDNA break. These technologies therefore reduce the unwanted effects associated

with DSB formation. The enhanced base editor technologies outlined in this research carry the potential to achieve remarkable precision in C>T (G>A) base conversions. This progress can be strategically harnessed for introducing stop codons or modifying splice sites, thereby influencing gene expression.

Several studies have undertaken a comparative analysis of translocation events occurring in the context of Cas9 editing and base editing. Notably, Webber, Lonetree (308) achieved successful disruption of *TRAC*, *B2M*, and *PDCD1* genes in primary human T cells using the BE3 base editing technology. The resulting CD19 CAR-T cells exhibited reduced frequencies of DSB and translocations in comparison to those edited with Cas9. In a separate study, an examination was conducted on CBE and its potential to induce translocations. This investigation revealed that translocations induced by SpCas9 at three specific on-target sites (*B2M*, *TRAC*, and *PDCD1*) occurred with frequencies ranging from 0.5% to 1.6%. Intriguingly, CBE did not lead to any detectable instances of translocations, as reported by Diorio, Murray (123).

Delivering base editors in the form of mRNA, rather than using plasmid DNA, significantly reduces all forms of off-target editing (368). When DNA encoding the editor is delivered, it can lead to prolonged expression, increasing the risk of off-target editing. In contrast, RNA has a shorter lifespan than DNA, and it does not require transcription to produce an active editor when delivered as mRNA along with the necessary sgRNA. This results in a shorter timeframe between delivery and editing for mRNA and gRNA compared to DNA, and transient expression of the editor. As an example, in recent *ex vivo* base editing experiments involving primary T cells, chemically modified mRNA encoding the base editor BE3 and synthetic gRNA were introduced through electroporation. In this setup, BE3 protein expression reached its peak at 12 hours post-electroporation and had almost entirely dissipated by 24 hours post-electroporation (72).

In this body of work, human-derived cytidine base editor (CBE) versions (either hAID or hA3A) alongside a rat APOBEC1 iteration were used to disrupt gene expression of *TRBC* and *CD7* by creating premature stop codons. It has been previously reported

that the base editing efficiency achieved by BE3 may exhibit variability, with some target C's located immediately downstream of a G demonstrating lower efficiency compared to others (297). In the pursuit of achieving efficient editing of specific targets, a group of researchers undertook the task of developing modified BE3 variants. In these engineered variants, a notable alteration involved the substitution of the APOBEC1 deaminase component with another enzymatic or functional element (299, 300, 310, 320, 327, 328). Furthermore, the study conducted by Doman assessed various base editors, including BE4 (BE3 was not evaluated in the study), as well as hAID and hA3A. While these editors demonstrated effective on-target editing capabilities, they also exhibited some degree of off-target effects (320) .

In the context of this study, an investigation was conducted into the possibility of achieving efficient knockout of both TCRαβ and CD7 expression in transduced cells by electroporating sgRNA of TRBC and CD7. A number of CD7 targeting sgRNAs were evaluated in terms of their on-target editing efficiency. These were evaluated in conjunction with a previously validated TRBC-targeting sgRNA to assess their collective potential in achieving dual knockout. The performance of these CD7 sgRNAs, along with both SpCas9 and coBE3 editing systems, indicated that the sgRNA designed to target exon 2 of the CD7 gene that introduces a premature STOP codon, exhibited the highest efficacy in terms of surface protein knockout, which had been used in a previous study (72), Additionally, in the same study, an investigation of 20 *in-silico* predicted guide-dependent Cas9-specific 'off-target' sites for each target demonstrated infrequently low levels of ectopic activity following BE3 editing (72). Next, the efficiency of primary T cell editing was compared between base editors coBE3, hAID and hA3A. Flow cytometry indicated efficient knockout of the *CD7* locus when using SpCas9, hA3A, and coBE3, with hAID showing relatively little cell surface removal of the CD7 protein. Sanger sequencing over the protospacer confirmed high levels of C>T conversion at the intended position C8 with both coBE3 and hA3A, producing a premature stop codon. Contrary to this hAID displayed a high degree of editing at alternative C positions within the editing window, but not at the desired nucleotide. Studies have shown that AID base editor predominantly deaminates

cytosine in WRC motifs (W = A/T, R = A/G) (336). In the case of the CD7 sgRNA, the target C (C8) did not fall within the optimal WRC motif, which helps to explain the relatively low editing at this site. This observation suggests that optimised CD7 sgRNA design may be necessary for the hAID base editor to enhance their targeting efficiency. Editing of the *TRBC* locus was efficient with all editors, however, editing with hA3A showed the highest C>T conversion outside of the predicted editing window. A similar result was observed by Gehrke and colleagues when A3A-BE3 did not exhibit a preference for deaminating cytidines in a TCR motif as expected (where R = A/G), which reduced the editor's fidelity (310).

The same sites were targeted using SpCas9, which as expected resulted in a high indel percentage at both the *CD7* and *TRBC* loci. Indels are problematic, as they can lead to translocation events and subsequent aberrant gene expression that can lead to oncogenic transformations. This disadvantage of SpCas9 usage is well documented and concurrent with current literature (367, 369).

As part of this work, the expression levels of both SpCas9 and CBE proteins (coBE3, hAID, and hA3A) were assessed by serial Western blot analysis, which detected transient expression of each base editor up to 72 hours after electroporation. However, following electroporation of SpCas9 mRNA, SpCas9 protein could be detected for up to 7 days post-delivery. mRNA delivery of SpCas9 or CBEs already reduces the risk of off-target effects associated with stable delivery via viral constructs, as it limits the proteins' life-span and, therefore, window of activity. This is consistent with earlier findings that demonstrated transient protein expression (<48 hours) of BE3 mRNA protein (72).

The expression of CBE protein varied slightly between the three base editors (coBE3, hA3A and hAID). coBE3 and hAID dissipated after 16 hours; however, hA3A persisted for roughly 72 hours. This finding could explain the high degree of editing outside the editing window of hA3A. It has been reported that effectiveness and accuracy of genome editing depend greatly on the extent of expression and the duration of presence of the editors in the cells (370). This study observed differences in SpCas9

and CBE protein expression, suggesting a decrease in the stability of the CBE fusion proteins, but additional research would be required for confirmation. This effect may however be beneficial as long as expression of the sgRNA coincides with the window of CBE protein expression. If editing was to be restricted to this time window, fidelity could be ensured with minimal off-target effects. Grünewald, Zhou *et al*. (2019) provided a potential reason for the rapid downregulation of CBE protein expression by showing that rAPOBEC1 used in BE3 was capable of editing its own mRNA sequence independently of sgRNA (327). In the case of this study, it could mean that CBE mRNA might be mutated by self-editing, preventing sustained CBEs protein expression.

The level and timing of protein expression can influence the occurrence of translocation events during CRISPR/Cas9 editing, as this process can lead to complex deletions and insertions at the target site, raising the risk of such genomic rearrangements. This study amplified the expected translocations between the *CD7* and *TRBC* genes using targeted PCR. Editing with SpCas9, as expected, showed the presence of matching bands in all predicted translocations among three primary T cells donors. Importantly though, samples treated with CBEs mostly lacked these bands, with Sanger sequencing further corroborating that no indel formation occurred when samples were edited through transient CBE mRNA electroporation. Furthermore, this observation provides additional support for the fact that AID and, notably, hA3A, despite its activity, do not consistently lead to indels and translocations. These findings are consistent with previous research from our lab, which also demonstrated the successful double knockout of *CD7* and *TRBC* using the same combination of sgRNAs with BE3 (72). From this previous work, the ddPCR results demonstrated the presence of translocations in the SpCas9 edited samples across all four combinations, with varying frequencies ranging from 0.25%-0.98%. On the other hand, BE3 edited samples exhibited significantly lower frequency of translocation events. The data supports the notion that the SpCas9 system tends to result in higher translocation frequencies compared to the coBE3 system (72). The differential frequencies of translocations observed between the two editing

approaches highlight the distinct outcomes and potential implications of using CBE in editing T cells.

Aberrant base conversion refers to the unintended or undesired changes that may occur in the DNA sequence during the editing process (371). Base editors are designed to convert one DNA base pair into another with high precision, however, aberrant base conversion can occur when the editing machinery induces changes at off-target sites or alters bases adjacent to the target site, leading to unintended genetic modifications (372). Studies on base editors have also revealed instances of aberrant base conversion caused by promiscuous reactivity of deaminase domains that lead to guide RNA-independent off-target editing in both DNA and RNA (317-319, 324, 325).

An important potential consequence of aberrant base conversion could be the alteration of antigen receptor sequences when a CAR is delivered by a lentiviral vector, especially if this was to affect regions that determine antigen binding specificity. Previous work interrogating the ABRs of CBE (coBE3) base-edited CAR3 and CAR7 cells, was unable to detect any promiscuity at the RNA level (72).This project extended the investigation to assess the potential for RNA editing promiscuity by testing hAID and hA3A base editors. AID is a natively DNA-focused enzyme primarily known for its crucial role in antibody diversification during the immune response, specifically in somatic hypermutation and class-switch recombination (373, 374). Given its DNA-centric role, it is reasonable to expect that AID would have limited involvement in RNA editing. Additionally, a study provided confirmation that there was no discernible evidence of RNA editing in experiments using hAID-BE3, reinforcing the idea that AID's primary activity is directed toward DNA rather than RNA (327). A3A is predominantly recognised for its role in inhibiting the replication of retroviruses and retrotransposons. However, there has been some speculation regarding whether A3A might also play a physiological role in RNA deamination. Researchers have demonstrated that A3A has the capability to deaminate cytidine bases within RNA molecules, extending its activity beyond its primary function of editing DNA (375). In a study investigating RNA off-target effects with CBEs, it was

detected that the use of a hA3A based CBE resulted in substantial RNA base edits (327). This observation highlights the potential of hA3A-based CBEs to induce RNA modifications in addition to their primary role in DNA base editing.

Interrogation of RNA collected 48 hours and 7 days post-electroporation from electroporation of mRNA found no evidence of ectopic deamination-mediated transitions, transversions, or other aberrations within the antigen-binding frameworks of the scFv for CAR7 with any of the three editors.

These results further reinforce the reliability and safety of the CBE-mediated base editing approach, specifically for its potential application in therapeutic settings.

6.2 Coupled CRISPR/Cas9 editing and CAR7 or CAR3 transgene expression

Our lab previously optimised a 3rd generation terminal-CRISPR lentiviral vector platform that couples transgene expression with CRISPR/Cas9 mediated gene knockout by incorporating a sgRNA expression cassette within the ΔU3 region of the 3'LTR. The sgRNA expression cassette is duplicated upon reverse transcription of the lentiviral genome prior to integration and its expression is effectively coupled with that of a CAR19 transgene for the generation of 'universal' CAR-T cell products against B-ALL. Upon delivery of SpCas9 mRNA to the T cells, *TRAC* knockout, restricted to the CAR expressing fraction is achieved, and downstream TCRαβ magnetic bead-based depletion allows for a highly homogenous CAR19^{+}TCR^{-} population (~97%) (329).

The current project applied the terminal-CRISPR platform with base editing to generate a TvT CAR product with the advantage of enriching the CAR-T cell population effectively using magnetic depletion. Our observation of surface antigen expression variability in primary T-ALL samples highlighted the heterogeneity of this disease and the need for the development of additional CAR constructs that could be used sequentially or in combination (72, 101). I therefore designed and cloned lentiviral vectors expressing either a CD3- or CD7-targeting CAR, coupled to

expression of a TRBC specific sgRNA, with a CD7 sgRNA delivered separately to avoid fratricide.

Lentivirus was produced from both configurations and titrated in a HEK 293T cell line. Both CAR3 and CAR7 transgenes showed high cell surface expression by flow cytometry, confirming the ability of these vectors to successfully transduce cells. These findings were in line with our expectations, given that HEK 293T cells lack the expression of both CD3 and CD7, making them suitable candidates for assessing the efficacy of CAR vector transduction. However, primary human T cells transduced with the TTRBC-CAR3 vector resulted in no detectible expression of the CAR3 transgene, while those transduced with CAR19 control vector demonstrated robust levels of expression. This finding aligns with prior research, which has demonstrated that transducing unedited T cells with a CAR3 vector leads to a notable absence of detectable transgene expression over time, primarily attributed to fratricide (101).

In the case of TTRBC-CAR7, expression of CAR7 could be detected in primary T cells transduced with the vector without editing. This coincided with a loss of surface CD7 staining, likely due to the scFv of the CAR binding CD7 on the cell surface blocking its detection. This finding is supported by previous work that detected the epitope masking with CAR7 (72, 139). CD7 expression on the cell surface could only be detected using an alternative anti-CD7 monoclonal antibody that recognised a different epitope to the 3A1e clone, used in the CAR7 scFv design, suggesting epitope masking was occurring. However, alternative mechanisms could also be contributing to this observation. Researchers have found that trogocytosis can result in reversible antigen loss in CAR19 T cells. During this process, the target antigen is transferred from cancer cells to CAR-T cells. Importantly, this phenomenon has been observed in CAR-T cells that use both CD28 and 41-BB co-stimulatory domains, indicating that trogocytic target acquisition is a general characteristic of CAR-T cells and likely applies to many, if not all, antigens (376). The expression of a CD7-specific CAR inhibited the expansion of transduced T cells as a result of residual CD7 expression and subsequent fratricide. Genomic deletion of CD7 by CRISPR/Cas9 improved CAR-T expansion and viability, without affecting their cytotoxicity (71).

In this project two different experimental timelines were explored for the efficient generation of fratricide resistant CAR7 or CAR3-T cells. Although, SpCas9 demonstrated higher knockout of CD7, I opted to use BE3 in this experiment to minimise genomic aberrations, which is especially critical when multiplex targeting is required.

One strategy relied upon an initial transduction of cells with TTRBC-CAR vectors followed by electroporation with coBE3 and CD7 sgRNA. Successful CAR7-T cells could be generated, however, there was limited disruption of TCRαβ. This could be linked to the potential transience of coBE3 mRNA expression, dissipating prior to peak expression of the TRBC sgRNA from the vector.

Furthermore, it was observed that CAR7 transduced cells led to a noticeable reduction of $CD8^+$ cells population which was not observed in in the CAR19 control group. This could be due to a disproportionate expansion of $CD4^+$ T cells as compared to effector/memory $CD8^+$ T cells or possibly due to an increased susceptibility of $CD8^+$ T cells to fratricide. Mamonkin, Rouce (115) also observed a skewed CD4:CD8 ratio in their CD5 specific CAR-T cells. However, in this case the bias was towards an increase of $CD8^+$ cells, which may have been the result of the expansion of effector/memory $CD8^+$ T cells or increased susceptibility of CD4 T cells to fratricide (115). One hypothesis to consider is that differences in the density of the CD7 on malignant T cells between CD8+ and CD4+ T cells could be a factor; these differences might influence the survival or proliferation of CD4+ or CD8+ CAR-T cells. Higher antigen levels could encourage CD8+ CAR7-T cell killing, known for their cytolytic activity. However, lower antigen levels on CD4+ T cells might lead to their expansion, which help boost the immune response by releasing cytokines. While this explanation seems reasonable, the literature may not provide much direct evidence to support it. These factors could affect how well CAR-T cells survive, grow and function in response to CAR signalling. Further studies are needed to validate these hypotheses and shed light on what causes an imbalance in the ratio between CD4 and CD8 in CAR7-T cell products.

Interestingly a study conducted by Lu, Liu (139) showed that CAR7 lentiviral transduction of naturally selected $CD7^-$ T cells has a significantly greater presence of the CD8 subset compared to the CD7 knocked out CAR7 obtained via gene editing (139). This approach (Strategy A) verified the genomic disruption of *CD7* in TTRBC-CAR7-T cells with a notable C>T conversion at the target C site. TCRαβ editing showed limited conversion at G5 and G6 in coBE3 mRNA-electroporated TRBC-CAR7 transduced cells. When the same strategy was explored in parallel for the generation of CAR3-T cells using the TTRBC-CAR3 vector, the presence of CAR3 failed to be detected on the surface of primary T cells. From our previous CAR3 TALEN studies it was apparent that timely disruption of TCRαβ ahead of CAR3 expression is critical for the generation of a product (101).

The alternative workflow, referred to as Strategy B, involved the initial electroporation of activated primary T cells with coBE3 mRNA and CD7 sgRNA, conducted 24 hours prior to transduction. This sequence of events resulted in the effective generation of CAR7-T cells characterised by high CD7 disruption, while the disruption of TCRαβ was comparatively restricted. Importantly, it was observed that the CD4:CD8 ratio remained balanced under this condition. In the case of CAR3, fratricide was even more prominent when this approach was used which stemmed from the ineffectiveness in removing TRBC to a sufficient extent and within a timely manner.

The observed decrease in CD8+ CAR7-T cells in Strategy A could lead to a potential decrease in CAR-T cell efficacy. This provides strong justification for adopting the second strategy, which involves the knockout of CD7 expression before transduction with CAR7. The presence of a $CD8^+$ cell population is a crucial factor impacting the effectiveness and persistence of CAR-T cell antitumor responses. Studies have shown that achieving a balanced ratio of $CD4^+$ and $CD8^+$ T cells, such as a 1:1 ratio, leads to superior outcomes in terms of antitumour activity and therapeutic persistence (91, 377). $CD8^+$ cells are known for their longer lifespan relative to $CD4^+$ cells, a key factor contributing to the prolonged effectiveness of CAR-T cell therapies, highlighting their importance in achieving sustained antitumor effects.

Additional measures were considered when optimising the delivery time of TTRBC-CAR7 in relation to coBE3 mRNA and CD7 sgRNA, which sheds light on whether expression of the CAR or TRBC knockout occurred first in the TTRBC-CAR cells. Following electroporation with coBE3 mRNA and CD7 sgRNA, cells were subsequently transduced with TTRBC-CAR19. Terminal CAR19 vector was chosen to mitigate the influence of fratricidal cells, and the transduction was carried out either immediately or at intervals up to 24 hours later. Despite this, there appeared to be no discernible coBE3-mediated TCRαβ disruption across the vector delivery timepoints.

As a consequence, the evaluation of the coupled TTRBC-CAR platform was extended in this project, to include alternative base editors hAID and hA3A, and to evaluate their potential in eliminating *TRBC* when sgRNA was expressed from the terminal CAR vector. Of the editors tested, only hA3A was able to disrupt TCRαβ successfully to allow for $CAR7^{+}/TCR^{-}$ cells to be generated, which could be explained by its prolonged protein expression (72 hours) compared to the other editors (16 hours) allowing for maximal vector driven TRBC sgRNA expression while hA3A was present and active. Molecular verification of *CD7* and *TRBC* disruption exhibited high editing at both loci, however, as described previously, hA3A induced substantial C>T (*CD7*) or G>A (*TRBC*) conversions outside the editing window. On the contrary, editing with hAID resulted in lower levels of the target cytidine for successful CD7 knockout, with the majority of editing seen at different Cs within the editing window, while editing at the *TRBC* was minimal.

CAR3 cells were unable to be generated using any of the editors due to the essential requirement for TCR disruption before CAR3 expression. Achieving this disruption within the necessary timeframe proved challenging when employing the terminal configuration.

6.3 Virus-free production of CAR-T cells via CRISPR/Cas9-mediated transgene insertion

There are numerous ways to redirect human T cells for targeted therapy, such as using integrated and non-integrated viral vectors described earlier, with each approach having its own advantages and disadvantages. Virus-mediated immunotherapy is severely limited by two factors; firstly, the long lead-time of vector manufacture coupled with high costs of clinical grade GMP vector production and associated biosafety challenges (351, 378-380), and secondly the safety concerns related to potential random integration into the host DNA which carries the risk of integration into an oncogenic locus, and subsequently triggering malignant transformation (379, 381, 382).

Therefore, to address these concerns it is important to adopt other feasible and safe methods for T cell engineering. Other groups have developed non-viral approaches by DNA transposon systems such as Sleeping Beauty (SB) (171) and *piggyBac* (PB) (172) for gene addition, which offers distinct advantages compared to retroviral delivery by circumventing the need for vector particle generation, potentially simplifying and reducing the cost of the process. However, two cases of lymphoma have been discovered in a CAR-T cell trial aimed at treating B cell malignancies using *piggyBac* delivery. In these cases, the transformed cells were found to harbour multiple integrated transposons and chromosomal rearrangements (173, 174).

Recently, several approaches have been developed to insert CAR transgenes into precise locations within the human genome, primarily relying on the HDR DNA repair pathway (274). The selection of the template type for HDR should align with both the delivery system employed and the specific engineered nuclease used, all in accordance with the clinical objectives (383).

Using a dsDNA template in a site-directed insertion approach allowed for replacing the native TCR. When primary human T cells were co-electroporated with CRISPR/Cas9 ribonucleoprotein complexes with linear dsDNA templates over 1kb, it

resulted in reduced toxicity, suggesting a protective effect possibly from the coating/masking of the naked DNA by the Cas9 (278). Subsequently, a study by Odé, Condori *et al*. (2020) employed non-viral dsDNA as a template for knock-in experiments. Through this approach, they achieved successful CRISPR/Cas9-mediated knock-in, demonstrating highly efficient integration of a large transgene encoding a CAR or bispecific T cell engagers (BiTEs) into the *TRAC* locus (287).

One of the main hurdles associated with the delivery of double-stranded DNA to primary T cells has been the high levels toxicity seen (242). Toxicity linked to the dsDNA in primary T cells arises from multiple factors. Firstly, dsDNA can be detected by cytoplasmic pattern recognition receptors (PRRs) like cyclic GMP-AMP synthase (cGAS) and stimulator of interferon genes (STING), triggering the initiation of innate immune responses (384). This cascade prompts the secretion of proinflammatory cytokines and chemokines, culminating in cell death and cytotoxic effects (384). Additionally, the activation of p53, a tumour suppressor protein, pivotal in DNA damage response and cell cycle control, plays a significant role (385). When activated, p53 induces cell cycle arrest, apoptosis, and senescence pathways, contributing further to the observed toxicity upon dsDNA introduction into primary T cells (386).

This was partially mitigated by using short single-stranded oligodeoxynucleotides (ssODN) HDR templates, which showed no notable T cell toxicity when compared to large linear dsDNA templates (387). However, there are limitations associated with ssODNs. They are constrained by size restrictions, making them suitable only for small insertions, deletions, or point mutations. Furthermore, ssODNs are less effective than double-stranded DNA donors when it comes to HDR-mediated gene editing (249). Therefore, this project explored the non-viral site-specific integration of a transgene using a dsDNA HDR template in combination with SpCas9 RNP complexes.

This approach was undertaken in this study achieving successful integration of the CAR20 and GFP controls into the *TRAC* locus, thereby demonstrating the effectiveness of the technique. However, challenges were encountered in the insertion of CAR7 and CAR3 into the same genomic site. Despite numerous attempts,

obstacles were faced in achieving both the desired expression of CAR7 or CAR3 and the verification of this integration at the genomic level.

The unsuccessful expression of CAR3 and CAR7 was likely due to fratricide, as TCR and CD7 expression may take longer to be removed from the cell surface, by which time HDR-mediated CAR template insertion may have occurred. It was therefore necessary to complete a time-course experiment using a control dsDNA GFP template directed to the *TRAC* locus following SpCas9 delivery to determine at which point knockout occurs. The time course experiment showed that the majority of GFP integration predominantly occurred within the initial 24-hour timeframe post-electroporation. However, when examining the knockout at that time point, almost all surface TCRαβ appeared to have been removed, while CD7 was still present, suggesting the time lag would need to be extended. This was corroborated by the MFI results, identifying simultaneous expression of CD7, and TCRαβ inserted GFP template, partially explaining the lack of both CAR3 and CAR7 expression.

When *CD7* and *TRBC* were disrupted two days before inserting the dsDNA template, CAR7 expression could be detected confirming the importance of extending the window between knockout and knock-in. Unfortunately, this approach couldn't yield a successful product for CAR3. Blockade of CD3 or the CAR single-chain variable fragment domain would mitigate production issues of generating CAR3-T cells. A similar approach was effectively employed to generate anti-CD38 CAR-T cells. This approach involved blocking the T cell surface expression of CD38 or the CAR scFv domain using mouse IgG1-type antibodies or proteins. The outcomes of this study demonstrated that the use of these antibodies and proteins had a positive impact on reducing CAR-T cell fratricide and fostering the expansion and enrichment of CAR-T cells (103).

Alternative integration sites were investigated to identify potential expression differences that could affect CAR-T cell behaviour while avoiding fratricide. Integrating CAR transgenes into the endogenous *CD3ζ* locus offers the advantage of using the existing transcriptional machinery that controls CD3ζ expression. This

shared regulatory context ensures more consistent CAR expression levels, as guided by CD3ζ-associated elements. Moreover, this approach preserves CD3ζ isoforms crucial for T cell signalling and maintains compatibility with T cell activation pathways. The strategy benefits from a smaller genetic alteration, potentially reducing stress on cells during modification, while enhancing the overall functionality and responsiveness of CAR-modified T cells.

In this study insertion of CAR7 in frame with the *CD3ζ* locus was successful among a number of primary T cell donors, as shown by cDNA synthesis and expression of the intracellular CD3ζ cytoplasmic tail. Again, CAR3 failed to integrate into *CD3ζ* locus due to fratricide. CAR7-T cells cytotoxic activity was comparable to pCCL-CAR7 T cells, indicating intact functional integrity after integration into *CD3ζ* locus. Future testing will involve *in vivo* anti-leukaemic function in humanised mice and ultimately against primary T cells from T-ALL patients. This approach has the potential to improve the durability and efficacy of CAR-T cell therapy by ensuring long-term CAR expression and activity. Differences in promoter activity and regulatory mechanisms between *CD3ζ* and *TRAC* genes can potentially influence the precise integration and expression of a CAR at a specific genomic site. In essence, selecting a promoter and its associated regulatory elements can critically impact managing CAR expression and functionality. Studies have investigated and compared site-directed CAR insertion at different genomic locations and regulated by various promoters, highlighting that choosing the genomic location and promoter selection can significantly affect the level of CAR expression (121, 275).

The *CD7* locus was also investigated as a potential alternative insertion site for the dsDNA CAR7 template providing a direct route to targeting the shared CD7 antigen and thereby protecting the cells from fratricide. In a recent study conducted this year, researchers achieved successful generation of CD7KO TRAC knock-in CAR-T cells by employing both gRNAs targeting *CD7* and *TRAC* locus, along with an AAV vector repair matrix containing a P2A sequence followed by a CD7 CAR. They employed a second-generation CAR backbone including CD28 and CD3ζ endodomains. The study compared three distinct strategies for knocking in the CAR7. In addition to the *CD7*

knockout *TRAC* knock-in approach mentioned above, the researchers also used an EF1α-driven CD7-specific CAR inserted at the knocked-out *CD7* locus with AAV, as well as a third strategy involving random integration of the CAR using a retrovirus (121). All three engineered CAR-T cell strategies, including CD7KO TRAC knock-in, EF1α-driven CD7-specific CAR inserted at the knocked-out *CD7* locus, and random integration with a retrovirus, demonstrated strong cytotoxicity against T-leukaemia and lymphoma cell lines, as well as primary tumour cells from patients. Notably, the site-specific knock-in CD7-specific CAR-T cells demonstrated superior anti-tumour activities compared to retrovirally transduced CAR-T cells in mouse xenograft models of T-ALL. Additionally, mice treated with CAR-T cells created by site-directed CAR7 insertion showed prolonged median survival compared to those treated with retrovirally transduced CAR-T cells. Compared to retroviral CAR-T cells, the superior tumour rejection seen in CD7KO and CD7 knock-in CAR-T cells was attributed to their higher numbers achieved during long-term expansion in two different donors. CD7KO TRAC knock-in CAR-T cells displayed minimal tonic signalling due to low CAR expression and downregulation upon antigen stimulation, leading to improved tumour control compared to retroviral CAR-T cells (121). These results underscore the significance of site-specific CD7 CAR-T cells in clinical settings, highlighting their potential as highly effective therapeutic agents.

After inserting a CAR transgene through HDR, the inserted sequences can exist in either a homozygous state or a heterozygous state, depending on several factors, such as the efficiency of the HDR process and the cell's ploidy. Homozygous insertion involves the precise modification of both alleles at the targeted gene locus to include the CAR sequence, thereby producing a homogeneous population of cells that express the CAR. This enhances the therapeutic efficacy and maintains constant CAR expression levels. Conversely, heterozygous insertion occurs when the CAR sequence is present in only one of the alleles at the targeted gene locus, with the other allele remaining unmodified. This results in a mixed population of cells, with some carrying the CAR on one allele and others remaining unmodified. Although heterozygous insertion may still provide therapeutic benefits, variation in CAR expression levels

across cells may compromise therapy effectiveness and consistency. The allelic status of the inserted CAR sequences must be assessed to evaluate the uniformity and efficacy of CAR-mediated therapeutic outcomes. Furthermore because of allelic exclusion, if the CAR were placed within the TRAC gene and incorporated into both alleles it might not show expression if integrated into the inactive allele. This underscores the importance of considering allelic status and potential regulatory mechanisms when evaluating CAR-mediated therapeutic efficacy.

A drawback associated with site-directed insertion is the modest knock-in efficiency compared to the vector (278, 287, 288, 294, 356). One way to increase the integration efficiency of site directed insertion strategy is by actively skewing the cellular repair pathway towards HDR as opposed to NHEJ (388). Following a dsDNA break, cells tend to favour NHEJ as a rapid repair response mechanism compared to HDR. NHEJ involves directly ligating the broken DNA ends together, without the need for a homologous template, which means additional measures would have to be undertaken to increase the propensity for HDR. This could be achieved by manipulating the cell cycle so that editing occurs during a phase that is more permissible for HDR, e.g., synchronising the cell cycle with small molecule inhibitors (231, 234). While comparably cheap, this approach would require extensive testing to ensure that the interference with the cell cycle does not affect cell viability or behaviour. Another approach would be to suppress/block key factors of NHEJ, such as DNA Ligase IV (targeted with SCR7) (389) or KU70/80 (237).

Overall, these findings highlight the need for continued research and development of innovative strategies to optimise the efficiency and safety of T cell redirection for targeted therapy.

6.4 Concluding remarks

In this study, genome-editing techniques were employed to eliminate the T cell receptor essential for the development of 'universal' CAR-T cells and to impart resistance to fratricide while targeting shared T lineage antigens.

Comparative analyses were conducted on various CBEs containing either the original rat APOBEC1, hAID-BE3, and hA3A-BE3, within primary human T cells by transient delivery of single guide sgRNA and CBE mRNA. Highly efficient multiplexed indel-free disruption of both *TRBC* and *CD7* loci was achieved using both human-derived CBE versions and ratAPOBEC1 control presenting alternative editor options where sequence context may be a factor. Efforts were also made to create CAR7/CAR3 T cells using different lentiviral strategies, including configurations that coupled expression of sgRNA with CAR highlighting the criticality of the orderly removal of shared antigens ahead of CAR expression. CAR7 was successfully generated using the terminal lentiviral configuration, while CAR3 failed due to fratricide-mediated elimination caused by the absence of protective TCRαβ disruption. This could be due to the degradation of base editor's mRNA before the expression of the vector carrying TRBC sgRNA.

An alternative virus-free method for CAR-T cell production was explored. This approach involved the use of CRISPR/Cas9 system as RNPs for the targeted integration of dsDNA donor CAR templates flanked by locus-compatible homology arms to the *TRAC*, *CD3ζ*, or *CD7* loci. Moderate integration of a dsDNA CAR7 donor template was achieved into the *CD7* and *CD3ζ* locus, with pilot testing demonstrating comparable cytotoxic potential of CD3ζ -CAR knock-in cells to lentiviral counterparts.

Overall, these findings contribute valuable insights into the development of CAR-T cell therapies and underscore the significance of antigen specificity in enhancing therapeutic efficacy. Furthermore, exploring alternative editing and production methods highlights the potential for advancing CAR-T cell technology towards safer and more efficient clinical applications while highlighting the need for further

optimisation and *in vivo* validation to fully harness their therapeutic benefits in immunotherapy applications.

6.5 Future directions

Further investigations could include the following:

1. Testing the next generation of base editors

This involves the evaluation and experimentation with advanced base editing tools such as BE4max (390), evoAPOBEC1-BE4max (391), which may offer enhanced precision, efficiency and reduce indels formation in genome editing compared to previous versions. Further testing could be carried out on hA3A as it is the only base editor that demonstrated compatibility with terminal vector configuration to generate CAR7-T cells. It successfully eliminated TCRαβ, where TRBC sgRNA was expressed from the terminal vector. However, an observed downside with hA3A was the high activity of the deaminase enzyme, leading to high bystander mutation and promiscuous activity. To address this issue, exploring the engineered version (eA3A) (310), hyeA3A-BE4max (392), or haA3A-CBE (393), which could potentially reduce bystander mutations and decrease off-target effects. By comparing these variants thoroughly, it would be possible to identify the most effective base editor for their specific experimental goals, considering factors such as editing efficiency, off-target effects, and indels.

2. Optimisation of HDR efficiency

This optimisation process may involve testing the efficacy of small molecule DNA-dependent protein kinase (DNA-PK) inhibitors to enhance HDR efficiency by pushing the cells towards the HDR pathway. These inhibitors, including Nu7026, M3814, and AZD7648, operate by inhibiting the activity of DNA-PK, an enzyme crucial in the NHEJ repair pathway. An alternative approach could explore the use of truncated Cas9 target sequences (tCTSs) flanking the end of the homology arms to 'drag' the template to the nucleus and improve localisation and template integration efficiency. Investigating strategies to mitigate fratricide by incorporating post-electroporation

steps involving blocking antibodies, for instance, blocking the CD7 antigen present on cells with recombinant anti-CD7 blocking antibodies. These experiments aim to prevent or minimise fratricide-related cell death, thereby enhancing the survival and efficacy of CAR-T cells in therapeutic applications.

3. Simultaneous non-viral CAR knock-in with multiplexed base editing

Multiplex gene editing with a single CRISPR/Cas nuclease system can cause high rates of translocations in edited cells. For non-viral CAR delivery approaches where additional edits for fratricide resistance or increased immune evasion are required, alternative strategies would have to be considered. A recent study has shown that multiplex editing with fewer translocations is possible when two CRISPR-Cas systems with distinct scaffold requirements and PAM recognition are combined, such as the Cas12a Ultra nuclease and the Cas9 BE ABE8.20 m (394). Accordingly, the following approach could be tested, which involves combining the Cas12a Ultra nuclease for CAR knock-in and SpCas9 BE for editing of CD7 and TCRαβ receptor, potentially allowing efficient multiplex editing and preventing translocations in T cells.

4. Testing alternative sites to insert CAR3

This initiative involves exploring alternative genomic loci for the insertion of CAR3. By investigating sites like CD3 epsilon, this strategy seeks site-specific insertion of CAR3 while minimising undesirable side effects of fratricide at the same time. Choosing CD3 epsilon is particularly relevant because our CAR targets the same locus, ensuring targeted and efficient CAR integration while reducing the risk of fratricide.

5. Phenotypic and functional studies of CAR products

A comparative analysis between CAR7-T cells generated via viral and non-viral methods can provide valuable insights into the phenotypic differentiation and functional response of distinct CAR-T cell subsets, such as CD4+ helper T cells and CD8+ cytotoxic T cells. A comprehensive analysis of cytokine profile and transcriptional signatures of anti-CD7 T cells upon antigen-specific stimulation can be thoroughly examined. Based on the preliminary results obtained, it would be highly

valuable to determine whether both CD4+ helper and CD8+ cytotoxic CAR-T cell subsets are equally effective in directly killing target tumour cells. Furthermore, it will also be essential to determine if their cytotoxic activity is associated with the increase in the range of TH1 and TH2 signature cytokines, e.g., Interferon γ, Tumour necrotic factor α, interleukin-5 (IL-5), and IL-13.

After successfully generating fratricide-resistant non-viral CAR7-T cells, their function and potency will be further assessed against primary T cell targets from T-ALL patients. Direct comparison *in vivo* will be required to evaluate any potential advantages of targeted CAR integration and expression under the control of the endogenous transcriptional machinery over conventional viral-derived vectors. To evaluate and compare the *in vivo* anti-leukemic activity of both viral and non-viral CAR7-T cells, a humanised NOD/SCID/γc-/- (NSG) xenograft model of leukaemic T cell inhibition will be utilised. Mice will be engrafted with 1 x 10^7 Jurkat T cells expressing CD7, labelled with $EGFP^+$ and LUC^+, and three days later, the establishment of leukaemia will be confirmed through bioluminescent signalling. Following this, mice will be inoculated with either viral CAR7-T cells, non-viral CAR7-T cells, or un-transduced cells after four days and leukaemic inhibition will be monitored through serial bioluminescent imaging.

Chapter 7 References

1. Kumar BV, Connors TJ, Farber DL. Human T Cell Development, Localization, and Function throughout Life. Immunity. 2018;48(2):202-13.
2. Germain RN. T-cell development and the CD4–CD8 lineage decision. Nature Reviews Immunology. 2002;2(5):309-22.
3. Janeway CA Jr, Travers P, Walport M. Immunobiology. 5th edition ed. New York: Garland Science; 2001.
4. Cresswell P. A personal retrospective on the mechanisms of antigen processing. Immunogenetics. 2019;71(3):141-60.
5. Mariuzza RA, Agnihotri P, Orban J. The structural basis of T-cell receptor (TCR) activation: An enduring enigma. J Biol Chem. 2020;295(4):914-25.
6. Cantrell D. T cell antigen receptor signal transduction pathways. Annu Rev Immunol. 1996;14:259-74.
7. Taylor J, Xiao W, Abdel-Wahab O. Diagnosis and classification of hematologic malignancies on the basis of genetics. Blood. 2017;130(4):410-23.
8. Casulo C, O'Connor O, Shustov A, Fanale M, Friedberg JW, Leonard JP, et al. T-Cell Lymphoma: Recent Advances in Characterization and New Opportunities for Treatment. JNCI: Journal of the National Cancer Institute. 2016;109(2).
9. Pui CH, Robison LL, Look AT. Acute lymphoblastic leukaemia. Lancet. 2008;371(9617):1030-43.
10. Cordo V, van der Zwet JCG, Canté-Barrett K, Pieters R, Meijerink JPP. T-cell Acute Lymphoblastic Leukemia: A Roadmap to Targeted Therapies. Blood Cancer Discov. 2021;2(1):19-31.
11. Karrman K, Johansson B. Pediatric T-cell acute lymphoblastic leukemia. Genes, Chromosomes and Cancer. 2017;56(2):89-116.
12. Bazarbachi A, Suarez F, Fields P, Hermine O. How I treat adult T-cell leukemia/lymphoma. Blood. 2011;118(7):1736-45.
13. Bene MC, Castoldi G, Knapp W, Ludwig WD, Matutes E, Orfao A, van't Veer MB. Proposals for the immunological classification of acute leukemias. European Group for the Immunological Characterization of Leukemias (EGIL). Leukemia. 1995;9(10):1783-6.
14. Shiraz P, Jehangir W, Agrawal V. T-Cell Acute Lymphoblastic Leukemia-Current Concepts in Molecular Biology and Management. Biomedicines. 2021;9(11).
15. Van Vlierberghe P, Ferrando A. The molecular basis of T cell acute lymphoblastic leukemia. J Clin Invest. 2012;122(10):3398-406.
16. Bornschein S, Demeyer S, Stirparo R, Gielen O, Vicente C, Geerdens E, et al. Defining the molecular basis of oncogenic cooperation between TAL1 expression and Pten deletion in T-ALL using a novel pro-T-cell model system. Leukemia. 2018;32(4):941-51.
17. Gordon WR, Roy M, Vardar-Ulu D, Garfinkel M, Mansour MR, Aster JC, Blacklow SC. Structure of the Notch1-negative regulatory region: implications for normal activation and pathogenic signaling in T-ALL. Blood. 2009;113(18):4381-90.
18. Liu Y, Easton J, Shao Y, Maciaszek J, Wang Z, Wilkinson MR, et al. The genomic landscape of pediatric and young adult T-lineage acute lymphoblastic leukemia. Nature genetics. 2017;49(8):1211-8.

19. Ragg S, Zehentner BK, Loken MR, Croop JM. Evidence for BCR/ABL1-positive T-cell acute lymphoblastic leukemia arising in an early lymphoid progenitor cell. Pediatr Blood Cancer. 2019;66(9):e27829.
20. Jotta PY, Ganazza MA, Silva A, Viana MB, da Silva MJ, Zambaldi LJ, et al. Negative prognostic impact of PTEN mutation in pediatric T-cell acute lymphoblastic leukemia. Leukemia. 2010;24(1):239-42.
21. Malczewska M, Kośmider K, Bednarz K, Ostapińska K, Lejman M, Zawitkowska J. Recent Advances in Treatment Options for Childhood Acute Lymphoblastic Leukemia. Cancers (Basel). 2022;14(8).
22. Samra B, Jabbour E, Ravandi F, Kantarjian H, Short NJ. Evolving therapy of adult acute lymphoblastic leukemia: state-of-the-art treatment and future directions. J Hematol Oncol. 2020;13(1):70.
23. Raetz EA, Teachey DT. T-cell acute lymphoblastic leukemia. Hematology 2014, the American Society of Hematology Education Program Book. 2016;2016(1):580-8.
24. Muffly L, Larson RA. Improving outcomes in childhood T-cell acute lymphoblastic leukemia: promising results from the Children's Oncology Group incorporating nelarabine into front-line therapy. Transl Pediatr. 2012;1(2):120-2.
25. O'Connor D, Demeulemeester J, Conde L, Kirkwood A, Fung K, Papaleonidopoulou F, et al. The Clinicogenomic Landscape of Induction Failure in Childhood and Young Adult T-Cell Acute Lymphoblastic Leukemia. Journal of Clinical Oncology. 2023;41(19):3545-56.
26. Kadia TM, Gandhi V. Nelarabine in the treatment of pediatric and adult patients with T-cell acute lymphoblastic leukemia and lymphoma. Expert Rev Hematol. 2017;10(1):1-8.
27. Brammer JE, Saliba RM, Jorgensen JL, Ledesma C, Gaballa S, Poon M, et al. Multi-center analysis of the effect of T-cell acute lymphoblastic leukemia subtype and minimal residual disease on allogeneic stem cell transplantation outcomes. Bone Marrow Transplant. 2017;52(1):20-7.
28. Huang Y-h, Wan C-L, Dai H-p, Xue S-l. Targeted therapy and immunotherapy for T cell acute lymphoblastic leukemia/lymphoma. Annals of Hematology. 2023;102(8):2001-13.
29. Tran TH, Hunger SP. The genomic landscape of pediatric acute lymphoblastic leukemia and precision medicine opportunities. Seminars in Cancer Biology. 2022;84:144-52.
30. Lustberg MB, Kuderer NM, Desai A, Bergerot C, Lyman GH. Mitigating long-term and delayed adverse events associated with cancer treatment: implications for survivorship. Nature Reviews Clinical Oncology. 2023;20(8):527-42.
31. Akhlaghi E, Lehto RH, Torabikhah M, Sharif Nia H, Taheri A, Zaboli E, Yaghoobzadeh A. Chemotherapy use and quality of life in cancer patients at the end of life: an integrative review. Health and Quality of Life Outcomes. 2020;18(1):332.
32. Lewandowska A, Rudzki G, Lewandowski T, Próchnicki M, Rudzki S, Laskowska B, Brudniak J. Quality of Life of Cancer Patients Treated with Chemotherapy. Int J Environ Res Public Health. 2020;17(19).
33. Schilstra CE, McCleary K, Fardell JE, Donoghoe MW, McCormack E, Kotecha RS, et al. Prospective longitudinal evaluation of treatment-related toxicity and health-related quality of life during the first year of treatment for pediatric acute lymphoblastic leukemia. BMC Cancer. 2022;22(1):985.

34. Swann JB, Smyth MJ. Immune surveillance of tumors. J Clin Invest. 2007;117(5):1137-46.
35. Tang L, Huang Z, Mei H, Hu Y. Immunotherapy in hematologic malignancies: achievements, challenges and future prospects. Signal Transduction and Targeted Therapy. 2023;8(1):306.
36. Katsnelson A. Drug development: Target practice. Nature. 2013;498(7455):S8-S9.
37. Zahavi D, Weiner L. Monoclonal Antibodies in Cancer Therapy. Antibodies. 2020;9(3):34.
38. Bechan GI, Lee DW, Zajonc DM, Heckel D, Xian R, Throsby M, et al. Phage display generation of a novel human anti-CD 1 A monoclonal antibody with potent cytolytic activity. British journal of haematology. 2012;159(3):299-310.
39. de Weers M, Tai YT, van der Veer MS, Bakker JM, Vink T, Jacobs DC, et al. Daratumumab, a novel therapeutic human CD38 monoclonal antibody, induces killing of multiple myeloma and other hematological tumors. J Immunol. 2011;186(3):1840-8.
40. Bertram JH, Gill PS, Levine AM, Boquiren D, Hoffman FM, Meyer P, Mitchell MS. Monoclonal antibody T101 in T cell malignancies: a clinical, pharmacokinetic, and immunologic correlation. Blood. 1986;68(3):752-61.
41. Tembhare PR, Sriram H, Khanka T, Chatterjee G, Panda D, Ghogale S, et al. Flow cytometric evaluation of CD38 expression levels in the newly diagnosed T-cell acute lymphoblastic leukemia and the effect of chemotherapy on its expression in measurable residual disease, refractory disease and relapsed disease: an implication for anti-CD38 immunotherapy. J Immunother Cancer. 2020;8(1).
42. Fu Z, Li S, Han S, Shi C, Zhang Y. Antibody drug conjugate: the “biological missile” for targeted cancer therapy. Signal Transduction and Targeted Therapy. 2022;7(1):93.
43. Frankel AE, Laver JH, Willingham MC, Burns LJ, Kersey JH, Vallera DA. Therapy of patients with T-cell lymphomas and leukemias using an anti-CD7 monoclonal antibody-ricin A chain immunotoxin. Leuk Lymphoma. 1997;26(3-4):287-98.
44. Lulla PD, Mamonkin M, Brenner MK. Adoptive Cell Therapy for Acute Myeloid Leukemia and T-Cell Acute Lymphoblastic Leukemia. Cancer J. 2019;25(3):199-207.
45. Li D, Li X, Zhou WL, Huang Y, Liang X, Jiang L, et al. Genetically engineered T cells for cancer immunotherapy. Signal Transduct Target Ther. 2019;4:35.
46. Hiltensperger M, Krackhardt AM. Current and future concepts for the generation and application of genetically engineered CAR-T and TCR-T cells. Front Immunol. 2023;14:1121030.
47. Want MY, Bashir Z, Najar RA. T Cell Based Immunotherapy for Cancer: Approaches and Strategies. Vaccines (Basel). 2023;11(4).
48. Shafer P, Kelly LM, Hoyos V. Cancer Therapy With TCR-Engineered T Cells: Current Strategies, Challenges, and Prospects. Front Immunol. 2022;13:835762.
49. Smith-Garvin JE, Koretzky GA, Jordan MS. T cell activation. Annu Rev Immunol. 2009;27:591-619.
50. Rath JA, Arber C. Engineering Strategies to Enhance TCR-Based Adoptive T Cell Therapy. Cells. 2020;9(6).

51. Qasim W, Brunetto M, Gehring AJ, Xue SA, Schurich A, Khakpoor A, et al. Immunotherapy of HCC metastases with autologous T cell receptor redirected T cells, targeting HBsAg in a liver transplant patient. J Hepatol. 2015;62(2):486-91.
52. Jahn L, Hombrink P, Hagedoorn RS, Kester MG, van der Steen DM, Rodriguez T, et al. TCR-based therapy for multiple myeloma and other B-cell malignancies targeting intracellular transcription factor BOB1. Blood. 2017;129(10):1284-95.
53. Robbins PF, Kassim SH, Tran TL, Crystal JS, Morgan RA, Feldman SA, et al. A pilot trial using lymphocytes genetically engineered with an NY-ESO-1-reactive T-cell receptor: long-term follow-up and correlates with response. Clin Cancer Res. 2015;21(5):1019-27.
54. Wooldridge L, Ekeruche-Makinde J, van den Berg HA, Skowera A, Miles JJ, Tan MP, et al. A single autoimmune T cell receptor recognizes more than a million different peptides. J Biol Chem. 2012;287(2):1168-77.
55. Morgan RA, Chinnasamy N, Abate-Daga D, Gros A, Robbins PF, Zheng Z, et al. Cancer regression and neurological toxicity following anti-MAGE-A3 TCR gene therapy. Journal of immunotherapy (Hagerstown, Md : 1997). 2013;36(2):133-51.
56. Bentzen AK, Such L, Jensen KK, Marquard AM, Jessen LE, Miller NJ, et al. T cell receptor fingerprinting enables in-depth characterization of the interactions governing recognition of peptide-MHC complexes. Nature biotechnology. 2018.
57. Bendle GM, Linnemann C, Hooijkaas AI, Bies L, de Witte MA, Jorritsma A, et al. Lethal graft-versus-host disease in mouse models of T cell receptor gene therapy. Nat Med. 2010;16(5):565-70, 1p following 70.
58. van Loenen MM, de Boer R, Amir AL, Hagedoorn RS, Volbeda GL, Willemze R, et al. Mixed T cell receptor dimers harbor potentially harmful neoreactivity. Proc Natl Acad Sci U S A. 2010;107(24):10972-7.
59. Schober K, Müller TR, Gökmen F, Grassmann S, Effenberger M, Poltorak M, et al. Orthotopic replacement of T-cell receptor α- and β-chains with preservation of near-physiological T-cell function. Nature Biomedical Engineering. 2019;3(12):974-84.
60. Stadtmauer EA, Fraietta JA, Davis MM, Cohen AD, Weber KL, Lancaster E, et al. CRISPR-engineered T cells in patients with refractory cancer. Science (New York, NY). 2020;367(6481).
61. Sadelain M, Brentjens R, Rivière I. The basic principles of chimeric antigen receptor design. Cancer Discov. 2013;3(4):388-98.
62. June CH, Sadelain M. Chimeric Antigen Receptor Therapy. N Engl J Med. 2018;379(1):64-73.
63. Eshhar Z, Waks T, Gross G, Schindler DG. Specific activation and targeting of cytotoxic lymphocytes through chimeric single chains consisting of antibody-binding domains and the gamma or zeta subunits of the immunoglobulin and T-cell receptors. Proc Natl Acad Sci U S A. 1993;90(2):720-4.
64. Hombach A, Hombach AA, Abken H. Adoptive immunotherapy with genetically engineered T cells: modification of the IgG1 Fc 'spacer' domain in the extracellular moiety of chimeric antigen receptors avoids 'off-target' activation and unintended initiation of an innate immune response. Gene Ther. 2010;17(10):1206-13.
65. Zhang C, Liu J, Zhong JF, Zhang X. Engineering CAR-T cells. Biomark Res. 2017;5:22.

66. Sadelain M, Rivière I, Riddell S. Therapeutic T cell engineering. Nature. 2017;545(7655):423-31.
67. Jayaraman J, Mellody MP, Hou AJ, Desai RP, Fung AW, Pham AHT, et al. CAR-T design: Elements and their synergistic function. EBioMedicine. 2020;58:102931.
68. Lindner SE, Johnson SM, Brown CE, Wang LD. Chimeric antigen receptor signaling: Functional consequences and design implications. Sci Adv. 2020;6(21):eaaz3223.
69. Gross G, Gorochov G, Waks T, Eshhar Z. Generation of effector T cells expressing chimeric T cell receptor with antibody type-specificity. Transplant Proc. 1989;21(1 Pt 1):127-30.
70. Brocker T. Chimeric Fv-zeta or Fv-epsilon receptors are not sufficient to induce activation or cytokine production in peripheral T cells. Blood. 2000;96(5):1999-2001.
71. Gomes-Silva D, Srinivasan M, Sharma S, Lee CM, Wagner DL, Davis TH, et al. CD7-edited T cells expressing a CD7-specific CAR for the therapy of T-cell malignancies. Blood. 2017;130(3):285-96.
72. Georgiadis C, Rasaiyaah J, Gkazi SA, Preece R, Etuk A, Christi A, Qasim W. Base-edited CAR T cells for combinational therapy against T cell malignancies. Leukemia. 2021.
73. Ottaviano G, Georgiadis C, Gkazi SA, Syed F, Zhan H, Etuk A, et al. Phase 1 clinical trial of CRISPR-engineered CAR19 universal T cells for treatment of children with refractory B cell leukemia. Science translational medicine. 2022;14(668):eabq3010.
74. Chiesa R, Georgiadis C, Syed F, Zhan H, Etuk A, Gkazi SA, et al. Base-Edited CAR7 T Cells for Relapsed T-Cell Acute Lymphoblastic Leukemia. N Engl J Med. 2023;389(10):899-910.
75. Li S, Wang X, Liu L, Liu J, Rao J, Yuan Z, et al. CD7 targeted “off-the-shelf” CAR-T demonstrates robust in vivo expansion and high efficacy in the treatment of patients with relapsed and refractory T cell malignancies. Leukemia. 2023.
76. Wang X, Li S, Gao L, Yuan Z, Wu K, Liu L, et al. Abstract CT052: Clinical safety and efficacy study of TruUCAR™ GC027: The first-in-human, universal CAR-T therapy for adult relapsed/refractory T-cell acute lymphoblastic leukemia (r/r T-ALL). Cancer Research. 2020;80(16_Supplement):CT052-CT.
77. Zhang M, Chen D, Fu X, Meng H, Nan F, Sun Z, et al. Autologous Nanobody-Derived Fratricide-Resistant CD7-CAR T-cell Therapy for Patients with Relapsed and Refractory T-cell Acute Lymphoblastic Leukemia/Lymphoma. Clin Cancer Res. 2022;28(13):2830-43.
78. van der Stegen SJ, Hamieh M, Sadelain M. The pharmacology of second-generation chimeric antigen receptors. Nat Rev Drug Discov. 2015;14(7):499-509.
79. Zhao Z, Condomines M, van der Stegen SJC, Perna F, Kloss CC, Gunset G, et al. Structural Design of Engineered Costimulation Determines Tumor Rejection Kinetics and Persistence of CAR T Cells. Cancer Cell. 2015;28(4):415-28.
80. Honikel MM, Olejniczak SH. Co-Stimulatory Receptor Signaling in CAR-T Cells. Biomolecules. 2022;12(9).
81. Carpenito C, Milone MC, Hassan R, Simonet JC, Lakhal M, Suhoski MM, et al. Control of large, established tumor xenografts with genetically retargeted human T cells containing CD28 and CD137 domains. Proc Natl Acad Sci U S A. 2009;106(9):3360-5.

82. Schubert M-L, Schmitt A, Neuber B, Hückelhoven-Krauss A, Kunz A, Wang L, et al. Third-generation CAR T cells targeting CD19 are associated with an excellent safety profile and might improve persistence of CAR T cells in treated patients. Blood. 2019;134:51.
83. Enblad G, Karlsson H, Gammelgård G, Wenthe J, Lövgren T, Amini RM, et al. A Phase I/IIa Trial Using CD19-Targeted Third-Generation CAR T Cells for Lymphoma and Leukemia. Clin Cancer Res. 2018;24(24):6185-94.
84. Chmielewski M, Abken H. TRUCKs: the fourth generation of CARs. Expert Opin Biol Ther. 2015;15(8):1145-54.
85. Zhang P, Zhang G, Wan X. Challenges and new technologies in adoptive cell therapy. Journal of Hematology & Oncology. 2023;16(1):97.
86. Schuster SJ, Bishop MR, Tam CS, Waller EK, Borchmann P, McGuirk JP, et al. Tisagenlecleucel in Adult Relapsed or Refractory Diffuse Large B-Cell Lymphoma. N Engl J Med. 2019;380(1):45-56.
87. Maude SL, Frey N, Shaw PA, Aplenc R, Barrett DM, Bunin NJ, et al. Chimeric antigen receptor T cells for sustained remissions in leukemia. N Engl J Med. 2014;371(16):1507-17.
88. Hirayama AV, Gauthier J, Hay KA, Voutsinas JM, Wu Q, Pender BS, et al. High rate of durable complete remission in follicular lymphoma after CD19 CAR-T cell immunotherapy. Blood. 2019;134(7):636-40.
89. Kochenderfer JN, Dudley ME, Kassim SH, Somerville RP, Carpenter RO, Stetler-Stevenson M, et al. Chemotherapy-refractory diffuse large B-cell lymphoma and indolent B-cell malignancies can be effectively treated with autologous T cells expressing an anti-CD19 chimeric antigen receptor. Journal of clinical oncology : official journal of the American Society of Clinical Oncology. 2015;33(6):540-9.
90. Brentjens RJ, Davila ML, Riviere I, Park J, Wang X, Cowell LG, et al. CD19-targeted T cells rapidly induce molecular remissions in adults with chemotherapy-refractory acute lymphoblastic leukemia. Science translational medicine. 2013;5(177):177ra38.
91. Turtle CJ, Hanafi LA, Berger C, Gooley TA, Cherian S, Hudecek M, et al. CD19 CAR-T cells of defined CD4+:CD8+ composition in adult B cell ALL patients. J Clin Invest. 2016;126(6):2123-38.
92. Neelapu SS, Locke FL, Bartlett NL, Lekakis LJ, Miklos DB, Jacobson CA, et al. Axicabtagene Ciloleucel CAR T-Cell Therapy in Refractory Large B-Cell Lymphoma. N Engl J Med. 2017;377(26):2531-44.
93. Maude SL, Laetsch TW, Buechner J, Rives S, Boyer M, Bittencourt H, et al. Tisagenlecleucel in Children and Young Adults with B-Cell Lymphoblastic Leukemia. New England Journal of Medicine. 2018;378(5):439-48.
94. Schuster SJ, Svoboda J, Chong EA, Nasta SD, Mato AR, Anak Ö, et al. Chimeric Antigen Receptor T Cells in Refractory B-Cell Lymphomas. N Engl J Med. 2017;377(26):2545-54.
95. Shah BD, Ghobadi A, Oluwole OO, Logan AC, Boissel N, Cassaday RD, et al. KTE-X19 for relapsed or refractory adult B-cell acute lymphoblastic leukaemia: phase 2 results of the single-arm, open-label, multicentre ZUMA-3 study. Lancet. 2021;398(10299):491-502.

96. Luo L, Zhou X, Zhou L, Liang Z, Yang J, Tu S, Li Y. Current state of CAR-T therapy for T-cell malignancies. Therapeutic Advances in Hematology. 2022;13:20406207221143025.
97. Chen KH, Wada M, Firor AE, Pinz KG, Jares A, Liu H, et al. Novel anti-CD3 chimeric antigen receptor targeting of aggressive T cell malignancies. Oncotarget. 2016;7(35):56219-32.
98. Chen KH, Wada M, Pinz KG, Liu H, Lin KW, Jares A, et al. Preclinical targeting of aggressive T-cell malignancies using anti-CD5 chimeric antigen receptor. Leukemia. 2017;31(10):2151-60.
99. Scherer LD, Brenner MK, Mamonkin M. Chimeric Antigen Receptors for T-Cell Malignancies. Frontiers in oncology. 2019;9:126.
100. Ren A, Tong X, Xu N, Zhang T, Zhou F, Zhu H. CAR T-Cell Immunotherapy Treating T-ALL: Challenges and Opportunities. Vaccines (Basel). 2023;11(1).
101. Rasaiyaah J, Georgiadis C, Preece R, Mock U, Qasim W. TCRalphabeta/CD3 disruption enables CD3-specific antileukemic T cell immunotherapy. JCI insight. 2018;3(13).
102. Png YT, Vinanica N, Kamiya T, Shimasaki N, Coustan-Smith E, Campana D. Blockade of CD7 expression in T cells for effective chimeric antigen receptor targeting of T-cell malignancies. Blood advances. 2017;1(25):2348-60.
103. Gao Z, Tong C, Wang Y, Chen D, Wu Z, Han W. Blocking CD38-driven fratricide among T cells enables effective antitumor activity by CD38-specific chimeric antigen receptor T cells. Journal of Genetics and Genomics. 2019;46(8):367-77.
104. Wong XFA, et al.,. Development of an Off-the-Shelf Chimeric Antigen Receptor (CAR)-T Cell Therapy for T-Cell Acute Lymphoblastic Leukemia (T-ALL) without Gene Editing. Blood. 2022;140(Supplement1):P.2358-9.
105. Ye J, Jia Y, Tuhin IJ, Tan J, Monty MA, Xu N, et al. Feasibility study of a novel preparation strategy for anti-CD7 CAR-T cells with a recombinant anti-CD7 blocking antibody. Mol Ther Oncolytics. 2022;24:719-28.
106. Freiwan A, Zoine JT, Crawford JC, Vaidya A, Schattgen SA, Myers JA, et al. Engineering naturally occurring CD7- T cells for the immunotherapy of hematological malignancies. Blood. 2022;140(25):2684-96.
107. Alcantara M, Tesio M, June CH, Houot R. CAR T-cells for T-cell malignancies: challenges in distinguishing between therapeutic, normal, and neoplastic T-cells. Leukemia. 2018;32(11):2307-15.
108. Di Stasi A, Tey SK, Dotti G, Fujita Y, Kennedy-Nasser A, Martinez C, et al. Inducible apoptosis as a safety switch for adoptive cell therapy. N Engl J Med. 2011;365(18):1673-83.
109. Yu S, Yi M, Qin S, Wu K. Next generation chimeric antigen receptor T cells: safety strategies to overcome toxicity. Mol Cancer. 2019;18(1):125.
110. Ruella M, Xu J, Barrett DM, Fraietta JA, Reich TJ, Ambrose DE, et al. Induction of resistance to chimeric antigen receptor T cell therapy by transduction of a single leukemic B cell. Nat Med. 2018;24(10):1499-503.
111. Qasim W, Zhan H, Samarasinghe S, Adams S, Amrolia P, Stafford S, et al. Molecular remission of infant B-ALL after infusion of universal TALEN gene-edited CAR T cells. Science translational medicine. 2017;9(374).

112. Pinz K, Liu H, Golightly M, Jares A, Lan F, Zieve GW, et al. Preclinical targeting of human T-cell malignancies using CD4-specific chimeric antigen receptor (CAR)-engineered T cells. Leukemia. 2016;30(3):701-7.
113. Ma G, Shen J, Pinz K, Wada M, Park J, Kim S, et al. Targeting T Cell Malignancies Using CD4CAR T-Cells and Implementing a Natural Safety Switch. Stem Cell Rev Rep. 2019;15(3):443-7.
114. Raikar SS, Fleischer LC, Moot R, Fedanov A, Paik NY, Knight KA, et al. Development of chimeric antigen receptors targeting T-cell malignancies using two structurally different anti-CD5 antigen binding domains in NK and CRISPR-edited T cell lines. Oncoimmunology. 2018;7(3):e1407898.
115. Mamonkin M, Rouce RH, Tashiro H, Brenner MK. A T-cell-directed chimeric antigen receptor for the selective treatment of T-cell malignancies. Blood. 2015;126(8):983-92.
116. Mamonkin M, Mukherjee M, Srinivasan M, Sharma S, Gomes-Silva D, Mo F, et al. Reversible Transgene Expression Reduces Fratricide and Permits 4-1BB Costimulation of CAR T Cells Directed to T-cell Malignancies. Cancer Immunol Res. 2018;6(1):47-58.
117. Dai Z, Mu W, Zhao Y, Cheng J, Lin H, Ouyang K, et al. T cells expressing CD5/CD7 bispecific chimeric antigen receptors with fully human heavy-chain-only domains mitigate tumor antigen escape. Signal Transduction and Targeted Therapy. 2022;7(1):85.
118. Wada M, Zhang H, Fang L, Feng J, Tse CO, Zhang W, et al. Characterization of an Anti-CD5 Directed CAR T-Cell against T-Cell Malignancies. Stem Cell Reviews and Reports. 2020;16(2):369-84.
119. Voynova E, Hawk N, Flomerfelt FA, Telford WG, Gress RE, Kanakry JA, Kovalovsky D. Increased Activity of a NK-Specific CAR-NK Framework Targeting CD3 and CD5 for T-Cell Leukemias. Cancers. 2022;14(3):524.
120. Cooper ML, Choi J, Staser K, Ritchey JK, Devenport JM, Eckardt K, et al. An "off-the-shelf" fratricide-resistant CAR-T for the treatment of T cell hematologic malignancies. Leukemia. 2018;32(9):1970-83.
121. Jiang J, Chen J, Liao C, Duan Y, Wang Y, Shang K, et al. Inserting EF1α-driven CD7-specific CAR at CD7 locus reduces fratricide and enhances tumor rejection. Leukemia. 2023;37(8):1660-70.
122. Wei W, Ma H, Yang D, Sun B, Tang J, Zhu Y, et al. SECTM1-based CAR T cells enriched with CD7-low/negative subsets exhibit efficacy in CD7-positive malignancies. Blood advances. 2023;7(13):2941-51.
123. Diorio C, Murray R, Naniong M, Barrera L, Camblin A, Chukinas J, et al. Cytosine base editing enables quadruple-edited allogeneic CART cells for T-ALL. Blood. 2022;140(6):619-29.
124. You F, Wang Y, Jiang L, Zhu X, Chen D, Yuan L, et al. A novel CD7 chimeric antigen receptor-modified NK-92MI cell line targeting T-cell acute lymphoblastic leukemia. Am J Cancer Res. 2019;9(1):64-78.
125. Wang D, Zeng C, Xu B, Xu JH, Wang J, Jiang LJ, et al. Anti-CD30 chimeric antigen receptor T cell therapy for relapsed/refractory CD30+ lymphoma patients. Blood Cancer Journal. 2020;10(1):8.

126. Ramos CA, Ballard B, Zhang H, Dakhova O, Gee AP, Mei Z, et al. Clinical and immunological responses after CD30-specific chimeric antigen receptor-redirected lymphocytes. J Clin Invest. 2017;127(9):3462-71.
127. Scarfo I, Ormhoj M, Frigault MJ, Castano AP, Lorrey S, Bouffard AA, et al. Anti-CD37 chimeric antigen receptor T cells are active against B- and T-cell lymphomas. Blood. 2018;132(14):1495-506.
128. Shi J, Zhang Z, Cen H, Wu H, Zhang S, Liu J, et al. CAR T cells targeting CD99 as an approach to eradicate T-cell acute lymphoblastic leukemia without normal blood cells toxicity. Journal of Hematology & Oncology. 2021;14(1):1-5.
129. Sánchez-Martínez D, Baroni ML, Gutierrez-Agüera F, Roca-Ho H, Blanch-Lombarte O, González-García S, et al. Fratricide-resistant CD1a-specific CAR T cells for the treatment of cortical T-cell acute lymphoblastic leukemia. Blood. 2019;133(21):2291-304.
130. Jiménez-Reinoso A, Tirado N, Martinez-Moreno A, Díaz VM, García-Peydró M, Hangiu O, et al. Efficient preclinical treatment of cortical T cell acute lymphoblastic leukemia with T lymphocytes secreting anti-CD1a T cell engagers. Journal for ImmunoTherapy of Cancer. 2022;10(12):e005333.
131. Huang J, Alexey S, Li J, Jones T, Grande G, Douthit L, et al. Unique CDR3 epitope targeting by CAR-T cells is a viable approach for treating T-cell malignancies. Leukemia. 2019;33(9):2315-9.
132. Perera LP, Zhang M, Nakagawa M, Petrus MN, Maeda M, Kadin ME, et al. Chimeric antigen receptor modified T cells that target chemokine receptor CCR4 as a therapeutic modality for T-cell malignancies. Am J Hematol. 2017;92(9):892-901.
133. Maciocia PM, Wawrzyniecka PA, Maciocia NC, Burley A, Karpanasamy T, Devereaux S, et al. Anti-CCR9 chimeric antigen receptor T cells for T-cell acute lymphoblastic leukemia. Blood, The Journal of the American Society of Hematology. 2022;140(1):25-37.
134. Maciocia PM, Wawrzyniecka PA, Philip B, Ricciardelli I, Akarca AU, Onuoha SC, et al. Targeting the T cell receptor beta-chain constant region for immunotherapy of T cell malignancies. Nat Med. 2017;23(12):1416-23.
135. Pan J, Tan Y, Wang G, Deng B, Ling Z, Song W, et al. Donor-Derived CD7 Chimeric Antigen Receptor T Cells for T-Cell Acute Lymphoblastic Leukemia: First-in-Human, Phase I Trial. Journal of Clinical Oncology. 2021;39(30):3340-51.
136. Tan Y, Pan J, Deng B, Ling Z, Weiliang S, Tian Z, et al. Efficacy and Safety of Donor-Derived CD7 CAR T Cells for r/r T-Cell Acute Lymphoblastic Leukemia/Lymphoma: Interim Analysis from a Phase 2 Trial. Blood. 2022;140(Supplement 1):4602-3.
137. Hu Y, Zhou Y, Zhang M, Zhao H, Wei G, Ge W, et al. Genetically modified CD7-targeting allogeneic CAR-T cell therapy with enhanced efficacy for relapsed/refractory CD7-positive hematological malignancies: a phase I clinical study. Cell Research. 2022;32(11):995-1007.
138. Zhang X, Zhou Y, Yang J, Li J, Qiu L, Ge W, et al. A Novel Universal CD7-Targeted CAR-T Cell Therapy for Relapsed or Refractory T-Cell Acute Lymphoblastic Leukemia and T-Cell Lymphoblastic Lymphoma. Blood. 2022;140(Supplement 1):4566-7.
139. Lu P, Liu Y, Yang J, Zhang X, Yang X, Wang H, et al. Naturally selected CD7 CAR-T therapy without genetic manipulations for T-ALL/LBL: first-in-human phase 1 clinical trial. Blood. 2022;140(4):321-34.

140. Brodeur JF, Li S, Damlaj O, Dave VP. Expression of fully assembled TCR-CD3 complex on double positive thymocytes: synergistic role for the PRS and ER retention motifs in the intra-cytoplasmic tail of CD3epsilon. Int Immunol. 2009;21(12):1317-27.
141. Sabattini E, Bacci F, Sagramoso C, Pileri S. WHO classification of tumours of haematopoietic and lymphoid tissues in 2008: an overview. Pathologica. 2010;102(3):83-7.
142. Kuhn C, Weiner HL. Therapeutic anti-CD3 monoclonal antibodies: from bench to bedside. Immunotherapy. 2016;8(8):889-906.
143. Frankel A, Zuckero S, Mankin A, Grable M, Mitchell K, Lee Y, et al. Anti-CD3 recombinant diphtheria immunotoxin therapy of cutaneous T cell lymphoma. Current drug targets. 2009;10(2):104-9.
144. Aruffo A, Seed B. Molecular cloning of two CD7 (T-cell leukemia antigen) cDNAs by a COS cell expression system. Embo j. 1987;6(11):3313-6.
145. Lobach DF, Haynes BF. Ontogeny of the human thymus during fetal development. Journal of Clinical Immunology. 1987;7(2):81-97.
146. Sempowski GD, Lee DM, Kaufman RE, Haynes BF. Structure and function of the CD7 molecule. Crit Rev Immunol. 1999;19(4):331-48.
147. Campana D, van Dongen JJ, Mehta A, Coustan-Smith E, Wolvers-Tettero IL, Ganeshaguru K, Janossy G. Stages of T-cell receptor protein expression in T-cell acute lymphoblastic leukemia. Blood. 1991;77(7):1546-54.
148. Foon KA, Todd RF, 3rd. Immunologic classification of leukemia and lymphoma. Blood. 1986;68(1):1-31.
149. Venditti A, Del Poeta G, Buccisano F, Tamburini A, Cox-Froncillo MC, Aronica G, et al. Prognostic relevance of the expression of Tdt and CD7 in 335 cases of acute myeloid leukemia. Leukemia. 1998;12(7):1056-63.
150. Miwa H, Nakase K, Kita K. Biological characteristics of CD7(+) acute leukemia. Leuk Lymphoma. 1996;21(3-4):239-44.
151. Reinhold U, Liu L, Sesterhenn J, Abken H. CD7-negative T cells represent a separate differentiation pathway in a subset of post-thymic helper T cells. Immunology. 1996;89(3):391-6.
152. Cooper ML, DiPersio JF. Chimeric antigen receptor T cells (CAR-T) for the treatment of T-cell malignancies. Best Pract Res Clin Haematol. 2019;32(4):101097.
153. Voisinne G, Gonzalez de Peredo A, Roncagalli R. CD5, an Undercover Regulator of TCR Signaling. Front Immunol. 2018;9:2900.
154. LeMaistre CF, Rosen S, Frankel A, Kornfeld S, Saria E, Meneghetti C, et al. Phase I trial of H65-RTA immunoconjugate in patients with cutaneous T-cell lymphoma. Blood. 1991;78(5):1173-82.
155. Xu Y, Liu Q, Zhong M, Wang Z, Chen Z, Zhang Y, et al. 2B4 costimulatory domain enhancing cytotoxic ability of anti-CD5 chimeric antigen receptor engineered natural killer cells against T cell malignancies. J Hematol Oncol. 2019;12(1):49.
156. Wang CM, Wu ZQ, Wang Y, Guo YL, Dai HR, Wang XH, et al. Autologous T Cells Expressing CD30 Chimeric Antigen Receptors for Relapsed or Refractory Hodgkin Lymphoma: An Open-Label Phase I Trial. Clin Cancer Res. 2017;23(5):1156-66.
157. Sims JE, Tunnacliffe A, Smith WJ, Rabbitts TH. Complexity of human T-cell antigen receptor beta-chain constant- and variable-region genes. Nature. 1984;312(5994):541-5.

158. Tunnacliffe A, Kefford R, Milstein C, Forster A, Rabbitts TH. Sequence and evolution of the human T-cell antigen receptor beta-chain genes. Proc Natl Acad Sci U S A. 1985;82(15):5068-72.
159. Yoshie O, Fujisawa R, Nakayama T, Harasawa H, Tago H, Izawa D, et al. Frequent expression of CCR4 in adult T-cell leukemia and human T-cell leukemia virus type 1-transformed T cells. Blood. 2002;99(5):1505-11.
160. Subramaniam JM, Whiteside G, McKeage K, Croxtall JC. Mogamulizumab: first global approval. Drugs. 2012;72(9):1293-8.
161. Sugiyama D, Nishikawa H, Maeda Y, Nishioka M, Tanemura A, Katayama I, et al. Anti-CCR4 mAb selectively depletes effector-type FoxP3+CD4+ regulatory T cells, evoking antitumor immune responses in humans. Proc Natl Acad Sci U S A. 2013;110(44):17945-50.
162. Shichijo T, Nosaka K, Tatetsu H, Higuchi Y, Endo S, Inoue Y, et al. Beneficial impact of first-line mogamulizumab-containing chemotherapy in adult T-cell leukaemia-lymphoma. Br J Haematol. 2022;198(6):983-7.
163. Coventry B, Heinzel S. CD1a in human cancers: a new role for an old molecule. Trends Immunol. 2004;25(5):242-8.
164. Bulcha JT, Wang Y, Ma H, Tai PWL, Gao G. Viral vector platforms within the gene therapy landscape. Signal Transduction and Targeted Therapy. 2021;6(1):53.
165. Milone MC, O'Doherty U. Clinical use of lentiviral vectors. Leukemia. 2018;32(7):1529-41.
166. Maetzig T, Galla M, Baum C, Schambach A. Gammaretroviral vectors: biology, technology and application. Viruses. 2011;3(6):677-713.
167. Knight S, Collins M, Takeuchi Y. Insertional mutagenesis by retroviral vectors: current concepts and methods of analysis. Curr Gene Ther. 2013;13(3):211-27.
168. Muñoz-López M, García-Pérez JL. DNA transposons: nature and applications in genomics. Curr Genomics. 2010;11(2):115-28.
169. Skipper KA, Andersen PR, Sharma N, Mikkelsen JG. DNA transposon-based gene vehicles - scenes from an evolutionary drive. Journal of Biomedical Science. 2013;20(1):92.
170. Ivics Z, Izsvák Z. The expanding universe of transposon technologies for gene and cell engineering. Mobile DNA. 2010;1(1):25.
171. Mátés L, Chuah MKL, Belay E, Jerchow B, Manoj N, Acosta-Sanchez A, et al. Molecular evolution of a novel hyperactive Sleeping Beauty transposase enables robust stable gene transfer in vertebrates. Nature genetics. 2009;41(6):753-61.
172. Yusa K, Zhou L, Li MA, Bradley A, Craig NL. A hyperactive piggyBac transposase for mammalian applications. Proc Natl Acad Sci U S A. 2011;108(4):1531-6.
173. Micklethwaite KP, Gowrishankar K, Gloss BS, Li Z, Street JA, Moezzi L, et al. Investigation of product-derived lymphoma following infusion of piggyBac-modified CD19 chimeric antigen receptor T cells. Blood. 2021;138(16):1391-405.
174. Bishop DC, Clancy LE, Simms R, Burgess J, Mathew G, Moezzi L, et al. Development of CAR T-cell lymphoma in 2 of 10 patients effectively treated with piggyBac-modified CD19 CAR T cells. Blood. 2021;138(16):1504-9.
175. Beatty GL, O'Hara MH, Lacey SF, Torigian DA, Nazimuddin F, Chen F, et al. Activity of Mesothelin-Specific Chimeric Antigen Receptor T Cells Against Pancreatic Carcinoma Metastases in a Phase 1 Trial. Gastroenterology. 2018;155(1):29-32.

176. Billingsley MM, Singh N, Ravikumar P, Zhang R, June CH, Mitchell MJ. Ionizable Lipid Nanoparticle-Mediated mRNA Delivery for Human CAR T Cell Engineering. Nano Lett. 2020;20(3):1578-89.
177. Sung YK, Kim SW. Recent advances in the development of gene delivery systems. Biomaterials Research. 2019;23(1):8.
178. Ghosh S, Brown AM, Jenkins C, Campbell K. Viral Vector Systems for Gene Therapy: A Comprehensive Literature Review of Progress and Biosafety Challenges. Appl Biosaf. 2020;25(1):7-18.
179. Vigna E, Naldini L. Lentiviral vectors: excellent tools for experimental gene transfer and promising candidates for gene therapy. The journal of gene medicine. 2000;2(5):308-16.
180. Durand S, Cimarelli A. The inside out of lentiviral vectors. Viruses. 2011;3(2):132-59.
181. Freed EO. HIV-1 assembly, release and maturation. Nat Rev Microbiol. 2015;13(8):484-96.
182. Dragic T, Litwin V, Allaway GP, Martin SR, Huang Y, Nagashima KA, et al. HIV-1 entry into CD4+ cells is mediated by the chemokine receptor CC-CKR-5. Nature. 1996;381(6584):667-73.
183. Miller MD, Farnet CM, Bushman FD. Human immunodeficiency virus type 1 preintegration complexes: studies of organization and composition. J Virol. 1997;71(7):5382-90.
184. Briggs JA, Krausslich HG. The molecular architecture of HIV. J Mol Biol. 2011;410(4):491-500.
185. Pluta K, Kacprzak MM. Use of HIV as a gene transfer vector. Acta biochimica Polonica. 2009;56(4):531-95.
186. Joglekar AV, Sandoval S. Pseudotyped Lentiviral Vectors: One Vector, Many Guises. Human gene therapy methods. 2017;28(6):291-301.
187. Cronin J, Zhang XY, Reiser J. Altering the tropism of lentiviral vectors through pseudotyping. Curr Gene Ther. 2005;5(4):387-98.
188. Dull T, Zufferey R, Kelly M, Mandel RJ, Nguyen M, Trono D, Naldini L. A third-generation lentivirus vector with a conditional packaging system. J Virol. 1998;72(11):8463-71.
189. Miyoshi H, Blomer U, Takahashi M, Gage FH, Verma IM. Development of a self-inactivating lentivirus vector. J Virol. 1998;72(10):8150-7.
190. Zufferey R, Dull T, Mandel RJ, Bukovsky A, Quiroz D, Naldini L, Trono D. Self-inactivating lentivirus vector for safe and efficient in vivo gene delivery. J Virol. 1998;72(12):9873-80.
191. Zufferey R, Donello JE, Trono D, Hope TJ. Woodchuck hepatitis virus posttranscriptional regulatory element enhances expression of transgenes delivered by retroviral vectors. J Virol. 1999;73(4):2886-92.
192. Hong S, Hwang DY, Yoon S, Isacson O, Ramezani A, Hawley RG, Kim KS. Functional analysis of various promoters in lentiviral vectors at different stages of in vitro differentiation of mouse embryonic stem cells. Molecular therapy : the journal of the American Society of Gene Therapy. 2007;15(9):1630-9.
193. Qin JY, Zhang L, Clift KL, Hulur I, Xiang AP, Ren BZ, Lahn BT. Systematic comparison of constitutive promoters and the doxycycline-inducible promoter. PloS one. 2010;5(5):e10611.

194. Li H, Yang Y, Hong W, Huang M, Wu M, Zhao X. Applications of genome editing technology in the targeted therapy of human diseases: mechanisms, advances and prospects. Signal Transduction and Targeted Therapy. 2020;5(1):1.
195. Urnov FD, Miller JC, Lee YL, Beausejour CM, Rock JM, Augustus S, et al. Highly efficient endogenous human gene correction using designed zinc-finger nucleases. Nature. 2005;435(7042):646-51.
196. Silva G, Poirot L, Galetto R, Smith J, Montoya G, Duchateau P, Pâques F. Meganucleases and other tools for targeted genome engineering: perspectives and challenges for gene therapy. Curr Gene Ther. 2011;11(1):11-27.
197. Scholze H, Boch J. TAL effector-DNA specificity. Virulence. 2010;1(5):428-32.
198. Jinek M, Chylinski K, Fonfara I, Hauer M, Doudna JA, Charpentier E. A programmable dual-RNA-guided DNA endonuclease in adaptive bacterial immunity. Science (New York, NY). 2012;337(6096):816-21.
199. Mali P, Yang L, Esvelt KM, Aach J, Guell M, DiCarlo JE, et al. RNA-Guided Human Genome Engineering via Cas9. Science (New York, NY). 2013;339(6121):823-6.
200. Gupta RM, Musunuru K. Expanding the genetic editing tool kit: ZFNs, TALENs, and CRISPR-Cas9. J Clin Invest. 2014;124(10):4154-61.
201. Osborn MJ, Webber BR, Knipping F, Lonetree CL, Tennis N, DeFeo AP, et al. Evaluation of TCR Gene Editing Achieved by TALENs, CRISPR/Cas9, and megaTAL Nucleases. Molecular therapy : the journal of the American Society of Gene Therapy. 2016;24(3):570-81.
202. Knipping F, Osborn MJ, Petri K, Tolar J, Glimm H, von Kalle C, et al. Genome-wide Specificity of Highly Efficient TALENs and CRISPR/Cas9 for T Cell Receptor Modification. Molecular therapy Methods & clinical development. 2017;4:213-24.
203. Cong L, Ran FA, Cox D, Lin S, Barretto R, Habib N, et al. Multiplex genome engineering using CRISPR/Cas systems. Science (New York, NY). 2013;339(6121):819-23.
204. Ishino Y, Shinagawa H, Makino K, Amemura M, Nakata A. Nucleotide sequence of the iap gene, responsible for alkaline phosphatase isozyme conversion in Escherichia coli, and identification of the gene product. J Bacteriol. 1987;169(12):5429-33.
205. Jansen R, Embden JD, Gaastra W, Schouls LM. Identification of genes that are associated with DNA repeats in prokaryotes. Mol Microbiol. 2002;43(6):1565-75.
206. Makarova KS, Aravind L, Grishin NV, Rogozin IB, Koonin EV. A DNA repair system specific for thermophilic Archaea and bacteria predicted by genomic context analysis. Nucleic Acids Res. 2002;30(2):482-96.
207. Bolotin A, Quinquis B, Sorokin A, Ehrlich SD. Clustered regularly interspaced short palindrome repeats (CRISPRs) have spacers of extrachromosomal origin. Microbiology. 2005;151(Pt 8):2551-61.
208. Mojica FJ, Díez-Villaseñor C, García-Martínez J, Soria E. Intervening sequences of regularly spaced prokaryotic repeats derive from foreign genetic elements. J Mol Evol. 2005;60(2):174-82.
209. Pourcel C, Salvignol G, Vergnaud G. CRISPR elements in Yersinia pestis acquire new repeats by preferential uptake of bacteriophage DNA, and provide additional tools for evolutionary studies. Microbiology (Reading). 2005;151(Pt 3):653-63.

210. Barrangou R, Fremaux C, Deveau H, Richards M, Boyaval P, Moineau S, et al. CRISPR provides acquired resistance against viruses in prokaryotes. Science (New York, NY). 2007;315(5819):1709-12.
211. Andersson AF, Banfield JF. Virus population dynamics and acquired virus resistance in natural microbial communities. Science (New York, NY). 2008;320(5879):1047-50.
212. Datsenko KA, Pougach K, Tikhonov A, Wanner BL, Severinov K, Semenova E. Molecular memory of prior infections activates the CRISPR/Cas adaptive bacterial immunity system. Nat Commun. 2012;3:945.
213. Deltcheva E, Chylinski K, Sharma CM, Gonzales K, Chao Y, Pirzada ZA, et al. CRISPR RNA maturation by trans-encoded small RNA and host factor RNase III. Nature. 2011;471(7340):602-7.
214. Garneau JE, Dupuis M, Villion M, Romero DA, Barrangou R, Boyaval P, et al. The CRISPR/Cas bacterial immune system cleaves bacteriophage and plasmid DNA. Nature. 2010;468(7320):67-71.
215. Gasiunas G, Barrangou R, Horvath P, Siksnys V. Cas9-crRNA ribonucleoprotein complex mediates specific DNA cleavage for adaptive immunity in bacteria. Proc Natl Acad Sci U S A. 2012;109(39):E2579-86.
216. Yosef I, Goren MG, Qimron U. Proteins and DNA elements essential for the CRISPR adaptation process in Escherichia coli. Nucleic Acids Res. 2012;40(12):5569-76.
217. Mojica FJM, Díez-Villaseñor C, García-Martínez J, Almendros C. Short motif sequences determine the targets of the prokaryotic CRISPR defence system. Microbiology (Reading). 2009;155(Pt 3):733-40.
218. Shah SA, Erdmann S, Mojica FJ, Garrett RA. Protospacer recognition motifs: mixed identities and functional diversity. RNA Biol. 2013;10(5):891-9.
219. Semenova E, Jore MM, Datsenko KA, Semenova A, Westra ER, Wanner B, et al. Interference by clustered regularly interspaced short palindromic repeat (CRISPR) RNA is governed by a seed sequence. Proc Natl Acad Sci U S A. 2011;108(25):10098-103.
220. Wiedenheft B, van Duijn E, Bultema JB, Waghmare SP, Zhou K, Barendregt A, et al. RNA-guided complex from a bacterial immune system enhances target recognition through seed sequence interactions. Proc Natl Acad Sci U S A. 2011;108(25):10092-7.
221. Makarova KS, Haft DH, Barrangou R, Brouns SJ, Charpentier E, Horvath P, et al. Evolution and classification of the CRISPR-Cas systems. Nat Rev Microbiol. 2011;9(6):467-77.
222. Liu C, Zhang L, Liu H, Cheng K. Delivery strategies of the CRISPR-Cas9 gene-editing system for therapeutic applications. J Control Release. 2017;266:17-26.
223. Hsu PD, Scott DA, Weinstein JA, Ran FA, Konermann S, Agarwala V, et al. DNA targeting specificity of RNA-guided Cas9 nucleases. Nature biotechnology. 2013;31(9):827-32.
224. Chakraborty A, Tapryal N, Venkova T, Horikoshi N, Pandita RK, Sarker AH, et al. Classical non-homologous end-joining pathway utilizes nascent RNA for error-free double-strand break repair of transcribed genes. Nat Commun. 2016;7:13049.

225. Mao Z, Bozzella M, Seluanov A, Gorbunova V. DNA repair by nonhomologous end joining and homologous recombination during cell cycle in human cells. Cell Cycle. 2008;7(18):2902-6.
226. Mari PO, Florea BI, Persengiev SP, Verkaik NS, Brüggenwirth HT, Modesti M, et al. Dynamic assembly of end-joining complexes requires interaction between Ku70/80 and XRCC4. Proc Natl Acad Sci U S A. 2006;103(49):18597-602.
227. Davis AJ, Chen DJ. DNA double strand break repair via non-homologous end-joining. Transl Cancer Res. 2013;2(3):130-43.
228. Truong LN, Li Y, Shi LZ, Hwang PY, He J, Wang H, et al. Microhomology-mediated End Joining and Homologous Recombination share the initial end resection step to repair DNA double-strand breaks in mammalian cells. Proc Natl Acad Sci U S A. 2013;110(19):7720-5.
229. Mao Z, Bozzella M, Seluanov A, Gorbunova V. Comparison of nonhomologous end joining and homologous recombination in human cells. DNA Repair (Amst). 2008;7(10):1765-71.
230. Frit P, Barboule N, Yuan Y, Gomez D, Calsou P. Alternative end-joining pathway(s): Bricolage at DNA breaks. DNA Repair. 2014;17:81-97.
231. Nambiar TS, Baudrier L, Billon P, Ciccia A. CRISPR-based genome editing through the lens of DNA repair. Mol Cell. 2022;82(2):348-88.
232. Karanam K, Kafri R, Loewer A, Lahav G. Quantitative live cell imaging reveals a gradual shift between DNA repair mechanisms and a maximal use of HR in mid S phase. Mol Cell. 2012;47(2):320-9.
233. Branzei D, Foiani M. Regulation of DNA repair throughout the cell cycle. Nat Rev Mol Cell Biol. 2008;9(4):297-308.
234. Wienert B, Nguyen DN, Guenther A, Feng SJ, Locke MN, Wyman SK, et al. Timed inhibition of CDC7 increases CRISPR-Cas9 mediated templated repair. Nat Commun. 2020;11(1):2109.
235. Jayavaradhan R, Pillis DM, Malik P. A Versatile Tool for the Quantification of CRISPR/Cas9-Induced Genome Editing Events in Human Hematopoietic Cell Lines and Hematopoietic Stem/Progenitor Cells. J Mol Biol. 2019;431(1):102-10.
236. Chu VT, Weber T, Wefers B, Wurst W, Sander S, Rajewsky K, Kühn R. Increasing the efficiency of homology-directed repair for CRISPR-Cas9-induced precise gene editing in mammalian cells. Nature biotechnology. 2015;33(5):543-8.
237. Li G, Liu D, Zhang X, Quan R, Zhong C, Mo J, et al. Suppressing Ku70/Ku80 expression elevates homology-directed repair efficiency in primary fibroblasts. Int J Biochem Cell Biol. 2018;99:154-60.
238. Riesenberg S, Kanis P, Macak D, Wollny D, Düsterhöft D, Kowalewski J, et al. Efficient high-precision homology-directed repair-dependent genome editing by HDRobust. Nature Methods. 2023.
239. Charpentier M, Khedher AHY, Menoret S, Brion A, Lamribet K, Dardillac E, et al. CtIP fusion to Cas9 enhances transgene integration by homology-dependent repair. Nat Commun. 2018;9(1):1133.
240. Chauhan VP, Sharp PA, Langer R. Altered DNA repair pathway engagement by engineered CRISPR-Cas9 nucleases. Proc Natl Acad Sci U S A. 2023;120(11):e2300605120.
241. Wang JY, Doudna JA. CRISPR technology: A decade of genome editing is only the beginning. Science (New York, NY). 2023;379(6629):eadd8643.

242. Charlesworth CT, Deshpande PS, Dever DP, Camarena J, Lemgart VT, Cromer MK, et al. Identification of preexisting adaptive immunity to Cas9 proteins in humans. Nat Med. 2019;25(2):249-54.
243. Crudele JM, Chamberlain JS. Cas9 immunity creates challenges for CRISPR gene editing therapies. Nat Commun. 2018;9(1):3497.
244. Liu J, Gaj T, Yang Y, Wang N, Shui S, Kim S, et al. Efficient delivery of nuclease proteins for genome editing in human stem cells and primary cells. Nature protocols. 2015;10(11):1842-59.
245. Yin H, Song CQ, Dorkin JR, Zhu LJ, Li Y, Wu Q, et al. Therapeutic genome editing by combined viral and non-viral delivery of CRISPR system components in vivo. Nature biotechnology. 2016;34(3):328-33.
246. Banasik MB, McCray PB, Jr. Integrase-defective lentiviral vectors: progress and applications. Gene Ther. 2010;17(2):150-7.
247. Dong W, Kantor B. Lentiviral Vectors for Delivery of Gene-Editing Systems Based on CRISPR/Cas: Current State and Perspectives. Viruses. 2021;13(7).
248. Moço PD, Aharony N, Kamen A. Adeno-Associated Viral Vectors for Homology-Directed Generation of CAR-T Cells. Biotechnol J. 2020;15(1):e1900286.
249. Shakirova A, Karpov T, Komarova Y, Lepik K. In search of an ideal template for therapeutic genome editing: A review of current developments for structure optimization. Front Genome Ed. 2023;5:1068637.
250. Oh SA, Senger K, Madireddi S, Akhmetzyanova I, Ishizuka IE, Tarighat S, et al. High-efficiency nonviral CRISPR/Cas9-mediated gene editing of human T cells using plasmid donor DNA. J Exp Med. 2022;219(5).
251. Wen W, Quan ZJ, Li SA, Yang ZX, Fu YW, Zhang F, et al. Effective control of large deletions after double-strand breaks by homology-directed repair and dsODN insertion. Genome Biol. 2021;22(1):236.
252. Gallagher DN, Haber JE. Single-strand template repair: key insights to increase the efficiency of gene editing. Current Genetics. 2021;67(5):747-53.
253. Shy BR, Vykunta VS, Ha A, Talbot A, Roth TL, Nguyen DN, et al. High-yield genome engineering in primary cells using a hybrid ssDNA repair template and small-molecule cocktails. Nature biotechnology. 2022.
254. Okamoto S, Amaishi Y, Maki I, Enoki T, Mineno J. Highly efficient genome editing for single-base substitutions using optimized ssODNs with Cas9-RNPs. Sci Rep. 2019;9(1):4811.
255. Jing R, Jiao P, Chen J, Meng X, Wu X, Duan Y, et al. Cas9-Cleavage Sequences in Size-Reduced Plasmids Enhance Nonviral Genome Targeting of CARs in Primary Human T Cells. Small Methods. 2021;5(7):2100071.
256. Fu Y, Foden JA, Khayter C, Maeder ML, Reyon D, Joung JK, Sander JD. High-frequency off-target mutagenesis induced by CRISPR-Cas nucleases in human cells. Nature biotechnology. 2013;31(9):822-6.
257. Gopalappa R, Suresh B, Ramakrishna S, Kim HH. Paired D10A Cas9 nickases are sometimes more efficient than individual nucleases for gene disruption. Nucleic Acids Res. 2018;46(12):e71.
258. Fu Y, Sander JD, Reyon D, Cascio VM, Joung JK. Improving CRISPR-Cas nuclease specificity using truncated guide RNAs. Nature biotechnology. 2014;32(3):279-84.

259. Kleinstiver BP, Pattanayak V, Prew MS, Tsai SQ, Nguyen NT, Zheng Z, Joung JK. High-fidelity CRISPR-Cas9 nucleases with no detectable genome-wide off-target effects. Nature. 2016;529(7587):490-5.
260. Vakulskas CA, Dever DP, Rettig GR, Turk R, Jacobi AM, Collingwood MA, et al. A high-fidelity Cas9 mutant delivered as a ribonucleoprotein complex enables efficient gene editing in human hematopoietic stem and progenitor cells. Nat Med. 2018;24(8):1216-24.
261. Kosicki M, Tomberg K, Bradley A. Repair of double-strand breaks induced by CRISPR-Cas9 leads to large deletions and complex rearrangements. Nature biotechnology. 2018;36(8):765-71.
262. Poirot L, Philip B, Schiffer-Mannioui C, Le Clerre D, Chion-Sotinel I, Derniame S, et al. Multiplex Genome-Edited T-cell Manufacturing Platform for "Off-the-Shelf" Adoptive T-cell Immunotherapies. Cancer Res. 2015;75(18):3853-64.
263. Sternberg SH, Doudna JA. Expanding the Biologist's Toolkit with CRISPR-Cas9. Mol Cell. 2015;58(4):568-74.
264. Pacesa M, Lin CH, Cléry A, Saha A, Arantes PR, Bargsten K, et al. Structural basis for Cas9 off-target activity. Cell. 2022;185(22):4067-81.e21.
265. Tsuchida CA, Brandes N, Bueno R, Trinidad M, Mazumder T, Yu B, et al. Mitigation of chromosome loss in clinical CRISPR-Cas9-engineered T cells. bioRxiv. 2023.
266. Wang DC, Wang X. Off-target genome editing: A new discipline of gene science and a new class of medicine. Cell Biol Toxicol. 2019;35(3):179-83.
267. Chen SJ. Minimizing off-target effects in CRISPR-Cas9 genome editing. Cell Biol Toxicol. 2019;35(5):399-401.
268. Ran FA, Hsu PD, Lin CY, Gootenberg JS, Konermann S, Trevino AE, et al. Double nicking by RNA-guided CRISPR Cas9 for enhanced genome editing specificity. Cell. 2013;154(6):1380-9.
269. Slaymaker IM, Gao L, Zetsche B, Scott DA, Yan WX, Zhang F. Rationally engineered Cas9 nucleases with improved specificity. Science (New York, NY). 2016;351(6268):84-8.
270. Naeem M, Majeed S, Hoque MZ, Ahmad I. Latest Developed Strategies to Minimize the Off-Target Effects in CRISPR-Cas-Mediated Genome Editing. Cells. 2020;9(7).
271. Bao XR, Pan Y, Lee CM, Davis TH, Bao G. Tools for experimental and computational analyses of off-target editing by programmable nucleases. Nature protocols. 2021;16(1):10-26.
272. Chuai GH, Wang QL, Liu Q. In Silico Meets In Vivo: Towards Computational CRISPR-Based sgRNA Design. Trends Biotechnol. 2017;35(1):12-21.
273. Tao J, Bauer DE, Chiarle R. Assessing and advancing the safety of CRISPR-Cas tools: from DNA to RNA editing. Nat Commun. 2023;14(1):212.
274. Dabiri H, Safarzadeh Kozani P, Habibi Anbouhi M, Mirzaee Godarzee M, Haddadi MH, Basiri M, et al. Site-specific transgene integration in chimeric antigen receptor (CAR) T cell therapies. Biomarker Research. 2023;11(1):67.
275. Eyquem J, Mansilla-Soto J, Giavridis T, van der Stegen SJ, Hamieh M, Cunanan KM, et al. Targeting a CAR to the TRAC locus with CRISPR/Cas9 enhances tumour rejection. Nature. 2017;543(7643):113-7.

276. Wang D, Tai PWL, Gao G. Adeno-associated virus vector as a platform for gene therapy delivery. Nat Rev Drug Discov. 2019;18(5):358-78.
277. Balke-Want H, Keerthi V, Cadinanos-Garai A, Fowler C, Gkitsas N, Brown AK, et al. Non-viral chimeric antigen receptor (CAR) T cells going viral. Immunooncol Technol. 2023;18:100375.
278. Roth TL, Puig-Saus C, Yu R, Shifrut E, Carnevale J, Li PJ, et al. Reprogramming human T cell function and specificity with non-viral genome targeting. Nature. 2018;559(7714):405-9.
279. Dimitri A, Herbst F, Fraietta JA. Engineering the next-generation of CAR T-cells with CRISPR-Cas9 gene editing. Mol Cancer. 2022;21(1):78.
280. Razeghian E, Nasution MKM, Rahman HS, Gardanova ZR, Abdelbasset WK, Aravindhan S, et al. A deep insight into CRISPR/Cas9 application in CAR-T cell-based tumor immunotherapies. Stem Cell Res Ther. 2021;12(1):428.
281. MacLeod DT, Antony J, Martin AJ, Moser RJ, Hekele A, Wetzel KJ, et al. Integration of a CD19 CAR into the TCR Alpha Chain Locus Streamlines Production of Allogeneic Gene-Edited CAR T Cells. Molecular therapy : the journal of the American Society of Gene Therapy. 2017;25(4):949-61.
282. Sachdeva M, Busser BW, Temburni S, Jahangiri B, Gautron AS, Maréchal A, et al. Repurposing endogenous immune pathways to tailor and control chimeric antigen receptor T cell functionality. Nat Commun. 2019;10(1):5100.
283. Feucht J, Sun J, Eyquem J, Ho YJ, Zhao Z, Leibold J, et al. Calibration of CAR activation potential directs alternative T cell fates and therapeutic potency. Nat Med. 2019;25(1):82-8.
284. Dai X, Park JJ, Du Y, Kim HR, Wang G, Errami Y, Chen S. One-step generation of modular CAR-T cells with AAV-Cpf1. Nat Methods. 2019;16(3):247-54.
285. Wiebking V, Lee CM, Mostrel N, Lahiri P, Bak R, Bao G, et al. Genome editing of donor-derived T-cells to generate allogenic chimeric antigen receptor-modified T cells: Optimizing αβ T cell-depleted haploidentical hematopoietic stem cell transplantation. Haematologica. 2021;106(3):847-58.
286. Mansilla-Soto J, Eyquem J, Haubner S, Hamieh M, Feucht J, Paillon N, et al. HLA-independent T cell receptors for targeting tumors with low antigen density. Nature Medicine. 2022;28(2):345-52.
287. Odé Z, Condori J, Peterson N, Zhou S, Krenciute G. CRISPR-Mediated Non-Viral Site-Specific Gene Integration and Expression in T Cells: Protocol and Application for T-Cell Therapy. Cancers (Basel). 2020;12(6).
288. Kath J, Du W, Pruene A, Braun T, Thommandru B, Turk R, et al. Pharmacological interventions enhance virus-free generation of TRAC-replaced CAR T cells. Molecular therapy Methods & clinical development. 2022;25:311-30.
289. Zhang J, Hu Y, Yang J, Li W, Zhang M, Wang Q, et al. Non-viral, specifically targeted CAR-T cells achieve high safety and efficacy in B-NHL. Nature. 2022;609(7926):369-74.
290. Foy SP, Jacoby K, Bota DA, Hunter T, Pan Z, Stawiski E, et al. Non-viral precision T cell receptor replacement for personalized cell therapy. Nature. 2022:1-10.
291. Glaser V, Flugel C, Kath J, Du W, Drosdek V, Franke C, et al. Combining different CRISPR nucleases for simultaneous knock-in and base editing prevents translocations in multiplex-edited CAR T cells. bioRxiv. 2022:2022.11.11.516008.

292. Mueller KP, Piscopo NJ, Forsberg MH, Saraspe LA, Das A, Russell B, et al. Production and characterization of virus-free, CRISPR-CAR T cells capable of inducing solid tumor regression. J Immunother Cancer. 2022;10(9).
293. Müller TR, Jarosch S, Hammel M, Leube J, Grassmann S, Bernard B, et al. Targeted T cell receptor gene editing provides predictable T cell product function for immunotherapy. Cell Rep Med. 2021;2(8):100374.
294. Nguyen DN, Roth TL, Li PJ, Chen PA, Apathy R, Mamedov MR, et al. Polymer-stabilized Cas9 nanoparticles and modified repair templates increase genome editing efficiency. Nature biotechnology. 2020;38(1):44-9.
295. Billon P, Bryant EE, Joseph SA, Nambiar TS, Hayward SB, Rothstein R, Ciccia A. CRISPR-Mediated Base Editing Enables Efficient Disruption of Eukaryotic Genes through Induction of STOP Codons. Mol Cell. 2017;67(6):1068-79.e4.
296. Rees HA, Liu DR. Publisher Correction: Base editing: precision chemistry on the genome and transcriptome of living cells. Nat Rev Genet. 2018;19(12):801.
297. Komor AC, Kim YB, Packer MS, Zuris JA, Liu DR. Programmable editing of a target base in genomic DNA without double-stranded DNA cleavage. Nature. 2016;533(7603):420-4.
298. Jiang T, Henderson JM, Coote K, Cheng Y, Valley HC, Zhang X-O, et al. Chemical modifications of adenine base editor mRNA and guide RNA expand its application scope. Nature Communications. 2020;11(1):1979.
299. Komor AC, Zhao KT, Packer MS, Gaudelli NM, Waterbury AL, Koblan LW, et al. Improved base excision repair inhibition and bacteriophage Mu Gam protein yields C:G-to-T:A base editors with higher efficiency and product purity. Sci Adv. 2017;3(8):eaao4774.
300. Wang X, Li J, Wang Y, Yang B, Wei J, Wu J, et al. Efficient base editing in methylated regions with a human APOBEC3A-Cas9 fusion. Nature biotechnology. 2018;36(10):946-9.
301. Gaudelli NM, Komor AC, Rees HA, Packer MS, Badran AH, Bryson DI, Liu DR. Programmable base editing of A•T to G•C in genomic DNA without DNA cleavage. Nature. 2017;551(7681):464-71.
302. Kim YB, Komor AC, Levy JM, Packer MS, Zhao KT, Liu DR. Increasing the genome-targeting scope and precision of base editing with engineered Cas9-cytidine deaminase fusions. Nature biotechnology. 2017;35(4):371-6.
303. Hu JH, Miller SM, Geurts MH, Tang W, Chen L, Sun N, et al. Evolved Cas9 variants with broad PAM compatibility and high DNA specificity. Nature. 2018;556(7699):57-63.
304. Nishimasu H, Shi X, Ishiguro S, Gao L, Hirano S, Okazaki S, et al. Engineered CRISPR-Cas9 nuclease with expanded targeting space. Science (New York, NY). 2018;361(6408):1259-62.
305. Tan J, Zhang F, Karcher D, Bock R. Engineering of high-precision base editors for site-specific single nucleotide replacement. Nature Communications. 2019;10(1):439.
306. Kleinstiver BP, Prew MS, Tsai SQ, Topkar VV, Nguyen NT, Zheng Z, et al. Engineered CRISPR-Cas9 nucleases with altered PAM specificities. Nature. 2015;523(7561):481-5.

307. Huang TP, Zhao KT, Miller SM, Gaudelli NM, Oakes BL, Fellmann C, et al. Circularly permuted and PAM-modified Cas9 variants broaden the targeting scope of base editors. Nature biotechnology. 2019;37(6):626-31.
308. Webber BR, Lonetree CL, Kluesner MG, Johnson MJ, Pomeroy EJ, Diers MD, et al. Highly efficient multiplex human T cell engineering without double-strand breaks using Cas9 base editors. Nat Commun. 2019;10(1):5222.
309. Jeong YK, Song B, Bae S. Current Status and Challenges of DNA Base Editing Tools. Molecular Therapy. 2020;28(9):1938-52.
310. Gehrke JM, Cervantes O, Clement MK, Wu Y, Zeng J, Bauer DE, et al. An APOBEC3A-Cas9 base editor with minimized bystander and off-target activities. Nature biotechnology. 2018;36(10):977-82.
311. Hess GT, Frésard L, Han K, Lee CH, Li A, Cimprich KA, et al. Directed evolution using dCas9-targeted somatic hypermutation in mammalian cells. Nat Methods. 2016;13(12):1036-42.
312. Kim K, Ryu SM, Kim ST, Baek G, Kim D, Lim K, et al. Highly efficient RNA-guided base editing in mouse embryos. Nature biotechnology. 2017;35(5):435-7.
313. Ma Y, Zhang J, Yin W, Zhang Z, Song Y, Chang X. Targeted AID-mediated mutagenesis (TAM) enables efficient genomic diversification in mammalian cells. Nat Methods. 2016;13(12):1029-35.
314. Nishida K, Arazoe T, Yachie N, Banno S, Kakimoto M, Tabata M, et al. Targeted nucleotide editing using hybrid prokaryotic and vertebrate adaptive immune systems. Science (New York, NY). 2016;353(6305).
315. Kim D, Lim K, Kim S-T, Yoon S-h, Kim K, Ryu S-M, Kim J-S. Genome-wide target specificities of CRISPR RNA-guided programmable deaminases. Nature biotechnology. 2017;35(5):475-80.
316. Liang P, Xie X, Zhi S, Sun H, Zhang X, Chen Y, et al. Genome-wide profiling of adenine base editor specificity by EndoV-seq. Nat Commun. 2019;10(1):67.
317. Jin S, Zong Y, Gao Q, Zhu Z, Wang Y, Qin P, et al. Cytosine, but not adenine, base editors induce genome-wide off-target mutations in rice. Science (New York, NY). 2019;364(6437):292-5.
318. Zuo E, Sun Y, Wei W, Yuan T, Ying W, Sun H, et al. Cytosine base editor generates substantial off-target single-nucleotide variants in mouse embryos. Science (New York, NY). 2019;364(6437):289-92.
319. Grünewald J, Zhou R, Garcia SP, Iyer S, Lareau CA, Aryee MJ, Joung JK. Transcriptome-wide off-target RNA editing induced by CRISPR-guided DNA base editors. Nature. 2019;569(7756):433-7.
320. Doman JL, Raguram A, Newby GA, Liu DR. Evaluation and minimization of Cas9-independent off-target DNA editing by cytosine base editors. Nature biotechnology. 2020;38(5):620-8.
321. Xu W, Song W, Yang Y, Wu Y, Lv X, Yuan S, et al. Multiplex nucleotide editing by high-fidelity Cas9 variants with improved efficiency in rice. BMC Plant Biol. 2019;19(1):511.
322. Rees HA, Komor AC, Yeh WH, Caetano-Lopes J, Warman M, Edge ASB, Liu DR. Improving the DNA specificity and applicability of base editing through protein engineering and protein delivery. Nat Commun. 2017;8:15790.

323. Kulcsár PI, Tálas A, Ligeti Z, Krausz SL, Welker E. SuperFi-Cas9 exhibits remarkable fidelity but severely reduced activity yet works effectively with ABE8e. Nat Commun. 2022;13(1):6858.
324. Rees HA, Wilson C, Doman JL, Liu DR. Analysis and minimization of cellular RNA editing by DNA adenine base editors. Sci Adv. 2019;5(5):eaax5717.
325. Zhou C, Sun Y, Yan R, Liu Y, Zuo E, Gu C, et al. Off-target RNA mutation induced by DNA base editing and its elimination by mutagenesis. Nature. 2019;571(7764):275-8.
326. Wang L, Xue W, Zhang H, Gao R, Qiu H, Wei J, et al. Eliminating base-editor-induced genome-wide and transcriptome-wide off-target mutations. Nat Cell Biol. 2021;23(5):552-63.
327. Grünewald J, Zhou R, Iyer S, Lareau CA, Garcia SP, Aryee MJ, Joung JK. CRISPR DNA base editors with reduced RNA off-target and self-editing activities. Nature biotechnology. 2019;37(9):1041-8.
328. Yu Y, Leete TC, Born DA, Young L, Barrera LA, Lee S-J, et al. Cytosine base editors with minimized unguided DNA and RNA off-target events and high on-target activity. Nature Communications. 2020;11(1):2052.
329. Georgiadis C, Preece R, Nickolay L, Etuk A, Petrova A, Ladon D, et al. Long Terminal Repeat CRISPR-CAR-Coupled "Universal" T Cells Mediate Potent Anti-leukemic Effects. Molecular therapy : the journal of the American Society of Gene Therapy. 2018;26(5):1215-27.
330. Doench JG, Fusi N, Sullender M, Hegde M, Vaimberg EW, Donovan KF, et al. Optimized sgRNA design to maximize activity and minimize off-target effects of CRISPR-Cas9. Nature biotechnology. 2016;34(2):184-91.
331. Afgan E, Baker D, Batut B, van den Beek M, Bouvier D, Cech M, et al. The Galaxy platform for accessible, reproducible and collaborative biomedical analyses: 2018 update. Nucleic Acids Res. 2018;46(W1):W537-w44.
332. Qasim W. Genome-edited allogeneic donor “universal” chimeric antigen receptor T cells. Blood. 2023;141(8):835-45.
333. Gapinske M, Luu A, Winter J, Woods WS, Kostan KA, Shiva N, et al. CRISPR-SKIP: programmable gene splicing with single base editors. Genome Biol. 2018;19(1):107.
334. Çakan E, Gunaydin G. Activation induced cytidine deaminase: An old friend with new faces. Front Immunol. 2022;13:965312.
335. Uriu K, Kosugi Y, Ito J, Sato K. The Battle between Retroviruses and APOBEC3 Genes: Its Past and Present. Viruses. 2021;13(1).
336. Kohli RM, Maul RW, Guminski AF, McClure RL, Gajula KS, Saribasak H, et al. Local sequence targeting in the AID/APOBEC family differentially impacts retroviral restriction and antibody diversification. J Biol Chem. 2010;285(52):40956-64.
337. Kouno T, Silvas TV, Hilbert BJ, Shandilya SMD, Bohn MF, Kelch BA, et al. Crystal structure of APOBEC3A bound to single-stranded DNA reveals structural basis for cytidine deamination and specificity. Nat Commun. 2017;8:15024.
338. Shi K, Carpenter MA, Banerjee S, Shaban NM, Kurahashi K, Salamango DJ, et al. Structural basis for targeted DNA cytosine deamination and mutagenesis by APOBEC3A and APOBEC3B. Nat Struct Mol Biol. 2017;24(2):131-9.

339. Nahmad AD, Reuveni E, Goldschmidt E, Tenne T, Liberman M, Horovitz-Fried M, et al. Frequent aneuploidy in primary human T cells after CRISPR-Cas9 cleavage. Nature biotechnology. 2022;40(12):1807-13.
340. Xin H, Wan T, Ping Y. Off-Targeting of Base Editors: BE3 but not ABE induces substantial off-target single nucleotide variants. Signal Transduct Target Ther. 2019;4:9.
341. Maul RW, Gearhart PJ. AID and somatic hypermutation. Adv Immunol. 2010;105:159-91.
342. Preece R, Georgiadis C, Gkazi SA, Etuk A, Christi A, Qasim W. 'Mini' U6 Pol III promoter exhibits nucleosome redundancy and supports multiplexed coupling of CRISPR/Cas9 effects. Gene Ther. 2020;27(9):451-8.
343. Irving M, Lanitis E, Migliorini D, Ivics Z, Guedan S. Choosing the Right Tool for Genetic Engineering: Clinical Lessons from Chimeric Antigen Receptor-T Cells. Human gene therapy. 2021;32(19-20):1044-58.
344. Fraietta JA, Nobles CL, Sammons MA, Lundh S, Carty SA, Reich TJ, et al. Disruption of TET2 promotes the therapeutic efficacy of CD19-targeted T cells. Nature. 2018;558(7709):307-12.
345. Shah NN, Qin H, Yates B, Su L, Shalabi H, Raffeld M, et al. Clonal expansion of CAR T cells harboring lentivector integration in the CBL gene following anti-CD22 CAR T-cell therapy. Blood advances. 2019;3(15):2317-22.
346. Ran T, Eichmüller SB, Schmidt P, Schlander M. Cost of decentralized CAR T-cell production in an academic nonprofit setting. Int J Cancer. 2020;147(12):3438-45.
347. Gándara C, Affleck V, Stoll EA. Manufacture of Third-Generation Lentivirus for Preclinical Use, with Process Development Considerations for Translation to Good Manufacturing Practice. Human gene therapy methods. 2018;29(1):1-15.
348. Kebriaei P, Izsvák Z, Narayanavari SA, Singh H, Ivics Z. Gene Therapy with the Sleeping Beauty Transposon System. Trends Genet. 2017;33(11):852-70.
349. Lin L, Cho SF, Xing L, Wen K, Li Y, Yu T, et al. Preclinical evaluation of CD8+ anti-BCMA mRNA CAR T cells for treatment of multiple myeloma. Leukemia. 2021;35(3):752-63.
350. Rogers GL, Huang C, Clark RDE, Seclén E, Chen H-Y, Cannon PM. Optimization of AAV6 transduction enhances site-specific genome editing of primary human lymphocytes. Molecular Therapy - Methods & Clinical Development. 2021;23:198-209.
351. van der Loo JC, Wright JF. Progress and challenges in viral vector manufacturing. Hum Mol Genet. 2016;25(R1):R42-52.
352. Ishibashi R, Abe K, Ido N, Kitano S, Miyachi H, Toyoshima F. Genome editing with the donor plasmid equipped with synthetic crRNA-target sequence. Scientific Reports. 2020;10(1):14120.
353. Zhang JP, Li XL, Li GH, Chen W, Arakaki C, Botimer GD, et al. Efficient precise knockin with a double cut HDR donor after CRISPR/Cas9-mediated double-stranded DNA cleavage. Genome Biol. 2017;18(1):35.
354. Song F, Stieger K. Optimizing the DNA Donor Template for Homology-Directed Repair of Double-Strand Breaks. Molecular Therapy - Nucleic Acids. 2017;7:53-60.
355. Veneziano R, Shepherd TR, Ratanalert S, Bellou L, Tao C, Bathe M. In vitro synthesis of gene-length single-stranded DNA. Sci Rep. 2018;8(1):6548.

356. Braun T, Pruene A, Darguzyte M, Vom Stein AF, Nguyen PH, Wagner DL, et al. Non-viral TRAC-knocked-in CD19(KI)CAR-T and gp350(KI)CAR-T cells tested against Burkitt lymphomas with type 1 or 2 EBV infection: In vivo cellular dynamics and potency. Front Immunol. 2023;14:1086433.
357. Balke-Want H, Keerthi V, Gkitsas N, Mancini AG, Kurgan GL, Fowler C, et al. Homology-independent targeted insertion (HITI) enables guided CAR knock-in and efficient clinical scale CAR-T cell manufacturing. Mol Cancer. 2023;22(1):100.
358. Fleischer LC, Spencer HT, Raikar SS. Targeting T cell malignancies using CAR-based immunotherapy: challenges and potential solutions. J Hematol Oncol. 2019;12(1):141.
359. Li H, Song W, Li Z, Zhang M. Preclinical and clinical studies of CAR-NK-cell therapies for malignancies. Front Immunol. 2022;13:992232.
360. Zhang L, Meng Y, Feng X, Han Z. CAR-NK cells for cancer immunotherapy: from bench to bedside. Biomarker Research. 2022;10(1):12.
361. Bergman H, Sissala N, HÄgerstrand H, Lindqvist C. Human NK-92 Cells Function as Target Cells for Human NK Cells - Implications for CAR NK-92 Therapies. Anticancer Res. 2020;40(10):5355-9.
362. Mitwasi N, Feldmann A, Arndt C, Koristka S, Berndt N, Jureczek J, et al. "UniCAR"-modified off-the-shelf NK-92 cells for targeting of GD2-expressing tumour cells. Scientific Reports. 2020;10(1):2141.
363. Cullot G, Boutin J, Toutain J, Prat F, Pennamen P, Rooryck C, et al. CRISPR-Cas9 genome editing induces megabase-scale chromosomal truncations. Nat Commun. 2019;10(1):1136.
364. Enache OM, Rendo V, Abdusamad M, Lam D, Davison D, Pal S, et al. Cas9 activates the p53 pathway and selects for p53-inactivating mutations. Nature genetics. 2020;52(7):662-8.
365. Wienert B, Cromer MK. CRISPR nuclease off-target activity and mitigation strategies. Front Genome Ed. 2022;4:1050507.
366. Yin J, Lu R, Xin C, Wang Y, Ling X, Li D, et al. Cas9 exo-endonuclease eliminates chromosomal translocations during genome editing. Nat Commun. 2022;13(1):1204.
367. Hunt JMT, Samson CA, Rand AD, Sheppard HM. Unintended CRISPR-Cas9 editing outcomes: a review of the detection and prevalence of structural variants generated by gene-editing in human cells. Hum Genet. 2023;142(6):705-20.
368. Gaudelli NM, Lam DK, Rees HA, Solá-Esteves NM, Barrera LA, Born DA, et al. Directed evolution of adenine base editors with increased activity and therapeutic application. Nature biotechnology. 2020;38(7):892-900.
369. Kosicki M, Allen F, Steward F, Tomberg K, Pan Y, Bradley A. Cas9-induced large deletions and small indels are controlled in a convergent fashion. Nat Commun. 2022;13(1):3422.
370. Guo C, Ma X, Gao F, Guo Y. Off-target effects in CRISPR/Cas9 gene editing. Front Bioeng Biotechnol. 2023;11:1143157.
371. Caso F, Davies B. Base editing and prime editing in laboratory animals. Lab Anim. 2022;56(1):35-49.
372. Arbab M, Shen MW, Mok B, Wilson C, Matuszek Ż, Cassa CA, Liu DR. Determinants of Base Editing Outcomes from Target Library Analysis and Machine Learning. Cell. 2020;182(2):463-80.e30.

373. Honjo T, Muramatsu M, Fagarasan S. Aid: How does it aid antibody diversity? Immunity. 2004;20(6):659-68.
374. Feng Y, Seija N, Di Noia JM, Martin A. AID in Antibody Diversification: There and Back Again. Trends Immunol. 2020;41(7):586-600.
375. Alqassim EY, Sharma S, Khan A, Emmons TR, Cortes Gomez E, Alahmari A, et al. RNA editing enzyme APOBEC3A promotes pro-inflammatory M1 macrophage polarization. Commun Biol. 2021;4(1):102.
376. Hamieh M, Dobrin A, Cabriolu A, van der Stegen SJC, Giavridis T, Mansilla-Soto J, et al. CAR T cell trogocytosis and cooperative killing regulate tumour antigen escape. Nature. 2019;568(7750):112-6.
377. Sommermeyer D, Hudecek M, Kosasih PL, Gogishvili T, Maloney DG, Turtle CJ, Riddell SR. Chimeric antigen receptor-modified T cells derived from defined CD8+ and CD4+ subsets confer superior antitumor reactivity in vivo. Leukemia. 2016;30(2):492-500.
378. Merten OW, Charrier S, Laroudie N, Fauchille S, Dugué C, Jenny C, et al. Large-scale manufacture and characterization of a lentiviral vector produced for clinical ex vivo gene therapy application. Human gene therapy. 2011;22(3):343-56.
379. David RM, Doherty AT. Viral Vectors: The Road to Reducing Genotoxicity. Toxicol Sci. 2017;155(2):315-25.
380. Tyagarajan S, Schmitt D, Acker C, Rutjens E. Autologous cryopreserved leukapheresis cellular material for chimeric antigen receptor-T cell manufacture. Cytotherapy. 2019;21(12):1198-205.
381. Hacein-Bey-Abina S, Von Kalle C, Schmidt M, McCormack MP, Wulffraat N, Leboulch P, et al. LMO2-associated clonal T cell proliferation in two patients after gene therapy for SCID-X1. Science (New York, NY). 2003;302(5644):415-9.
382. Nam CH, Rabbitts TH. The role of LMO2 in development and in T cell leukemia after chromosomal translocation or retroviral insertion. Molecular therapy : the journal of the American Society of Gene Therapy. 2006;13(1):15-25.
383. Wan T, Niu D, Wu C, Xu F-J, Church G, Ping Y. Material solutions for delivery of CRISPR/Cas-based genome editing tools: Current status and future outlook. Materials Today. 2019;26:40-66.
384. Charlesworth CT, Hsu I, Wilkinson AC, Nakauchi H. Immunological barriers to haematopoietic stem cell gene therapy. Nature Reviews Immunology. 2022;22(12):719-33.
385. Conti A, Di Micco R. p53 activation: a checkpoint for precision genome editing? Genome Med. 2018;10(1):66.
386. Dorset SR, Bak RO. The p53 challenge of hematopoietic stem cell gene editing. Molecular therapy Methods & clinical development. 2023;30:83-9.
387. Hornung V, Latz E. Intracellular DNA recognition. Nat Rev Immunol. 2010;10(2):123-30.
388. Yang H, Ren S, Yu S, Pan H, Li T, Ge S, et al. Methods Favoring Homology-Directed Repair Choice in Response to CRISPR/Cas9 Induced-Double Strand Breaks. Int J Mol Sci. 2020;21(18).
389. Lieber MR. The mechanism of double-strand DNA break repair by the nonhomologous DNA end-joining pathway. Annu Rev Biochem. 2010;79:181-211.

390. Koblan LW, Doman JL, Wilson C, Levy JM, Tay T, Newby GA, et al. Improving cytidine and adenine base editors by expression optimization and ancestral reconstruction. Nature biotechnology. 2018;36(9):843-6.
391. Thuronyi BW, Koblan LW, Levy JM, Yeh W-H, Zheng C, Newby GA, et al. Continuous evolution of base editors with expanded target compatibility and improved activity. Nature biotechnology. 2019;37(9):1070-9.
392. Zhang X, Chen L, Zhu B, Wang L, Chen C, Hong M, et al. Increasing the efficiency and targeting range of cytidine base editors through fusion of a single-stranded DNA-binding protein domain. Nat Cell Biol. 2020;22(6):740-50.
393. Yang L, Huo Y, Wang M, Zhang D, Zhang T, Wu H, et al. Engineering APOBEC3A deaminase for highly accurate and efficient base editing. Nature Chemical Biology. 2024.
394. Glaser V, Flugel C, Kath J, Du W, Drosdek V, Franke C, et al. Combining different CRISPR nucleases for simultaneous knock-in and base editing prevents translocations in multiplex-edited CAR T cells. Genome Biol. 2023;24(1):89.